The Spatial Organization of EPH Receptor Tyrosine Kinase Activity

By: Ola Sabet

Dissertation

Der Fakultät für Chemie der
Technische Universität Dortmund

Vorlegt am 18 Juni 2013

von Ola Sabet

Erster Gutachter: Prof. Dr. Philippe Bastiaens
Zweiter Gutachter: Prof. Dr. Roland Winter

Tag der mündlichen Prüfung: 25.07.2013

Work presented in this dissertation was performed in the laboratory of
Prof. Dr. Philippe Bastiaens at the Max-Planck-Institute of Molecular Physiology,
Dortmund, Germany.

Ola Sabet was affiliated to the
International Max-Planck Research School
for Chemical Biology, Dortmund, Germany.

Eidesstattliche Versicherung

Ich versichere hiermit an Eides statt, dass die vorgelegte Dissertation von mir selbständig und ohne unerlaubte Beihilfe angefertigt ist.

Dortmund, den …….. ……..…….
(Unterschritt)

Erklärung

Hiemrmit erkläre ich, dass ich mich anderweitig einer Doktorprüfung ohne Erfolg nicht unterzogen habe.

Dortmund, den …….. ……..…….
(Unterschritt)

Adam & Ismail

"Thanks for being my kind of light at the end of the tunnel"

CONTENTS

LIST OF PUBLICATIONS

Results and methodologies presented in this thesis have contributed to the following peer-reviewed publications:

- Janes PW, Wimmer-Kleikamp S, Fragakis AS, Griesshaber B, **Sabet O**, Grabenbauer M, Ting AY, Saftig P, Bastiaens PIH, Lackmann M (2009) Cytoplasmic Relaxation of Active Eph Controls Ephrin Shedding by ADAM10 PLoS Biology.
- Haj FG, **Sabet O**, Kinkhabwala A, Wimmer-Kleikamp S, Roukos V, Han HM, Grabenbauer M, Bierbaum M, Anthony C, Neel BG, Bastiaens PIH (2012) Regulation of Signaling at Regions of Cell-Cell Contact by Endoplasmic Reticulum-Bound Protein-Tyrosine Phosphatase 1B PLoS ONE.
- Schaupp A, **Sabet O**, Dudanova I, Ponserre M, Bastiaens PIH and Klein R (2013) Composition of EphB2 Clusters Determines Strength of Cellular Response, (Submitted).
- **Sabet O**, Stockert R, Schmick M, Bastiaens PIH (2013) The Spatial Organizaiton of Eph Receptor Signaling, (Submitted).
- Hou J*, **Sabet O***, Grecco H, Bastiaens P (2013) Enzyme Substrate Imaging of Eph Receptors, (In preparation).
  * equal contribution

The work was presented at the following conferences:

- IMPRS-CB Symposium 2011 – "Spatial-Temporal Activity Profiling of EPH/Ephrin Signaling".
- 3rd EMBO Conference Series – "Cellular Signaling and molecular Medicine" – won the EACR poster prize.

LIST OF FIGURES

ABBREVIATIONS

&	and
‘	minute(s)
‘’	second(s)
°C	degree Celsius
µl	microliter
a.u.	arbitrary units
Å	angstrom
AL	activation loop
ADAM	A-Disintegrin-And-Metalloprotease
ATP	Adenosine triphosphate
BSA	bovine serum albumin
CMV	Cytomegalovirus
COS	CV-1 origin, SV-40
C-terminus	carboxy terminus
DMEM	Dulbecco’s modified Eagle’s medium
DNA	deoxyribonucleic acid
dNTPs	deoxyribonucleoside triphosphates
e.g.	*exempli gratia*
ECM	extracellular matrix
EDTA	ethylenediaminetetraacetic acid
EGF	epidermal growth factor
EGFP	enhanced green fluorescent protein
EGFR	epidermal growth factor receptor
Eph	erythropoietin-producing hepatocellular carcinoma cell
ephrin	Eph receptor interacting protein
ER	endoplasmatic reticulum
Fc	human Fc-antibody fragment
FGFR	Fibroblast growth factor receptor
Fig.	figure
FL	fluorescence
FNIII	type-III fibronectin protein
FP	fluorescent protein
FRET	Förster resonance energy transfer
GFP	green fluorescent protein
GPI	glycosylphosphatidylinositol
GRIP	glutamate receptor interacting protein
HEK	human embryonic kidney
HEPES	N-2-hydroxyethylpiperanzine-N’-2-ethanesulfonic acid
hr(s)	hour(s)
i.e.	*id est*
IC_{50}	half maximal inhibitory concentration
ICD	Intracellular domain
IP	immunoprecipitation
JM	juxtamembrane
JMS	juxtamembrane segment
kd	kinase-dead / deficient
KD	Kinase domain
l	liter
LB_0	lysogeny broth
LBD	ligand binding domain

MCF-7	Michigan cancer foundation-7
MDCK	Madin-darby canine kidney cells
min	minute(s)
ml	milliliter
NGF	Nerve growth factor
n.s.	not significantly different
N/A	numerical aperture
ns	nanosecond(s)
N-terminus	amino terminus
PAGE	poly-acrylamide gel electrophoresis
PBM	PDZ-binding motif
PDZ	PSD95/Dlg/ZO1
pH	*potentium hydrogenii*
PM	plasma membrane
PTB	phospho-tyrosine binding
PTP	phosophotyrosine phosphatases
PTP1B	protein tyrosine phosphatases 1B
pTyr	phosphotyrosine
RBD	receptor binding domain
RE	recycling endosome
RT	room temperature
RTK(s)	receptor tyrosine kinase(s)
s	second(s)
SAM	sterile-α-motif
SEM	standard error of mean
SH2	src homology 2
SPIM	single plane illumination microscopy
TM	transmembrane
Tris	Tris[hydroxymethyl]aminomethane
TyrK	Tyrosine kinases
VEGF	vascular endothelial growth factor
WT	wild type

Units were abbreviated using the International System of Units (SI). The triple and single letter codes were used for abbreviations of amino acids. Chemicals are abbreviated according to guidelines by the International Union of Pure and Applied Chemistry.

ABSTRACT

Eph receptors (Ephs) and their membrane bound ephrin ligands constitute one of the major guidance cues that control developmental and pathological cell positioning. As in other receptor tyrosine kinases (RTKs), ligand binding induces oligomerization of Ephs at the plasma membrane (PM), activation of their intrinsic autocatalytic activity and phosphorylation of key tyrosine residues in their intracellular domain. In this thesis, we asked how the autocatalytic activity of Eph is dynamically controlled inside cells to prevent spurious self-activation yet allow for robust activation upon exposure to ligand.

The current view in Eph signaling is that ligand-driven oligomerization of Ephs converts inactive monomers to active oligomers. However, in this thesis we show that the mechanism of receptor clustering is not that simple. Using an FKBP-based dimerizing system, we investigated the effect of cluster size composition on EphB2 cellular output. We found that small-sized EphB2 clusters produce a functional response, whose strength is determined by the abundance of multimers over dimers within a cluster population. In addition, we identified a positive regulatory effect on EphB2 clustering by GRIP1 protein and a negative regulatory effect on ephrin-induced clustering by C-terminal domains of EphB2. Together these results showed how the cell's pre-established molecular context could determine the response of Ephs to ephrins, which is then translated into clusters with different size, composition and/or stability.

The *auto*catalytic activity of Eph receptors is regulated by reversible *auto*phosphorylation and dephosphorylation cycles that are spatially and temporally partitioned within cells due to the interactions with protein tyrosine phosphatases (PTPs). Using quantitative cellular imaging approaches, we found that the endoplasmic reticulum (ER)-anchored PTP1B comes in close proximity to regions of cell-cell contact rich in Eph receptors and identified EphA2 as a new substrate for PTP1B specifically at those regions. These results highlighted ER-PM interactions as an emerging new paradigm in cellular signaling.

To investigate how Eph conformational dynamics as well as its spatial organization within cells can affect its inherent *auto*catalytic activity, we designed a genetically encoded biosensor that monitors EphA2 conformation, termed Linker optimized Intramolecular-FRET based sensor for EphA2 (LIFEA2). By measurements of LIFEA2 conformational dynamics, we could describe EphA2

activation with precise spatial temporal resolution. In addition, by correlating the cell-to-cell variance in LIFEA2 expression level to its activity state, we demonstrated the propensity of this *auto*catalytic system to self-activate in the absence of ligand. Finally, we described two levels of regulation for EphA2 activation, a *cis*-inhibitory dynamic interaction between the kinase domain and the juxtamembrane segment, and a novel PM-recycling mediated mechanism. The continuous recycling of EphA2 to the PM acts as a safeguard mechanism by maintaining a low steady-state level of receptor at the PM and by trafficking the receptor through peri-nuclear areas with high PTP1B activity that dephosphorylates spuriously *auto*activated receptors.

ZUSAMMENFASSUNG

Eph-Rezeptoren (Ephs) und ihre membrangebundenen Ephrin-Liganden bilden eine der wichtigsten Orientierungsmarken, für die Kontrolle der Zellpositionierung im Rahmen ontogenetischer und pathologischer Prozesse. Wie bei anderen Rezeptortyrosinkinasen (RTKs) induziert die Ligandenbindung die Oligomerisierung der Ephs an der Plasmamembran (PM), die Aktivierung der autokatalytischen Aktivität und die Phosphorylierung wichtiger Tyrosinreste in der intrazellulären Domäne. In dieser Arbeit wird der Frage nachgegangen, wie die autokatalytische Aktivität von Eph innerhalb der Zelle dynamisch derart kontrolliert wird, dass einerseits spontane Autoaktivierung verhindert und andererseits eine robuste Aktivierung des Rezeptors nach Ligandenbindung erzielt wird.

Nach dem derzeit geläufigen Modell für Eph konvertiert die Liganden induzierte Oligomerisierung des Ephs inaktive Monomere in aktive Oligomere. In dieser Arbeit wird jedoch gezeigt, dass der Mechanismus des Clustering der Rezeptoren komplexer ist. Mithilfe eines FKBP-basierten Dimersierungssystems wurde der Effekt der Clustergröße auf die EphB2 vermittelte Zellantwort untersucht. Dabei zeigte sich, dass kleine EphB2 Cluster eine funktionelle Zellantwort induzieren, deren Stärke vom Verhältnis der Multimere zu Dimeren innerhalb der Clusterpopulation bestimmt wird. Desweiteren wurde ein positiver regulatorischer Effekt des GRIP1 Proteins auf EphB2 und ein inhibierender Effekt C-terminaler Domänen des EphB2 auf die Ephrin-induzierte Oligomerisierung identifiziert. Zusammen zeigen diese Ergebnisse, wie der vorhandene molekulare Kontext der Zelle die Antwort von Ephs auf Ephrine bestimmen und wie sich dies in in Bezug auf die Clustergröße, -Zusammensetzung und/oder -Stabilität von Eph auswirken kann.

Die autokatalytische Aktivität des Eph wird in Zellen durch Zyklen reversibler Autophosphorylierung und Dephosphorylierung reguliert, die durch Interaktion mit Proteintyrosinphosphatasen (PTPs) räumlich und zeitlich separiert sind. Mit quantitativen, mikroskopischen Verfahren konnten wir zeigen, dass am Endoplasmatischen Retikulum (ER) verankertes PTP1B in unmittelbare Nähe zu Zell-Zell-Kontakten kommt, die reich an Ephs sind, und konnten EphA2 als neues Substrat für PTP1B in genau diesen Regionen identifizieren. Diese Ergebnisse

untermauern das derzeit aufkeimende Modell der Bedeutung von ER-PM Interaktionen für die zelluläre Signalregulation.

Um zu untersuchen, wie die Dynamik der Konformationsänderungen von Eph sowie seine räumliche Organisation in Zellen die autokatalytische Aktivität beeinflussen, entwickelten wir einen genetisch-kodierten Biosensor namens „Linker optimized Intramolecular-FRET based sensor for EphA2" (LIFEA2), der die Konformation von EphA2 anzeigt. Durch Messung der Konformationsdynamik von LIFEA2 konnten wir die EphA2 Aktivierung mit hoher räumlicher und zeitlicher Auflösung beschreiben. Weiterhin konnten wir durch Korrelation der Zell-zu-Zell-Varianz in LIFEA2-Expressionsleveln zum LIFEA2-Aktivitätszustand auch die Neigung des autokatalytischen Systems zur Selbstaktivierung in Abwesenheit des Liganden aufzeigen. Abschließend beschreiben wir zwei Regulationsebenen für die EphA2 Aktivierung – eine cis-inhibitorische, dynamische Interaktion zwischen der Kinasedomäne und dem Juxtamembran-Segment sowie einen neuen Recycling-Mechanismus zur PM. Das kontinuierliche Recycling des EphA2 zur PM dient als Schutzmaßnahme, indem es niedrige Gleichgewichtslevel des Rezeptors an der PM aufrechterhält und durch das Schleusen des Rezeptors durch den peri-nukleären Bereich mit hoher PTP1B-Aktivität spontan autoaktivierte Rezeptoren dephosphoryliert.

1. INTRODUCTION

Despite the successes achieved by reductionist research of the twentieth-century in identifying and describing the molecular components of cellular signaling pathways, little is known about how these multicomponent pathways process extracellular signals to generate a defined cellular response. To understand signal processing, it is no longer sufficient to depend on linear reaction schemes that consider an active state of a given protein. Rather, one needs to consider how external and internal stimuli are dynamically processed by a given multicomponent signaling system[1]. Dynamically here refers to the spatial organization of signaling, which does not only include the topology of a given simple network but also the initial concentration of each protein state over space and time. Dynamic biological systems are kept in-check by operating under constant opposing tendencies, favoring one or the other depending on the context. Amplification and attenuation or robustness and adaptability of signaling systems are examples of opposing tendencies underlying every level of organization [2]. Even on a molecular level, such duality can be seen between individual proteins, allowing local sources to affect global patterns. The emerging patterns will in return affect the interactions of individual proteins at local sources, in a negative or positive manner.

The function of a subfamily of receptor tyrosine kinases (RTKs) called Eph (from erythropoietin-producing hepatocellular carcinoma cell) family is an excellent example of such duality in signaling. Like other RTK family members, the signaling capacity of Eph is mediated by *auto*phosphorylation of intracellular tyrosine residues that can serve as docking sites for downstream effectors. Interactions of Ephs with their cognate membrane-bound ephrin ligands can either prolong cell-cell adhesion and communication or promote cell-cell repulsion. Upon ligand binding, activated Ephs form expansive clusters that need to be terminated for cell-cell repulsion to take place. Promotion versus termination of signaling is therefore the balance that Eph RTKs must maintain at every level of organization. Local factors influencing this balance include, gradients of interacting Eph/ephrins, duration of their contact, clustering capacity of Ephs and the cell's own clustering history, spatial organization of the phosphorylation-dephosphorylation cycle and recycling versus termination of signaling.

In this thesis, my main aim is to study the spatial organization of Eph signaling while focusing on local factors contributing to such organization. Factors such as regulation by the ER-anchored PTP1B, Eph trafficking, Eph clustering and Eph conformational dynamics are analyzed and their link to Eph regulation in space and time is assessed. These questions required a method, capable of measuring Eph clustering and/or Eph activation in living cells. For the former, fluorescence anisotropy coupled to a dimerizer controlled clustering system of Ephs was used to measure cluster sizes of fluorescently labeled EphB2. For the latter, high-resolution fluorescence microscopy and a genetically encoded sensor monitoring EphA2 active conformation was designed and used.

This thesis is divided into (4) major parts. Chapter 1 summarizes the current structural, biochemical and cell biological knowledge of the Eph/ephrin system as well as describing the basis of FLIM and Anisotropy. Chapter 2 gives a detailed description of the experimental procedures and reagents used in this thesis. Chapter 3 presents experimental results that study the spatial organization the ER-anchored phosphatase (PTP1B) towards points of cell-cell contact, with the aim of addressing the regulation of signaling at these points by PTP1B. Furthermore, the role of clustering in Eph signaling is presented, to test the hypothesis that clustering can allow Ephs to modulate the signaling capacity in a graded fashion when exposed to ephrin gradients during cellular patterning. Moreover, local factors affecting Eph active conformation will be presented while following the activity of Eph with a linker optimized intra-molecular FRET based sensor for EphA2 (LIFEA2). A discussion of the experimental results is given in chapter 4.

1.1 Cell signaling by receptor tyrosine kinases

In order to understand Eph signaling in space and time, one has to start with the parental cellular communication system, i.e. phosphotyrosine signaling by receptor tyrosine kinases (RTKs). Phosphotyrosine (pTyr)-based signaling is mediated by three distinct functional components: tyrosine kinases (TyrK) that phosphorylate specific tyrosine residues on proteins, Src Homlogy 2 (SH2) and phospho-tyrosine binding (PTB) domains that identify the tyrosine modification and phosophotyrosine phosphatases (PTP) that remove the phosphates. Together, these components play a pivotal role in many cell-to-cell communication pathways, including differentiation, proliferation, adhesion, immune defense and hormone responses (**Figure 1.1**) [3,4]. Since the cloning of the first cell surface RTK, the Epidermal Growth Factor Receptor (EGFR) more than two decades ago, RTKs have dwelled in the spotlight as key players of critical cellular responses. Unraveling the RTK signaling networks that connect extracellular signals with key cellular processes, such as differentiation and proliferation, cell migration and cell cycle control, cell survival and metabolism has now evolved into the well-established field of signal transduction [5,6]. TyrK can be divided into either nonreceptor or receptor tyrosine kinases (RTKs). There are 58 known RTKs in humans, with similar molecular topology, yet divided into twenty subfamilies (**Fig 1.2**).

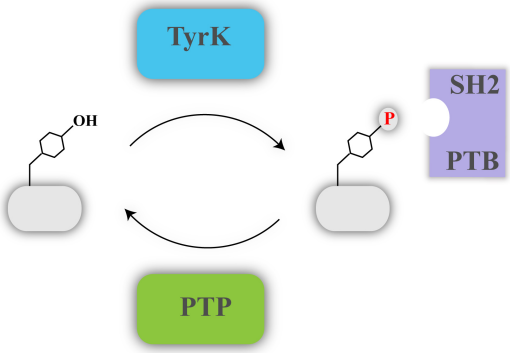

Fig 1.1 The three-part toolkit of phosphotyrosine signaling
In phosphor-Tyrosine (pTyr) signaling, the tyrosine kinase (TyrK), Src Homology 2(SH2), phosphor tyrosine-binding domain (PTB) and phosphotyrosine phosphatase (PTP) domains form a highly interdependent signaling platform. Adapted from [4].

All RTKs have their ligand-binding domain (LBD) on the extracellular side of the membrane, a single-pass transmembrane (TM) helix, followed by an intracellular domain (ICD) that contains the protein tyrosine kinase (TK) catalytic region, plus additional regulatory domains in the juxtamembrane (JM) and carboxy (C-) terminus region of the molecule [7].

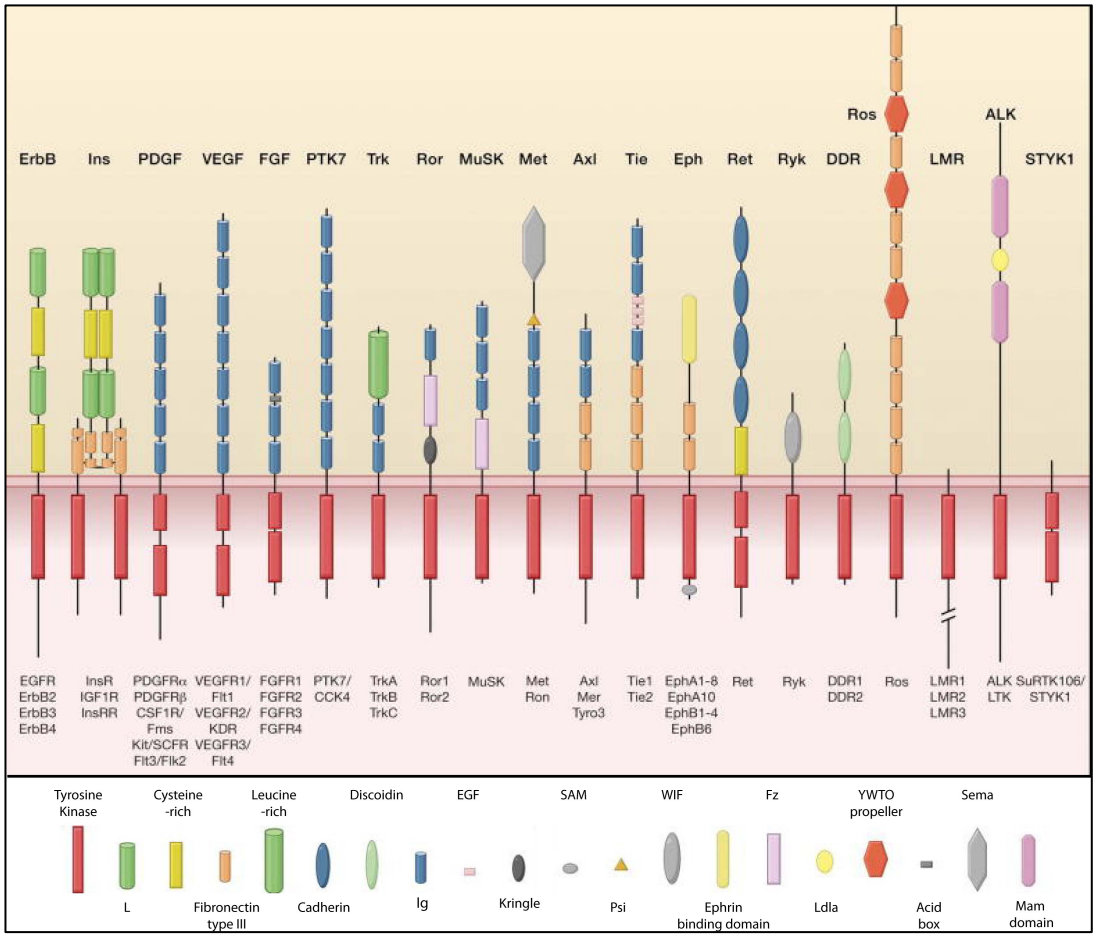

Fig 1.2 Receptor tyrosine kinase families
In human, there are 58 receptor tyrosine kinases (RTKs) that fall in 20 subfamilies, shown here schematically with the family members listed below each receptor. Structural domains in the extracellular regions identified by structure determination or sequence analysis, are marked according to the key. The intracellular domains are shown as red rectangles. Adapted from [7].

1.1.1 Receptor activation through Ligand-induced dimerization of RTKs

Growth factor binding generally leads to RTK activation by inducing receptor dimerization. There is however, a subset of RTKs that exist in an oligomeric form even before ligand activation. Ligand-induced activation of RTK whether the "inactive" state is a monomer or an oligomer, will still require the bound ligand to stabilize the "active" form of RTK, be it dimeric or oligomeric [5]. Early work on "ligand mediated" RTK dimerization suggested that a divalent ligand interacts with and thereby cross-links two receptor molecules, forming a 2:2, ligand: receptor complex. This model was supported by various crystal structures including, vascular endothelial growth factor (VEGF) receptor [8,9], nerve growth factor (NGF)/neurotrophin receptor TrkA [10], stem cell factor receptor KIT1 [11] and Eph receptors [12]. Recent structural studies of full extracellular regions of RTKs,

has replaced the generic "ligand-mediated" mode of receptor dimerization, with a range of mechanisms (**Fig 1.3**). At one end, the ligand holds the sole responsibility for inducing receptor dimerization, and the two receptors do not directly contact, as for the NGF/TrkA, ligand/receptor interaction [10,13] (**Fig 1.3A**). At the other end, receptors mediate dimerization and ligands do not contribute to the dimer interface, as for the EGFR/ErbB family [14,15] (**Fig 1.3D**). Dimerization can also involve both receptor and ligand-mediated components (**Fig 1.3B and 1.3C**).

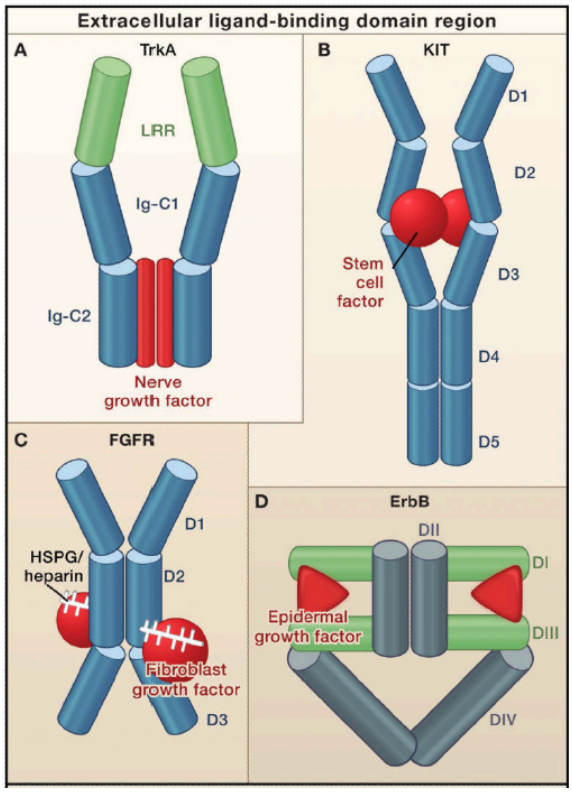

Fig 1.3 Receptor tyrosine kinase dimerization
RTKs associate into dimers when ligand (red) binds to their extracellular domains. The bound ligand activates the receptors by stabilizing a certain relationship between two separate receptor molecules. **(A)** Nerve growth factor dimers (red) cross-links two TrkA molecules without any direct contact between the two receptors [13]. **(B)** Stem cell factor dimer (red) cross-links two KIT molecules, accompanied by interaction of the two Ig-like domains (D4 and D5) across the dimer interface [16]. **(C)** Two fibroblast growth factor receptors (FGFRs) as well the necessary molecule heparin (white) contact one another through the Ig-like domain D2. In addition the fibroblast growth factor (FGF) ligand (red) contacts Ig-like domain D2 and D3 of both FGFRs [17]. **(D)** Dimerization of ErbB receptors is mediated entirely by the receptor. When the ligand binds to the two sites (DI and DIII) it drives the exposure of the dimerization interface in Domain II.

1.1.2 Activation of tyrosine kinase domain

The central question in RTK signaling is how the ligand-induced dimerization of the extracellular domain gets translated into kinase domain (KD) activation on the intracellular side of the membrane. All tyrosine KDs consist of an N-lobe and a C-lobe (**Fig 1.4**), and exhibit a similar structure when crystallized in an active form [18]. Crucial regulatory elements such as the αC helix in the kinase N-lobe and the activation loop (AL) adopt a specific structure in the active KD form that is essential for phosphotransfer [19]. Structures of the inactive tyrosine KDs are on the other hand quite versatile between the different receptor, depending on the set of intramolecular inhibitory interactions that are receptor specific.

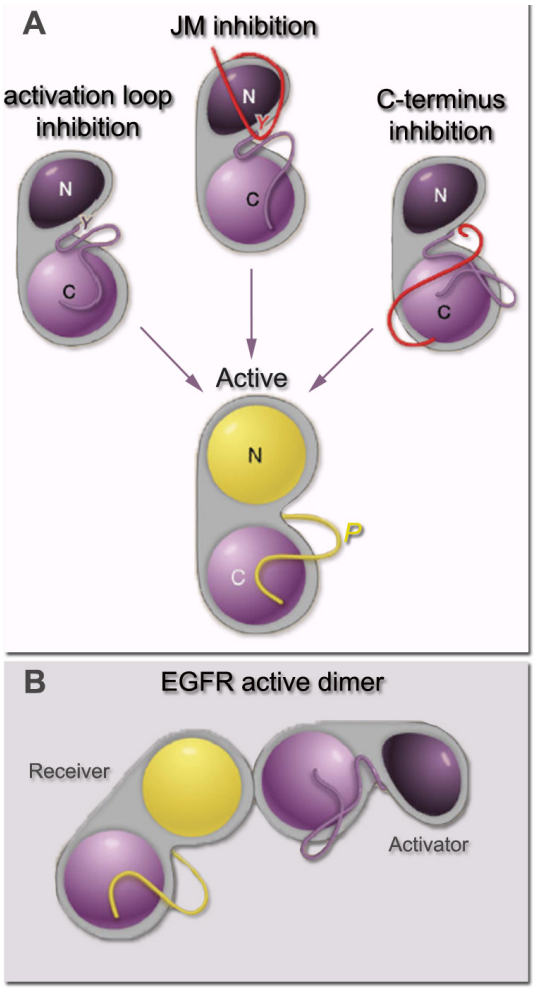

Fig 1.4 Receptor tyrosine kinase (RTK) activation upon extracellular dimerization Intracellular tyrosine kinase domains (TKDs), contain a C-lobe (light purple), N-lobe (dark purple or yellow). Many receptors are inhibited by a set of intramolecular (or *cis*) interactions: **(A)** Activation loop inhibition. In FGFR, insulin receptor and IGF1 receptor, the activation loop interacts directly with the kinase active site thereby blocking access to protein substrates or both ATP and protein substrates. Phosphorylation of key tyrosines releases this inhibition allowing the kinase a "relaxed" active state. Juxtamembrane (JM) inhibition. In KIT, PDGFR and Eph receptors, the JM region (red) interacts with and disrupts the kinase domain. Phophorylation of key tyrosines in the JM region destabilizes these autoinhibitory *cis* interactions and allows the kinase domain to attain an active conformation. C-terminal tail inhibition. In Tie1 and Tie2, the C-terminus tail interacts with the kinase active site to stabilize an inactive conformation[20]. **(B)** EGFR kinase domain is activated allosterically by direct contacts between C-lobe of one kinase, the "Activator" and the N-lobe of another kinase, "Receiver" [21].

1.1.2.1 Inhibition of the kinase domain by the activation loop

Activation loop autoinhibition was first demonstrated by the structure of the insulin receptor KD. An essential tyrosine residue in the activation loop (Y1162) blocks access of ATP and protein substrates to the active site ("activation loop inhibition" in **Fig 1.4A**). Upon insulin binding, *trans*-phosphorylation of Y1162 disrupts its *cis*-autoinhibitory effect, allowing the kinase domain to adopt the generic RTK active state (Fig1.4A) [22]. The KD of Fibroblast Growth Factor Receptor1 (FGFR1) is also *cis*-autoinhibited by the activation loop, but through a different set of activation loop interactions that stabilize an inactive conformation. Ligand-induced dimerization, again releases this *cis*-autoinhibition through *trans*-phosporylation of activation loop tyrosines [23].

1.1.2.2 *Inhibition of the kinase domain by the juxtamembrane*

In addition to *cis*-autoinhibition by the KD itself, many RTKs are inhibited by elements outside of the KD, best example of which is the juxtamembrane segment (JMS), as seen in KIT [24] and Eph family RTKs [25]. Through extensive contacts with the KD, that involve key tyrosines in the JM region, the inactive autoinhibied KD conformation is stabilized ("JM inhibition" in **Fig. 1.4A**). Ligand-induced dimerization promotes *trans*-phosphorylation of those JM-tyrosines, thereby disrupting *cis*-autoinhibitory interactions of JM and promoting KD activation [22].

1.1.2.3 *Inhibition of the kinase domain by C-terminal sequences*

Despite the fact that the activation loop of Tie2 kinase domain exists in an active-like conformation prior to phosphorylation, its nucleotide-binding loop adopts an inactive configuration [20]. The tyrosine-containing C-terminal tail of Tie2 is involved in *cis*-autoinhibition of KD by blocking substrate access to the kinase active site ("C-terminus inhibition in **Fig. 1.4A**). Autophosphorylation of the C-terminal located tyrosines, may lead to the disruption of this autoinhibitory interaction and thereby activate Tie2 [26].

1.1.2.4 *Allosteric activation of kinase domain*

Most RTKs follow the general dogma of trans-phosphorylation alleviating KD *cis*-autoinbibition and thereby leading to kinase activation. The EGFR/ErbB family of proteins and Ret stand as exception to this rule, since they do not require *trans*-phosphorylation for activation [21,27]. The kinase domain of EGFR forms an asymmetric dimer (**Fig 1.4B**) where the C-lobe of one KD "Activator" is in contact with the N-lobe of the second KD "Receiver". This interaction allows the receiver-kinase to adopt an active conformation without phosphorylation of activation loop.

1.1.2.5 *Conformational coupling across the plasma membrane*

Recent work done on the EGF receptor, uncovered the involvement of the transmembrane (TM) helices in intracellular kinase domain (KD) activation. Activation requires an N-terminal interaction between the TM helices that facilitates antiplarallel interaction between JM domains and release of inhibition by the membrane. Ligand binding would release steric constrains in the extracellular domain and translate that across the TM to an activation of intracellular KD [28,29].

1.2 Eph receptors and ephrin ligands

Eph receptors constitute the largest subfamily of RTKs. Together with their membrane-associated ephrin ligands, they function as principal guidance cues during developmental tissuegenesis, normal tissue homeostasis and tumorigenesis [30,31]. The ability of Ephs to alter cell positioning is achieved principally by modulating the adhesion or repulsion between receptor and ligand expressing cells upon their contact [32]. Interaction of Ephs and ephrins in *trans* leads to typical RTK forward signaling in receptor expressing cells and unique reverse signaling in ligand expressing cells, which is a distinguishing feature of the Eph/ephrin system known as bidirectional signaling [30]. Bidirectionality arises because Ephs are unique among other RTKs in their dependency on membrane-anchored ephrin ligand for activation [33]. Contrary to other RTKs, which are activated by dimerization, Ephs form higher-ordered oligomers with ephrins for proper biological response [34].

1.2.1 Nomenclature of Ephs and ephrins

The acronym EPH comes from the cell line from which the first family member (EphA1) was isolated, namely an *E*rythropoietin-*P*roducing *H*epatocellular carcinoma cell line [35]. Based on sequence conservation and their affinities towards ephrins, Ephs are divided into two subclasses, A and B. EphA subtype, consists of nine members in mammals (EphA1-EphA8 and EphA10) that bind promiscuously to six glycosylphosphatidylinositol (GPI)-anchored ephrinsAs (ephrin-A1-A6). EphB subtype, consists of five members (EphB1-EphB4 and EphB6) that interact with three transmembrane ephrinBs (ephrin-B1-B3) [36]. Inter-subclaass interactions between Eph and ephrin has been reported, for example EphA4 binds both ephrin A- and B-type [37,38], and ephrinA5 can bind and thereby activateEphB2 [39].

1.2.2 Eph/ephrin domains

The general domain topology of Ephs is conserved throughout the animal kingdom (**Fig. 1.5**) [40]. Eph extracellular region starts with an N-terminal globular ligand-binding domain (LBD), a cysteine-rich domain composed of a sushi domain and an EGF-like domain and two fibronectin type-III repeats (FNIIIa and b). In addition to ligand binding, the Eph globular domain, together with the cysteine-rich domain, contribute to ephrin-independent receptor dimerization and clustering [41-43]. Smilar to other RTKs, Eph receptors contain a single-pass transmembrane (TM) α-helical domain. Eph intracellular region consists of a

juxtamembrane (JM) segment containing two conserved regulatory tyrosine residues, the catalytic tyrosine kinase domain, a sterile-α-motif (SAM) protein interaction domain and a PDZ-binding motif (PBM) [31,44].

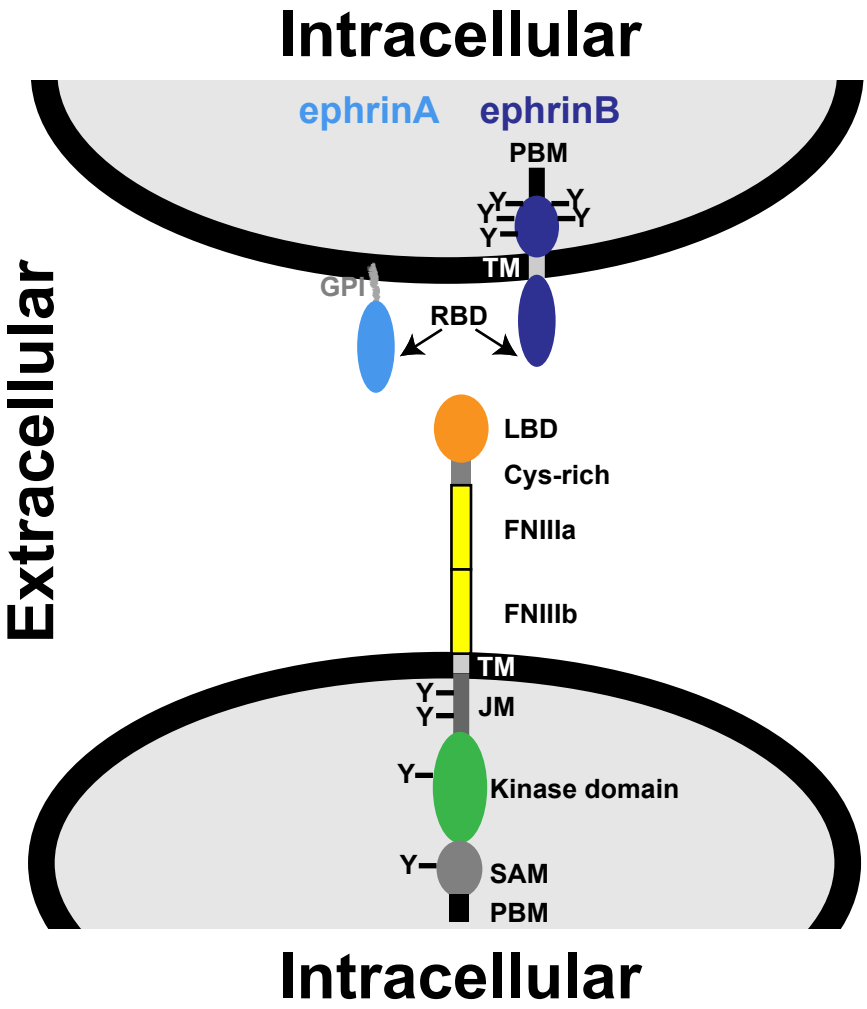

Fig 1.5 Domain structure of Eph receptors and ephrin ligands
Eph receptors contain an extracellular region with a globular ligand-binding domain (LBD), followed by cysteine-rich (Cys-rich) and fibronection type III repeats (FNIIIa and FNIIIb). Similar to other type 1 RTKs, the receptor contains a single-pass trans-membrane (TM) domain. The intracellular region contains a juxtamembrane (JM) domain, the kinase catalytic domain, sterile-alpha-motif (SAM) and PSD95/Dlg/Zo1 (PDZ)-binding motif (PBM). Ligand binding promotes clustering and phosphorylation at key tyrosines indicated by (Y). The transmembrane ephrin-Bs also become phosphorylated on tyrosine residues by Src family kinases, which are probably also promoting signaling by the GPI-anchored ephrin-As. RBD, receptor-binding domain; LBD, ligand-binding domain; GPI, glycosylphosphatidylinositol-anchor.

EphrinAs are membrane anchored via a glycosylphosphatidylinositol (GPI), while ephrinBs contain a single-pass TM domain and a short cytoplasmic tail with five conserved tyrosines followed by a PDZ-binding motif (PBM) (**Fig 1.5**). Both

ephrin subclasses posses an extracellular globular receptor-binding domain (RBD), and both lack intrinsic catalytic activity [31,45].

1.2.3 Signaling clusters of Ephs/ephrins

Contrary to ligands of other RTK subfamilies, only artificially clustered ephrins or naturally occurring membrane-bound ligand can trigger receptor signaling [33]. It has even been shown that the soluble non-clustered form of the ligand acts as an antagonist [46-48]. Prior to ligand contact, Ephs are scarcely distributed within the plasma membrane, and showing an expression level-dependent basal kinase activity [49-51]. The initiator step in Eph-ephrin signaling is a 1:1 high-affinity heterodimer between the Eph globular LBD and the conserved RBD of ephrins [52]. It has been shown for EphB2/ephrinB2, that additional interactions tether the formed heterodimers so that each ephrin now binds two Ephs and vice versa, to form a ring-like tetramer with distinct dimerization and tetramerization interfaces [41] (**Fig. 1.6 a**). Using a mutagenesis screen to study the molecular determinants of EphA3/ephrin-A5 binding, three extracellular receptor surface areas were defined as essential for the receptor/ligand interaction [53]. Two of those areas map to the previously identified dimerization and tetramerization interfaces in the EphB2/ephrinB2 complex, while the third interface lies outside the structurally characterized interaction domains (**Fig. 1.6 b**). A cluster of 10 residues on eprhinA5 was later on identified to be responsible for the formation of the third surface required for oligomerization and activation of EphA3 signaling [54]. Moving from this so-called Eph/ephrin nucleus to higher-order oligomers could be explained if one takes into account the aforementioned third interaction interface, as well as Eph-Eph homotypic ectodomain interactions [42,43,55] (**Fig. 1.6 c**), all of which can help propagate Eph signaling laterally independent of ephrin contact [56]. It is, however, important to mention that structures of other Eph/ephrin complexes [39,57,58] have not shown the previously described heterotetramer, and therefore nucleation via tetramerization, cannot be taken as a general mechanism of Eph/ephrin clustering. A recent study on the formation of expansive Eph/ephrin signaling clusters coined the term "extracellular steric seeding mechanism" [42]. The study confirmed the aforementioned "lateral propagation" concept [56], and suggested a "nucleation mechanism" whereby few EphA2-ephrinA5 interactions would "seed" an arrangement of receptors that can propagate into expansive signaling arrays. Further studies on EphBs/ephrinBs are needed to confirm or refute the existence of such a steric-seeding mechanism. In

addition to Eph extracellular domain, Eph TM segment [59], and Eph SAM domain [60-63] have also been implicated in receptor clustering, however, their functional role is yet to be confirmed.

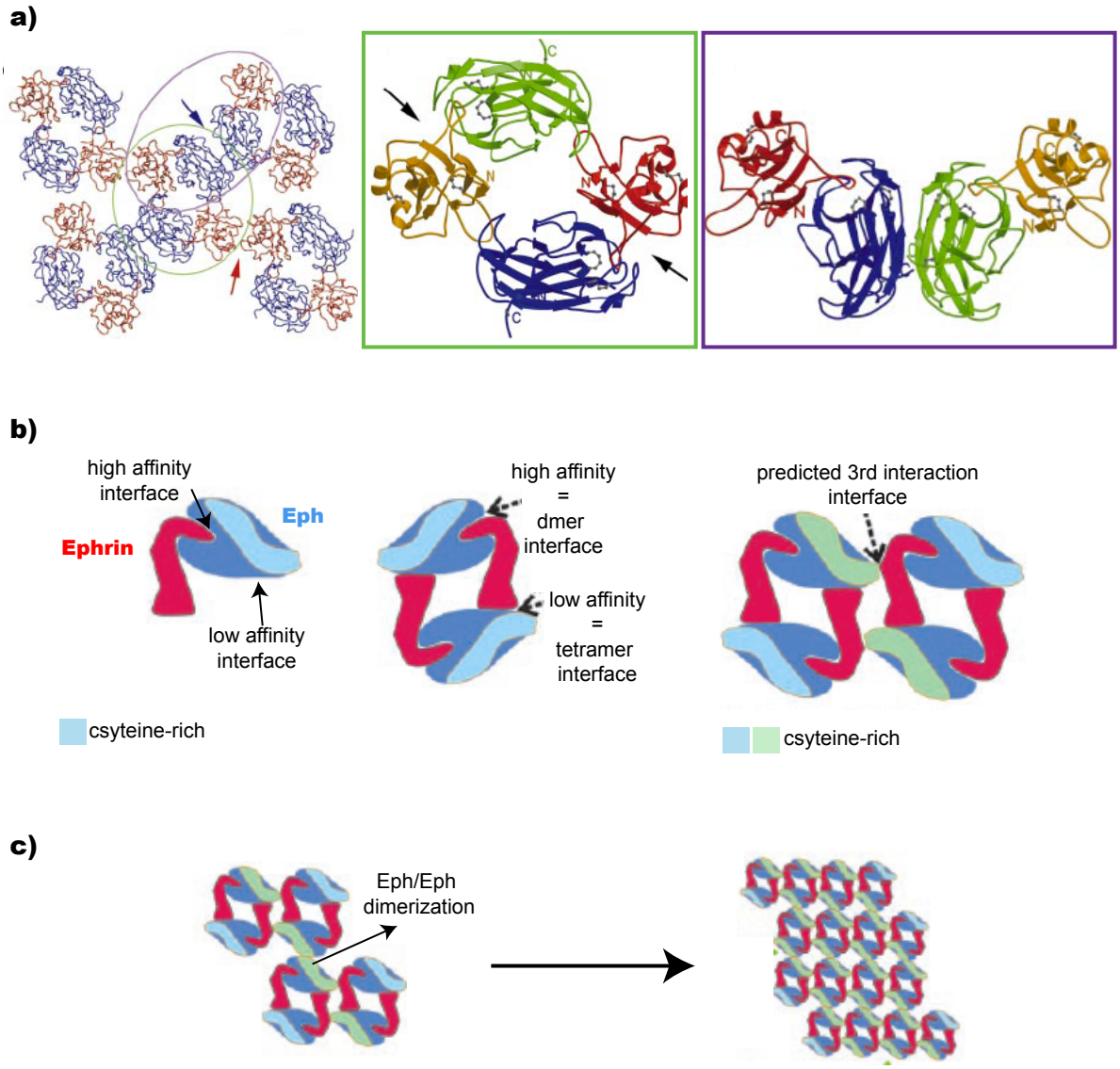

Fig 1.6 Eph/ephrin clustering
(a) Crystal arrangement of EphB2 (blue) and ephrinB2 (red) molecules shows four ligand and four receptor molecules [41]. Two possible tetramers are indicated with green and purple lines; ligand-lignad crystal packing (red arrow) and receptor-receptor crystal packing (blue arrow) are shown. First tetramer (green box): ligand molecules in red and orange, and the receptors in blue and green. Tetramer is generated by two receptor-ligand dimers joined together. Black arrows show receptor-ligand dimerization interfaces. Second tetramer (purple box): two EphB2 molecules joined through receptor-receptor interfaces, and each EphB2 is bound to a single ligand molecule. **(b)** Model of ephrin-induced Eph clustering. Monomeric ephrinA5 (red) and EphA3 (blue) combine into high affinity Eph/ephrin dimers [52]; those then assemble via a lower affinity interface into Eph/ephrin heterotetramers [41]. A cluster of 10 residues on the eprhinA5 were later on identified to be responsible for the formation of the third surface required for oligomerization and activation of EphA3 signaling [53,54]. **(c)** Moving from this Eph/ephrin nucleus to higher-order oligomers could be explained if one takes into account the aforementioned third interaction interface, as well as Eph-Eph homotypic ectodomain interactions [42,43].

1.2.4 Eph/Eph clustering

The contribution of various domains to Eph clustering, and in particular the involvement of intracellular, ligand-independent domains, raises the possibility of intra- and inter-subclass cross talk. The concept of RTK hetero-oligomerization, although common for receptors of other RTK subfamilies [64], was yet to be confirmed and investigated for the Eph subfamily. Given the promiscuity of Eph-ephrin interactions intra-subclass, co-expression of same subclass Ephs will likely lead to their interaction with the same ephrin. In fact, EphB1 and EphB4 were shown to form functional hetero-oligomeric complexes when co-expressed with kinase dead EphB6, resulting in its transphosphorylation [65,66]. Evidence for cross-class trans-phosphorylation has been accumulated from many studies, for example, the capability of EphA4 to phosphorylate the JM tyrosines of EphB2 and EphA2 *in vitro* [67], the capability of ephrinB1 to simulate phosphorylation of EphA2/A3/A7 in addition to EphB4/B2 and EphB3 [68], and the capability of ephrinB1-expressing cells to modulate phosphorylation of various EphAs in EphB2-expressing HEK293 cells [69]. In addition to cross-class transphorphorylation, cross clustering has also been observed. Activation of EphA3 with a selective monoclonal antibody, managed to co-cluster and activate the co-expressed EphB2 in HEK293T cells [70], as well as endogenous EphA and EphB receptors in tumour cells [71]. Taken together, this would mean that upon cell-cell contact, the resulting cell behavior will not be limited to those Ephs able to directly bind the activating ephrin, but will depend on the overall abundance of Ephs inside the cell.

1.2.5 Eph activation

Similar to other RTKs, activation of Ephs follows a general framework, beginning with ligand binding, receptor reorientation or oligomerization, and consequent *trans*-phosphorylation by the tyrosine kinase domain. Tyrosine phosphorylation affects the signaling properties of RTKs in at least two ways. First, autophosphorylation of a key tyrosine residue within the kinase activation loop (AL), known as Tyr_{ACT} changes the local structure of the receptor and stabilizes the active conformation of the kinase domain (**Fig. 1.7**). In the inactive state, Tyr_{ACT} blocks ATP binding by protruding into the active site. Auto-phosphorylation of Tyr_{ACT} and adjacent residues reposition the AL into a catalytically competent conformation, thereby freeing the active site to interact with substrates [72,73]. Second, phosphorylation of neighboring noncatalytic sites creates docking sites for the Src Homology 2 (SH2) and/or phosphotyrosine binding (PTB) domain necessary for

downstream effectors [74-77]. All tyrosine KDs consist of an N-lobe, that assists in the binding and coordination of ATP, and a C-lobe, that orients the substrate for productive transfer of γ-phosphate (**Fig 1.7**), and a similar structure when crystallized in an active form [18]. Crucial regulatory elements such as the αC helix in the kinase N-lobe and the AL adopt a specific structure in the active KD form that is essential for phosphotransfer [19]. Owing to an inherent interlobe flexibility that allows for both, open and closed conformations, protein kinases are capable of adopting a range of conformations. However, the catalytically competent conformation is the one in which the two lobes clamp together to form an interfacial nucleotide binding site and catalytic cleft, i.e. it is superficially a closed structure [25].

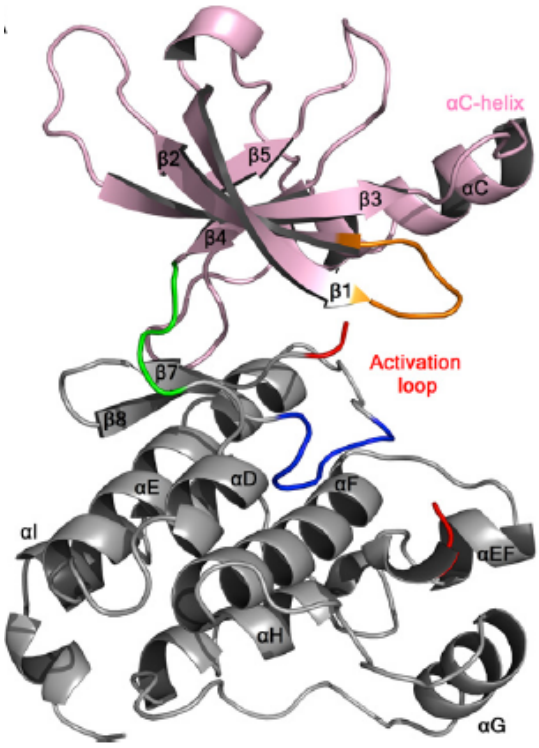

Fig 1.7 Phosphorylated, active tyrosine kinase domain of RTK represented by EphA4
Ribbon diagram of phosphorylated, and therefore active form of murine EphA4. First, the αC –helix of the kinase N-lobe is in the ATP proximal position allowing the formation of the conserved Lys^{653}-Glu^{670} salt bridge, which coordinates the alpha and beta phosphate groups of ATP. Second, the activation loop (AL) is disorganized and adopts the so-called "DFG-in" conformation with the side-chain of Phe^{765} pointing towards the interior of the molecule. N-terminal lobe (pink) and consists of five-stranded anti-parallel β-sheet and one α-helix (αC). The C-terminal lobe (grey), is mainly α-helical. The p-loop (orange), hinge region (green), the catalytic loop (blue) and the activation loop (red). PDB accession number 2Y6M [78].

1.2.5.1 *Mechanism of Eph cis-inhibition by JMS*

In addition to serving as docking sites, phosphorylation of non-catalytic tyrosines in the JM region of Ephs regulates catalytic activity. More specifically, activation of Ephs correlates with auto-phosphorylation of two conserved tyrosines (Tyr604 and Tyr610, for murine EphB2; Tyr587 and Tyr593, for EphA2) embedded in a highly conserved ~10-amino acid motif within the JM segment (JMS), in addition to phosphorylation of the aforementioned Tyr_{ACT} (Tyr788 for murine EphB2; Tyr 771 in the case of EphA2)[79]. It has been shown that mutation of the conserved JM tyrosines to phenylalanine impairs kinase activity, while glutamic acid substitution preserves kinase activity [80,81]. *In-vitro* kinetic analysis of EphA4 showed a decreased affinity for peptide substrate when AL or JM tyrosines are substituted, and suggested a two step inhibitory mechanism, released by autophosphorylation of Tyr_{ACT} and JM tyrosines [79]. In the crystal structure of murine EphB2, the JMS in its non-phosphorylated form, adopts an ordered α-helical conformation that interacts with several elements in the kinase domain, and prevents it from adopting an ordered, active structure (**Fig. 1.8 a**). As a whole, the autoinhibited EphB2 kinase domain adopts a closed conformation that superficially resembles an active state. From a closer perspective, JM-mediated autoinhibition mainly arises from contacts with the N-lobe of the kinase. One way the JMS was thought to represses kinase activity, is by distorting the key αC helix in the kinase N-lobe [25]. However, subsequent crystal structures of EphA2 and EphA4 lacking JMS exhibited a similar kink in the αC helix [78,82] (**Fig 1.8 c**). In addition, contact with the C-lobe of the kinase prevents the activation segment from adopting an ordered productive conformation, and restricts inter-lobe flexibility through bridging of N- and C-lobes [25]. Whether the observed autoinhibited structure would be oriented in a certain fashion with respect to the inner surface of the membrane is impossible to extrapolate considering the lengthy sequence between the plasma membrane and the start of strand Ex1 [83] (**Fig 1.8 a**). Subsequent NMR studies done on autoinhibited and activated EphB2 and EphA4, suggested that increased interlobe flexibility and the dynamic sampling of catalytically competent conformations for helix αC and the AL, rather than a transition to a static active conformation is the basis for Eph RTK activation [84]. In contrast to EphA4, kinase activation mutations (Tyr742A) in a double EphA3 YYFF background did not lead to the dissociation of the JMS, suggesting an alternative activation mechanism [85]. Crystal structures of dephosphorylated, fully

phosphorylated or partially phosphorylated wild type EphA3, revealed the relationship between the JM and AL (**Fig. 1.8 d**). At the crystallographic level, the extent to which the AL after the conserved DFG segment is structured is commonly correlated with the phosphorylation state of the protein and the absence of the JMS from the crystal's electrons density. However, some EphA3 structures indicate that the relationship between the AL and JMS regions and kinase activity is not binary (**Fig 1.8 d cyan structure**). Other conserved tyrosine residues (660, 744, 750 and 939) have been identified as *in vivo* phosphorylation site in EphB2 and EphB5 receptors [86,87]. However, their role in regulating Eph receptor activation and their contribution, if any, in attaining an active conformation is sill unknown. Using a semisynthetic EphA4 receptor, activation of Ephs upon ephrin binding was proposed to follow a sequential and ordered autophosphorylation process, where Tyr_{JM2} is phosphorylated first, followed by Tyr_{JM1}, and finally by Tyr_{ACT} [88]. It remains to be established how subtle, sequential phosphorylation events can affect the activity and conformation of Ephs *in vivo*.

Fig 1.8 Mechanisms of Eph Activation, inferred from crystallographic studies
(a) Ribbon diagram of murine EphB2 in complex with AMP-PNP (black). N-terminal lobe (pink), C-terminal lobe (grey), p-loop (orange), hinge region (green), and the juxtamembrane segment (JMS) in (cyan) with the phophoregulatory residues Tyr/Phe604 and Tyr/Phe610 depicted in sticks, the catalytic loop (blue) and the activation loop (AL) in red. Protein Data Bank accession number 1JPA [25]. **(b)** Schematic diagram comparing the autoinhibited (upper) and active states (lower) of Eph receptor. The autoinhibited scheme is based on crystal structure of 2YF-Ephb2 (1JPA) [25], and the active configuration is based on the crystal structure of active Insulin receptor kinase (IRK) (Accession no. 1IR3) [73]. Dashed lines indicate regions of activation segment disorder. Numbering scheme corresponds to murine EphB2. **(c)** Comparison of EphA2 crystal structure (1MQB [82], green) with the kinase domain of other Ephs. Superimposition of phosphorylated murine EphA4-kinase domain (2Y6M [78], grey), Y596/602F, Y742A EphA4-kinase domain + JM (however JM is disordered and cannot be seen here) (2HEL [84], red). Crystal structure of the EphB2 active state, comprising a D754A activating mutation in the activation loop (2HEN [84], blue), and the autoinhibited EphB2-kinase domain + JMS, comprising Y604/610P (1JPA [25], yellow). **(d)** Structures of wild type EphA3 kinase showing relationship between AL and JMS. In summary, differences between the wild type structures presented occur mainly in the N-terminal region of the AL and the N-terminal region of the JMS. The AL tyrosine, Tyr779, is autophosphorylated, however the conformational consequence of this phosphorylation event is unclear, as the electron density in this region is always interpretable (magenta dashed line). Except for the segment surrounding the second JM tyrosine (Tyr602), which is disordered (grey dashed line), the conformation of the wile type JMS of CIP treated EphA3-apo (PDB: 2QO2, green) and basal (partially phosphorylated) EphA3-AMP-PNP (PDB: 2QOQ, yellow) matches closely with that of the dominant negative Y604/608F double mutant of EphB2 (PDB: 1JPA). Basal JMS-EphA3 kinase-apo structure (PDB: 2GSF, cyan) is considered intermediate low activity conformation. CIP treated JMS-EphA3 kinase-AMP PNP (PDB: 2QO7, red) and ATP treated JMS-EphA3 kinase-AMP PNP (PDB: 2QO9, blue) [85].

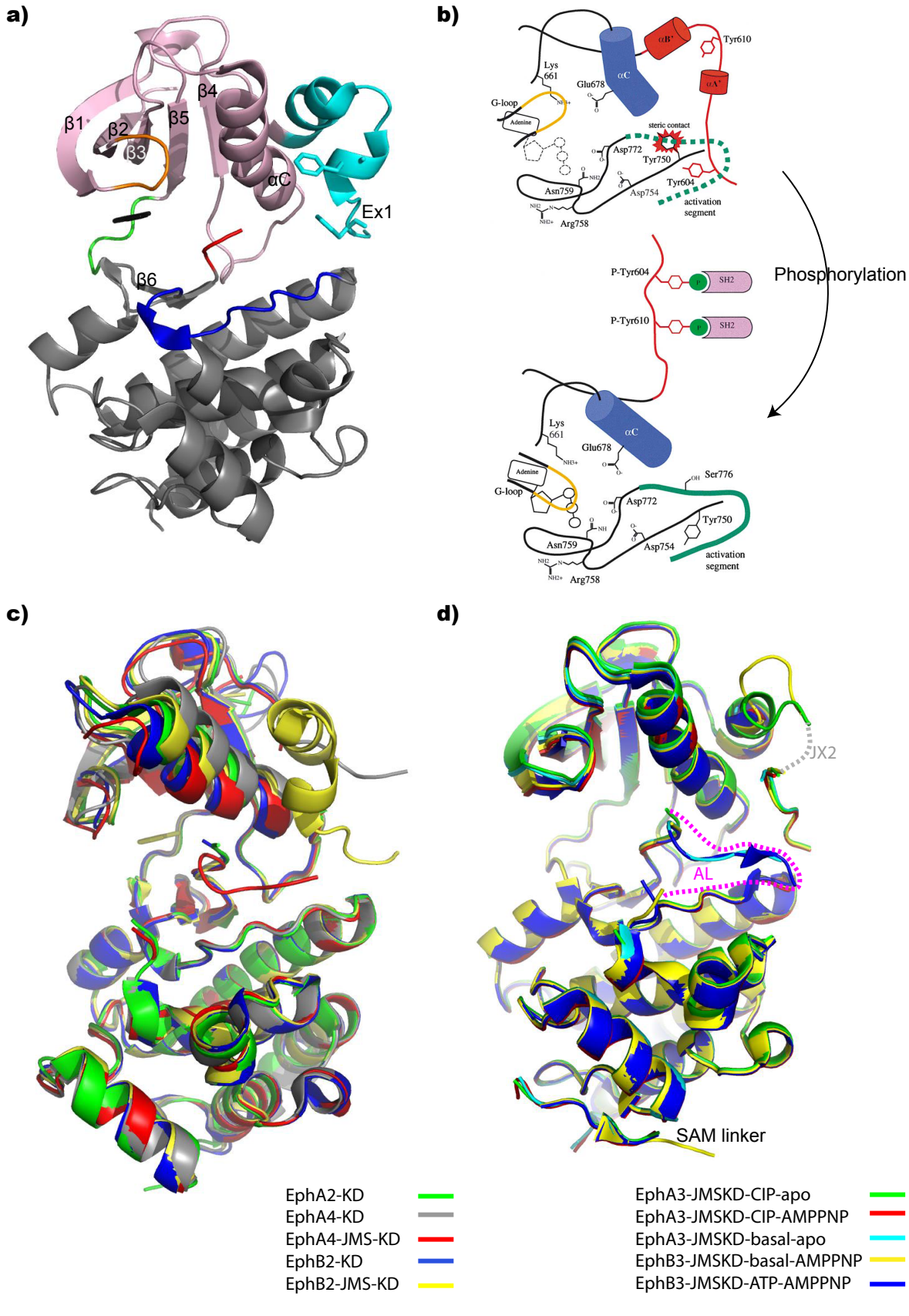
a)
β1
β2
β3
β4
β5
αC
Ex1
β6
b)
Tyr610
αB'
αA'
Lys 661
Glu678
αC
G-loop
Adenine
steric contact
Asp772
Tyr750
Asn759
Asp754
Tyr604
activation segment
Arg758
P-Tyr604
P-Tyr610
SH2
Phosphorylation
Ser776
c)
d)
JX2
AL
SAM linker
EphA2-KD
EphA4-KD
EphA4-JMS-KD
EphB2-KD
EphB2-JMS-KD
EphA3-JMSKD-CIP-apo
EphA3-JMSKD-CIP-AMPPNP
EphA3-JMSKD-basal-apo
EphB3-JMSKD-basal-AMPPNP
EphB3-JMSKD-ATP-AMPPNP

1.3 Biological roles of Eph/ephrin signaling

Originally identified as axon guidance molecules, the role of Ephs/ephrins in the developing vascular system is their next best-studied function. Their expression and function in adult tissues is now well established during tumor invasion, neoangiogenesis and metastasis. Upon cell-cell contact, interactions between Ephs and ephrins initiate bi-directional signaling in both, receptor-expressing and ligand-expressing cells. Signaling cascades are propagated laterally and/or vertically with the help of various adaptors, mediators, and effector proteins. Several reviews sum up the current knowledge about Eph/ephrin biological roles [31,32,89]. Some of those Eph-mediated functions will be detailed here.

1.3.1 Eph as the central integrator of cell positioning

During embryogenesis, Eph receptors position motile cells and cell layers within their surrounding tissues. They can do that, by affecting the assembly and/or disassembly of cell-cell contacts, thereby controlling the direction of motion and the choice of interacting cells. This coupled with the spatially and temporally restricted pattern of expression in developing tissues and organs, can eventually affect tissue patterning [89]. Due to the dependency of Eph signaling on cell-cell contact, the final cell position will depend on many factors including; slope, shape, composition and orientation of Eph/ephrin gradients, abundance of interacting Ephs and ephrins, and crosstalk with other signaling systems [90-92]

1.3.2 Cell sorting and boundary formation

The ability of Eph/ephrin signaling system to modulate cell positioning during development, has endowed them with the ability to mediate cell-cell segregation necessary for boundary formation. One of the earliest studied Eph-mediated boundary formation processes during development, is zebrafish rhombomeres. Complementary expression of Ephs and ephrins in the different segments, coupled with their unique bi-directional signaling maintains rhombomeres boundaries [93]. This biological concept has been replicated in various other models including recently, mammalian cell co-cultures of Eph- and ephrin-expressing cells [69]. Eph-mediated pathways involved in cell-cell segregation include, MAPK activation downstream of EphB2 [94], inhibition of gap junction communication [95], and Wnt pathway-dependent RhoA activation [96].

1.3.3 Vasculogenesis and angiogenesis

Class-B Ephs and ephrins, especially interactions between EphB2/B4 and ephrin-B2, play crucial roles during the development of the embryonic cardiovascular system [97,98]. Studies have shown that ephrin-B2 is prominently expressed on embryonic arteries, while its cognate receptor EphB4 on veins. This, together with lethal vascular defects in knock-out mice, have promoted the idea that reciprocal signaling at arterial-venous boundaries prevents arterial and venous endothelial cell intermingling [99]. Class-A Ephs and ephrins on the other hand, have limited roles during cardiovascular development, mostly attributed to the expression of EphA3 and ephrin-A1 during embryogenesis on major blood vessels and heart valves [100,101]. In contrast to embryonic vasculature, recent evidence suggested important roles for Eph/ephrin type-A, especially EphA2 and ephrin-A1, in post-natal angiogenesis and pathological neo-angiogenesis [102,103]. Not surprisingly, and owing to a common role of Eph/ephrin- and VEGFR-signaling in blood vessel assembly, growth and differentiation, interactions of the two signaling pathways have recently been reported. Ephrin-B2 was shown to regulate VEGFR2 internalization and thus its function in developmental and tumor angiogenesis. In addition, ephrin-B2 was able to directly activate VEGFR2, while ephrin-B2 PDZ signaling-deficient mice with abrogated VEGFR2 regulation showed reduced multi-tissue vascularization [104,105].

1.3.4 Eph signaling in cancer

Considering the fact that most Eph family members were first identified in tumor cell lines, it is not surprising to see the volumes of data documenting their roles in various epithelial and mesenchymal tumors. The aforementioned crucial role of Ephs in defining cell position during tissue and organ development now re-emerges in adult tissues in a deregulated fashion, affecting cell-cell, cell-matrix attachment and survival during invasion, metastasis and neoangiogenesis [106-108]. Eph overexpression often marks invasive, metastatic tumors and poor prognosis [109]. The expression of EphA2 for example, is more elevated in distant metastases than primary melanomas [110]. Also expression of EphA2 in MCF10A, which are non-transformed mammary epithelial cells, increases invasiveness in matrigel, induces anchorage-independent growth and induces tumor formation in nude mice [111]. In addition to breast cancer and melanoma, elevated expression of Ephs has been documented in various other cancers, including, lung, kidney, colon, prostate and ovarian cancers [106]. Neovascularisation is another aspect of cancer Ephs and

ephrins play a role in. EphA2 and ephrinA1, as well as EphB4 and ephrinB2 are elevated in tumor vasculature, where the ligand is usually marking endothelial cells [102,112]. Depending on the context, Ephs can act as tumor suppressors rather than tumor promoters. Compared to its aforementioned roles in tumor progression, EphA2 knockout mice are more susceptible to skin tumors induced by carcinogen [113]. EphB4 can also either promote or suppress tumor growth [114,115]. This opposing effect can be explained by stage-dependent changes of Eph expression, which increases in initial stages of cancer progression, then it is either subjected to epigenetic silencing or modulation of function at later stages of tumor progression [107]. Another explanation for this dichotomy is the activity of Eph system in question. Treating EphB4^{+ve} mouse xenografts with ephrinB2 inhibits tumor progression, which suggests that EphB4 promotes tumor progression in a ligand-independent manner or in the presence of low ligand levels, but at high kinase activity shifts to inhibition of tumor progression [115]. Overexpressing kinase-dead (kd) EphB4 in breast cancer cells enhanced tumor vascularization by promoting recruitment and proliferation of ephrinB2^{+ve} endothelial cells [116].

1.4 Tipping the balance at points of cell-cell contact

Eph-ephrin interactions at points of cell-cell contact usually lead to, cell retraction, contraction and segregation. However, depending on the context, Eph-ephrin signaling can also lead to enhanced cell adhesion within the same cell type. The output of a given Eph/ephrin complex depends on various aspects, including composition of signaling clusters, Eph and ephrin cell surface densities, termination and internalization of formed Eph/ephrin clusters, regulation by phosphatases and cross-talk with other signaling systems [117]. The specifics of some of those factors will be outlined here.

1.4.1 Signaling capacity of interacting Ephs/ephrins

Eph kinase activity and the strength of bidirectional signaling are important factors governing the switch between repulsion and adhesion at points of cell-cell contact. Co-expression of a cytoplasmic-truncated form of EphA7 decreased phosphorylation of wild type full-length receptor and switched cellular response upon exposure to ephrinA5 from cell-cell segregation to adhesion [118], confirming the crucial role of Eph-kinase in determining the fate of cell-cell contact site. Mice carrying mutations that disrupt bidirectional signaling between B-subclass Ephs and ephrins on the developing urethra, developed with incomplete fusion events

that tabularize the urethra, indicating the importance of intact Eph-ephrin bidirectional signaling for midline cell-cell adhesion and fusion events [119]. It has been shown earlier that ephrinB1 can cause EphB1-expressing HEK293 cells to retract above a certain concentration, below which the same ephrin can promote integrin-mediated extracellular matrix (ECM) attachment [120]. Such a graded dependency on ephrin concentration has also been reported for retinal axons [121], and HEK293T cells expressing the kinase-deficient EphB6 receptor. Despite kinase deficiency of EphB6, higher ephrin-B2 concentrations inhibited migration and shifted response to retraction through the EphB6-associated Src family kinase Fyn [122]. The aforementioned examples suggest a model where kinase activation with sufficient concentration of ligand is needed for retraction at points of cell-cell contact [123].

1.4.2 Protein tyrosine phosphatases (PTPs)

Similar to other RTKs, one cannot account for the signaling capacity of a given Eph-ephrin system inside the cell without taking into consideration the competing and coordinated roles played by protein tyrosine phosphatases (PTPs). Consistent with this idea, elevated PTP activity in EphA3-positivie leukaemia cells provokes adhesion to an ephrin-A5 surface, while its inhibition reverses the adhesive response to a repulsive one [124]. EphA4 is negatively regulated by PTP receptor type O [125], while EphB2 activation is regulated by the leukocyte common antigen related receptor tyrosine phosphatase (LAR-1) [94]. In addition, insulin secretion, triggered by glucose-induced increase in PTP activity, reduces EphA5 forward and enhances ephrinA reverse signaling [126]. Furthermore, changing expression of the endoplasmic reticulum (ER)-anchored PTP1B can modulate duration and amplitude of EphA3 phosphorylation and biological function [127]. The ability of ER-anchored PTP1B to interact with and affect a PM receptor in a spatial-temporal manner is a conceptual dilemma that has been extensively investigated. Recent studies support a dynamic interplay between PTP1B and its PM substrates, in space and time, whereby dephosphorylation by PTP1B takes place when endocytosed RTK transit past the ER [128,129]. Other studies suggest a direct on-site contact between PTP1B and its PM and/or adhesion sites localized substrates [130,131], a microtubule (MT)-dependent positioning of ER-bound PTP1B to the periphery of growth cones [132], or a possible recruitment of PTP1B to the cell surface upon Eph-ephrin cell-cell contact [133]. We recently found that the ER network is in close proximity to the PM at regions of cell-cell contact, thereby allowing the ER-

anchored PTP1B to interact with substrates at those sites. Inhibition of PTP1B causes increased tyrosine phosphorylation of EphA2 specifically at sites of cell-cell contact, thereby identifying those sites as important target regions for regulation by PTP1B [134]. Inactivation of PTPs by thiol-reactive compounds like pervanadate, causes ligand-independent phosphorylation of RTKs, indicating a functional role of PTPs in maintaining a dephosphorylated receptor prior to stimulation [135,136]. Ligand-dependent activation of RTKs on the other hand, may also be coupled to transient PTP inactivation in order to enhance signal efficiency. This happens through increased production of H_2O_2 upon activation of the NADPH oxidase complex and the subsequent inactivation of PTPs [137-141]. These data suggest that a gradient of PTP activity counterbalanced by a gradient of active Eph-dependent H_2O_2 inside the cells can comprise a reaction cycle that may be required for the establishment of a signaling threshold close to the PM and points of cell-cell contact (see Results and Discussion).

1.4.3 Termination of Eph-ephrin complexes shifts adhesion to repulsion

Upon cell-cell contact, large Eph-ephrin complexes, which physically tether receptor-and ligand-expressing cells, form and need to be disrupted to allow for cell-cell repulsion. The transmembrane metalloprotease ADAM10 (a disintegrin and a metalloprotease 10) plays a much-investigated role in termination of Eph/ephrin class-A complexes. The Eph receptor associated ADAM10 cleaves ephrin ligand in *trans* following receptor activation [142,143]. Association of ADAM10 with EphAs depends on ephrin-induced Eph clustering [144], while ligand cleavage relies on a conformational change in the activated Eph cytoplasmic domain that relieves inhibitory JM/KD interactions, and allows productive association with ADAM10 [145]. In regulating Eph/ephrin signaling, ADAMs seem to be shed from both receptors and ligands, but under different conditions. In addition to the aforementioned ligand mediated cleavage, ADAM facilitates EphB2 extracellular domain shedding in the absence of ligand and in the presence of calcium influx, leaving behind a fragment that γ–secretase further cleaves [146]. The concept of sequential cleavage applies also to ephrin-B1 and ephrin-B2, where possible extracellular domain shedding by ADAM13 [147] is followed by γ–secretase cleavage of the remaining intracellular domain [148]. The contribution of other proteases to the termination of Eph/ephrin complexes has also been described, including cleavage of ligand-activated EphB2 by matrix metalloproteases MMP-2/MMP-8 [149], and TM

cleavage of ephrin-Bs by rhomboid serine protease RHBDL2 [150]. Termination of Eph/ephrin complexes can also occur in a protease-independent manner, namely through "transendocytosis" of the entire complex. Interactions between EphB/ephrinB-expressing cells result in normal endocytosis of activated, phosphorylated EphB mainly into receptor-expressing cells, and unique transendocytosis of ephrinB also into receptor expressing cells. Transendocytosis depends on Rac and cytoskeletal signaling and an intact cytoplasmic domain of both receptor and ligand [151,152]. With the presence of different mechanisms to terminate Eph/ephrin complexes, the common theme is the dependence on intracellular, kinase signaling controlling endocytosis, to achieve cytoskeletal reorganization and cell retraction.

1.5 Recycling versus processing

The amplitude and kinetics of RTK activation; Eph included; upon ligand binding are influenced by a highly regulated endocytic process. The decision between sorting activated receptors for lysosomal processing or recycling back to the plasma membrane is another level of spatial organization of RTK activity [153]. All organelles on the exocytic and endocytic pathways, be it plasma membrane, endoplasmic reticulum or lysosomes are connected by rapid, bidirectional membrane traffic mediated by vesicular transport. Several members of the Ras superfamily of small guanosine triphosphatases (GTPases) play essential roles in regulating vesicular transport. Here, we will focus on the branch of Rab GTPases, which control all aspects of vesicular trafficking. This includes, the formation of vesicles or tubular intermediates, their active transport along cytoskeletal elements, their tethering to acceptor membranes and the regulation of their fusion with target compartment [154].

1.5.1 RAB proteins as membrane organizers

Rab proteins comprise the largest family of monomeric small GTPases, with 11 Rab proteins in yeast *Saccharomyces cerevisiae* and over 60 members in humans. Rab proteins are organized on different intracellular compartments and involved in the regulation of transport between organelles [154-156]. Like other GTPases, the minimal regulatory cycle of Rabs involves their capacity to switch between an active GTP-bound and an inactive GDP-bound conformation. Exchange of GDP with GTP is catalyzed by guanine nucleotide exchange factors (GEFs), while conversion from GTP-bound to GDP-bound state is catalyzed by GTPase-

activating proteins (GAPs) [157]. GTP-bound Rab recruits several effectors, including kinases, phosphatases, motors, sorting adaptors and tethering factors. Newly synthesized, GDP-bound Rab is recognized by a Rab escort protein (REP), which presents Rab-GDP to geranylgeranyl transferase (GGT). Rab GDP dissociation inhibitor (GDI) can chaperon the geranylgeranylated form of Rab GTPases in the cytosol, mediates their delivery to target membranes and recycles them back into the cytosol. Targeting of Rab GTPases to their cognate membranes is partly attributed to the membrane-bound GDI displacement factors (GDFs), which displaces GDI from Rab-GDI complexes, thereby facilitating the association of geranylgeranylated Rab GTPase with its cognate membrane (**Fig 1.9**) [158].

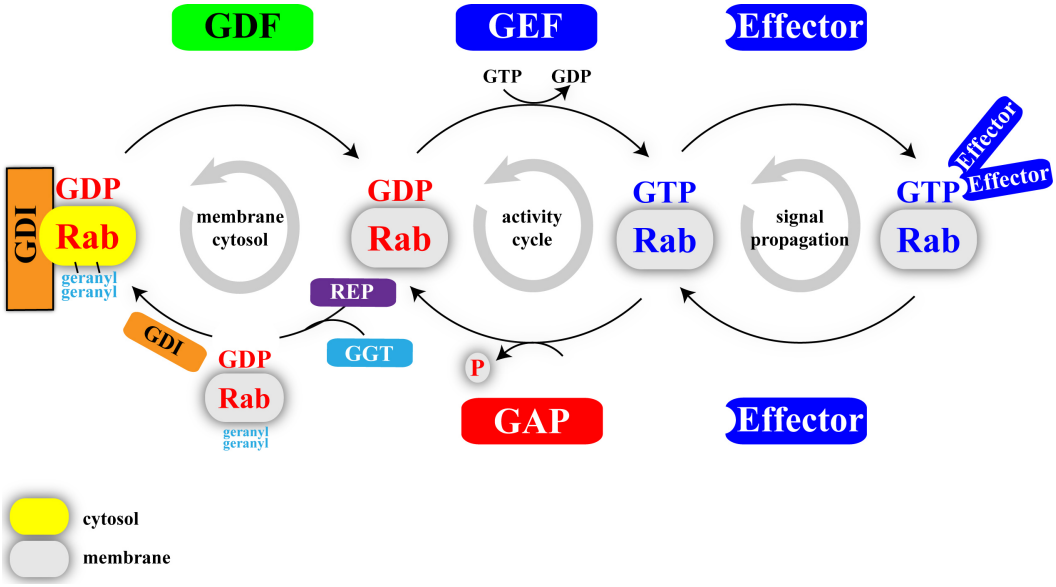

Fig 1.9 The Rab switch and its cycle
Conversion of GDP-bound Rab (red) to GTP-bound Rab (blue) is catalyzed by a guanine nucleotide exchange factor (GEF). The GTP-bound "active" conformation can be converted back to the GDP-bound "inactive" form through hydrolysis of GTP and release of inorganic phosphate, a reaction catalyzed by GTP-ase activating protein (GAP). The GTP-bound conformation is recognized by various effectors (blue), which further propagate the signal of active Rab. Newly synthesized GDP-bound Rab is captured by a Rab escort protein (REP) (purple) and introduced to a geranylgeranyl transferase (GGT). GDP-bound, geranygeranylated Rab is recognized by Rab GDP dissociation inhibitor (GDI) (orange), which captures the geranylgeranylated form in the cytosol, mediates its delivery to the respective membrane and recycles it back to the cytosol. Membrane-bound GDI displacement factor (GDF) (green) recognizes specific Rab-GFI complexes, promotes GFI release and thereby aids in the association of geranylgeranylated Rab GTPase with the cognate membrane. Adapted from [159] and [157].

1.5.2 RAB proteins in membrane traffic

In the early endocytic pathway, homotypic fusion of the initial endocytic vesicles and their fusion to the early endosome require Rab5. Rapid recycling of early endosomal vesicles to the cell surface requires Rab4. Transformation of the early endosome (EE) to a late endosome (LE) requires Rab7 and transport of material from the recycling endosome (RE) back to the cell surface requires Rab11 [154] . Early endosomes contain Rab4 and Rab11, in addition to the aforementioned Rab5. However, these Rabs form their own subdomains on EE membranes (**Fig 1.10**) [160]. Similarly, the LE contains Rab9 in addition to Rab7, each of which has its own subdomains [161].

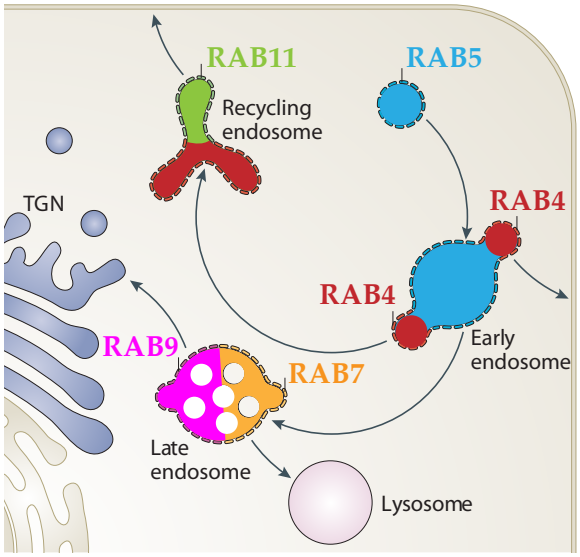

Fig 1.10 Rab domains on endosomes
Early endosomes has distinct domains enriched in Rab5 (blue), which is involved in vesicle endosome fusion and Rab4 (red), which is involved in endocytic recycling. The recycling endosome has distinct domains enriched in Rab5 and Rab11 (green), which is involved in vesicle trafficking to the plasma membrane. Late endosomes has distinct domains enriched in Rab7 (orange), which mediates trafficking to lysosomes and Rab9 (magenta), which mediates trafficking to the *trans*-Golgi network (TGN). Adapted from [157].

1.5.3 RAB proteins and receptor signaling

There is a tight correlation between receptor signaling and membrane trafficking Membrane trafficking can affect many cellular processes by regulating the number of functional receptors available at the cell surface [156]. Activation of several growth factor receptors leads to their internalization and subsequent sorting along the endosomal pathway. Rabs, being the main players in the endocytic pathway are involved in facilitating receptor trafficking, transmitting receptor signals for cytoskeletal regulation, modulating the amplitude and duration of signaling based on receptor sorting and even taking direct part in signaling pathways downstream of RTKS through their effector proteins. For detailed review, refer to [155,157].

1.5.4 Eph trafficking

The contribution of the early, recycling and late endosome to the regulation of basal receptor activity and ligand-induced activation is still poorly understood. However, the immediate outcome of regulated endocytosis is to reduce the number of cell-surface receptors, thereby attenuating cellular responsiveness to extracellular ligands (**Fig 1.11**) [156]. Little is yet known about Eph trafficking prior to ligand-induced activation and clustering. Eph receptors and ephrin ligands can traffic through both caveolin- and clathrin-mediated endocytic routes, activating small GTPases involved in membrane trafficking and actin remodeling [162]. In support of clathrin-mediated endocytosis, EphrinA5-Fc mediated endocytosis of EphA8 co-localized with clathrin, transferrin and EEA1 [163], and EphA4 was detected in clathrin-coated vesicles *in vivo* [164]. In support of caveolin-mediated endocytosis, ephrinB1 and EphB1 co-localized with caveolin, and EphA2 bound caveolin1 in response to ephrinA1-Fc stimulation [165,166]. Upon ligand induced EphA4 activation, the Rab5-GEF, Rin1 (Ras/Rab interactor 1), which targets phosphorylated receptors to Rab5$^+$ early endosomes, bound EphA4 via its SH2 domain [167]. Similar to other RTKs, the final fate of an activated Eph receptor is speculated to be lysosomal degradation. Ligand stimulation induces Cbl phosphorylation and Cbl-dependent ubiquitinylation and downregulation of Eph-A and –B receptors through the lysosomal pathway [168-170]. However, how consistent these findings are among other Eph family members and how efficient they can reflect the physiological membrane-bound ligand response is still not clear.

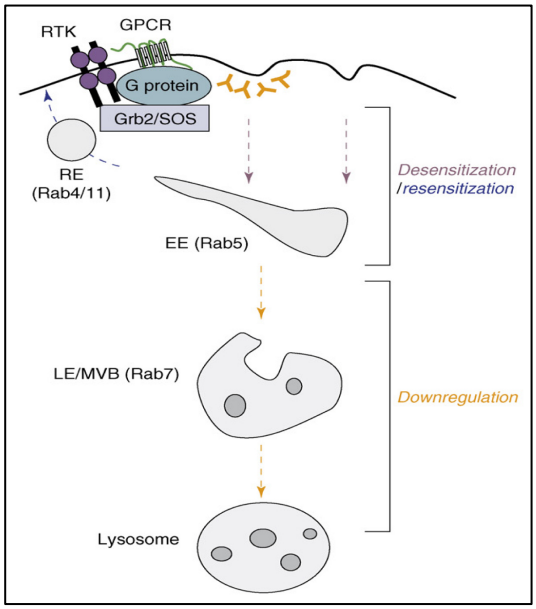

Fig 1.11 Regulation of signaling by endocytosis
Regulated endocytosis via clathrin-independent or –dependent pathways removes receptors (EGFR and GPCR as examples) from the cell-surface, linked via scaffold proteins such as Grb2 or a heterotrimeric G protein. This contributes to "desensitization" of cell signaling (violet arrows). Recycling back to the plasma membrane via the recycling endosome (RE) can reverse this effect (blue arrow). Sorting of internalized receptors into multivesicular bodies (MVB) and their fusion with lysosomes results in receptor "downregulation" (orange arrows)[156].

1.6 Fluorescence-based methods for studying protein states

The use of fluorescence technology has expanded over the years, making it a primary research tool in most disciplines. In the field of molecular biology, fluorescence-based imaging techniques offer a superior resolution for detecting protein localization and function, sometimes even up to a single-molecule detection level. The introduction of genetically encoded fluorophores (FPs) combined with advanced fluorescence microscopy techniques, allow precise quantifications of protein functionality in space and time [171]. The work presented in this thesis is based on fluorescence microscopy techniques, therefore proper introduction into the phenomena of fluorescence will be provided.

1.6.1 Photophysics of fluorescence

Fluorescence (FL) is the emission of a photon from an electron in an excited singlet state, as it relaxes to a spin-allowed, paired ground state. FL emission rates are rapid, and lay typically in the range of nanoseconds. The Jablonski diagram (**Fig. 1.12**) is often used to describe the processes occurring between absorption and emission of light. [172]. Following light absorption, an electron in the ground state S_0 is often excited to some higher vibrational level of either S_1 or S_2. The excited singlet state can either relax back to the ground state radiatively through the emission of a photon (fluorescence-k_F), or nonradiatively to the lowest vibrational level of S_1 (internal conversion-k_{IC}). The excited singlet state in S_1 can alternatively undergo a spin conversion to the first triplet state T1 (inter-system crossing-k_{IST}), radiative emission from which is dubbed phosphorescence (k_P), and is several orders of magnitude longer than FL[172]. The rate of singlet state radiative emission (k_F) cannot be measured indirectly from the fluorescence lifetime (τ). Fluorescence lifetime is defined as the average time the molecule spends in the excited state prior to return to the ground state and is given by:

$$\tau = \frac{1}{k_F + k_{IC} + k_{IST}} \qquad (1)$$

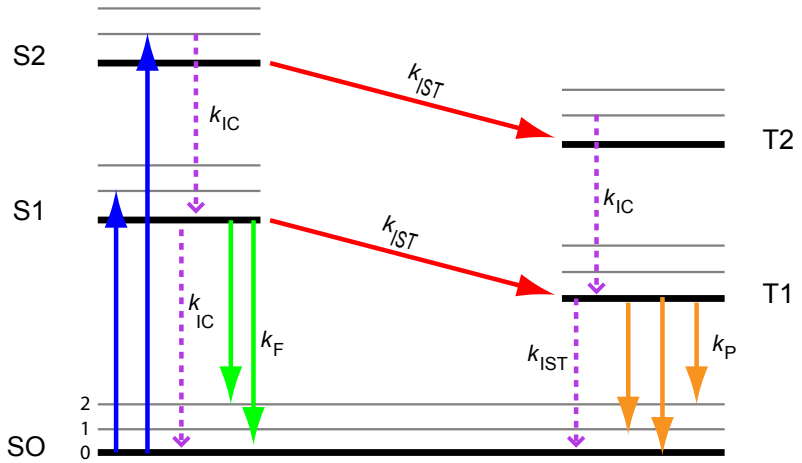

Fig 1.12 Jablonski diagram
Following light absorption (blue arrows), electrons from the singlet ground state (S_O) can be excited to some higher vibrational level of the first two excited singlet states (S_1, S_2). Molecules rapidly relax to the lowest vibrational level of S_1 in a process termed internal conversion (ex. dashed magenta arrow from S2 to S1). Molecules in S_1 or S_2 can also undergo a spin conversion to the triplet state (T_1, T_2) in a process termed intersystem crossing (red arrows). Electrons loose their energy and return to ground state through radiative (green and orange arrows) or non-radiative (dashed magenta arrows) decay. Radiative decay from excited singlet states is termed fluorescence (green arrows), while radiative decay from excited triplet states is termed phosphorescence (orange arrows).

1.6.2 Fluorescence anisotropy

Anisotropy measurement is one application of Fluorescence that is commonly used to provide information on size and/or amount of proteins in a cluster, fluidity of membranes, proteins-protein interactions and for biochemical assays of numerous substances. Anisotropy measurements are based on the concept of photoselective excitation of FPs by polarized light. In an isotropic solution, the FPs are randomly oriented and upon excitation will emit unpolarized light. However, if polarized light was used, excitation will only occur to a subset of FPs whose absorption transition dipole is parallel to the electric vector of the excitation light (**Fig 1.13**). Selective excitation results in a partially polarized fluorescence emission and a partially oriented subset of FPs (photoselection). The extent of emitted light polarization is described by fluorescence anisotropy (r) and defined by:

$$\boldsymbol{r} = \frac{\boldsymbol{I}_{\parallel} - \boldsymbol{I}_{\perp}}{\boldsymbol{I}_{\parallel} + 2\boldsymbol{I}_{\perp}} \qquad (2)$$

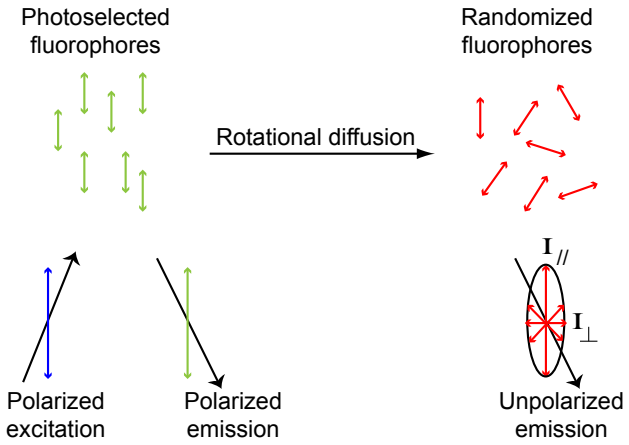

Fig 1.13 Effects of polarized excitation and rotational diffusion on anisotropy [172].

Several factors can decrease the measured anisotropy through depolarization of the light emitted by FPs. The most common factor being rotational diffusion of the FP, (**Fig.1.10**), which takes place during the lifetime of the excited state and randomizes the polarization of the emission dipole. When the FP lifetime is much shorter than rotational diffusion time scale, Förster resonance energy transfer becomes the dominating factor in the depolarization of emitted light [172]. Anisotropy measurements allow the detection of FRET between identical FPs (Homo-FRET), thereby providing a straightforward technique for measuring oligomerization and homo-dimerization of proteins [173,174].

1.6.3 Förster Resonance Energy Transfer (FRET)

Förster resonance energy transfer (FRET) is another process that takes place in the excited state. FRET occurs when the emission spectrum of an excited FP, called the donor (D), overlaps with the absorption spectrum of another FP, called the acceptor (A) (**Fig. 1.14**). FRET is a non-radiative process that occurs in the nanometer range and for which the acceptor does not need to be fluorescent to occur [175,176]. The donor and acceptor molecules are coupled via dipole-dipole interactions and the rate of energy transfer (k_T) between them is given by:

$$k_T = \frac{1}{\tau_D}\left(\frac{R_0}{r}\right)^6 \qquad (3)$$

where (r) is the distance between donor and acceptor molecules, (τ_D) is the fluorescence lifetime of the donor and (R_0) is the Förster distance between donor and acceptor at which the transfer efficiency drops to 50% (**Fig.1.14**).

The efficiency of energy transfer (E) is also distance dependent and is defined by:

$$E = \frac{{R_0}^6}{{R_0}^6 + r^6} \quad (4)$$

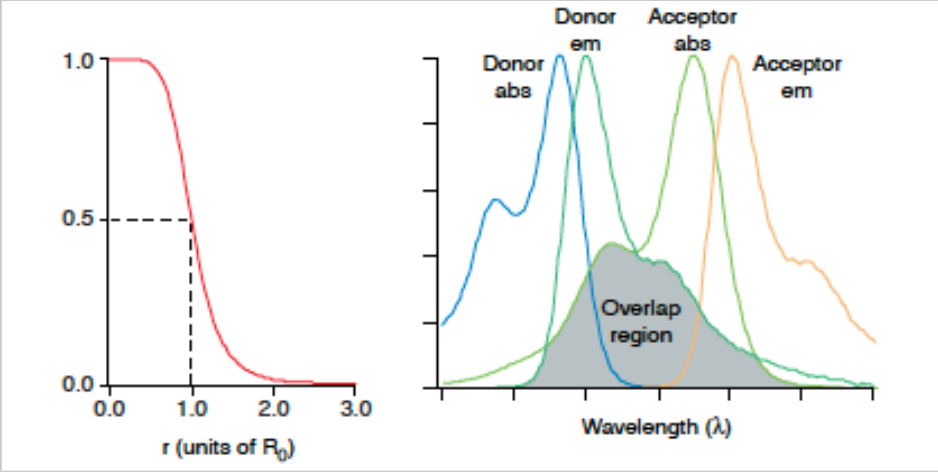

Fig 1.14 Factors affecting FRET
(**Left**) Förster radius (R_0) is the distance at which 50% of the energy transfer is taking place between to molecules. (**Right**) The overlap integral ($J(\lambda)$) depends on the overlap area between donor emission spectrum and acceptor absorbance spectrum (grey area) [177].

R_0 is dependent on the photophysical properties of the FP pair and for most biologically relevant FRET pairs, falls around the value of 5 nm [178], which is well below the resolution limit of light microscopy and compares to typical globular protein radii. R_0 is defined by:

$$R_o = [\kappa^2 \times J(\lambda) \times n^{-4} \times Q]^{1/6} \times 9.7 \times 10^2 \quad (5)$$

Factors affecting R_0 include: (κ^2), which is the relative orientation of the transition dipoles of the FPs, ($J(\lambda)$; $cm^6.mol^{-1}$) the overlap integral, which depends on the extent of spectral overlap between donor emission and acceptor absorbance (**Fig.1.11**), (n) the refractive index of the intervening medium and (Q) the quantum yield of the donor [177]. FRET reduces the excited state lifetime of the donor FP by providing an additional pathway for depopulating the excited state (compare to **Equation 1**):

$$\tau = \frac{1}{k_F + k_{IC} + k_{IST} + k_{FRET}} \quad (6)$$

FRET efficiency can be measured experimentally by monitoring the drop in donor intensity (I) or lifetime (τ) in the presence of acceptor:

$$E = 1 - \frac{I_{DA}}{I_D} = 1 - \frac{\tau_{DA}}{\tau_D} \quad (7)$$

Imaging techniques designed to detect FRET therefore monitor the photophysical changes occurring to the excited donor FP in the presence of an acceptor FP. Intensity-based and fluorescence lifetime measurements are both used to detect FRET between different donor/acceptor molecules (Hetero-FRET). Donor lifetime measurement is independent of FP concentration, is less prone to errors arising from intensity fluctuations, allows precise quantification of donor fraction undergoing FRET and is therefore superior to intensity-based FRET measurements. In this thesis only lifetime measurement of FRET will be further discussed. For extensive review of intensity-based FRET measurements, please refer to [172,177,179].

1.6.4 Fluorescence Lifetime Imaging Microscopy (FLIM)

Fluorescence lifetime (τ) is an inherent property of each FP that is independent of probe concentration and light path length, but depends on processes affecting depolarization of FP excited state, such as FRET [177]. In combination with advanced microscopy techniques, lifetime-measurement allows superior spatial-temporal resolution of protein dynamics. As discussed earlier in (**Equation 7**), FRET efficiency (E) for a certain donor/acceptor pair, can be calculated from donor lifetime (τ), in presence or absence of acceptor. Measurement of donor lifetime (τ) can be done in the frequency or time domain, but for the purpose of work done in this thesis, only time-domain FLIM will be discussed in details. For extensive review of frequency-domain FLIM, please refer to [180,181].

1.6.4.1 Time-domain FLIM

In time-domain FLIM measurements, the sample is excited with a pulsed light source, whose width is made as short as possible to be discernable from the decay time (τ) of the sample. Following the excitation pulse, time-dependent emission fluorescence intensity is measured. The decay time (τ) is calculated from the slope of a plot of time versus log $I(t)$ (decay profile), but more commonly from

fitting the data to presumed decay models. Intensity decay curves are often measured with a polarizer inclined at 54.7° from the vertical z-axis, thereby avoiding effects by anisotropy and/or rotational diffusion on decay curves [172]. This relates to lifetime (τ), because when a fluorophore (FP) is excited with an infinitely sharp (δ-function) pulse of light, a population of FP molecules (n_0) is initially excited, to further decay exponentially with a rate:

$$\frac{dn(t)}{dt} = (\Gamma + k_{nr})\, n_0\, exp(-t/\tau) \qquad (8)$$

where *n(t)* represents the number of excited FP molecules at time *t*, Γ is the emissive rate, k_{nr} is the non-radiative decay rate. Fluorescence-based experiments, are not based on counting the number of excited molecules, but rather on fluorescence intensity, which is relative to *n(t)*. If we now substitute (Eq.8) with time-dependent intensity changes *I(t)* we get single exponential decay expression:

$$I(t) = I_0\, exp(-t/\tau) \qquad (9)$$

where I_0 is the intensity at time 0. The lifetime τ is the inverse of the total decay rate, $\tau = (\Gamma + k_{nr})^{-1}$ and can be seen as the average length of time a FP remains in the excited state following excitation. Excited FP molecules emit randomly throughout their decay, therefore lifetime is considered a statistical average. The distribution of emitted photons across time is the intensity decay [172]. Time-domain FLIM is mostly done using time-correlated single-photon counting (TCSPC). Instrumentation of TCSPC use high repetition rate picosecond (ps) or femtosecond (fs) lasers, coupled to very sensitive and extremely fast detection systems. Detectors used for TCSPC are either micro-channel plates (MCPs), photomultiplier tubes (PMTs) or single photon avalanche diodes (SPADs) [172]. In principle, the sample is excited with a pulse of light (**Fig 1.15** upper panel "green") with a frequency allowing good resolution of fluorescence lifetime in question. For fluorescence lifetime within the range of 2.5-4 ns, the pulse rate is typically 25MHz. In TCSPC, the detection rate is normally set to less than one photon per pulse. For each observed photon, the time difference between detection and excitation pulse is noted and stored in a histogram (**Fig 1.15** lower panel), in which the x-axis represents time-difference and the y-axis the number of photons per a given time-difference. So far in TCSPC,

only the first photon is detected, therefore one has to adjust count rate in order to avoid bias to early (short-lifetime) photons [172].

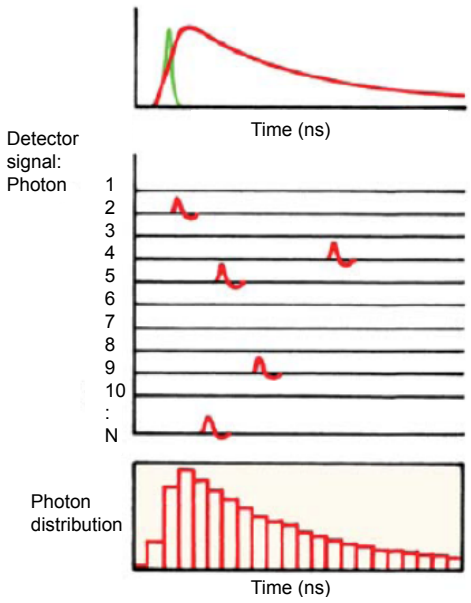

Fig 1.15 Principles of TCSPC

(Upper) Sample is excited with a pulse of light, resulting in the waveform observed (red), instrument response function is shown in green. (Middle) The pulses represent the output from a constant fraction discriminator. The x-axis is the time difference (in ns) and the y-axis is the number of photons detected for the time difference. (Lower) Shows a histogram-representing fraction of photons detected at a certain time difference.

In case of FRET, the measured decay profile in each pixel becomes the sum of the different decay profiles scaled by their respective populations. The analysis in this case will require a multi-exponential decay model for fitting. Multi-exponential model assumes that intensity decays as the sum of individual single exponential decays [172]:

$$I(t) = \sum_{i=1}^{n} \alpha_i \, exp(-t/\tau_i) + B \qquad (10)$$

where (B) is the background, (n) is the number of decay times present, (α_i) represents the amplitudes of the components at t = 0, and (τ_i) are the fluorescence decay times. If we assume that the free donor molecules have a single lifetime (τ_D) and that the acceptor molecules exist in a single spatial configuration with respect to the donor in the complex (i.e. a single reduced lifetime of the donor (τ_F), then the decay profile in each pixel becomes the sum of these two populations, plus an additional background term (B) that accounts for the dark noise of the detector [182]:

$$I(x,y,t) = A_D(x,y) \, exp(-t/\tau_D) + A_F(x,y) \, exp(-t/\tau_F) + B \qquad (11)$$

The population of free donor molecules has amplitude of (A_D) and the population of acceptor-bound donor molecules has amplitude of (A_F). The fraction of donor

molecules in close proximity to acceptor molecules (α) can be calculated on pixel basis as follows:

$$\alpha(x,y) = \frac{A_F(x,y)}{A_D(x,y) + A_F(x,y)} \quad (12)$$

It is often useful to determine average lifetime ($\bar{\tau}$), when using the multi-exponential decay law. The average lifetimes is given by:

$$\bar{\tau} = \frac{\alpha_1 \tau_1^2 + \alpha_2 \tau_2^2}{\alpha_1 \tau_1^2 + \alpha_2 \tau_2^2} \quad (13)$$

The connotation of (α and τ) depends on the context of the system under investigation. For a fluorophore displaying a complex decay, (α_i) values represent the fraction of molecules in each conformation at t = 0, which is the ground-state equilibrium [172]. Following acquisition of enough photons, TCSPC data are analyzed by fitting fluorescence decay histograms according to any given model that accounts for or excludes the instrument response function (IRF). In this thesis, most of the data are analyzed with precision FLIM (pFLIM), which uses a specific parameterized IRF model to account for the true IRF [183]. In the time-domain, a minimum number of photons are required to distinguish two lifetimes, which sometimes limits the quantitative analysis of the data. This can be overcome if time-domain data is analyzed in the Fourier space by applying global analysis [184].

1.7 Outline of thesis

Within each level of organization, dynamic biological systems are kept in-check by operating under constant opposing tendencies. Even on a molecular level, such duality can be seen between individual proteins, allowing local sources to affect global patterns. The emerging patterns will in return affect the interactions of individual proteins at local sources, in a negative or positive feedback manner [2]. There is no better signaling system defining the link between local opposing tendencies and global pattern formation than the Eph subfamily of RTKs. The same receptor-ligand pair can enhance adhesion or repulsion between two cells upon their contact. How local factors affecting the signaling output of the system can lead to such a switch at points of cell-cell contact is of utmost interest. Local factors influencing this balance include, clustering capacity of Ephs and the cell's own clustering history, spatial organization of the phosphorylation-dephosphorylation cycle and recycling versus termination of signaling (**Fig 1.16**). In this thesis my main aim is to understand how the activity Eph RTKs, with inherent *auto*catalytic properties and intrinsic structural features that promote dimerization and clustering is spatially organized (**Fig 1.16**). To accomplish this, the following specific questions were addressed:

1. The formation of higher-order clusters is a unique and essential feature of Eph/ephrin family among other RTKs [12]. Is there a link between composition of Eph clusters and cellular output? Does the cell's historical context determine the response to incoming ephrin? How important is clustering for robust kinase activity? Is it a prerequisite or a consequence?
2. The effect of the ER-anchored PTP1B on amplitude and duration of EphA3 signaling was highlighted before [133]. Whether the ER is polarized actively or passively towards cell contact points and whether it contributes to spatial organization of Eph signaling at these points is still poorly understood. If PTP1B actively contributes to regulation of Eph signaling at points of cell-cell contact, then the question is how the balance shifts between dominating Eph activity and dominating PTP1B activity at these points?
3. In addition to serving as docking sites, the two tyrosines in the Eph JM domain regulate catalytic activity [79-81]. Does the molecule exist in either an *auto*inhibited or a catalytically active conformation or is the process of activation more dynamic allowing the kinase to "breath" and sample many conformations?

4. The immediate outcome of regulated endocytosis is to reduce the number of cell-surface receptors, thereby attenuating responsiveness to ligand [156], but is the endocytosed Eph receptor still active and what is the contribution of the early, recycling and late endosome to the spatial organization of Eph activity? Finally, how does the cell differentiate between an active monomer and a ligand clustered active receptor in terms of different trafficking routes and thereby fate of signaling?

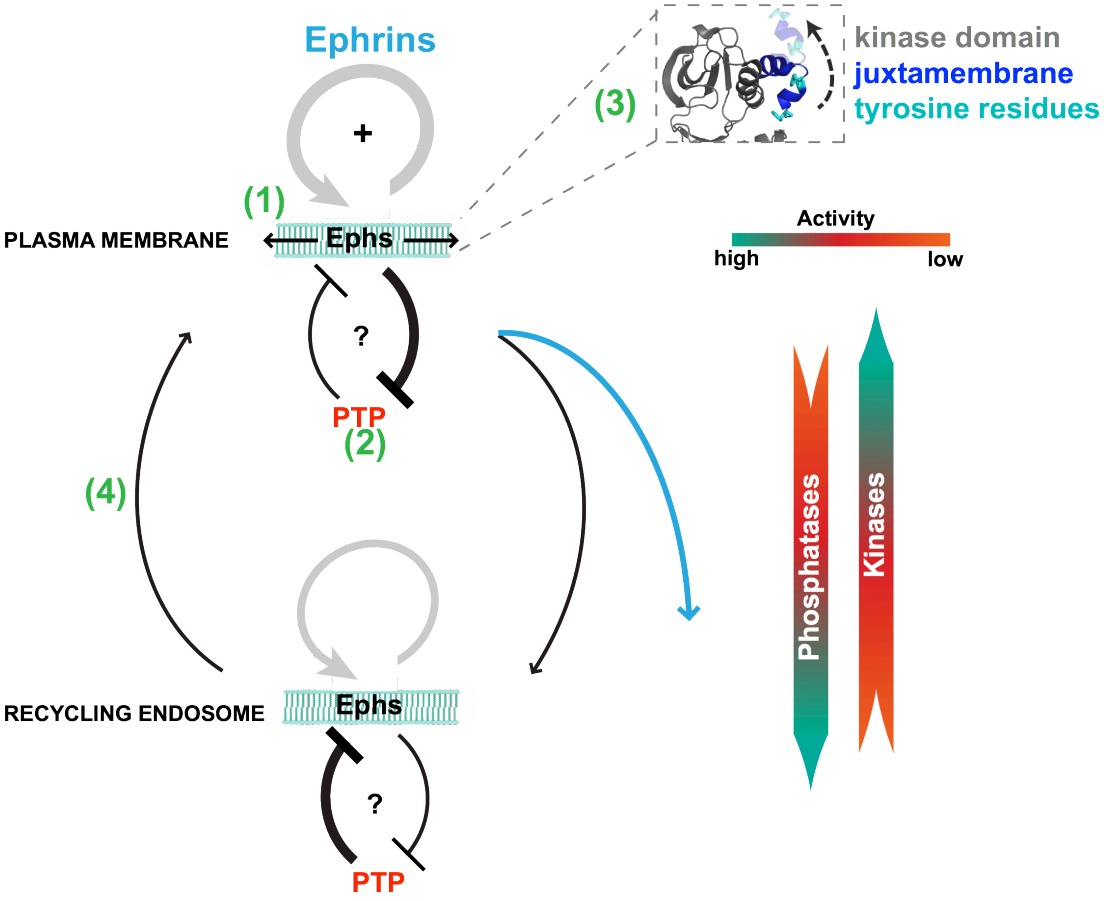

Fig 1.16 Model depicting possible determinants of Eph activity spatial organization
(1) The formation of higher-order clusters, (2) spatial organization of phosphorylation-dephosphorylation cycles, (3) *auto*regulation of Eph kinase activity by its juxtamembrane segment, (4) the effect of different trafficking routes on the output of Eph signaling.

2. MATERIALS AND METHODS

2.1 Materials

2.1.1 Chemicals

Acetic acid	Sigma-Aldrich®
Adenosin-5′-triphosphate (ATP)	Sigma-Aldrich®
Ammonium persulfate (APS)	SERVA Electrophoresis GmbH
Ampicillin sodium salt	SERVA Electrophoresis GmbH
Bromophenolblue	Sigma-Aldrich®
Dasatinib (10mM stock)	kind gift from Dr. Ralf Schneider
Dasatinib #9052	Cell Signaling Technology ®
2′-deoxyadenosine-5′-triphosphate (dATP)	Invitrogen™ Life Technologies
2′-deoxythymidine-5′-triphosphate (dTTP)	Invitrogen™ Life Technologies
2′-deoxycytidine-5′-triphosphate (dCTP)	Invitrogen™ Life Technologies
2′-deoxyguanosine-5′-triphosphate (dGTP)	Invitrogen™ Life Technologies
Dimethyl sulfoxide (DMSO)	SERVA Electrophoresis GmbH
Disodium hydrogen phosphate (Na_2HPO_4)	Merck KG
Dithiothreitol (DTT)	Fluka® Analytical
Ethanol	J.T.Baker
Ethidium bromide (EtBr) (10 mg/ml)	Fisher Scientific
Ethylenediaminetetracetic acid (EDTA)	Fluka® Analytical
Fluorescein isothiocyanate #F245-6	EGA-Chemie
Glycerol	GERBU Biotechnik GmbH
N-(2-Hydroxyethyl)Piperazine-N′-ethane-2-sufonic acid (HEPES)	GERBU Biotechnik GmbH
Isopropanol	J.T.Baker
Isopropyl β–D-thiogalactopyranoside (IPTG)	AppliChem GmbH
Kanamycin sulfate	GERBU Biotechnik GmbH
Magnesium chloride ($MgCl_2$)	Merck KG/J.T.Baker
Methanol	AppliChem GmbH
2-Mercapto-ethanol	SERVA Electrophoresis GmbH
Monopotassium phosphate (KH_2PO_4)	J.T. Baker
Nocodazole	Sigma-Aldrich®
Phosphatase Inhibitor Cocktail 1	Sigma-Aldrich®
Phosphatase Inhibitor Cocktail 2	Sigma-Aldrich®
Sodium chloride (NaCl)	Fluka® Analytical
Sodium dodecyl sulfate (SDS)	SERVA Electrophoresis GmbH
N,N,N′,N′-Tetramethylene-diamine (TEMED)	Sigma-Aldrich®
Tris-base	Carl Roth GmbH
Tris-HCl	J.T.Baker
Tritox X-100	SERVA Electrophoresis GmbH
Tween 20	SERVA Electrophoresis GmbH
UltraPure™ Agarose	Invitrogen™ Life Technologies

2.1.2 Enzymes, Proteins and Antibodies

AccuPrime™ *Pfx* DNA polymerase	Invitrogen™ Life Technologies
Age I-HF (10,000 U/ml)	New England Biolabs Inc.
*BamH*I (20,000 U/ml)	New England Biolabs Inc.
*BsrG*I (10,000 U/ml)	New England Biolabs Inc.
Calf Intestinal Phosphatase (10,000 U/ml)	New England Biolabs Inc.
*Dpn*I	New England Biolabs Inc.
*EcoR*I-HF	New England Biolabs Inc.
EphA2 rabbit polyclonal AB (C-20) #sc-924	Santa Cruz ® Biotechnology
mEphrin A1/Fc Chimera #602-A1	R & D Systems ®
mEphrin B2/Fc Chimera #496-EB	R & D Systems ®
Enolase (rabbit muscle) #E0379	Sigma-Aldrich®
*Hind*III (20,000 U/ml)	New England Biolabs Inc.
IRDye® 680 donkey anti-mouse IgG	LI-COR® Biosciences
IRDye® 800 donkey anti-goat IgG	LI-COR® Biosciences
IRDye® 680 donkey anti-rabbit IgG	LI-COR® Biosciences
IRDye® 800 donkey anti-mouse IgG	LI-COR® Biosciences
Living colors® GFP rabbit polyclonal AB	Clontech
Living colors® GFP mouse monoclonal AB	Clontech
*Not*I	New England Biolabs Inc.
Paq5000 DNA polymerase	Agilent Technologies
PfuUltra High-Fidelity DNA polymerase AD	Stratagene
Phusion High-Fidelity DNA Polymerase	FINNZYMES
Platinum® Pfx DNA polymerase	Invitrogen™ Life Technologies
PTB1B allosteric inhibitor #539741	Calbiochem
Purified mouse anti- phosphotyrosine (P172.1)	InVivo Biotech Services GMBH
Purified mouse anti-PTP1B (Ab-1) #PH01	Calbiochem
Purified mouse anti- α-tubulin	Sigma-Aldrich®
Purified mouse anti β-Catenin #610153	BD Transduction Laboratories™
Purified mouse anti-human Rab11 #610656	BD Transduction Laboratories™
Purified goat anti-human EphA2 #AF3035	R & D Systems ®
Purified rabbit anti-EphA2 +A3+A4 (phospho Y588+596) #ab62256	Abcam
Purified mouse anti-humanIgG Fc #411455	Calbiochem
RNaseA (100 mg/ml)	QIAGEN
*Sal*I	New England Biolabs Inc.
*Spe*I (10,000 U/ml)	New England Biolabs Inc.
*Xho*I (20,000 U/ml)	New England Biolabs Inc.
*Xma*I (10,000 U/ml)	New England Biolabs Inc.

2.1.3 Oligonucleotides

All oligonucleotides were purchased from Sigma-Aldrich Chemie GmbH in salt-free or HPLC purified form. All primer sequences are found in APPENDIX I

2.1.4 Plasmids

mCherry-N1	Clontech Laboratories Inc.
mCitrine-N1	Clontech Laboratories Inc.
mEGFP-N1	Clontech Laboratories Inc.
mTFP-N1	Clontech Laboratories Inc.
mTagBFP-N1	Evrogen Laboratories Inc.
PTP1B (D/A)-RFP-TK	generated by inserting cDNA encoding catalytic domain of human PTP1B (D/A) (residues 1-407) flanked by AgeI restriction sites into pRFP-tkB-C1 vector (gift from Dr. M. Lackmann).
mCherry-Rab7	kind gift by Dr. Yaowen Wu (MPI, Dortmund)
mTagBFP-Rab11	generated by inserting cDNA encoding human Rab11 into mTagBFP-C1 vector.
mTagBFP-PTP1B	generated by inserting cDNA encoding human PTP1B into mTagBFP-C1 vector.
dSH2-cherry	dimer SH2 domain from $pp60^{src}$ labeled with mCherry, generated by swapping YFP from the original dSH2-YFP [185], (cloned by Rabea Stockert).

2.1.5 Buffers and Solutions

LB agar plates	add 15 g agar per litre LB medium, pour plates when the autoclaved medium has approximately 55°C, add antibiotic of choice at desired concentration
LB medium	10 g/l Bacto-Trypton, 5 g/l bacto-yeast extract, 10 g/l NaCl and finally autoclave
HNTG	20 mM HEPES pH 7.5, 150 mM NaCl, 10% glycerol, 0.1% Triton X100, adjust volume with ddH_2O
KRB	125 mM HEPES pH 7.5, 12.5 mM $MgCl_2$, 20 mM $MnCl_2$ 0.5 mM Na vanadate, 100 mM β-glycerophosphate, adjust volume with ddH_2O
1x PBS (pH 7.4)	137 mM NaCl, 10 nM Na_2HPO_4, 2.6 mM KCl, 1.8 mM KH_2PO_4
4% PFA	4 g paraformaldehyde, 1x PBS (pH 7.4)
RIPA lysis buffer	50mM Tris pH 7.5, 150 mM NaCl, 1 mM EGTA, 1 mM EDTA, 1% IGEPAL, 0.25% Na deoxycholate, 2.5 mM Na pyrophosphate, 1 mM β-glycerophosphate, 0.1 mM PMSF, adjust volume with ddH_2O
5x SDS sample buffer	60 mM Tris-HCl (pH 6.8), 25 % glycerol, 2 % SDS, 14.4 mM 2-mercapto-ethanol, 0.1 % bromo-phenolblue
SDS running buffer	25 mM Tris-base, 192 mM glycine, 0.1 % SDS
Separating gel buffer	1.5 M Tris-HCl (pH 8.8)
SOC medium	20 g/l Bacto-Trypton, 5 g/l bacto-yeast extract, 0.5 g/l NaCl, 2.5 mM KCl, 10 mM $MgCl_2$ (SOB medium), autoclave and before usage add 20 mM glucose to obtain SOC

Stacking gel buffer	0.5 M Tris-HCl (pH 6.8)
STET	8% sucrose, 5% triton x100, 50 mM EDTA, 50 mM Tris pH 7.9 and adjust total volume with ddH_2O
1x TAE buffer	40 mM Tris/Acetate (pH 7.5), 20 mM NaOAc, 1 mM EDTA
1x TBS	100 mM Tris-HCl (pH 7.4), 150 mM NaCl
1x TBST	100 mM Tris-HCl (pH 7.4), 150 mM NaCl, 0.1 % Tween 20
Transfer buffer	25 mM Tris-base, 192 mM glycine, 20 % methanol.

2.1.6 Kits and Commercial Solutions

For DNA work

BigDye® Terminator v3.1 cycle sequencing kit	Applied Biosystems
100x BSA	New England Biolabs Inc.
6 x DNA gel loading buffer	Novagen
2-log DNA ladder	New England Biolabs Inc.
100 mM dNTP mix	Invitrogen™ Life Technologies
DyeEx® 2.0 Spin kit	QIAGEN
GelPilot loading dye, 5x	QIAGEN
50 mM Magnesium Sulfate	Invitrogen™ Life Technologies
NucleoBond® Xtra Maxi EF kit	Macherey-Nagel GmbH & Co. KG.
10x *Pfu* amplification buffer	Invitrogen™ Life Technologies
QIAprep® Spin Miniprep kit	QIAGEN
QIAquick® Gel Extraction kit	QIAGEN
QIAquick® PCR Purification kit	QIAGEN.
QuickChange XL Site-Directed Mutagenesis kit	Stratagene
RedSafe nucleic acid staining solution #21141	iNtRON
10x Restriction Enzyme Buffer 1	New England Biolabs Inc.
10x Restriction Enzyme Buffer 2	New England Biolabs Inc.
10x Restriction Enzyme Buffer 3	New England Biolabs Inc.
10x Restriction Enzyme Buffer 4	New England Biolabs Inc.
T4 DNA Ligase # 15224-017	Invitrogen™ Life Technologies
5x T4 DNA Ligation Buffer # 46300-018	Invitrogen™ Life Technologies
Zero Blunt® TOPO® PCR cloning kit	Invitrogen™ Life Technologies

For protein work

30 % Acrylamide/Bis solution	Bio-Rad Laboratories, Inc.
Bradford reagent #B6916	Sigma-Aldrich®
10x Cell lysis buffer	Cell Signaling Technology®
Complete Mini EDTA-free protease inhibitor tablets	Roche Applied Science
Odyssey Infrared Imaging System blocking	

buffer	Li-Cor® Biosciences
Precision Plus Protein™ standards	Bio-Rad Laboratories, Inc.
Protein G Sepharose ®, fast flow #P3296	Sigma-Aldrich®
1x TBS	Sigma-Aldrich®

For cell-culture work

DPBS	PAN™ Biotech GmbH
Dulbecco's Modified Eagle's Medium (DMEM)	PAN™ Biotech GmbH
Effectene® transfection reagent	QIAGEN
Fetal calf serum (FCS)	PAN™ Biotech GmbH
Fugene® 6 transfection reagent	Roche Applied Science
L-Glutamine	GIBCO®/Invitrogen™
Lipofectamine ™ 2000.	Invitrogen™
Trypsin/EDTA	PAN™ Biotech GmbH

2.1.7 Bacterial Strains

One Shot® TOP10 Competent Cells	Invitrogen™ Life Technologies
Rosetta™ 2(DE3) Singles™ Competent	Novagen
XL10 Gold	Stratagene (regrown in-house)

2.1.8 Mammalian Cell Lines

Cell Line	Origin	Supplier	Reference
COS-7	African green monkey kidney fibroblast	ATCC	[186]
HEK-293	Human embryonic kidney	ATCC	
HeLa	Human cervical adenocarcinoma	ATCC	
MCF-7	Human mammary gland adenocarcinoma	ATCC	
MDA-MB468	Human mammary gland adenocarcinoma	ATCC	
MDCK	Madin-darby canine kidney cells	ATCC	

2.1.9 Material and Equipment

Centrifuges & Rotors

Centrifuge 5415R	Eppendorf
Centrifuge 5810R	Eppendorf
Centrifuge RC 26 Plus	Sorvall®
Rotor SH-3000	Sorvall®
Rotor FA-45-24-11	Eppendorf
Rotor FL 064-04053	Eppendorf
Vacuum centrifuge	Eppendorf

For DNA work

Gel Imaging Station	Bio-Rad Laboratories
Gene Pulser™	Bio-Rad Laboratories
PCR-Cycler	Eppendorf
Power Pac™ 1000	Bio-Rad Laboratories
Pulse controller	Bio-Rad Laboratories

For protein work

Amicon Ultra-15 centrifugal filter unit	Millipore™
1.0 mm cassettes for western blots	Invitrogen™ Life Technologies
1.0 mm 10-well combs	Invitrogen™ Life Technologies
Incubation box for western blots	Li-Cor® Biosciences
Incubator Shaker Series I26	New Brunswick Scientific
Odyssey Infrared Imager	Li-Cor® Biosciences
PVDF membrane	Bio-Rad Laboratories, Inc.
Sonicator needle (MS 73)	Bandelin Electronic GmbH
Ultraschall HD 2200	Bandelin Electronic GmbH
Test tube rotator 34528	Snijders
Cuvettes (1 ml) Ref. 67.742	Sarstedt Aktiengesellschaft & Co.

For cell-culture work

Cell scraper	BD Falcon™
Cryo vials	
Easy Grip™ tissue culture dish (60 mm)	BD Falcon™
75 mm filter unit	Nalge Nunc International
Glass Pasteur pipettes (150 mm, 230 mm)	Brand GmbH & Co. KG
2-well LabTek® chambers No. 1.0	Nalge Nunc International
4-well LabTek® chambers No. 1.0	Nalge Nunc International
8-well LabTek® chambers No. 1.0	Nalge Nunc International
NALGENE® Cryo 1 °C freezing container	Nalge Nunc International
35-mm MatTek petri dishes No. 1.5	MatTek Corporation
NUAIRE™ Cellgard class II biological safety cabinet	Integra Biosciences
T75 tissue culture flask	BD Falcon™
Tissue culture plate (6 well)	BD Falcon™
Vacusafe comfort	Integra Biosciences
Vi-Cell™ XR cell viability analyzer	Beckman Coulter, Inc.

General Material and Equipment

Bunsen burner LABOGAZ® 206	Campinggaz®
Eppendorf safe lock tubes (0.5/1.5/2 ml)	Eppendorf
Falcon tubes (15/50 ml)	BD Falcon™
Gas cartridge C 206	Campinggaz®
Gene Pulser	Bio-Rad
Heatable magnetic stirrer “IKMAG®RCT”	IKA®Labortechnik

Heating block "QBD4"	Grant Instruments
Nanodrop® ND-1000 spectrophotometer	Peqlab Biotechnologie GmbH
Parafilm®	Pechiney Plastic Packaging
PFE powder-free latex exam gloves (S)	Kimberly-Clark
Pipetboy acu	Integra Biosciences
Pulse Controller	Bio-Rad
Safegrip® nitril gloves (S)	Süd-Laborbedarf GmbH
Sarstedt serological pipettes (5/10/25 ml)	Sarstedt Aktiengesellschaft & Co.
Scale "Precisa 62 A"	Precisa Instruments AG
Scale "Precisa 620 C"	Precisa Instruments AG
Surgical disposable scalpel (No. 11, No.21)	Braun Melsungen AG
Thermomixer comfort	Eppendorf
"Vortex Genie 1" touch mixer	Scientific Industries

2.1.10 Microscopes

Axiovert 200M: inverse FL microscope	Carl Zeiss MicroImaging GmbH
Cell R	Olympus
Fiber coupling unit	PicoQuant GmbH
Fluo View FV1000	Olympus
IU-LH75XEAPO: 75W xenon APO lamp	Olympus
IX 81: inverse microscope	Olympus
IX2-UCB controlling unit	Olympus
Leica TCS SP5	Leica MICROSYSTEMS
PR-IX2 motorised stage	Olympus
Scan Stage	Olympus
Sepia II	PicoQuant GmbH
U-HSTR2: hand switch	Olympus
UPLSAPO 40x/0.9 NA	Olympus
UPLSAPO 60x/1.2 NA	Olympus
U-RFL-T	Olympus

2.1.11 Software

Adobe Illustrator	Adobe Systems Inc.
DNASTAR Navigator v2.2.1.1	DNASTAR Inc.
FV10-ASW Fluoview Software	Olympus
IgorPRo v6.12	WaveMetrics
ImageJ64 v1.44	http://rsbweb.nih.gov/
Microsoft Excel 2011	Microsoft Corporation
MacPyMOL	http://www.pymol.org/
SymPhoTime v5.12	PicoQuant GmbH

2.2 Methods

2.2.1 Cloning

2.2.1.1 Bacterial Cultures

Unless otherwise stated, *E*.coli cells were grown in LB medium (+ appropriate antibiotic) at 37 °C and 225 rpm. Single clones (colony) grown on agar plates were then inoculated into cultures of 4 ml LB medium. This pre-culture was left to grown for 6-10 h, then used to inoculate the desired volume of main culture.

2.2.1.2 Transformation of Chemically Competent E.coli

Chemical transformation of foreign DNA into competent bacterial cells is a method of amplification for recombinant DNA and it usually has a transformation efficiency of 1 x 10^6 - 1 x 10^8 colonies/μg DNA.

For each tube of chemically competent *E*.coli XL 10 Gold cells (100 μl), 3.25 μl of 2.25 mM DTT was added. Aliquots of 50µl cells were used for each transformation reaction, and were inoculated with either ~1 μl plasmid DNA (50ng), or 2 – 4 μl ligation mix, then left on ice for 30 min. Tubes with transformation mix were then heat shocked for 60 sec at 42 °C and returned to settle on ice for 2-5 min. On each 50-µl tube, 250 μl of SOC medium was added and then tubes were left for 60 min at 37 °C, 225 rpm. In case of ligation mix, all cell suspension was plated on LB agar plates containing the required antibiotics and placed at 37 °C overnight or at RT over the weekend. In case of recombinant DNA amplification, 50 μl cell suspension was used for plating.

2.2.1.3 Transformation of Electro-Competent E.coli

For complicated or difficult cloning experiments electroporation of recombinant DNA was used instead of chemical competent cells, because electroporation has a higher transformation efficiency of up to 1 x 10^{10} colonies/μg DNA.

On each tube of electro-competent *E*.coli XL 10 Gold cells (50 μl), 50 μl of 10% glycerol and 5.0 μl recombinant DNA was added and tubes were left on ice. The transformation mix was later transferred to a sterile, pre-cooled electroporation cuvette and exposed to an electric field (1.3 V, 25 μF, 800 Ω) in the electroporation chamber. Time constants were monitored on the Gene Pulser device and were always between 6 and 8 milliseconds. Afterwards, cells were transferred to a 15 ml Falcon tube containing 950 μl SOC medium and then tubes

were left for 60 min at 37 °C, 225 rpm. In case of ligation mix, all cell suspension was plated on LB agar plates containing the required antibiotics and placed at 37 °C overnight or at RT over the weekend. In case of recombinant DNA amplification, 50 μl cell suspension was used for plating.

2.2.1.4 DNA Preparation Using Boiling Miniprep

This procedure is used for quick yet dirty DNA preparations, to check the identity of clones before clean, large-scale DNA preps are undertaken. It is a small-scale, fast and simple plasmid preparation method that works well with smaller plasmids (< 15 kb in size). It works with most strains of *E.coli*, except those strains that release large amounts of carbohydrates such as HB101. The procedure is also not recommended for endA+ strains because endonuclease A is not entirely inactivated during the boiling procedure. The resulting DNA can only be used for electrophoresis and restriction digestion.

Bacterial cultures were grown overnight as described earlier in (2.2.1.1). Spin down 1.5 ml of the cell suspension for 30 sec at max speed, 4 °C. Supernatant was then removed leaving the pellet to dry as much as possible. The pellet was then resuspended in 200 μl STET by vortexing and 20 μl of 10 mg/ml fresh lysozyme was mixed gently before boiling the tube for 45 sec. Samples were centrifuged at max speed for 10 min, and clot formed was removed by toothpick before precipitating nucleic acids by adding 200 μl isopropanol. Contents of the tube were then mixed, left for 5-10 min at RT then centrifuged at max speed for 10 min. Supernatant was then removed with care and tubes drained on paper towel. Pellet was rinsed with 170 µl 70% ethanol, spun down for 2 min, left to dry (~30min) and afterwards resuspended in 20-50 μl TE. For restriction digestion, 2 µl DNA were used in a total of 20 µl digestion mix. After complete digestion, RNAseA (0.01 µg/ul) was added and missed with digestion mix a few sec before gel loading.

2.2.1.5 DNA Preparation Using QIAprep® Spin Miniprep Kit

The QIAprep® Spin Miniprep Kit is routinely used for molecular biology applications. It is a small-scale, fast and simple plasmid preparation method designed for the purification of up to 20 μg high-copy plasmid DNA. The resulting DNA is in sequencing quality and can be used for restriction analysis, cloning and

PCR. The kit is based on initial alkaline analysis of bacterial cells and the consequent absorption of the plasmid DNA onto a patent silica membrane in the presence of high-salt buffers. DNA can be eluted form the membrane with ddH_2O or low-salt buffer.

Plasmid DNA was prepared following the QIAprep® Miniprep Handbook. Bacterial cultures were grown overnight as described earlier in (2.2.1.1). Cell suspensions then centrifuged for 15 min at 6,800 x *g*, 4 °C. Plasmid DNA was finally eluted by adding 50 μl ddH_2O to the centre of the spin column. Tubes were left aside for 5 min, then subsequently centrifuged for 1 min at 16,100 x *g*, RT.

2.2.1.6 *Endotoxin-Free Plasmid DNA Preparation Using NucleoBond® Xtra Maxi EF Kit*

Endotoxin-free plasmid DNA was prepared on a large-scale in order to be used for mammalian cells transfection. Endotoxins are amphiphilic lipopolysaccharides (LPS) that constitute the outer layer of a membrane enclosing the inner membrane of Gram-negative bacteria's lipid bilayer membrane. During cell growth, endotoxins are released from cells in small amount. However, upon cell death and cell lysis occurring during plasmid DNA purification, large amounts of endotoxins are released. Free LPS induce inflammatory reactions of the mammalian immune system, and therefore their removal is essential to ensure high transfection rates and high viability of transfected cells. The amphiphilic nature of LPS makes it hard to separate them from DNA using common plasmid purification systems. NucleoBond® Xtra EF purification system is a fast and efficient way of reducing endotoxin level to <0.05 EU/*u*g plasmid DNA for up to 1000 *u*g high-copy plasmid DNA.

Endotoxin-free plasmid DNA was prepared following the NucleoBond® Xtra Maxi EF Kit user manual. Bacterial cultures (usually 300 ml) were inoculated with 4 ml pre-culture grown overnight as described earlier in (2.2.1.1). Cells were collected by centrifugation for 20 min at 4500 x *g*, 4 °C. Endotoxin-free plasmid DNA was finally eluted from NucleoBond® finalizers twice with the same 8000 μl TE-EF buffer. To increase DNA yield, the finalizer was washed once again with 200 μl TE-EF buffer.

2.2.1.7 *Agarose Gel Electrophoresis of dsDNA*

Agarose gel electrophoresis is used to separation DNA fragments starting from ~50 by their size. Polymerized agarose forms pores with sizes dependent on

the agarose concentration used. The distance between the DNA bands being separated will also depend on the percent of agarose in the gel. Because nucleic acids bears negative charges, DNA fragments migrate towards the anode upon applying an electric field. The smaller the fragment, the faster it migrates and the closer it is towards the anode (the lower end of the gel).

For electrophoresis, agarose gels are prepared with 1x TAE buffer supplemented with RedSafe nucleic acid staining solution (5 μl/100 ml) or ethidium bromide (EtBr) (4 μl/100 ml). EtBr can visualize DNA owing to its ability to intercalate into double stranded DNA molecules and emitting orange light at 590 nm when excited with UV light of wavelength 312 nm. RedSafe is a new and safer alternative to EtBr, that emits green fluorescence when bound to DNA. Fluorescence emission of RedSafe is centered at 537 nm and it has two fluorescence excitation maxima, one at 309 nm and the other at 419 nm. After leaving the gel aside to dry, it is transferred to an electrophoretic chamber and the chamber is filled up with 1x TAE buffer. Electrophoresis takes place at constant voltage of 100V for small gels and 120 for bigger gels for about 20-30 min. For sample preparation, DNA samples to be resolved (volumes appropriate to comb size used for gel preparation) were mixed with DNA loading buffer (6 x). For proper size estimation of resolved DNA fragments, a DNA-marker is added in one lane of the gel. Agarose concentration in gels is chosen according to the size DNA molecule to be separated as follows:

Agarose concentration in % (w/v)	Size of DNA fragments
2.5	<100bp
2.0	0.1 - 1.0 kb
1.8	0.2 – 2.0 kb
1.5	0.3 – 3.0 kb
1.2	0.5 – 5.0 kb
1.0	0.5 – 7.0 kb
0.8	0.8 – 12.0 kb
0.5	1.0 30.0 kb

2.2.1.8 Isolation of DNA Fragments from Agarose Gels

The QIAquick® Gel Extraction Kit is a fast and simple procedure for gel extraction of up to 10 μg DNA (70 bp to 10 kb). The method is based on a simple and fast bind-wash-elute procedure, where DNA binds to silica-membrane-based columns in the presence of high salt concentrations. Contaminants are washed off through the column and DNA fragments can be eluted at the last step with 30-50 μl ddH_2O. Before applying sample to the column, DNA fragments to be extracted are

excised from the agarose gel (up to 400 mg slices) and completely dissolved in the appropriate buffer at 50 °C for 10 min. Purification is then continued according to the manufacturer's manual.

2.2.1.9 *Purification of DNA Fragments*

The QIAquick® PCR Purification Kit is a fast and simple procedure for DNA purification of up to 10 μg PCR or restriction digestion products (100 bp to 10 kb). The method is based on a simple and fast bind-wash-elute procedure, where DNA binds to silica-membrane-based columns in the presence of high salt concentrations. Contaminants are washed off through the column and DNA fragments can be eluted at the last step with 30-50 μl ddH_2O.

2.2.1.10 *Restriction Digestion*

Restriction endonucleases type II bind to and cleave DNA molecules at specific sites termed "restriction sites", which are short sequences of bases specific to each enzyme. s are washed off through the column and DNA fragments can be eluted at the last step with 30-50 μl ddH_2O. Restriction enzymes catalyze the hydrolysis of 3' -> 5'-phosphodiesterbonds in each of the DNA strands and thereby creates a double strand break. Restriction digestion was performed to create DNA fragments with sticky ends for eventual ligation and cloning of new recombinant DNA, for checking correct insertion of fragments and for linearization of vector DNA.

For complete digestion of 1 μg DNA, appropriate reaction buffer (10x) was added at 1/10 of final reaction mix volume. Reaction mix was supplemented with BSA (10x) when indicated, excess of restriction enzyme units, ddH_2O to final volume and incubated from 1 h up to O/N at 37 °C to achieve complete digestion.

2.2.1.11 *Dephosphorylation of 5'-Phosphorylated DNA fragments*

An essential step during cloning and before the ligation of two DNA fragments is the dephosphorylation of 5'-end of destination vector to prevent its self-ligation. Self-ligation of cut vector will prevent fragment insertion and produce empty vectors. For dephosphorylation, 0.5 U/μg DNA of alkaline phosphatase (calf intestinal phosphatase CIP) is added directly on the restriction mix (as long as restriction buffer was not NEB buffer 1) and reaction tubes are incubated for 1 h at 37 °C. If the restriction reaction buffer was NEB buffer 1, it is advisable to purify the reaction and do the CIP treatment (0.5 U/μg DNA) in NEB reaction buffer 3

(10x), while adjusting final volume with ddH_2O. Once dephosphorylaiton reaction has reached completion (~1 h), DNA is purified using the QIAquick® PCR Purificaiton Kit.

2.2.1.12 Ligation of DNA Fragments

DNA ligation requires the action of DNA ligase, which catalyzes the formation of a 3′ -> 5′ phosphodiester bond between the free 5′-phosphate and the 3′-hydroxyl groups of linearized DNA fragments, in the presence of ATP. The starting ligation conditions required 50 ng vector DNA and three-fold molar excess of insert DNA ends. The ratio of vector: insert was varied when optimization was needed. The required amount of insert for any given ligation reaction was calculated according to the following formula:

$$\text{Amount insert [in ng]} = \frac{\text{amount vector [in ng] x insert size [in bp]}}{\text{vector size [in bp]}}$$

In addition to vector DNA and the calculated amount of insert/inserts DNA, ligation mix is supplemented with 5 x T4 DNA ligase buffer, 1 U T4 ligase and final volume adjusted with ddH_2O. Ligation reaction is then incubated O/N at 16 °C or for 1 h at RT before transformation into competent *E*.coli XL10 Gold.

2.2.1.13 TOPO® - Blunt Cloning

Zero Blunt® TOPO® PCR cloning is the easiest, fastest method for highly efficient insertion of blunt-end PCR products into a cloning vector. Blunt ligation kits include a linearized and topoisomerase I-activated (covalently bound to the 3′-end of each DNA strand) pCR®Blunt II-TOPO® cloning vector, for fast ligations without ligase. The Zero Blunt® TOPO® PCR cloning kit was used when saving and storing hard-to-get PCR products was needed, as well as a template for some PCR products for sequential subcloning.

Zero Blunt® TOPO® PCR cloning was carried out by gently mixing 4 µl blunt-end PCR product with 1 µl of the kit salt solution and 1 µl pCR®-Blunt TOPO® cloning vector. The mixture was then incubated for 5-15 min at RT and subsequently placed on ice. Finally 2 µl of the TOPO® cloning reaction were used for transformation into chemically competent *E*.coli One Shot® TOP10.

2.2.2 Polymerase Chain Reaction (PCR)

2.2.2.1 Amplification of DNA fragments

The polymerase chain reaction (PCR) is a method for amplifying a particular DNA sequence without the need for cloning into vectors. PCR utilizes heat-stable DNA polymerase, to synthesize DNA from single-stranded template. Double stranded DNA molecules are divided into single strands by heat denaturation. Two oligonucleotide primers direct the specificity of the reaction, through their hybridization to the DNA sequence of interest on opposite strands and acting as primers for the polymerase enzyme. Hybridization of primers to the single stranded DNA will occur at a temperature dependent on the primer of choice (usually 45-60 °C). Primers are added in excess to ensure that the formation of primer-template complexes takes precedence over renaturation of DNA single strands. Heat-stable DNA polymerase elongates bound primers as an exact copy of the original template, doubling the target DNA sequence for every cycle. Since each dsDNA molecule synthesized per cycle can serve a template for the following cycle, cycle repetitions leads to exponential amplification of the target sequence. The final specific product obtained after 25-35 cycles of denaturation, primer annealing and extension, can be visualized as a single band of DNA in agarose gels [187]. Special consideration for primer length, %GC in primer sequence, primer secondary structure and primer self-complementation was taken through checking designed primers in:

(http://eu.idtdna.com/analyzer/applications/oligoanalyzer/).

For standard PCR, AccuPrime™ *Pfx* (a recombinant DNA polymerase isolated from *Thermococcus* species strain KOD), was used. AccuPrime™ *Pfx* polymerase is a high fidelity enzyme owing to its proofreading 3′ -> 5′ exonuclease activity and a highly processive enzyme with a fast chain extension capability. It is provided in an inactive form, owing to its specific binding to an antibody that is inactive at ambient temperatures, but its activity is restored after the initial denaturation step at 94 °C in the PCR cycler. This "automatic hot start" increases sensitivity, specificity and yield of the PCR reaction, while allowing assembly of the reactants at RT. PCR reaction mixtures consisted of the equivalent of 20 ng template DNA, 5.0 µl 10x AccuPrime™ *Pfx* reaction buffer, 1.5 µl of a 2 mM dNTP mix, 1.5 µl of 10mM forward primer, 1.5 µl of 10 mM reverse primer, 2.5 U AccuPrime™ *Pfx* DNA polymerase and total volume adjusted to 50 µl with ddH_2O. The PCR reaction started with 2 min of denaturation at 95 °C, followed by 25-35

cycles of amplification. Each cycle consisted of an initial denaturation at 95 °C for 15 s, followed by primer annealing at the appropriate annealing temperature (-5°C from primer T_m) for 45 s, and ending with extension at 68°C for 1 min per kb. The last PCR cycle was followed by an additional extension step at 68°C for 15 min. Afterwards, the reaction was left in the PCR cycler to cool down at 4°C and PCR product was analyzed by agarose gel electrophoresis. PCR reaction was supplemented with 5% DMSO in case of GC-rich templates. Sometimes a two-step PCR reaction was essential to optimize primer annealing, in which case the initial phase was performed for 5 cycles, and the second phase for 25 cycles.

2.2.2.2 In-Vitro Site-Directed Mutagenesis

Stratagene's QuickChange® *In-Vitro* site directed mutagenesis kit was used for introduced of site-specific mutation in virtually any double-stranded plasmid. Mutations included point mutations and/or exchange, deletion or insertion of a single or limited number of amino acids in a protein sequence of interest. The basic procedure utilizes double stranded DNA vector with an inserted protein of interest and two synthetic, complementary oligonucleotide primers bearing the desired mutation. The primers, each complementary to opposite strands of the vector DNA, are extended and amplified with PCR, thereby generating a mutated plasmid with staggered single strand nicks. Following PCR, the product is treated with type II endonuclease *Dpn* I. DNA isolated from most *E*.coli strains is dam-methylated and is therefore susceptible to digestion by *Dpn* I. Digestion of the mutagenesis PCR product with *Dpn*I would therefore ensure that clones formed after transforming PCR product into competent *E*.coli are specific to the mutated DNA. Transformed bacteria repairs the single strand nicks, producing a functional, mutated plasmid with efficiencies greater than 80%.

The mutagenic oligonucleotide primers containing the desired mutation and binding to the same sequence on opposite DNA strands were designed according to some rules. The desired mutation was placed in the middle of the primer with 15-25 nucleotides flanking the mutation on both sides. Primers always ended with one or more C- or G- bases and had a melting temperature (T_m) of ≥78 °C. Primer melting temperature was estimated according to the following equation:

$$T_m = 81.5 + 0.41(\%GC) - 675/N - \%mismatch$$

Where N is the primer length in bases. For mutagenesis it is important to keep primer concentration in excess, so 125 ng of each primer were used. To convert nanograms to picomoles, the following formula was used:

X pmol of oligo = (ng primer x 1000) / (330 x number of oligo bases)

For mutagenesis PCR either Platinum® *Pfx* DNA polymerase, Pfu Ultra High-Fidelity DNA polymerase or Phusion High-Fidelity DNA polymerase were used as suggested by the respective manufacturer. Mutaion PCR was performed as a 50 μl reaction including, 50 ng template DNA 5.0 μl respectice 10x reaction buffer, 2.0 μl of a 2mM dNTP mix, 1.0 μl mM $MgSO_4$ (only for Platinum® *Pfx* DNA polymerase), 125 ng of each primer, 2.5 U DNA polymerase, and ddH_2O up to 50 μl. Cycling parameters consisted of an initial denaturation of template DNA and activation of DNA polymerase for 30 sec at 95 °C (depends on type of polymerase used). This was followed by 12-18 PCR amplification cycles of denaturation at the enzyme's specific denaturation temperature for 30 sec, primer annealing at 55 °C for 45 sec and extesnsion at the appropriate temperature and rate. Final extension for 10 min was followed by cooling to 4 °C until gel check or *Dpn*I treatment (1.0 μl of *Dpn*I 10U/ μl) for 60 min at 37 °C. Afterwards 2.5 μl of *Dpn*I treated PCR product were transformed into chemically competent *E*.coli as described in (2.2.1.2).

2.2.2.3 Directed Mutagenesis of dsDNA by PCR

Mutagenesis PCR can be done with primers that bind to non-identical sequences inside the protein of interest. . The 3'-end of each primer encodes for 15-25 amino base pairs of opposite strands of the original gene directly adjacent to the desired mutation. Their 5'-end contains one of two halves of the mutation to be introduced. As mentioned earlier the primers should end with one or more C- or G-bases. The mutagenesis oligonucleotide primers will bind to their complementary sequences on opposite strands, thereby amplifying the vector DNA with PCR. The resulting PCR produce is a linera, blunt end DNA molecule encoding for the entire plasmid with the mutations resting at its 3'- and 5'- ends. The length of the insertion was limited by the length of the oligonucleotide primers, than can be synthesized and used in PCR. For deletion of a specific nucleotide sequence, the primers used will not include the sequence to be deleted, and the amplified plasmid region will therefore exclude the respective amino acid sequence. Parental DNA is digested by *Dpn*I, after which blunt ends were ligated and subsequently transformed into competent *E*.coli.

For mutagenesis PCR either Platinum® *Pfx* DNA polymerase, Pfu Ultra High-Fidelity DNA polymerase or Phusion High-Fidelity DNA polymerase were

used as suggested by the respective manufacturer. Mutaion PCR was performed as a 50 µl reaction including, 50 ng template DNA 5.0 µl respectice 10x reaction buffer, 2.0 µl of a 2mM dNTP mix, 1.0 µl mM $MgSO_4$ (only for Platinum® *Pfx* DNA polymerase), 125 ng of each primer, 2.5 U DNA polymerase, and ddH_2O up to 50 µl. Cycling parameters consisted of an initial denaturation of template DNA and activation of DNA polymerase for 30 sec at 95 °C (depends on type of polymerase used). This was followed by 12-18 PCR amplification cycles of denaturation at the enzyme's specific denaturation temperature for 30 sec, primer annealing at 55 °C for 45 sec and extesnsion at the appropriate temperature and rate. Final extension for 10 min was followed by cooling to 4 °C until gel check or *Dpn*I treatment (1.0 µl of *Dpn*I 10U/ µl) for 60 min at 37 °C. Afterwards 2.5 µl of *Dpn*I treated PCR product were transformed into chemically competent *E*.coli as described in (2.2.1.2).

2.2.2.4 Two-Step Fusion PCR

When the mutant DNA molecule to be created was too long to be synthesized synthetically on oligonucleotide primer, then two-step fusion PCR reaction was used. The two fragments to be linker were amplified in separate PCR reactions. Both products form the initial PCR reactions were fused in a second standard PCR, by using amplification of both fragments in the same reaction using the 5'- and 3'- end primers for the N- and C- terminal parts of the final fusion protein, respectively. An overlapping sequence in both DNA fragments allows the annealing of the two separate fragments. For the second fusion PCR, fragments encoding C- and N-terminal parts of the final DNA were used at equimolar concentrations. After the amplification of the whole construct, fused DNA was cloned into pCR®-Blunt II-TOPO® vector for storage, sequencing and identity check with restriction digestion.

2.2.2.5 DNA sequencing

Sequencing of dsDNA was done following the dideoxy chain terminating method [188]. This is based on using fluorescently labeled 2',3'-dideoxy-nucleotides (ddNTPs) in addition to 2'-deoxynucleotides (dNTPs), that cannot form new phosphodiester-bonds due to the missing 3'-OH group. This leads to the termination of the synthesized DNA strand after insertion of ddNTP. The last incorporated nucleotide, which is the fluorescent ddNTP, can be detected by capillary gel electrophoresis. This was subsequently done in-house at our Zentrale Einrichtung Biotechnolgie.

Sequencing PCR was performed using the BigDye® Terminator v3.1 Cycle Sequencing Kit. In a total of 20 μl reaction adjusted with ddH_2O, 150-300 ng plasmid DNA, 4.0 μl ready reaction premix, 2.0 μl BigDye® sequencing buffer and 0.35 μl primer (100 pmol/ μl) were added. PCR protocol started with an initial denaturation cycle at 96 °C for 1 min, followed by 25 cycles of denaturation (96 °C for 10 sec), annealing (50 °C for 5 sec) and extension (60 °C for 4 min). Excess ddNTPs were removed from PCR product using the DyeEx® 2.0 Spin kit according to the manufacturer's manual. Cleaned product was transferred to 0.5 ml, dried in a vacuum centrifuge and sent for analysis.

2.2.3 Biochemistry

2.2.3.1 Preparation of Whole Cell Lysates

Whole cell lysates for protein analysis in western blots were prepared from mammalian cells cultured in 35-mm and/or 100-mm Easy Grip ™ tissue culture dishes. Cells were washed once with ice-cold PBS and then ice-cold RIPA buffer supplemented with 1 tablet Complete Mini EDTA-free protease inhibitor and 100 μl phosphatase inhibitor cocktail 1 and 2 was added. Cells with lysis buffer were left for 15 min, then cells were scrapped with a plastic cell-scarper, and contents of each dish/well were transferred to pre-cooled 1.5 ml Eppendorf tubes. Samples were sonicated for 12 sec, cycle 3, 30% and then transferred to a bench-top centrifuge for 15 min, 13,000 rpm at 4 °C. Supernatant was then transferred to fresh pre-cooled 1.5 ml Eppendorf tubes and at this stage samples could be snap-frozen in liquid nitrogen if experiment was to be carried out on a different day and stored at -80 °C. All steps were performed on ice to avoid protein degradation.

2.2.3.2 Determination of Protein Concentration with Bradford Assay

For determination of protein concentrations in cell extracts the Bradford assay was used. Bradford assay is a colorimetric protein determination assay, based on the absorbance shift occurring to the Cossmassie Brilliant Blue G-250 dye in the presence of proteins. The binding of dye to proteins stabilizes the blue form of Cosomassie dye, therefore the amount of blue complex present in solution is a measure for protein concentration and can be estimated by reading the absorbance at 595 nm. The cationic unbound form of the dye is usually red, and it shifts to the anionic blue form when bound to proteins, seen as an increase in absorbance at 595 nm. Bradford assay is sensitive to high levels of detergents; therefore a control reading is always measured for lysis buffer alone.

The assay was performed in UV cuvettes, one cuvette per sample. Protein standards were prepared by diluting a BSA standard 1 mg/ml (16 μl) in ddH_2O and making a serial dilution out of this 1-16 μg/ μl. Each protein standard (500 μl) was added in a separate cuvette and mixed with 500 μl Bradford reagent. For each sample, 1 μl were added to 500 μl ddH_2O and mixed with 500 μl Bradford reagent. Control sample consisted of 1 μl lysis buffer, 500 μl ddH_2O mixed with 500 μl Bradford reagent. Absorbance values obtained at 595 nm with the spectrophotometer were plotted against standard protein concentration. Protein concentrations of the various samples were then determined by mapping their absorbance values at 595 nm to the standard curve.

2.2.3.3 Denaturing Polyacrylamide Gel Electrophoresis (SDS-PAGE)

SDS-PAGE is used to separate proteins according to their size via an electric current. SDS is an anionic detergent that can bind to proteins in an amount proportional to their size (~ one molecule SDS per two amino acids). SDS breaks hydrogen bonds and unfolds proteins creating complexes that display a similar charge/size ration. SDS-protein complexes carry a negative charge and therefore migrate towards the anode when subjected to an electric current. When an electric current is applied to a vertical polyacrylamide gel, smaller proteins will migrate faster and the distance they migrate will be proportional to the pore size formed by the polymerized acrylamide. The concentration of acrylamide used was 8, 10 or rarely 12%, depending on the molecular weight of the protein of interest. Two gels were prepared in sequential order, separating and stacking and both poured into 1.0 mm western blot cassette according to the following protocol:

	8 %	**10 %**	**12 %**	
Acrylamide 30%	1.7 ml			**Stacking gel**
1.0M Tris (pH 6.8)	1.25 ml			
10 % SDS (w/v)	100 μl			
ddH_2O	6.8 ml			
10 % APS (w/v)	100 μl			
TEMED	10 μl			
Acrylamide 30%	4.0 ml	5.0 ml	6.0 ml	**Separating gel**
1.5M Tris (pH 8.8)	3.8 ml	3.8 ml	3.8 ml	
10 % SDS (w/v)	150 μl	150 μl	150 μl	
ddH_2O	7.0 ml	5.9 ml	5.0 ml	
10 % APS (w/v)	150 μl	150 μl	150 μl	
TEMED	9 μl	6 μl	6 μl	
Total	15 ml			

Separating gels were poured first, covered with ddH_2O and left to dry for ~15 min. After drying, water overload was removed and stacking gels poured on top. 10- or 15-well combs were inserted into the stacking gel immediately after pouring and allowed to dry to form sample pockets. Prepared gels can be stored at 4 °C for a maximum of 1 week, if properly humidified with ddH_2O and protected from drying by wrapping in a plastic bag or aluminum foil.

Whole cell lysates or IP samples (20 μl) were mixed with 5 μl 5x SDS sample buffer and incubated for 5 min at 95 °C before loading, to heat denature proteins and allow their reduction by 2-mercapto-ethanol in the sample buffer. Samples were then centrifuged for 1 min used for loading. For electrophoresis, combs were removed from gels, sample pockets cleaned with ddH_2O and gels were inserted into (BioRad…), gel chambers. Gel chambers were then assembled and filled with 1x running buffer and samples loaded. For size determination of separated proteins, 4 μl () standard containing different bands of known molecular weight were loaded in one well. Empty pockets were loaded with sample buffer and electrophoresis was performed with constant voltage of 80 V until samples leave separating gel, followed by an increase to 150 V for roughly 90 min.

2.2.3.4 Western Blot

One form of immuno-blotting is western blotting. In this technique proteins that were separated electrophoretically are transferred to a nitrocellulose or PVDF membrane to enable immunological protein detection with antibodies.

After electrophoresis blots were assembled in () semidry bot modules according to the manufacturer's manual. PVDF membranes were activated for 5 min in methanol, then left to equilibrate in 1 x transfer buffer together with the gel and two pieces of (whatmann) filter paper. The blot sandwich was assembled in the following sequence from bottom-up: filter paper, PVDF membrane, gel and the second filter paper. For a mini-gel semidry transfer was done at 15 V for 25 min.

Following semi-dry transfer, PVDF membrane was transferred to Li-Cor® incubation box for the remaining binding sites of the membrane blocked with Odyssey infrared imaging system blocking buffer (Li-Cor® Biosciences) for 1 h at RT on a shaker. Membranes were then incubated with primary antibodies diluted in 1 ml 0.1% TBST solution. PVDF membrane was sealed in a plastic bag after discarding air bubbles and incubated overnight at 4 °C. Next day, blots were transferred again to Li-Cor® incubation boxes, washed 3 times, 5 min each with

0.1% TBST. Blots were then incubated with the appropriate secondary antibodies (diluted 1:15,000) diluted in 10 ml TBS for 20 min, RT. Finally, blots were washed 3 times, 10 min each with 0.1% TBST solution and detected with Odyssey Imaging System.

2.2.3.5 *Immunoprecipitation*

Cell lysis and protein quantification were performed as described in 2.2.4.1 and 2.2.4.2. For immunoprecipitation, Protein-G Sepharose® (PG-Seph) beads were first pre-cleared. Purification of PG-Seph beads involved washing 5-6 times with ice cold PBS (~1 mL) and centrifugation at 850 g for 2 min at 4 °C after each wash. For lysate preclear, 25 μl of PG-Seph slurry were added to 600 μl lysate for 2 h at 4 °C on the wheel-over-wheel-shaker. Lysates were cleared by centrifugation at 850 g for 2 min at 4 °C followed by transferal into new tubes and addition of anti-GFP antibody (living colors rabbit, #632592 at 1:200) overnight at 4 °C on the wheel-over-wheel-shaker. Next day 40 μl of PG-Seph slurry were added to the 600 μl lysate for 2 h at 4 °C on the wheel-over-wheel-shaker. IP lysates were then washed 4-5 times with lyssis buffer. The last wash was removed with a syringe and beads were resuspended in 20 μl lysis buffer and boiled at 95 °C for 5 min after adding 5 μl 6X Lammeli buffer. Western blotting was undertaken according to section 2.2.4.2.

2.2.3.6 *Immunofluorescence*

Cells were fixed with 4% paraformaldehyde in PBS for 10 min at RT, rinsed three times (3X) with TBS. For phosphorylation labeling of Eph receptors, cells were permeabilized for 5 min with 0.1 % Triton X-100 in PBS at RT, then rinsed again 3X with TBS at RT. Blocking was performed for 30 min at RT or overnight at 4 °C with 4 % goat serum (v/v) (varies according to secondary antibody), 2 % BSA (w/v) in PBS. Primary antibodies were applied for 60 min at RT. After washing with PBS secondary antibodies diluted 1:200 in blocking solution were applied for 1 hr at RT. Cells were wash 3X with PBS at RT and imaged fin PBS with the appropriate microscope.

2.2.3.7 *In-Vitro kinase assays*

In-vitro auto- and transphosphorylation assays were preformed as described earlier [79,189]. COS-7 cells were transected with cDNA-encoding the construct in question. Cells were lysed 18-20 hr later as described in 2.2.4.1 and constructs were

immunoprecipitated according to section 2.2.4.5. Following IP, beads were washed 2 times in lysis buffer and 2X in HNTG buffer. Prior to auto-phosphorylation kinase assay, samples were dephosphorylated using calf intestinal phosphatase (CIP, #M0290, 0.5 U/μg protein) for 60 min at RT. IP lysates were then washed 2X with KRB buffer (1X). Last wash was removed completely with a syringe and beads were resuspended in 50 μl KRB. For an experiment with 5 time points, sample was prepared as follows: 50 μl IP beads, 20 μl 5X KRB, 10 μl 1 mM ATP (stock at 10 mM), adjust to 100 μl with dd H_2O. IP mix was left at RT until chosen time points, at which 20 μl were transferred to a new tube and 5 μl 6X Lammeli sample buffer were added, boiled with sample at 95 °C for 5 min to terminate reaction. For trans-phosphorylation kinase assay, acid denatured enolase was used as an external substrate. The equivalent of 100 μg enolase (from rabbit muscle, Sigma-Aldrich®, #E0379) was centrifuged at max speed for 5 min at 4 °C. Supernatant was discarded and 10 μl of (1 mM DTT/50 mm HEPES), pH 7.0 was added to the pellet and mixed thoroughly. This mixture was then incubated for 60 min on ice followed by the addition of 10 μl glycerol. Tubes were left on ice if the assay was to be done on the same day (otherwise stored at -80 °C). Immediately prior to assay, 20 μl of 100 mM acetid acid were added to the enolase solution and mixed thoroughly. Mixture was then incubated for 5 min at a 30 °C water bath, then kept on ice until required (maximum 1 hour). IP lysates to be assayed were washed 2X with KRB buffer (1X). Last wash was removed completely with a syringe and beads were resuspended in 50 μl KRB. For an experiment with 5 time points, sample was prepared as follows: 20 μl 5X KRB, 10 μl 1 mM ATP (stock at 10 mM), acid denatured enolase (5 μg/reaction) and 10 μl dd H_2O. Tubes were warmed for 5 min at 30 °C then 50 μl IP lysates were added to make the final volume 100 μl. IP mix was left at RT until chosen time points, at which 20 μl were transferred to a new tube and 5 μl 6X Lammeli sample buffer were added, boiled with sample at 95 °C for 5 min to terminate reaction.

2.2.4 Mammalian Cell Culture

2.2.4.1 Subculture of Mammalian Cells

Cells were maintained in Dulbecco's Modified Eagle's Medium (DMEM) supplemented with 10% fetal bovine serum (FBS), 1% L-glutamine and 1% non-essential amino acids (NEAA), grown at 37 °C in a 90% humidified incubator with 5% CO_2. For starving, phenolred free DMEM with 0.5% FBS wss used.

Exponentially growing cells become confluent and reach a density where all available substrate of the culture dish is occupied. When this happens, cell growth is usually inhibited by contact inhibition and cells need to be subcultured to new dishes with much less density to allow for further cell growth. When cultured cells reached 80-90% confluency, cells were washed once with PBS, covered with 1 ml trypsin for a few seconds, then trypsin was removed and dishes returned for 5 min at 37 °C (MDCK cells required longer time ~ 20 min). Detached cells were washed with 10 ml complete growth media to inactivate any remaining trypsin and cell suspension transferred to a falcon tube and pipetted gently up and down to separate cells to a single cell suspension. If cell number and/or viability were to be determined, 50 μl of cell suspension in a total of 500 μl media were used in Vi-Cell™ XR cell viability analyzer and the desired number of cells required for seeding into different cell culture dishes was calculated. For maintenance of cells lines, cells were subcultured at a ratio of 1:10 into new culture dishes.

2.2.4.2 Cryo-Preservation and Long-Term Storage of Cell Lines

For long-term storage, cells were cryo-preserved by freezing at temperatures below -80 °C. For maximal cell viability during the process of cryo-preservation, the use of cryo-preservative such as DMSO is essential since intracellular ice crystal formation and regional formation of high-concentration solutes can reduce cell viability drastically.

Sub-confluent 10cm cell-culture dishes and/or T75 flasks were split as described above. Cells were counted and diluted to a concentration of 1.5- 2 x 10^6 cells/ml in cryo-medium (90% FBS, 10% DMSO). Cells were aliquoted into cryo-vials and transferred to a NALGENE® Cryo 1 °C freezing box. NALGENE Cryo 1 °C boxes are filled with isopropanol and allow for controlled freezing rates of 1 °C per minute to avoid freezing associated cell damage. Cryo-boxes were then transferred to the -80 °C freezer overnight and cryo-vials were moved to the -150 °C freezer for long-term storage.

When frozen vials were needed, cell thawing was done as quickly as possible to avoid the toxic effect of DMSO on cells. Cryo-vials were thawed out in the 37 °C water bath and cell suspension was quickly transferred to prepared dishes with 10 ml complete growth media. Media was exchanged next day from thawed out cells with fresh 10 ml complete growth media with or without G418 depending on type of thawed out cells.

2.2.4.3 *Transfection with DNA*

Transfection is defined as the deliberate introduction of genetic material or nucleic acids into eukaryotic cells by non-viral means. Transfection can be done by various methods and it typically involves opening transient pores in the cell membrane to allow the uptake of genetic material. Transfection can be carried out by classical calciumphosphate co-precipitation, electroporation or by lipofection. In this study, all cells were transfected with plasmid DNA via lipofection, the mixing of a cationic lipid with the DNA to produce liposomes, which fuse with the cell membrane and deposit their content inside cells. The transfection reagent used was either Fugene® 6 or Lipofectamine ™ 2000 and transfection proceeded according to manufacturer's manual guidelines. Cells were either plated in 60-mm or 100-mm Easy Grip™ tissue culture dishes, 35-mm MatTek petri dishes or 4-well LabTek® chambers. Cells were plated one day prior to transfection to reach 50-80% confluency in case of Fugene® 6 or 90% confluency in case of using Lipofectamine ™ 2000. On the day of transfection, Fugene® 6: DNA ratios used were always 3:1 and Lippofectamine ™ 2000: DNA ratios were always 2.5:1.

For Fugene® 6 transfection of cells in 35-mm dishes, 3.0 μl Fugene® 6 in a total of 100 μl serum free media was incubated for 5 min at RT. Afterwards, 1 μg plasmid DNA was added and mixed properly either by pipetting up and down several times, or by vortexing. Transfection mix was left for 15 min at RT before adding to cells. Fugene® 6–DNA complexes were finally added to cells drop-wise and culture vessels swirled gently to ensure equal distribution of transfection complex over the entire surface. Cells were incubated at 37 °C in a 90% humidified incubator with 5% CO_2 until next day. For transfection of cells in other formats, amounts of Fugene® 6, DNA and serum free media were adjusted according to the following table:

Culture vessel	Surface area	No. Cells	Starting amount of Fugeme6	DNA	Medium
96-well 16-well Labtek	0.3 cm^2 0.4 cm^2	0.6-1.8 x 10^4	0.15 μl	0.05 μg	24.85 μl
48-well 8-well Labtek	1 cm^2 0.8 cm^2	1.2-3.6 x 10^4	0.3 μl	0.10 μg	24.7 μl
24-well 4-well Labtek	2 cm^2 1.8 cm^2	2.5-7.5 x 10^4	0.6 μl	0.20 μg	24.4 μl
12-well 2-well Labtek	4 cm^2	0.5-1.5 x 10^5	1.5 μl	0.50 μg	43.5 μl
6-well 35 mm dishes	10 cm^2 9.6 cm^2	1-3 x 10^5	3 μl	1 μg	97 μl
60-mm	20 cm^2	1.5 - 6 x 10^5	6 μl	2 μg	94 μl
10-cm	60 cm^2	0.3 –1.2 x 10^6	18 μl	6 μg	182 μl

For Lipofectamine ™ 2000 transfection of cells in 35-mm dishes, 10 µl Lipofectamine ™ 2000 in a total of 250 µl serum free media was incubated for 5 min at RT. In another tube, dilute 4 µg plasmid DNA in 250 µl serum free media an leave aside till the end of the 5 min. Afterwards diluted DNA was added to diluted transfection reagent and mixed properly either by pipetting up and down several times, or by vortexing. Transfection mix was left for 20 min at RT before adding to cells. Lipofectamine ™ 2000–DNA complexes were finally added to cells drop-wise and culture vessels swirled gently to ensure equal distribution of transfection complex over the entire surface. Cells were incubated at 37 °C in a 90% humidified incubator with 5% CO_2 for 4-6 hours, then media exchanged with fresh complete growth media to minimize cell toxicity. For transfection of cells in other formats, amounts of Lipofectamine ™ 2000, DNA and serum free media were adjusted according to the following table:

Culture vessel	Surface area	No. Cells	Starting amount of Lipofectamine	DNA	Medium
96-well 16-well Labtek	0.3 cm^2 0.4 cm^2	1-5 x 10^4	0.5 µl	0.2 µg	2 x 25 µl
48-well 8-well Labtek	1 cm^2 0.8 cm^2	0.25-1 x 10^5	1.0 µl	0.4 µg	2 x 50 µl
24-well 4-well Labtek	2 cm^2 1.8 cm^2	0.5-2 x 10^5	2.0 µl	0.8 µg	2 x 50 µl
12-well 2-well Labtek	4 cm^2	1-4 x 10^5	4.0 µl	1.6 µg	2 x 100 µl
6-well 35 mm dishes	10 cm^2 9.6 cm^2	0.25-1 x 10^6	10 µl	4.0 µg	2 x 250 µl
60-mm	20 cm^2	0.5 - 2 x 10^6	20 µl	8.0 µg	2 x 500 µl
10-cm	60 cm^2	1.5 –6 x 10^6	60 µl	24 µg	2 x 1.5 ml

2.2.5 Microscopy

2.2.5.1 Laser Scanning Confocal Microscopy (LSCM)

Confocal images of live and fixed cells were obtained with an Olympus FluoView FV1000 confocal laser-scanning microscope. TagBFP was excited with 405 nm, mTFP with 458 nm and EGFP and mCitrine with the 488 line of a multiline Argon laser. mCherry was excited with the 561 nm line of a DPSS laser. Excitation light was focused into the sample by a 60x/1.2 NA oil objective or a 40x/0.9 NA air objective using either the DM405/488/561/633 or the DM458/515 dichroic mirror. Detection of fluorescence was done by an acousto-optic tunable filter (AOTF) and SIM scanner. Blue fluorescence (Alexa 405 or TagBFP) was detected in a channel with bandwidth 425-478 nm and through a SDM490 emission beam splitter. Green and Yellow FPs were collected between 498-551 nm and through a SDM 510

emission beam splitter or SDM 560 if sequential imaging with the 561 nm laser was used. mCherry fluorescence was detected by collecting photons within the range of 575-675 nm. mCitrine and mCherry were separated by a SDM560 emission beam splitter (**Fig. 2.1 a**) while mTFP and mCitrine were separated by a SDM510 beam splitter (**Fig. 2.1 b**). Live cell imaging was performed in an incubation chamber adjusted to 37 °C, while fixed cells experiments were performed at RT (~ 25 °C).

Fig 2.1 Instrumental alignment for LSCM
Lasers (vertical black lines) and AOTF adjustments (colored, transparent rectangles) used for laser scanning confocal microscopy. (a) Excitation and emission spectra of mCitrine and mCherry are displayed with the corresponding excitation lines (488nm for mCitrine and 561nm for mCherry) and collection channel bandwidth (transparent green for mCitrine and transparent orange for mCherry). (b) Excitation and emission spectra of mTFP and mCitrine are displayed with the corresponding excitation lines (458nm for mTFP and 515nm for mCitrine) and collection channel bandwidth (transparent green for mCitrine and transparent blue for mTFP). Spectra from: (http://hernan.client.mpi-dortmund.mpg.de:8080/)

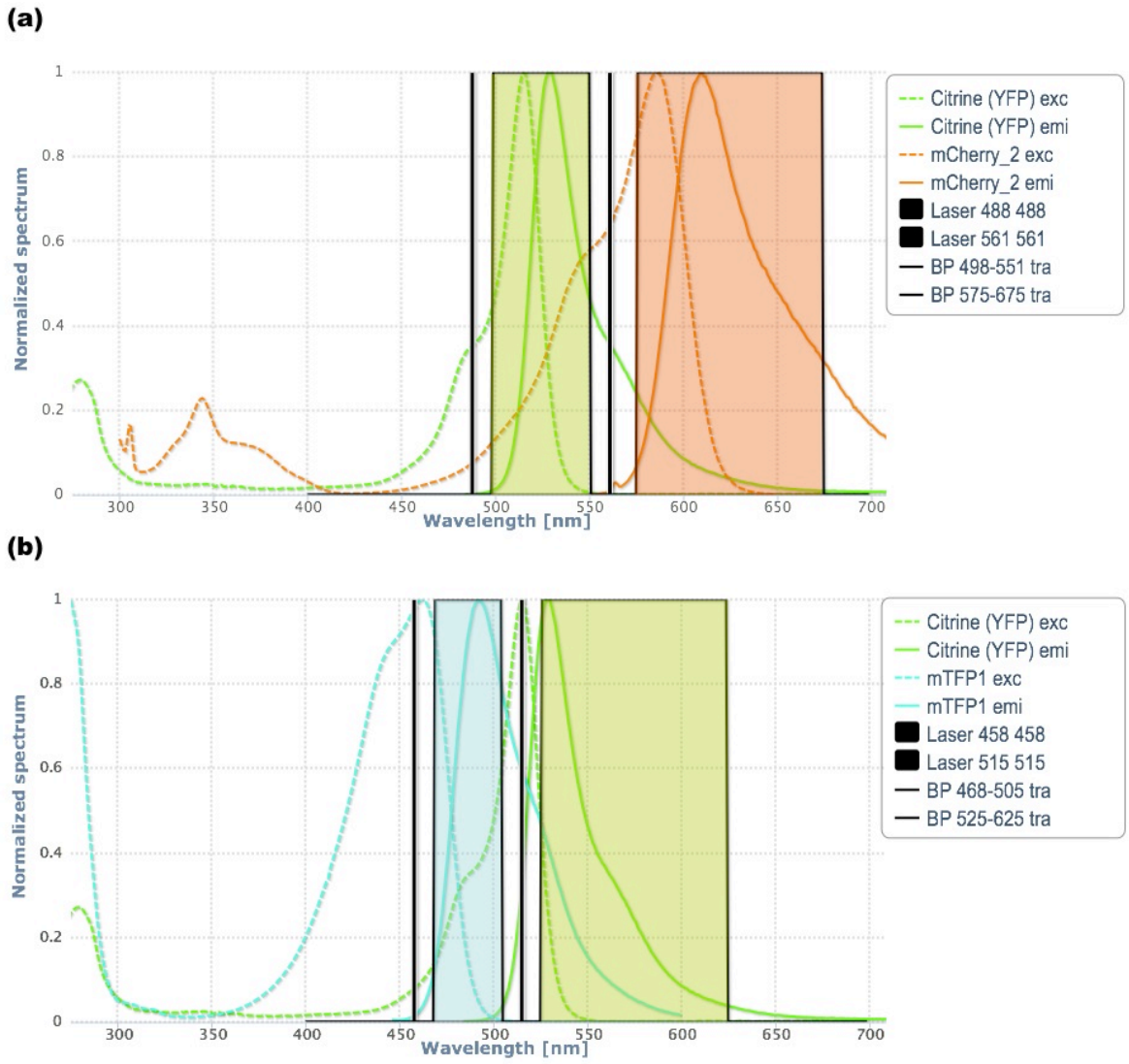

2.2.5.2 *Fluorescence Lifetime Imaging Microscopy (FLIM)*

FLIM measurements were made in a commercial setup composed of an Olympus FluoView FV1000 laser scanning confocal microscope equipped with an external unit, PicoQuant's compact FLIM and FCS upgrade kit for laser scanning microscopes. Pulsed lasers are coupled to the FV1000 through an independent port and are controlled by a driver that can be digitally modulated (PicoHarp 300). Detection of photons can be directed to one or a combination of two single photon avalanche diodes (SPAD), which then transfer their signal to the PicoHarp 300 data acquisition unit. FLIM imaging was mostly done using the 60x/1.35 NA oil objective by Olympus. All pulsed lasers (440, 470 and 510 nm) were were controlled with the Sepia II software (PicoQuant GmbH) (pulse repetition every 25 ns) and detected via the first APD. Image integration time was ~ 3 min. with an average total photon count of 3.0-5.0 x 10^6 per image. For mTFP, the 440 nm pulsed laser line (at 38% power) and the DM440/470 dichroic mirror were used. mTFP emission was detected by APDs equipped with 480/20 bandpass filter (**Fig2.2 a**). For mCitrine, the 470 nm pulsed laser line (at 37%) or the 510 nm pulsed laser (at 64%) and the DM440/470 or the DM458/515 dichroic mirror were used. mCitrine fluorescence was detected by APDs equipped with 525/15 bandpass filter (**Fig2.2 b**) or with the 537/26 bandpass filter (**Fig2.2 c**).

Fig 2.2 Instrumental alignment for FLIM.
Lasers (vertical black lines) and filters (colored, transparent rectangles) for FLIM. (a) Excitation and emission spectra of mTFP and mCitrine are displayed with the corresponding pulsed laser used when mTFP is the donor (440nm pulsed laser) and detection channel bandwidth (transparent blue for mTFP). (b) Excitation and emission spectra of mCitrine and mCherry are displayed with the corresponding pulsed laser used when mCitrine is the donor (470nm for mCitrine) and detection channel bandwidth (transparent green for mCitrine). (c) Excitation and emission spectra of mCitrine and mCherry are displayed with the another option for pulsed laser used when mCitrine is the donor (510nm for mCitrine) and detection channel bandwidth (transparent green for mCitrine). Spectra from (http://hernan.client.mpi-dortmund.mpg.de:8080/).

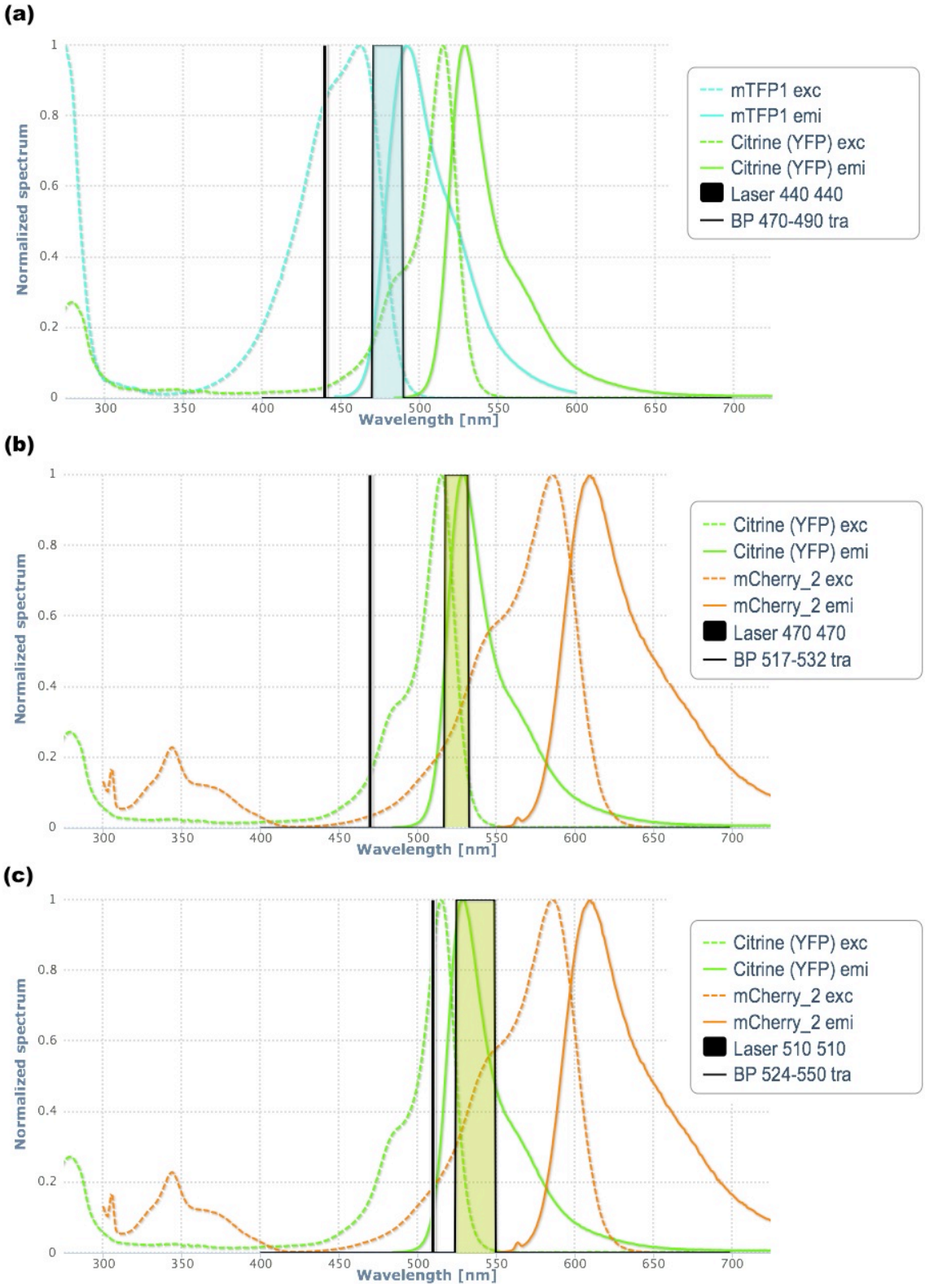
(a)
Normalized spectrum
Wavelength [nm]
mTFP1 exc
mTFP1 emi
Citrine (YFP) exc
Citrine (YFP) emi
Laser 440 440
BP 470-490 tra
(b)
Normalized spectrum
Wavelength [nm]
Citrine (YFP) exc
Citrine (YFP) emi
mCherry_2 exc
mCherry_2 emi
Laser 470 470
BP 517-532 tra
(c)
Normalized spectrum
Wavelength [nm]
Citrine (YFP) exc
Citrine (YFP) emi
mCherry_2 exc
mCherry_2 emi
Laser 510 510
BP 524-550 tra

2.2.5.3 *Fluorescence Loss After Photoactivation (FLAP)*

FLAP experiments were carried out at 37 °C on a Leica SP5 confocal microscope in imaging medium as described earlier [190]. Transiently transfected 15-24 hrs post-transfection post transfection, cells were allowed to equilibrate in the incubation chamber on the microscope and imaged with laser setting adjusted to minimize photobleaching (typically 488 and 561 lasers used at 10%). The fluorescence was collected via a 63x/1.4 NA oil objective, with a custom routine that followed through the three stps of FRAP/FLAP analysis: (1) Pre-bleach imaging (3 images with 488 and 561 lasers only). (2) Bleaching/Photoactivation (2 times with the 405 laser only at 80%) in a pre-defined region of interest (ROI). (3) Post-bleach imaging (20 frames at 40 sec interval using the 488 and 561 lasers only). At the end of the experiment an image of Rab11-BFP was acquired with 5% 405-laser power to identify the recycling compartment in a given experiment.

After standard image processing, mean intensities of photoactivatable EphA2-GFP (EphA2-paGFP) in the photoactivated ROI yielded fluorescence loss curves, which were normalized to EphA2-cherry to account for changes in the structure and intensity in the ROI resulting from the dynamic nature of live cells. Another ROI processed and normalized in the same manner was chosen at the cell periphery to investigate vesicular transport form the recycling endosome to the plasma membrane. For measuring half time of plasma membrane gain or recycling endosome loss of EphA2 fluorescence in the selected ROIs, normalized fluorescence decay cures were averaged and average curve was then fitted to a single exponential function in Igor Pro.

$$I = I_o + A\ exp(-t/\tau)$$

Where (I) is the intensity, (A) exponential constant, (t) is time, (τ) is the exponential time-constant.

2.2.5.4 *Image Manipulation and FLIM Analysis*

Quantifications done on images required their initial conversion to 32-bit in ImageJ, followed by background correction. When required, brightness and contrast of images were changed to improve signal-to-noise ratio. FLIM data were analyzed with precisionFLIM (pFLIM) [183] analysis code. Precision FLIM is an accurate, efficient code for time-domain FLIM that considers all significant instrumental artifacts. The analysis code uses a parameterized model to account for the instrument response function (IRF) (**Fig.2.4**). Fitting of full decay curves is done by conventional χ^2 minimization and single pixel fitting of lifetime populations is done with "maximum fidelity". When fluorophores followed a single-exponential decay, as in the case of mCitrine donor only images, a mono-exponential decay model according to equation (**9**) was used. When more than one lifetime was to be expected in the sample, a double-exponential model was used for fitting according to the following equation [172]:

$$I(t) = A_1\, exp(-t/\tau_1) + A_2\, exp(-t/\tau_2) + B \qquad (12)$$

where B is the background, A_1 and A_2 are amplitudes, τ_1 and τ_2 are the fluorescent lifetimes. Lifetime maps analyzed by the code in IgorPro were presented as pseudo-colored lifetime maps. Lifetime ranges displayed were adjusted manually in IgorPro.

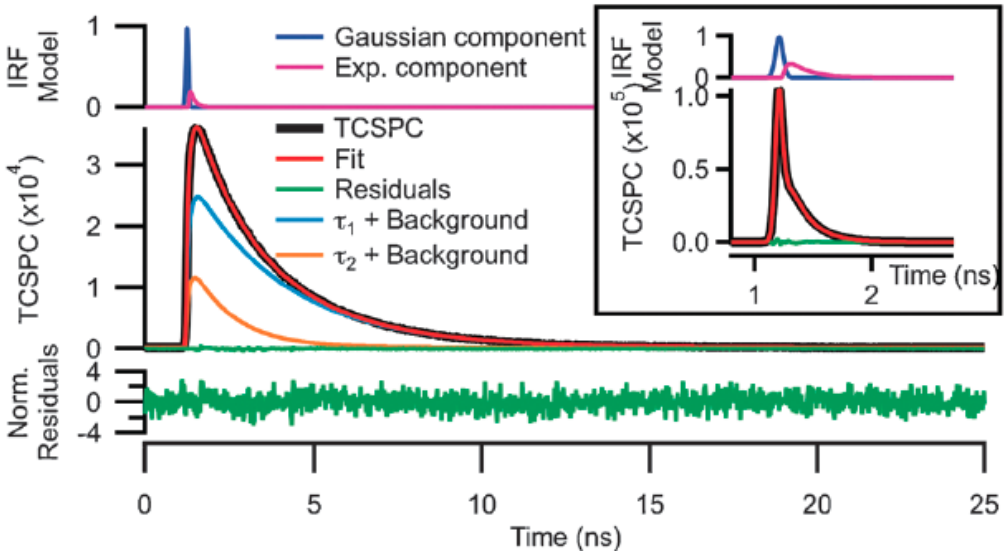

Fig 2.4 Outline of precision FLIM analysis.
χ^2 fit of a parameterized model decay function (red) to the full decay histogram (black). The concluded instrument response function (IRF) obtained from the fit is displayed above the TCSPC with the two IRF fitting components, a Gaussian and an exponential component. Normalized fit residuals are displayed below the TCSPC. Inset shows a representative fit of IRF model as compared to an IRF estimate obtained from the scattered excitation light of 470 nm pulsed laser at 36% power [183].

2.2.5.5 *Fluorescence Anisotropy Microscopy*

FRET (Förster resonance energy transfer) between identical fluorophores (homo-FRET) can be monitored by fluorescence anisotropy [191]. Fluorescence anisotropy was used to study protein structure [192], protein oligomerization [193,194], the organization of GPI-anchored proteins in submicrodomains at the cell surface [195] and the spatial distribution of monomeric versus dimeric proteins in living cells [196]. For each measurement two images were taken, an image with the emission polarizer oriented parallel to the excitation polarizer ($\boldsymbol{I}_{\parallel}$) and an image with the emission polarizer oriented perpendicular to the excitation polarizer ($\boldsymbol{I}_{\perp}$). Steady state anisotropy was calculated in each pixel *i* by:

$$\boldsymbol{r^i} = \frac{\boldsymbol{G^i}\,\boldsymbol{I_{\parallel}}^{\boldsymbol{i}} - \boldsymbol{I_{\perp}}^{\boldsymbol{i}}}{\boldsymbol{G^i}\,\boldsymbol{I_{\parallel}}^{\boldsymbol{i}} + 2\boldsymbol{I_{\perp}}^{\boldsymbol{i}}} \qquad (13)$$

The *G*-factors $\boldsymbol{G^i}$ were determined by acquiring the ratio of the intensities at perpendicular and parallel orientations for a fluorophore in solution (fluorescein) with a steady-state anisotropy that was close to zero:

$$\boldsymbol{G} = \frac{\boldsymbol{I_{\perp}}^{\boldsymbol{i}}}{\boldsymbol{I_{\parallel}}^{\boldsymbol{i}}} \qquad (14)$$

For reference measurement, fluorescein solution in water was placed in a glass bottomed tissue culture dish (MaTek, Ashland, MA, USA) and imaged as mentioned before. Average values of *G* images measured for 20x air objective was used for equation (13). As mentioned in the introduction, excitation with polarized light results in photoselective excitation of a subset of fluorophores (FPs) whose absorption transition dipole is parallel to the electric vector of the excitation light. The lifetime of the fluorophores we use (EGFP and Citrine) in anisotropy experiments is much shorter than rotational diffusion time scale. Therefore, förster resonance energy transfer (homo-FRET) becomes the dominating factor in the depolarization of emitted light [172].

Steady-state anisotropy of EGFP and Citrine was measured using Olympus MT-20 150W mercury arc burner as described before by Squire et *al*. [197]using an Olympus IX81 inverted microscope (Olympus, Hamburg, Germany). Three high extinction linear dichroic polarizers (Meadowlark optics, Frederick, Colorado) were used for anisotropy measurements; one was placed in the illumination path of the microscope, and the other two, parallel and perpendicular oriented

polarizers with respect to the polarization of the excitation light, placed in the motorized filter wheel. The filter block was set up with a bandpass (BP) 460-480 HQ filter for excitation light, a 485 dichroic and a 495-540 HQ filter for emission light. Fluorescence was collected using a 20x 0.7 N/A air objective and images of perpendicular and parallel emission light were acquired sequentially with an Orca CCD camera (Hamamatsu Photonics, Hamamatsu City, Japan). The CellR software was used for data acquisition and instrumental control. Images of the same cells were taken prior to and 20 min post dimerization, stimulation or 1 hr post-drug treatment. The acquired ($\boldsymbol{I}_{\parallel}$) and ($\boldsymbol{I}_{\perp}$) images were slightly shifted with respect to each other, therefore they were manually aligned and vertical and horizontal shift values were used for all experiments done with the same settings. ($\boldsymbol{I}_{\perp}$) and ($\boldsymbol{I}_{\parallel}$) images were background corrected before calculating steady-state anisotropy [197].

2.2.5.6 *Quantification of cluster sizes for Anisotropy Analysis*

Image processing in ImageJ was applied to compute anisotropy from the periphery of the cell. Two binary masks were created, one covered the whole area of a given cell and the other covered an eroded version of the cell same cell (10-15 pixels removed from the 8-bit binary mask). Subtraction of the second mask from the first created a new binary mask that represents the periphery of the cell that was multiplied with the original anisotropy image. The distribution of anisotropy values for a given FKBP construct as obtained from multiple samples incubated with the AP20187 dimerizer was then plotted (histograms represents binned images, bins size =50). The average molecular brightness of each state was used as a weighing factor in computing the relative contribution of each association state to the anisotropy. This intensity-weighted contribution of each association state was divided by their summed anisotropy, to give the cumulative relative contribution of each association state to a given anisotropy value.

2.2.5.7 *Total Internal Reflection Fluorescence (TIRF) microscopy*

Total internal reflection fluorescence (TIRF) microscopy (TIRFM) is based on the principle that when excitation light is reflected in a transparent solid at its boundary with liquid, then an evanescent wave with the same frequency as the excitation wave is produced at the solid-liquid interface. The intensity of this evanescent wave decays exponentially with distance from the solid surface (~100 nm), allowing for excitation of fluorescent molecules only within a few hundred nanometers of the solid surface "optical section". This thin axial region can be used

for the visualization of the basal plasma membrane (~7.5 nm thick) with a small section of the cytoplasm adjacent to the membrane [198].

TIRFM was performed using an Olympus IX81 inverted microscope with a 60x N/A 1.8 TIRM APOCHROMAT oil objective. The microscope is equipped with Argon lasers that pass through condensers that allow for the manipulation of the incident angle of light onto the specimen to obtain proper TIRF angle. Image analysis and background corrections were done later in ImageJ.

2.2.5.8 Fluorescence Calibrated Confocal Time-Lapse Microscopy

Fluorescence-calibrated time-lapse imaging was performed on a Zeiss LSM 510 Meta confocal microscope equipped with a ConfoCor 3 unit and a C-Apochromat 40x/1.2 N.A water immersion objective at 37 °C. mTFP and mCitrine were excited with 458 nm and 514 nm argon lasers, respectively, whereas RFP was excited with a 561 DPSS laser. The fluorescent light was passed through a NFT 565 beam splitter and detected with PMT detectors through a BP 475–525 band pass filter for mTFP, a LP 530 long pass filter for mCitrine, and a LP 575 long pass filter for RFP. To minimize cross talk between individual channels, mTFP and RFP were recorded simultaneously, whereas mCitrine was imaged separately. Pinhole diameter was set to 192 μm for mTFP, 296 μm for RFP, and 1000 μm for mCitrine. Images were recorded at a resolution of 512x512 pixels (0.15 μm /pixel) and a bit depth of 12 bit. For time-lapse imaging, single-plane multi-color images were recorded at 1-minute intervals.

To correlate the image intensity of mCitrine to absolute protein concentrations, we acquired single-channel images of cells expressing mCitrine-PTP1B D/A CD at exactly the same settings used for the time-lapse experiments. Fluorescence correlation spectroscopy (FCS) measurements were performed at randomly chosen positions in the cytoplasm of the same cells. Background corrected average image intensities were determined in a 1 μm radius around the FCS measurement point. For FCS, mCitrine was excited with the 514 nm line of an argon laser, while an APD detector recorded the fluorescence through a LP 530 long pass filter and a 70 μm pinhole. The raw intensity data were correlated using the microscope manufacturer's software, and for each measurement, correlation curves were averaged for ten consecutive 10-second intensity recordings. Averaged correlation curves were fit by using a model accounting for anomalous diffusion and a triplet term in order to determine the average number of particles in the confocal observation volume, using a non-linear least squares minimization

algorithm implemented in Matlab (MathWorks). Confocal volume was determined from calibration measurements of an Alexa 546 dye solution, assuming diffusion coefficient of 280 $\mu m^2/s$ at 25 °C that was extrapolated to 308 $\mu m^2/s$ at 37 °C. (Data analysis was performed by Dr. Martin Bierbaum).

2.2.6 Statistical Analysis

Results are expressed as the mean ± SEM, unless otherwise mentioned. Statistical significance was estimated either by the Mann-Whitney nonparametric *t*-test, one-way ANOVA or Student's *t*-test. Datasets that passed the Komogorov and Sminov test for Gaussian distribution are indicated in the figure legend. Significance level of p=0.05 was used, $p<0.05$ (*), $p<0.01$ (**) and $p<0.001$ (***).

2.2.7 Ephrin stimulation

Mouse ephrinB2-Fc, mouse ephrinA1-Fc and Alexa-647 labeled ephrinA5-Fc (M.Lackmann laboratory) fusion proteins were used for stimulations. Clustered ephrin-Fc fusion proteins were prepared by incubating with goat anti-human Fc at a ratio of 5:1 for 30 min at room temperature. Stimulations were carried out in a CO_2-controlled incubator at 37 °C for the indicated time.

3. RESULTS

3.1 Regulation of signaling at points of cell-cell contact by PTP1B

3.1.1 PTP1B substrate-trapping mutant localizes to regions of cell-cell contact

The ubiquitously expressed non-receptor protein tyrosine phosphatase (PTP1B) is bound to the cytosolic face of the endoplasmic reticulum (ER) through its C-terminal hydrophobic sequence [199,200]. Despite the initial thought that their anchor restricts its access to key substrates, many new findings have shown that PTP1B not only interacts with substrates as they transit past the ER, but also directly at specialized regions of the plasma membrane. We investigated the ability of PTP1B to access and spatially-temporally regulate signaling at points of cell-cell contact. Expression of GFP-labeled wild type (WT) PTP1B and its "substrate trapping" mutant D181A (D/A) in PTP1B-null fibroblasts showed that both localized to the ER network (**Fig. 3.1**). The PTP1B (D/A) mutant which is catalytically impaired but retains substrate binding [233], additionally accumulated at regions of cell-cell contact, labeled using anti-β catenin antibodies (**Fig. 3.1 white arrows**).

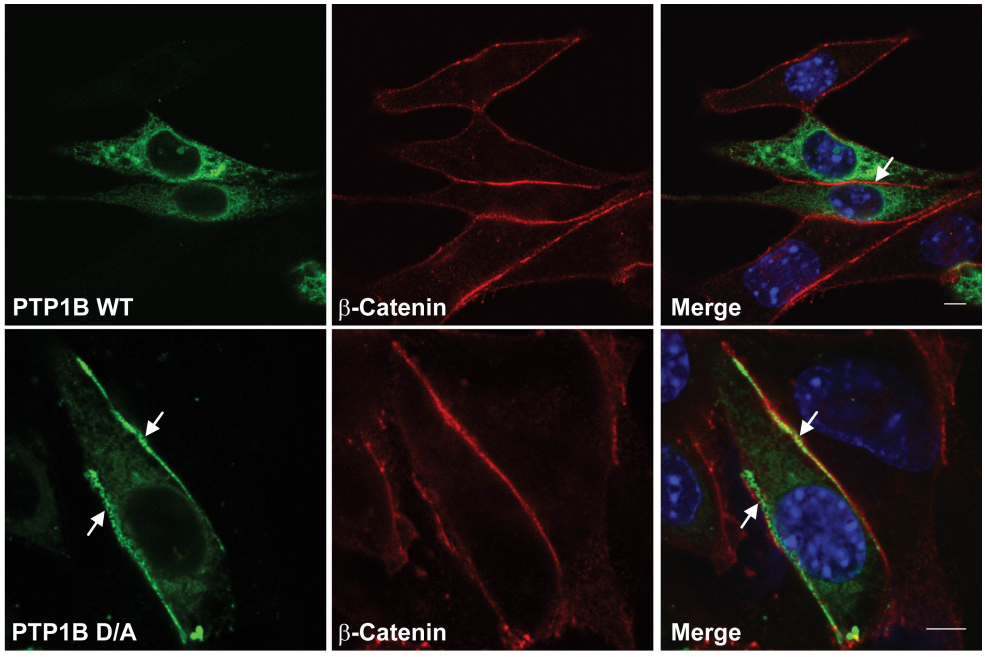

Fig 3.1 PTP1B localizes to regions of cell-cell contact.
PTP1B-null fibroblasts transiently expressing PTP1B WT-GFP or PTP1B D/A-GFP fixed and stained for β- catenin and DAPI. Regions of cell-cell contact are highlighted with white arrows. Scale bars 5 μm. (reproduced from Haj, Sabet et al. [134]).

3.1.2 The endoplasmic reticulum extends to regions of cell-cell contact

To confirm that the ER can extend to regions of cell-cell contact, mCherry-labeled PTP1B (D/A) was co-expressed in MDCK cells with YFP-labeled general ER marker, stress-related ER protein (SREP) (**Fig. 3.2 (a)**). Co-localization of SREP with cell-cell contact proximal PTP1B (D/A) confirmed that the ER extends out to the plasma membrane at regions of cell-cell contact (**Fig. 3.2 (a), white arrows**). Similar results were obtained when the rough ER marker, Sec61 was co-expressed with PTP1B (D/A) (**Fig. 3.2 (b), white arrows**).

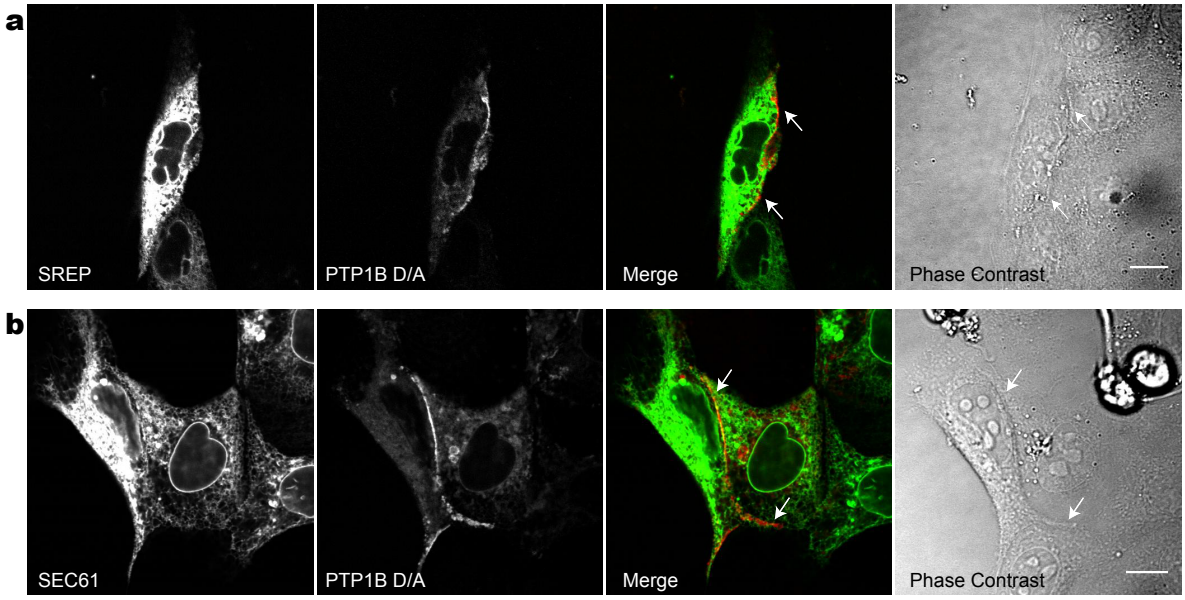

Fig 3.2 The ER is at close proximity to the PM at regions of cell-cell contact
(**a**) MDCK cells coexpressing a general ER marker, stress-related ER protein (SREP-YFP) and PTP1B D/A-mCherry. (**b**) MDCK cells coexpressing a rough ER marker, (Sec61-YFP) and PTP1B D/A-mCherry. White arrows indicate regions of colocalization at points of cell-cell contact. Scale bars 10 μm.

3.1.3 The endoplasmic reticulum is polarized towards regions of cell-cell contact

To investigate the inherent tendency of the ER to polarize towards points of cell-cell contact, and address the possible involvement of PTP1B in this process, we decided to disrupt the ER network. Microtubules (MTs) play a major role in the formation and stabilization of the ER network [201,202], therefore we opted to disrupt MTs using nocodazole. Total internal reflection microscopy (TIRF) was used to monitor ER retraction at cell periphery and at points of cell-cell contact. COS-7 cells were co-transfected with mTFP-calreticulin and RFP-tagged TK-Ras as a general marker for plasma membrane that can account for cell shape changes and mark

points of cell-cell contact (**Fig. 3.3**). Consistent with previous reports, the ER collapsed after nocodazole treatment [203], with the peripheral tubular ER changing into sheet-like structures. The ER retracted from cell periphery, but persisted at points of cell-cell contact (**Fig. 3.3** compare ROI 1 and 2).

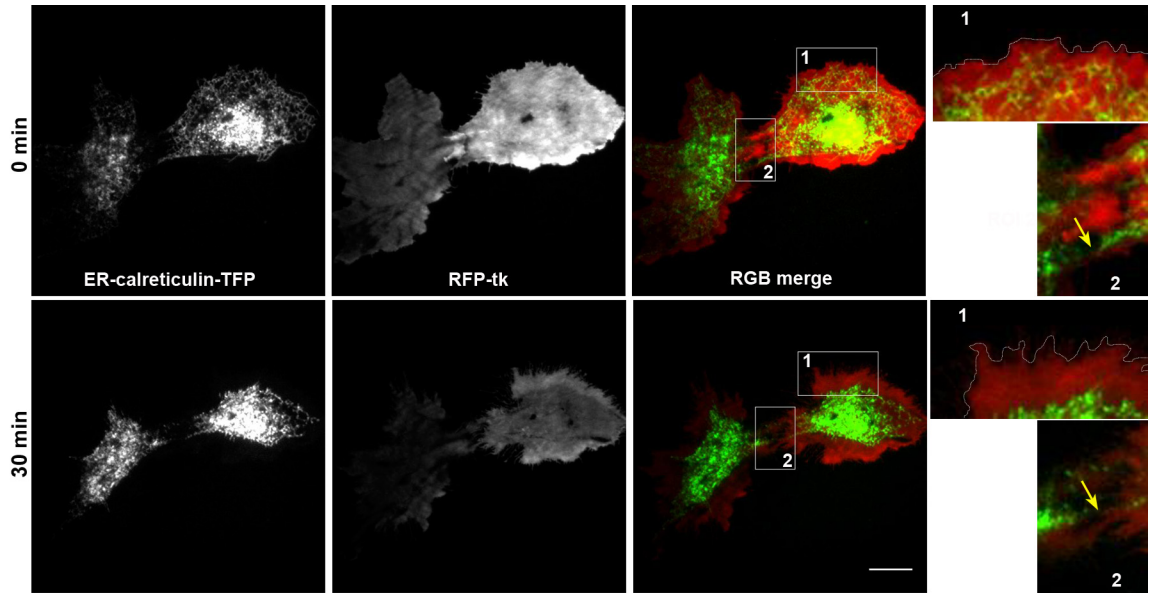

Fig 3.3 Polarity of the ER
COS-7 cells co-expressing calreticulin-mTFP and RFP-tk. Cells were treated with ncodazole (33 μM) and imaged for 30 min using TIRF microscope. Two regions of interest (1) and (2) are highlighted in the merged image and magnified. ROI (1) shows a peripheral region of the plasma membrane to which the ER is reaching out before drug treatment (upper panel) and retracting from which after drug treatment (lower panel). ROI (2) depicts a region of cell-cell contact, where the ER network persists even after drug treatment (yellow arrow). Scale bars 10 μm.

COS-7 cells were co-transfected with mCitrine-wt PTP1B and RFP-tagged TK-Ras as a general marker for plasma membrane (**Fig. 3.4 (A)**) or mCitrine PTP1B (D/A) and RFP-tagged TK-Ras (**Fig. 3.4 (B)**). Here again the ER collapsed after nocodazole treatment, with the peripheral tubular ER changing into sheet-like structures. The ER retracted from cell periphery, but persisted at points of cell-cell contact (**Fig. 3.4 (A)** compare ROI 1 and 2). The degree of ER reorganization varied between experiments depending on cell shape, type and confluence. In isolated cells expressing the substrate trapping mutant of PTP1B, the ER retracted only partially after nocodazole treatment, leaving behind long stretches of tubular ER left attached to the plasma membrane probably at sites of cell attachment to the glass coverslip (focal adhesions) (**Fig 3.4 (B)** white arrows).

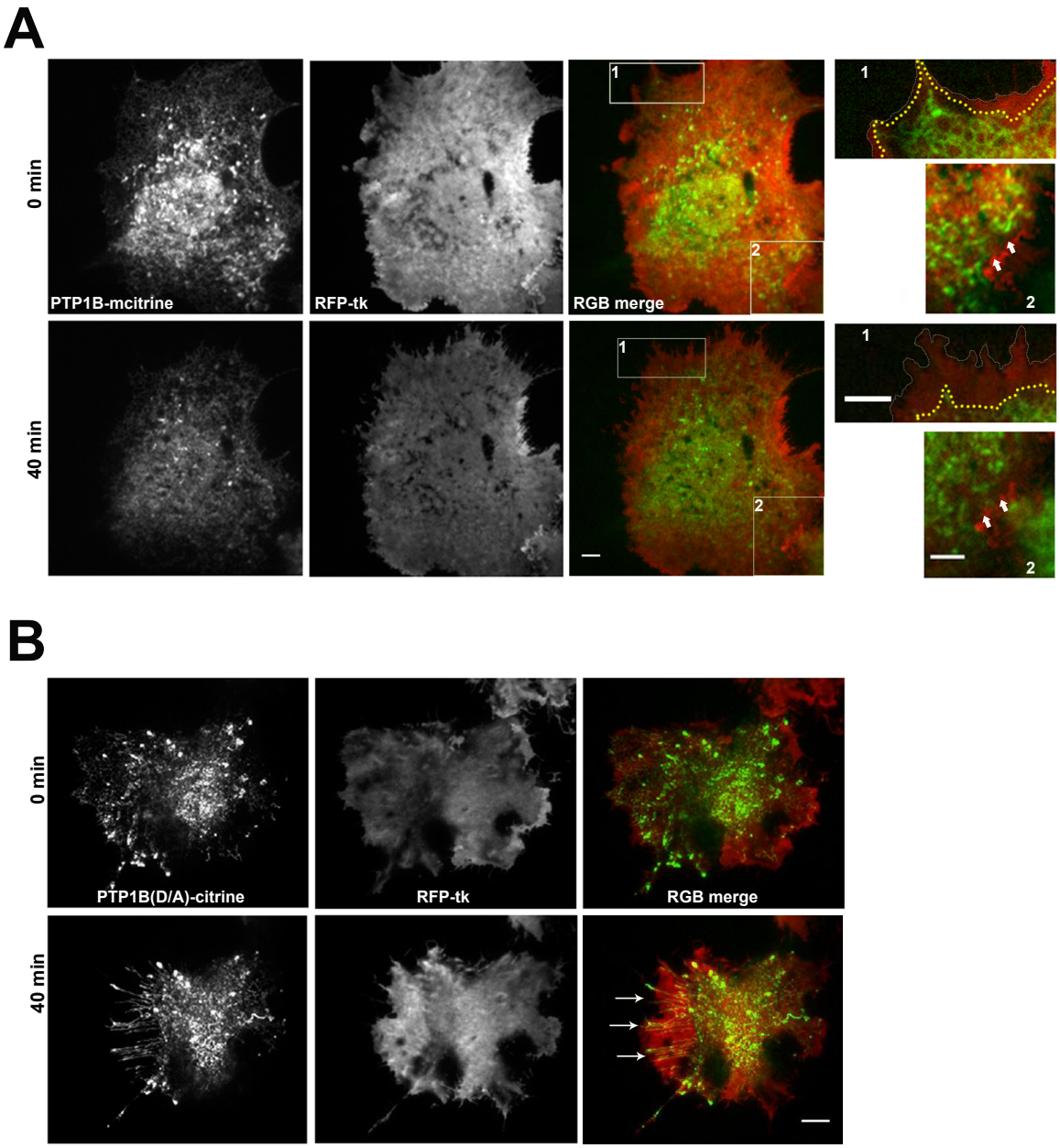

Fig 3.4 PTP1B and the intrinsic polarity of the ER
(**A**) COS-7 cells co-expressing PTP1B WT-mCitrine and RFP-TK. Cells were treated with nocodazole (33 μM) and imaged for 40 min using TIRF microscope. Two regions of interest (1) and (2) are highlighted in the merged image and magnified. ROI (1) shows a peripheral region of the plasma membrane to which the ER is reaching out before drug treatment (upper panel) and retracting from which after drug treatment (lower panel). ROI (2) depicts a region of cell-cell contact, where the ER network persists even after drug treatment (white arrow). The PM outline is traced in white and the ER outline is traced in yellow, to facilitate the observation of ER retraction relative to PM. (**B**) COS-7 cells co-expressing PTP1B D/A-mCitrine and RFP-tk were treated with nocodazole (33 μM) and imaged for 40 min using TIRF microscope. In the lower right panel, white arrows indicate the long stretches of ER left behind attached to sites of adhesion to the glass coverslip following drug treatment. This was only observed in the case of cells overexpressing PTP1B D/A. All scale bars 10 μm.

3.1.4 PTP1B-substrate interactions do not by themselves stabilize the polarity of ER to regions of cell-cell contact

The previous findings raised the possibility that the //interactions// of PTP1B with cell-contact based substrates might have a role in polarizing the ER towards these points. Competing out endogenous PTP1B from its interaction with substrates using an overexpressed cytosolic catalytic domain of PTP1B D/A (PTP1B D/A CD) should allow the ER to retract from points of cell-cell contact after nocodazole treatment if this was the case. MDCK cells were co-transfected with PTP1B D/A-CD-mCitrine, mTFP-calreticulin, RFP-TK and unlabeled EGFR. Following starvation, cells were stimulated with EGF (100ng/ml) for 5 minutes to enhance phosphorylation of EGFR and thereby recruitment of PTP1B (D/A)-CD to its substrates and then cells were treated with nocodazole. Similar peripheral ER retraction was observed, with no apparent retraction of ER from regions of cell-cell contact (**Fig 3.5**). To evaluate whether the expression of PTP1B (D/A)-CD was high enough at regions of point of cell-cell contact, fluorescence correlation spectroscopy (FCS) was used. FCS was used to correlate image intensity of cytoplasmic PTP1B (D/A)-CD to its absolute concentration across the cells [204]. A linear fit to this correlation allowed for the estimation of PTP1B (D/A)-CD at points of cell-cell contact (by extrapolation) to be ~ 9 μM. At areas close to points of cell-cell contact, PTP1B (D/A)-CD concentration remained in the μM range, which is comparable to K_D values previously calculated for PTP1B (D/A)-substrate interactions [205]. This means that in principle, PTP1B (D/A)-CD should be able to compete with endogenous PTP1B for substrates at regions of cell-cell contact.

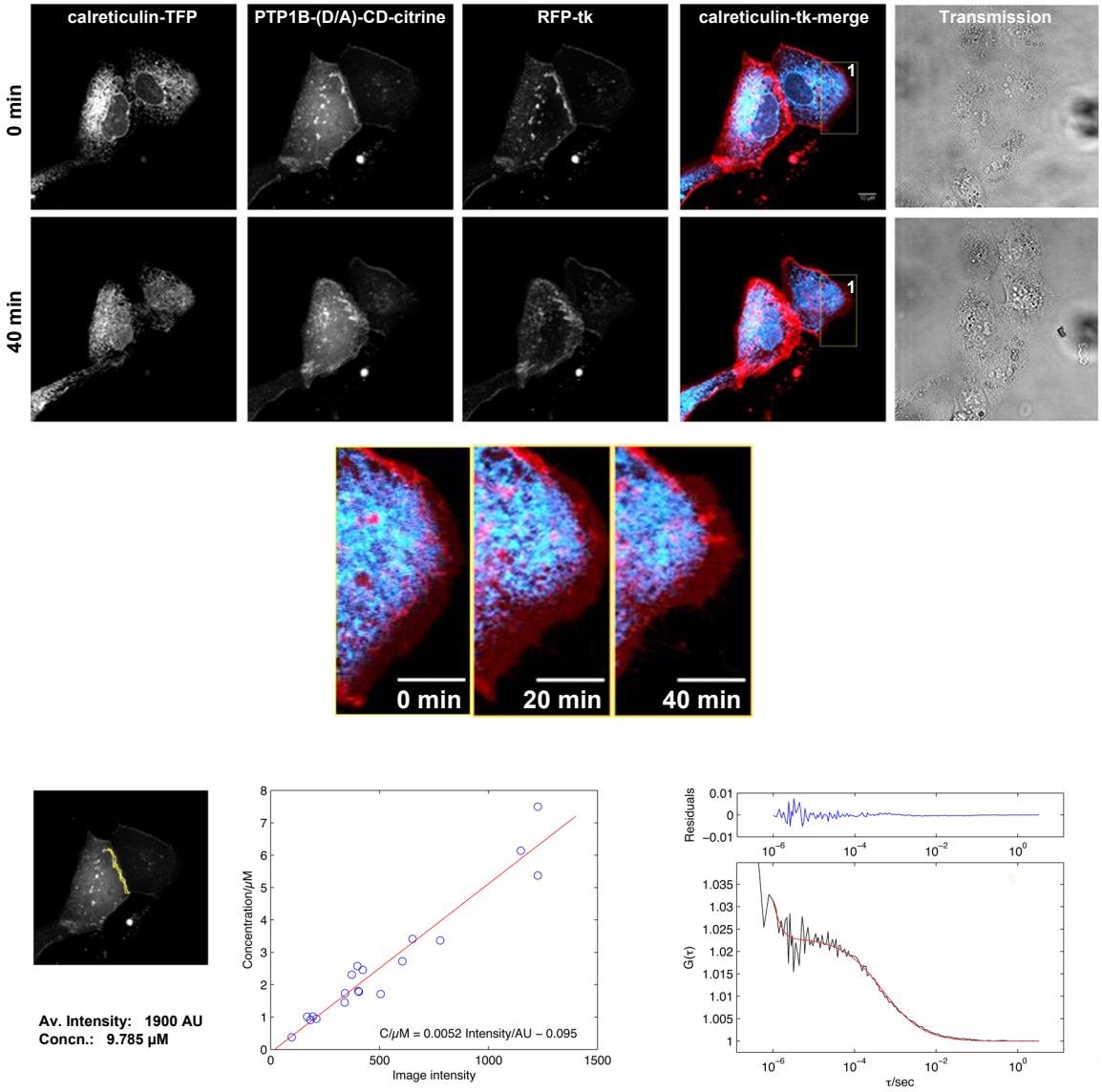

Fig 3.5 PTP1B substrate competition cannot destabilize the ER at of cell-cell contact
MDCK cells co-expressing calreticulin-TFP, PTP1B D/A-CD-mCitrine and RFP-TK. Cells were treated with ncodazole (33 μM) and imaged for 40 min using confocal microscope. ROI (1) highlighted in the merged image is magnified for three time points (0, 20 and 40 min) to show peripheral retraction of ER post drug treatment. Lower left image shows calculated concentration of PTP1B (D/A)-CD at cell-contact region (yellow line) based on the fluorescence calibrated imaging. Lower middle graph is a correlation of the average image intensity of PTP1B D/A-CD measured in the cytoplasm to the absolute concentration as measured from FCS graphs. A linear fit (red line) returned the calibration function used late to calculate absolute concentrations from image intensities. Lower right graph is an example of an auto-correlation G (τ) curve of PTP1B D/A-CD-mCitrine (black line) fit by a model for anomalous diffusion and triplet term (red line). All scale bars correspond to 10 μm.

Being ER-anchored (2D), endogenous PTP1B has a "geometric" advantage in its search for substrates, thereby invalidating arguments about K_D, which assumes 3D search for substrates. To overcome the high (2D) concentration of endogenous PTP1B, additional competition experiments were done with a PTP1B chimera, which lacks its natural ER anchor, but has a C-terminal CAAX box sequence from KRas (TK) to anchor it to plasma membrane (PTP1B D/A-RFP-TK). The hypothesis was that anchoring PTP1B (D/A) to the PM should give it a similar geometric advantage to endogenous ER-anchored PTP1B. Expression of PTP1B D/A-RFP-TK with TFP-calreticulin and unlabeled EGFR followed by nocodazole treatment was performed as previously described. Nevertheless, the ER did not retract from regions of cell-cell contact post drug treatment (**Fig 3.6**). Taken together, these experiments indicate that PTP1B-substrate interactions stand-alone cannot account for ER polarization at points of cell-cell contact. PTP1B might not be the reason for intrinsic ER polarity towards these regions, but the ER polarity might still have a functional significance for the spatial organization of PTP1B activity.

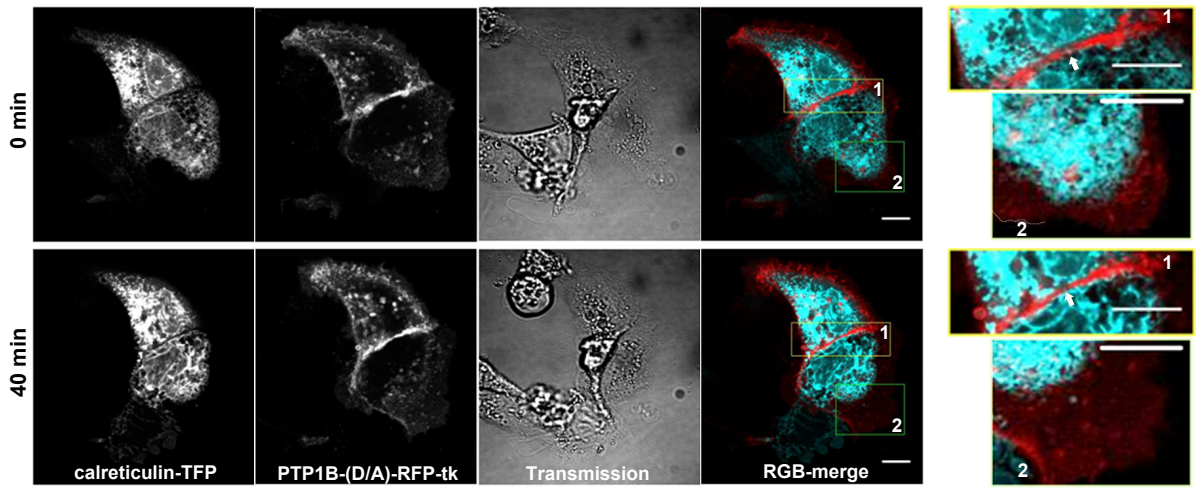

Fig 3.6 PTP1B D/A-RFP-TK cannot compete out endogenous PTP1B
MDCK cells co-expressing calreticulin-TFP, PTP1B D/A-RFP-TK and unlabeled EGFR were treated with nocodazole (33 μM) and imaged for 40 min using confocal microscope. Two ROIs are highlighted in the merged image, ROI (1) shows a region of cell-cell contact and ROI (2) shows a peripheral region of the cell. Drug treatment increases the distance between peripheral plasma membrane and ER as seen in ROI (2), while the ER stays unchanged at regions of cell-cell contact as seen in ROI (1). All scale bars =10 μm.

3.1.5 Regulation of signaling at regions of cell-cell contact by PTP1B

The above observations raised the possibility that PTP1B may play a significant role in the regulation of signaling at points of cell-cell contact. To test this hypothesis, the effect of PTP1B specific inhibition on phosphorylation of cell-cell contact based substrates was tested. COS-7 cells were co-transfected with EphA2-mCherry, a closely related member to the recently described substrate of PTP1B, EphA3 [133]. Tyrosine phosphorylation of EphA2 was monitored using YFP fused to SH2 domain of $pp60^{src}$ (dSH2-YFP) [185]. Cells were treated with an allosteric PTP1B inhibitor [206], that show higher selectivity when compared to active site inhibitors, and monitored after 1 hour of incubation with drug (**Fig. 3.7 a/b v,vi,vii**). Prior to PTP1B inhibition, EphA2 showed typical membrane distribution of a RTK, with occasional accumulation at points of cell-cell contact (**Fig 3.7 a/b, ii**). dSH2-YFP localized to the nucleus, punctuate clusters surrounding the cell typical of focal adhesions (**Fig.3.7 a iii**) and in some instances at regions of cell-cell contact (**Fig 3.7 b iii, yellow arrowheads**). Minimal co-localization was observed between dSH2-YFP and EphA2-mcherry prior to inhibition, even at regions of cell-cell contact (**Fig. 3.7 a/b iv cyan arrowheads**). After 1hr of PTP1B inhibition, the extent of co-localization was higher, especially at points of cell-cell contact (**Fig. 3.7 a/b vii**). The enhanced tyrosine phosphorylation of EphA2 upon PTP1B inhibition indicates that EphA2 is a novel PTP1B substrate at points of cell-cell contact. The above findings show that the ER-anchored PTP1B, by virtue of the intrinsic polarization of ER towards points of cell-cell contact, can access and regulate its potential substrates at these regions, in other words, a polarized safeguard mechanism.

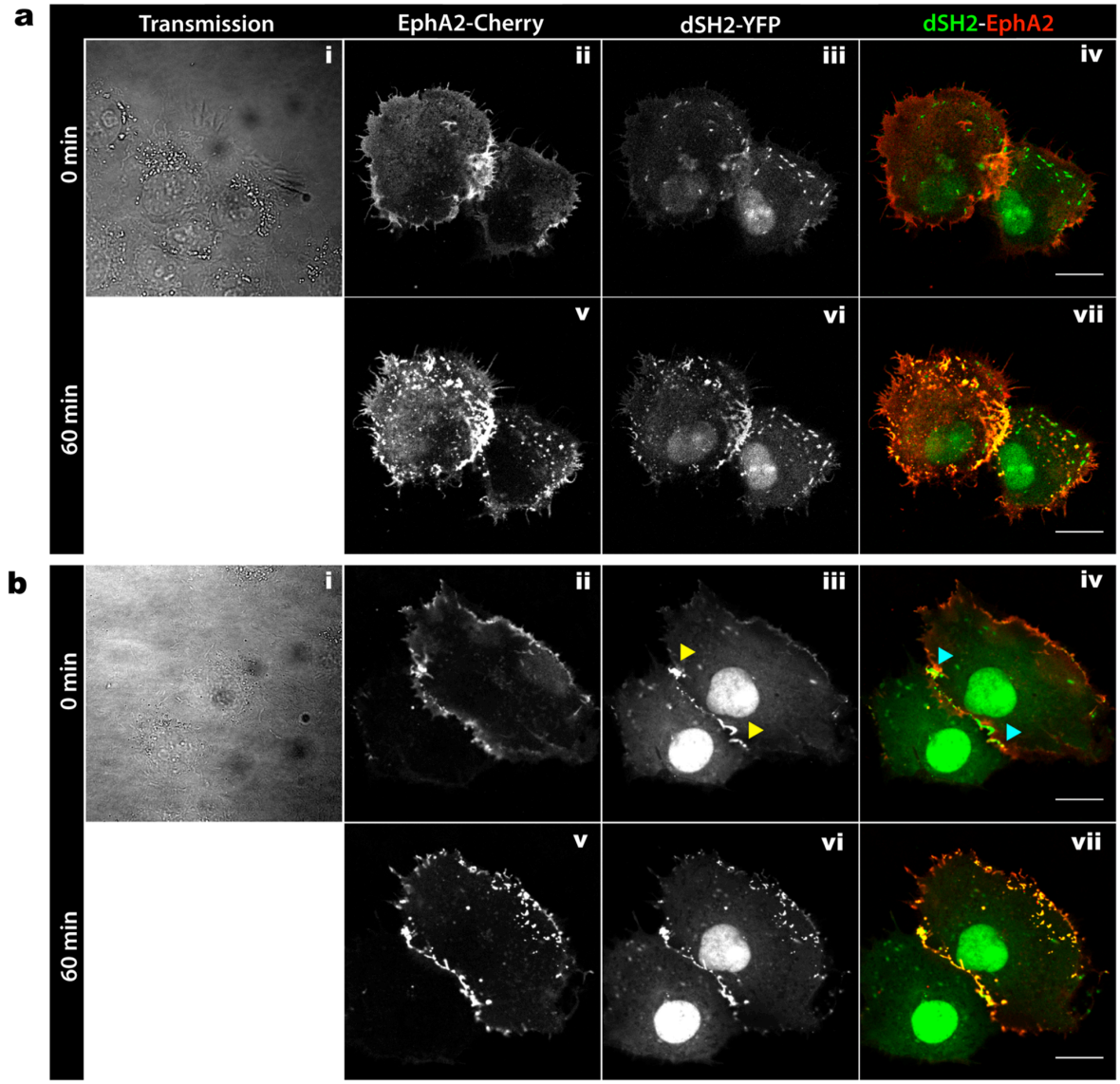

Fig 3.7 PTP1B access specific substrates at cell-cell contacts
(**a,b**) COS-7 cells co-expressing EphA2-mCherry (ii.v) and dSH2-YFP (iii,vi) were incubated with PTP1B allosteric inhibitor (250μM) for 1 hr at 37 °C and imaged using confocal microscope. Transmission images (i) define cell confluency and help define regions of cell-cell contact. Merge images (iv, vii) show the spatial localization of EphA2 (red) and SH2 (green), before (iv) and after (vii) PTP1B inhibitor treatment. Notice the increased co-localization of EphA2 and SH2 at regions of cell-cell contact after inhibitor treatment, indicating increased EphA2 phosphorylation. All scale bars correspond to 20 μm.

3.2 Clustering as the central integrator of Eph signaling

3.2.1 Decision making at Eph/ephrin cell-contact interfaces

Regulation of signaling at points of cell-cell contact can also be addressed from a kinase point of view. The Eph/ephrin signaling system is the center of this study and will therefore be addressed with more detail. The Eph/ephrin system exemplifies opposing tendencies in biology. The same receptor/ligand interaction can either lead to cell-cell repulsion or adhesion depending on the context. To put this into perspective, a co-culture assay was performed with two populations of cells [69,152]. One cell type, (HEK293) is expressing ephrinA5 ligand, and the other cell type (COS-7) is expressing EphA2 receptor. COS-7 cells were transfected with EphA2-mCitrine (**Fig. 3.8 (A) green cells**), HEK293 cells were transfected with mCherry-ephrinA5 (**Fig. 3.8 (A) purple cells**). Three regions of interest (ROIs) were chosen to monitor decision-making at points of Eph/ephrin contact (**Fig. 3.8 (A)).** Three points of Eph/ephrin contact were formed after adding HEK293 cells expressing mCherry-ephrinA5 on top of COS-7 cells expressing EphA2-mCitrine. In the 1st case (**Fig. 3.8 (B) ROI1)**, Eph/ephrin clusters (**white in merged RGBs "3rd row"**), persisted over time without obvious changes. In the second case (**Fig. 3.8 (B) ROI2)**, Eph/ephrin clusters were terminated over time and endocytosed into receptor-expressing cells. The two cells eventually underwent contact-repulsion. In the third case (**Fig. 3.8 (B) ROI3**), Eph/ephrin clusters persisted and even grew larger over time. Taken together, live-cell imaging of Eph/ephrin co-cultures displayed the concept of "opposing tendency of the system at points of cell-cell contact. The same receptor and ligand interactions can lead to enhanced cell-cell adhesion or cell-repulsion depending on the context.

Fig 3.8 Formation of Eph/ephrin complexes at points of cell-cell contact
(**A**) Co-culture of COS-7 cells expressing EphA2-mCitrine (green) and HEK293 cells expressing mCherry-ephrinA5 (magenta) imaged using confocal microscope. RBD stands for receptor binding domain, LBD stands for ligand binding domain. Three ROIs were monitored with more details during the course of the movie. (**B**) ROI1 in three channels, upper row (ephrinA5), middle row (EphA2) and lower row (merged RGB) depicts no changes in cell-cell contact point with time. ROI2 depicts cell-cell repulsion. ROI3 depicts enhanced adhesion and increased Eph/ephrin cluster formation with time. All scale bars correspond to 20 μm.

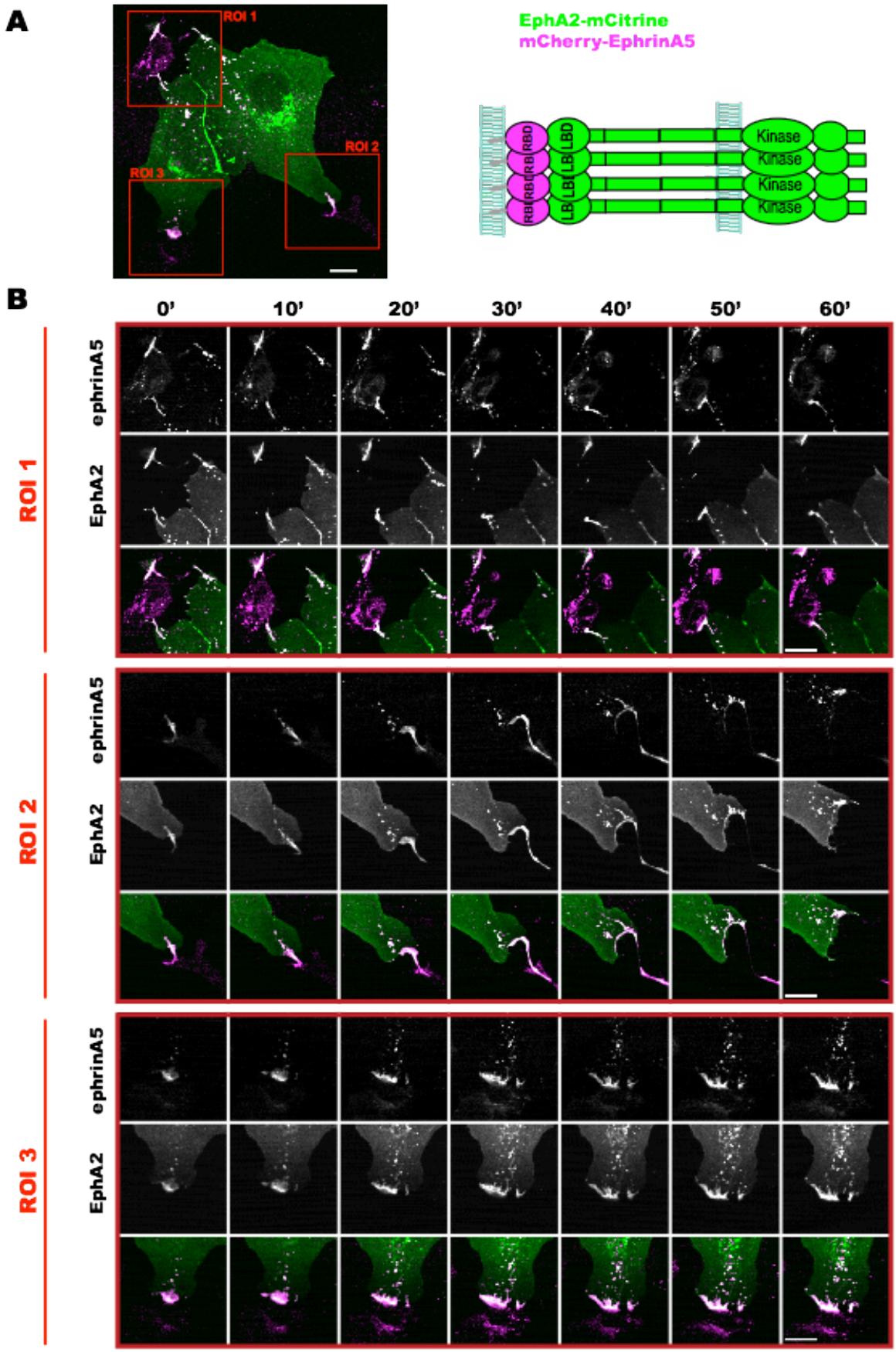
A
ROI 1
ROI 2
ROI 3
EphA2-mCitrine
mCherry-EphrinA5
LBD
RBD
Kinase
B
0'
10'
20'
30'
40'
50'
60'
ROI 1
ROI 2
ROI 3
ephrinA5
EphA2

3.2.2 Generation of a clustering-readout in living cells

Live cell confocal imaging of co-cultures does not offer enough spatial resolution to describe the composition of Eph/ephrin complexes formed at points of cell-cell contact. Contact between ligand- and receptor-expressing cells is random, non-controllable and the outcome cannot be predicted beforehand. To visualize clustering directly and to study its impact on Eph signaling, a dimerizer-induced system of Eph/ephrin clustering was generated in the laboratory of Ruediger Klein (Max Plank Institute for Neurobiology). The approach was based on the ARGENT® Regulated Homo (Hetero) dimerization kit from Ariad Pharmaceuticals. Cloning, optimization and biochemical characterization of the different clones was done by Dr. Andreas Schaupp. In principle either no, 1, 2 or 3 FKBP domains were inserted downstream of the transmembrane (TM) domain of murine EphB2 (**Fig. 3.9**). Keeping the extracellular intact meant that the chimeras were still sensitive to physiological ephrin stimulation, but the FKBP domains allowed for controlled clustering initiation with the high affinity homodimerizer AP20187 or the low affinity homodimerizer AP1887 when needed.

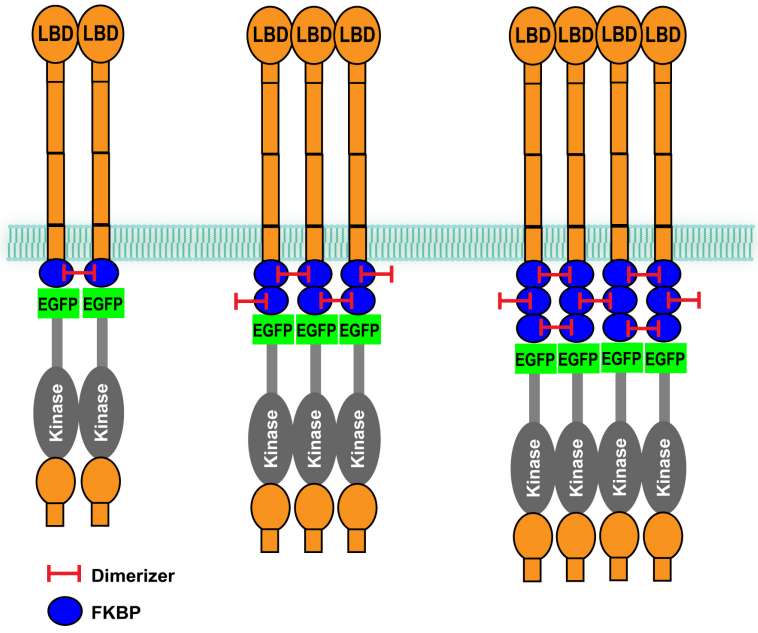

Fig 3.9 Generation of a synthetic dimerizer-induced, Eph clustering system
Schematic representation of Eph receptors showing sites of insertion of 1-3 FKBPs. Receptors are tagged with a fluorescent protein (in that case monomeric EGFP) in the cytoplasmic tail, downstream of the transmembrane (TM) domain. Model predicts outcome of homodimerizer-dependent receptor clustering of 1-3 FKBP chimeras. High-affinity homodimerizer AP20187 (IC_{50}= 1.8 nM) or low-affinity dimerizer AP1887 (IC_{50}= 40nM) non-covalently crosslink the different FKBP domains of adjacent Eph receptors. LBD: ligand binding domain.

3.2.3 Imaging EphB2 cluster populations

Theoretically speaking, the more the number of FKBP domains inserted in a receptor, the higher-order cluster that can be formed. To test this hypothesis, homo-FRET was measured with fluorescence anisotropy using widefield microscopy. Homo-FRET involves non-radiative transfer of energy between similar FPs (in this case EGFP) at nanometer distances and leads to a decrease in the fluorophore's steady-state anisotropy [193]. Basal steady-state anisotropy values of all FKBP isoforms prior to dimerization was similar over different fluorescence intensities except at very low fluorescence signals, where anisotropy tailed off due to background noise (**Fig 3.10 (B)**). Addition of AP20187 dimerizer to cells decreased anisotropoy of all FKBP isoforms in a manner correlating with number of FKBP domain insertions due to the extended Förster energy migration within larger clusters of mGFP (**Fig 3.10**). Quantification of anisotropy was done in the peripheral regions of the cell, excluding central regions of the cells where signals would be originating from receptors residing on endo-membranes.

Fig 3.10 Imaging of EphB2 cluster populations
COS-7 cells transiently expressing kinase dead EphB2 carrying different numbers of FKBP domains and fused to mGFP was used for steady-state anisotropy imaging before and after dimerization with 250 nM AP20187. (**A**) Fluorescence and Anisotropy images of representative cells pre- and 20 min post-stimulation with AP20187 are shown. Anisotropy values decrease with increasing numbers of FKBP domains indicating a higher degree of homo-FRET/clustering. Scale bars in anisotropy panels: 10 μm. The color scale of anisotropy images is shown on the bottom. (**B**) Anisotropy plots of pre- and post-stimulation of 0 to 3 FKBP isoforms. Data represent mean anisotropy ± SEM of n=57, 28, 22 and 20 cells for 3FKBP, 2FKBP, 1FKBP and 0FKBP. Post-stimulation curves of 0-3FKBP are all significantly different from each other and controls. (0/1FKBP, 0/2FKBP, 0/3FKBP, 1/3FKBP, 2/3FKBP: $p < 0.001$; 1/2FKBP: $p < 0.01$; Mann-Whitney nonparametric test).

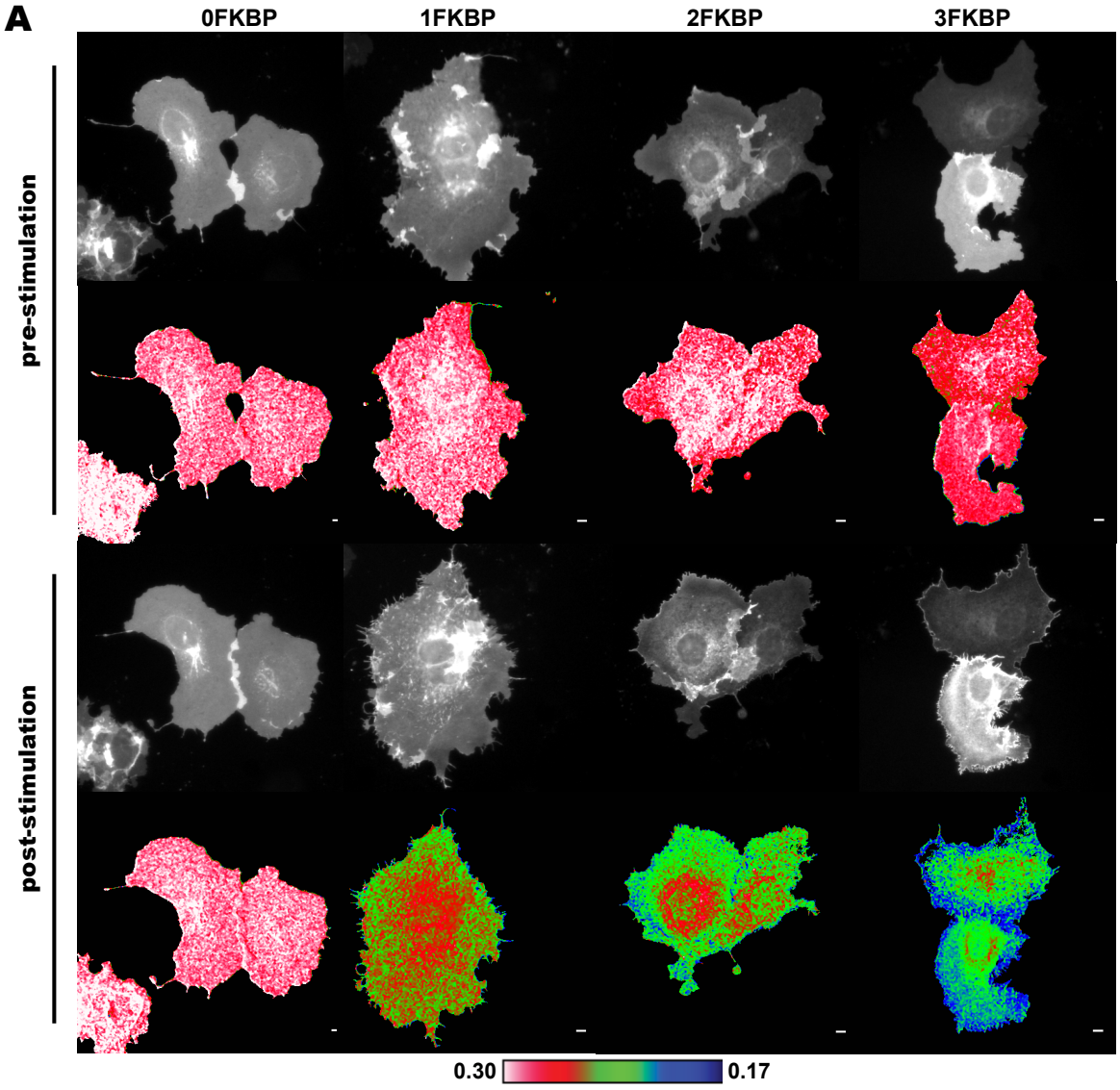

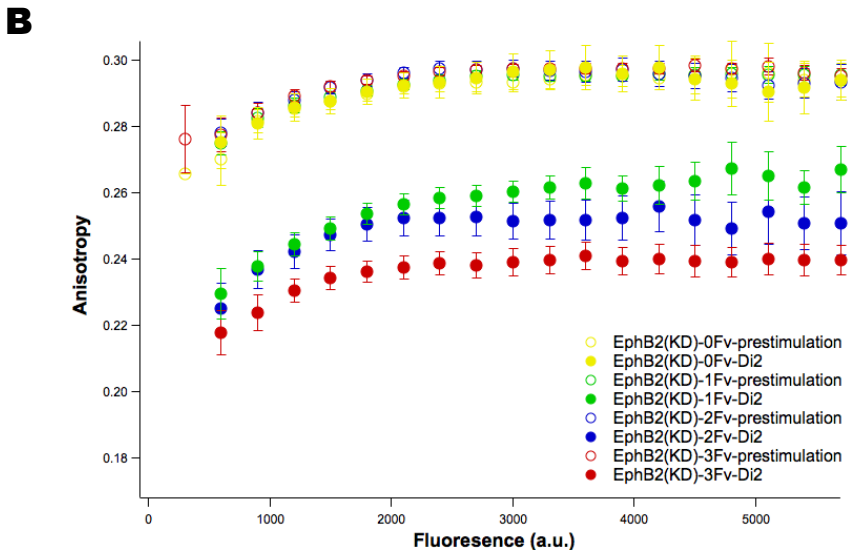

Significance level (0.05)

	0-Fv	1-Fv	2-Fv	3-Fv
0-Fv		***	***	***
1-Fv			**	***
2-Fv				***

We backed up our graded clustering response detected by anisotropy microscopy with blue-native polyacrylamide gel electrophoresis (**Fig. 3.11 (A**)). Following transient expression of the different FKBP-EphB2 constructs in COS-7 cells and dimerization with AP20187, EphB2 clusters were resolved with blue-native PAGE and blotted with anti-EphB. FKBP and FP insertions did not affect signaling the properties of EphB2 upon stimulation with clustered ligand as seen in *auto*phosphorylation blots, cell collapse assays and internalization kinetics (data not shown). Blue-native PAGE gels showed that upon dimerization with AP20187, the 1FKBP isoform formed dimers with residual amounts of monomers. Dimerization of the 2FKBP isoform resulted in the formation of oligomers, primarily trimers, with dimers still present and no residual monomers. Dimerization of the 3FKBP isoform formed large oligomers with no apparent residual dimers or monomers (**Fig. 3.11** (**A**)). The relative contribution of monomers, dimers and multimers in each FKBP isoform was determined and used later to determine the relative contributions of these different association states to a given anisotropy value. 2D histograms representing the distribution of anisotropy values (at the periphery of cells) for a given FKBP isoform after dimerization were plotted. The molecular brightness of each state was taken into consideration as a weighing factor in computing the relative contribution of each association state to the steady-state anisotropy (**Fig 3.11 (B)**). Three association states and their corresponding anisotropy were thereafter distinguished. All FKBP isoforms had a monomeric state prior to dimerization with an average anisotropy value of A_M ± std. = 0.278 ± 0.009. Dimerization of the 1FKBP isoform, formed the dimeric state with an anisotropy value of A_D ± std. = 0.237± 0.011. Finally, a mixture of oligomeric association states of trimers and higher-order clusters with an anisotropy value of A_O ± std. = 0.218± 0.013 (**Fig 3.11 (B)**). Time-resolved anisotropy changes of the different FKBP isoforms showed a sigmoidal decrease in anisotropy after dimerization (for the 2FKBP and 3FKBP constructs), reaching steady-state after ~ 20 min time series (**Fig 3.11 (C)**).

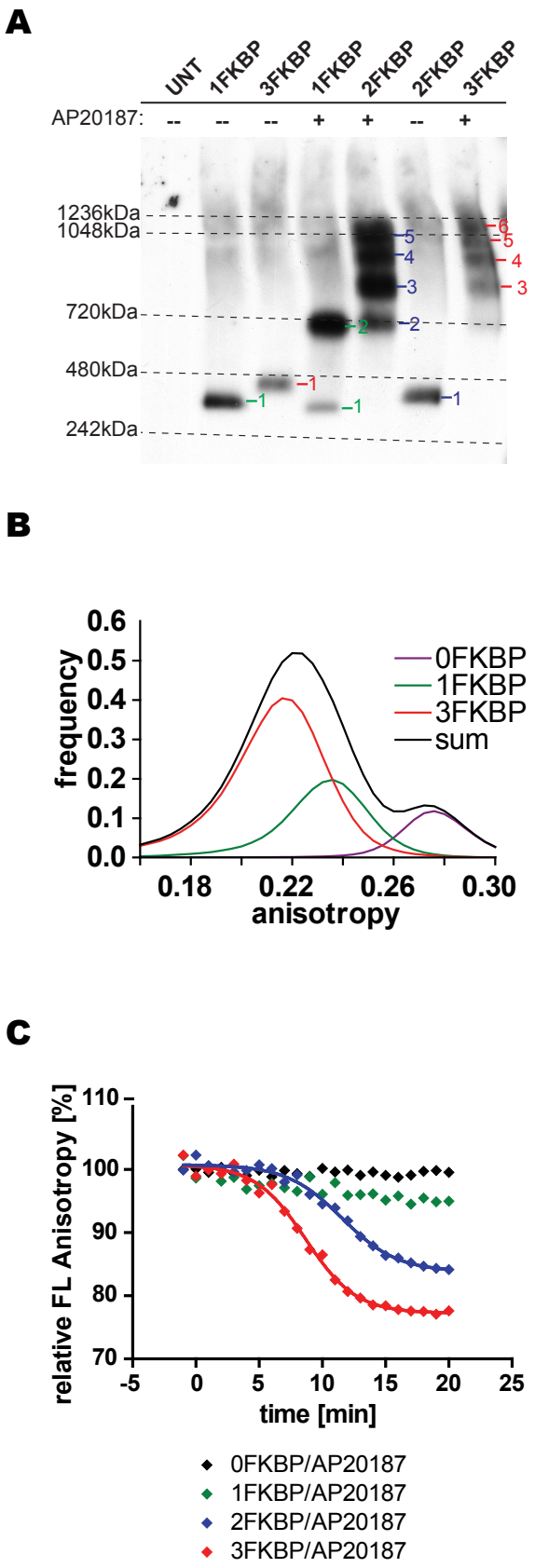

Fig 3.11 Characterization of EphB2 cluster composition
(**A**) Blue-native PAGE gel showing different cluster populations of FKBP isoforms prior to and after dimerization. UNT: untransfected cells. FKBP isoforms of kinase dead EphB2 in the absence of dimerizer migrated as monomeric species. Upon dimerization with AP20187 (250 nm for 20 min) a shift in migration was observed for all FKBP isoforms. 1FKBP, now forms mostly dimers, 2FKBP and 3FKBP forms higher-order clusters. (**B**) Graph shows the intensity-weighted distribution of anisotropy values for the different FKBP association states. Data was extracted from raw eroded (10-15 pixels) anisotropy images in ImageJ, 0FKBP was used to represent monomeric state (purple trace), 1FKBP for the dimeric state (green trace), and 3FKBP for the multimeric state (red trace). Summed anisotropy distributions (black trace) was later used for calculating the contribution of each association state to a given anisotropy value. (**C**) Representative time-lapse anisotropy measurements of the different FKBP isoforms. COS-7 cells were transiently transfected with the indicated FKBP-EphB2 isoforms. Following dimerization with AP20187, a sigmoidal decrease in anisotropy could be observed for 20 min. Fluorescence (FL) anisotropy is plotted as percent relative to predimerization condition and normalized to 0FKBP isoform. Blot was Experiments were done by Dr. A. Schaupp data analysis by O. Sabet (submitted).

We next moved to comparing the artificially controlled cluster populations attained by the dimerizer to the physiological ephrin-induced oligomers. The calculated anisotropy values of monomers, dimers and oligomers from the dimerizer system, were used to estimate the complexity of EphB2 clusters formed at points of cell-cell contact with ephrinB2-expressing ells. COS-7 cells expressing kinase dead EphB2 tagged with mGFP (kdEphB2-mGFP) (**Fig 3.12 (I)**) were co-cultured with HEK293 cells expressing ephrinB2 (tagged with mCherry) (**Fig 3.12 (II)**). Points of cell-cell contact were identified by the colocalization of the two fluorophores (**Fig 3.12 (III)**). Homo-FRET imaging by showed areas of very low anisotropy indicative of higher-order EphB2 clustering (**Fig 3.12 (IV)**). The intensity-weighted distribution of anisotropy values (**Fig 3.11 (B)**) was used to map the cumulative relative contribution of each association state for a given anisotropy value (**Fig 3.12 (V')**). The contribution of each association state was mapped on the anisotropy image of co-cultures of ephrinB2$^+$ and EphB2$^+$ cells (**Fig 3.12 (V'', V''')**), allowing for the identification of areas with multimers, dimers and monomers.

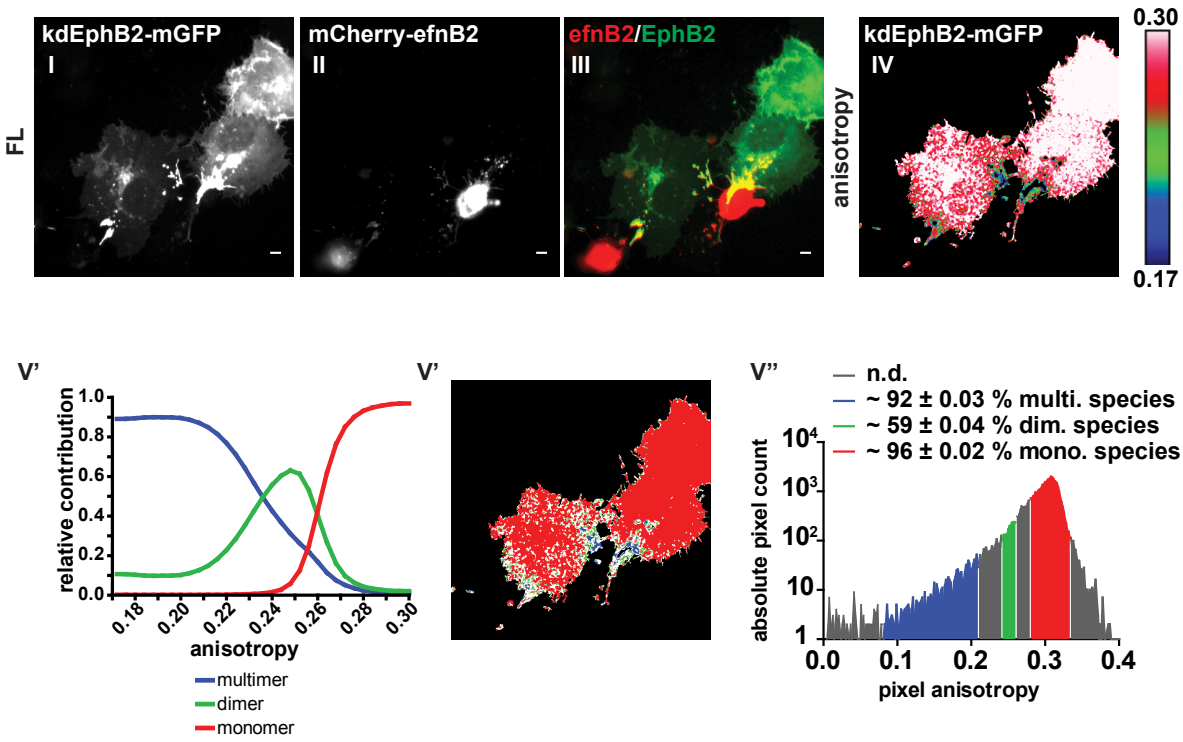

Fig 3.12 Physiological clustering of kdEphB2 upon contact with ephrinB2$^+$ cells
COS-7 cells transfected with kdEphB2-mGFP (**I**) and co-cultured with HEK293 cells stably expressing wild type mCherry-ephrinB2 (**II**). Anisotropy map of clustered kdEphB2-mGFP was determined (**IV**). For calibration of anisotropy values to cluster size distributions the cumulative relative contributions of 0FKBP (monomer), 1FKBP (dimer) and 3FKBP (oligomer) were plotted to the range of anisotropy values on the X-axis (**V'**). Distribution of monomers, dimers and multimers (**V''**) according to the histogram in (**V'''**) is shown.

3.2.4 Correlation between degree of clustering and receptor phosphorylation

To determine the relative contributions of the different EphB2 oligomeric species to receptor *auto*phosphorylation levels, EphB2 constructs without and with the different FKBP insertions (1-3) were separated using blue-native PAGE (**Fig 3.13 A**). Following transient expression of the different FKBP-EphB2 constructs in COS-7 cells and dimerization with AP20187, EphB2 clusters were resolved with blue-native PAGE and blotted with anti-phospho EphB2 antibodies (**Fig. 3.13 (A**)). Blots were stripped and reblotted for total EphB2 to calculate relative phosphorylation of each FKBP isoform ((**Fig. 3.13 (B**)). Quantification of relative phosphorylation levels showed that trimers and larger oligomers were 2-fold more phosphorylated as compared to dimers, with no apparent difference between the 2FKBP and 3FKBP cluster populations.

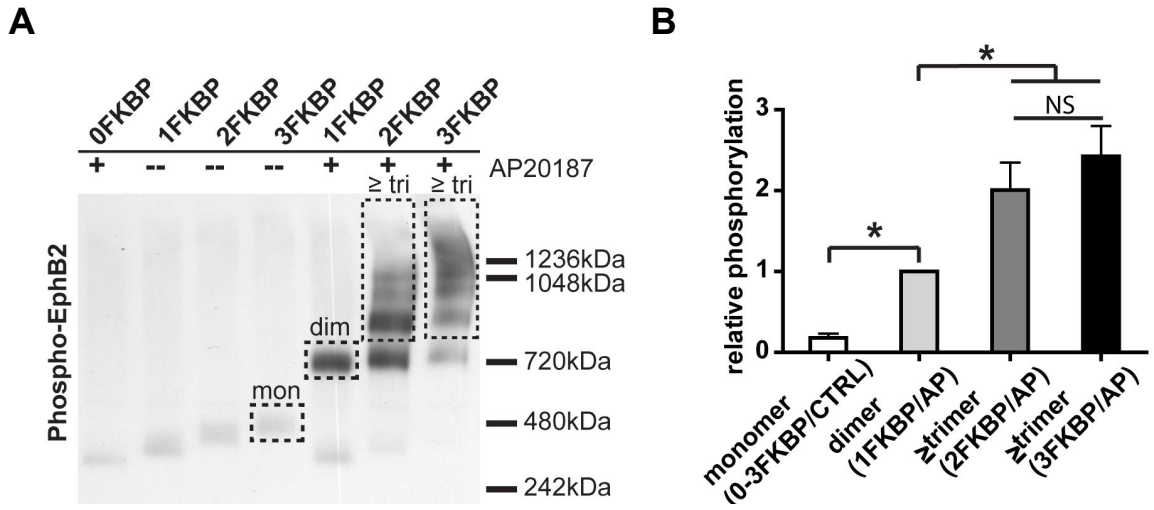

Fig 3.13 Degree of Eph clustering determines receptor activation
(A) Blue-native PAGE of lysates of COS-7 cells expressing different FKBP isoforms of wtEphB2 and stimulated with either vehicle (-) or AP20187 (250 nM for 20 min). Western blot was performed with anti-phospho-EphB2 antibodies; blots were stripped and reblotted for total EphB2 protein, (not shown). The relative phosphorylation levels of single oligomeric species were measured according to example regions outlined by stippled boxes for monomers, dimers and species ≥ trimers. **(B)** Quantitative autophosphorylation analysis of single cluster species displayed as mean ratio ± SEM of phosphorylated versus total EphB2 protein from example regions in (A) from n= 4 blue-native PAGE experiments normalized to dimer species phosphorylation level set to 1.0 (* $p < 0.05$, one-way ANOVA with post-hoc Bonferroni test). All EphB2 monomers (irrespective of the number of FKBP domains present) exhibited only a small fraction of autophosphorylated receptors. EphB2 dimers were hypophosphorylated relative to trimers and species ≥trimers in the 2FKBP and 3FKBP cluster populations. Blots were done by Dr. Andreas Schaupp (submitted).

3.2.5 Intracellular modulation of Eph oligomerization alters response to stimulation

After comparing the link between EphB2 clustering and the resulting signal output, we next asked whether clustering determinants involving the Ephb2 intracellular domain could modulate clustering induced by extracellular ephrins. So we first asked if the multi PDZ domain-containing scaffolding protein GRIP1, a physiological adaptor protein of EphB2 [207], was capable of clustering EphB2. We co-expressed GRIP1-mCherry and wtEphB2-mGFP in COS-7 cells and visualized the degree of EphB2 clustering in living cells by fluorescence anisotropy. In the absence of ephrinB2-Fc, the degree of EphB2 clustering was low, independently of the presence of GRIP1 (**Fig. 3.14 (A)**). Upon addition of unclustered ephrinB2-Fc, EphB2 clustering was induced and this effect was significantly enhanced in cells co-expressing GRIP1 (**Fig. 3.14 (B**)). When we applied the same dose of ephrinB2-Fc to HeLa cell populations expressing wtEphB2-mGFP, we observed both a significantly enhanced cellular collapse response and accelerated rounding kinetics when GRIP1-mCherry was co-expressed (data not shown**)**. Together these results indicate that GRIP1 enhances EphB2 clustering in the presence of extracellular ephrins and further suggest that this enhanced clustering leads to a stronger cell collapse response.

Fig 3.14 GRIP1 enhances EphB2 clustering in response to ephrinB2
(**A**) Steady-state FL anisotropy of ephrinB2-induced EphB2 clusters. COS-7 cells transiently expressing wtEphB2-mGFP with and without GRIP1-mCherry were stimulated with 0.5 μg/ml unclustered ephrinB2-Fc. Anisotropy values of representative cells pre (upper panels) and 20 min post-stimulation (lower panels) with ephrinB2 are shown. Higher-power magnifications from overlayed FL channels and the corresponding EphB2-mGFP anisotropy panels are displayed from regions indicated with numbered boxes to the right. GRIP1 presence in subcellular regions leads to a decrease of FL anisotropy. Scale bars: 10 μM. The color-coding of anisotropy values is shown. (**B**) Quantification of steady-state FL anisotropy plots from (a) pre- and post-stimulation (20 min) with 0.5μg/ml unclustered ephrinB2-Fc. Data represent mean anisotropy ± SEM of n=36 and 45 cells for wtEphB2-mGFP in absence or presence of GRIP1-mCherry, respectively. Post-stimulation curves are significantly different from each other; $p< 0.001$, Mann-Whitney nonparametric test.

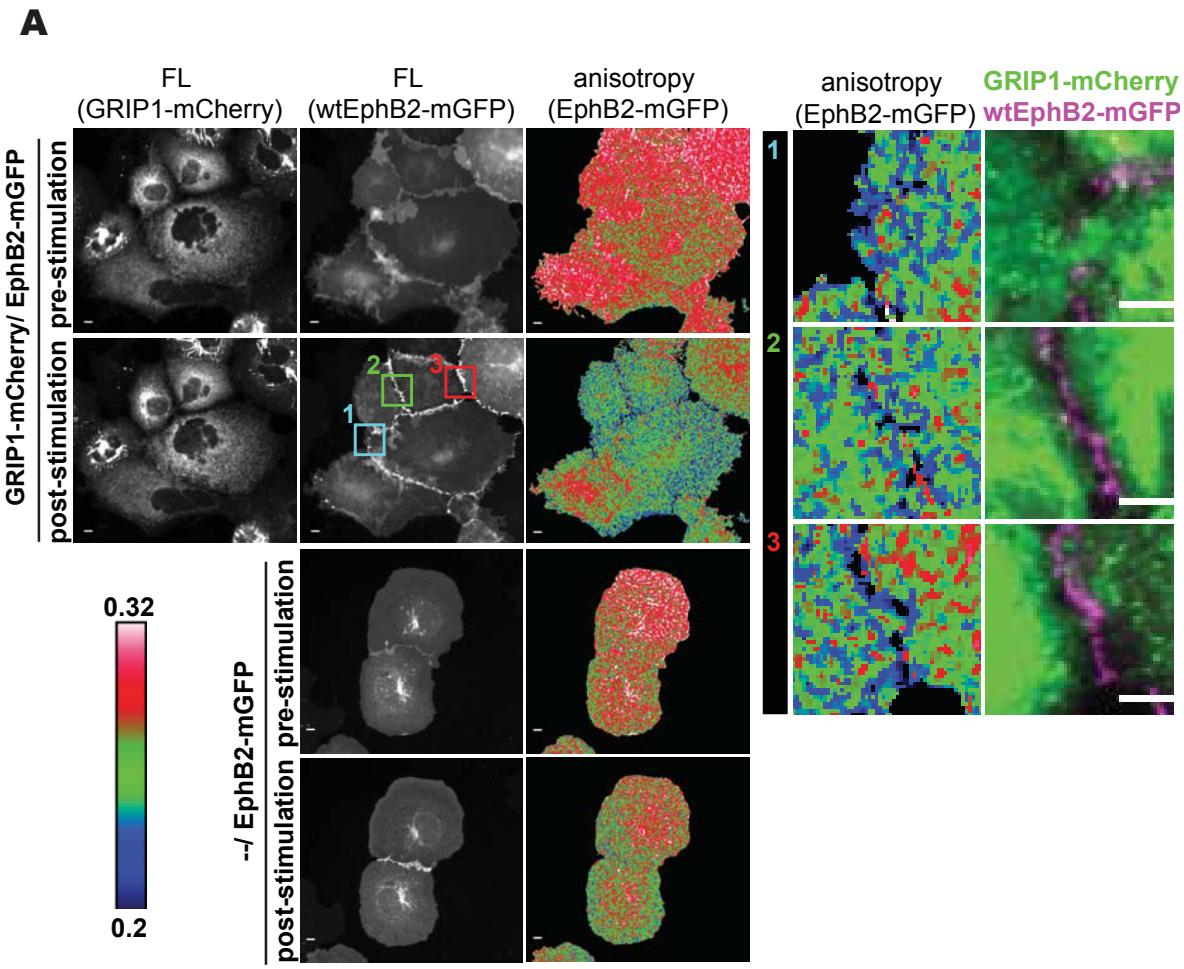
A
FL
(GRIP1-mCherry)
FL
(wtEphB2-mGFP)
anisotropy
(EphB2-mGFP)
anisotropy
(EphB2-mGFP)
GRIP1-mCherry
wtEphB2-mGFP
GRIP1-mCherry/ EphB2-mGFP
pre-stimulation
post-stimulation
1
2
3
0.32
0.2
-/ EphB2-mGFP
pre-stimulation
post-stimulation

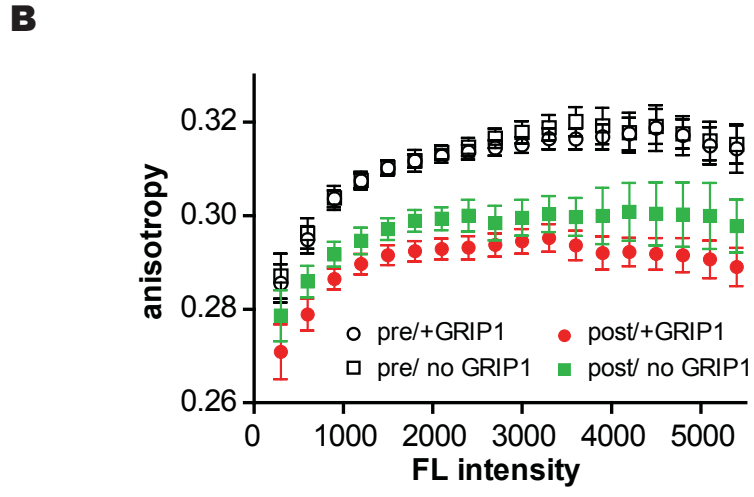
B
anisotropy
0.32
0.30
0.28
0.26
0
1000
2000
3000
4000
5000
FL intensity
pre/+GRIP1
pre/ no GRIP1
post/+GRIP1
post/ no GRIP1

We then asked if the presence of the C-terminal SAM domain and the PDZ-binding motif (PBM) would influence EphB2 clustering. Co-expression of GRIP1-mcherry with an EphB2 deletion mutant lacking both SAM & PBM (EphB2ΔSAM/PBM) did not alter clustering response. Because SAM/PBM may bind other scaffolding or adaptor protein complexes that positively or negatively regulate clustering, we decided to repeat the experiment in the absence of GRIP1. Using fluorescence anisotropy, we compared the clustering propensities of wtEphB2-mGFP to the EphB2ΔSAM/PBM-mGFP in COS-7 cells. At steady state the degree of EphB2 clustering was low in both constructs (**Fig. 3.15 (A), left panels & (B)**). Upon stimulation with unclustered ephrinB2-Fc (500ng), more clustering was observed in cells expressing mutant EphB2ΔSAM/PBM (**Fig. 3.15 (A), right panels & (B)**), suggesting that SAM/PBM negatively influence EphB2 clustering. In line with the increased clustering, EphB2ΔSAM/PBM induced more cell collapse when expressed at comparable levels as wild type EphB2 **(Fig. 3.14 (C), courtesy of Marion Ponsere)**. Moreover, EphB2ΔSAM/PBM showed significantly increased *auto*phosphorylation compared to wild type EphB2 specifically after ephrinB2-Fc stimulation (**Fig. 3.15 (D,E), courtesy of Marion Ponsere)**. Together these results indicate that the intracellular domain of EphB2 significantly influences EphB2 clustering and that SAM domain and PBM have a negative impact on EphB2 clustering.

Fig 3.15 Negative regulatory effect on EphB2 ligand-induced clustering
(**A**) Steady-state FL anisotropy of ephrinB2-induced EphB2 clusters. COS-7 cells transiently expressing wtEphB2-mGFP or EphB2ΔSAM/PBM-mGFP were treated with 0.5 μg/ml unclustered ephrinB2-Fc. Anisotropy values of representative cells pre (left panels) and 20 min post-stimulation (right panels) with ephrinB2 are shown. Deletion of SAM and PBM domains leads to a decrease of FL anisotropy. Scale bars: 10 μM. The color-coding of anisotropy values is shown on the right side. (**B**) Quantification of steady-state FL anisotropy plots from pre- and post-stimulation (20 min) with 0.5μg/ml unclustered ephrinB2-Fc. Data represent mean anisotropy ± SEM of n=35 and 46 cells for wtEphB2-mGFP and EphB2ΔSAM/PBM-mGFP respectively. Post-stimulation curves are significantly different from each other; ***p< 0.001, Mann-Whitney nonparametric test. (**C**) Cell collapse assays done on HeLA cells expressing either wtEphB2 or EphB2ΔSAM/PBM and clustered by equal concentrations (500ng) of unclustered human-Fc fragment or ephrinB2-Fc. Cell assay was quantified by measuring the cell's surface area (Mean cell area ± SEM from n= 25 cells per condition; **** p< 0.0001, *** p< 0.001, ** p< 0.01, * p< 0.05, two-way ANOVA with post Bonferroni test, n= 8 separate experiments). (**D**) Representative Western blots of anti-Flag immunoprecipitated wtEphB2 or EphB2ΔSAM/PBM after treatment with equal concentration of Fc control or ephrinB2-Fc (0.5 μg/ml, t= 20 min) using mouse anti-phospho tyrosine antibody (clone G410); blots were stripped and reblotted for total EphB2 protein levels (mouse anti-FLAG M2 antibody). (**E**) Quantitative analysis of autophosphorylation (** p< 0.01, * p< 0.05, unpaired t-test, n=7 separate experiments). C,D and E are data from experiments done by Marion Ponsere (submitted).

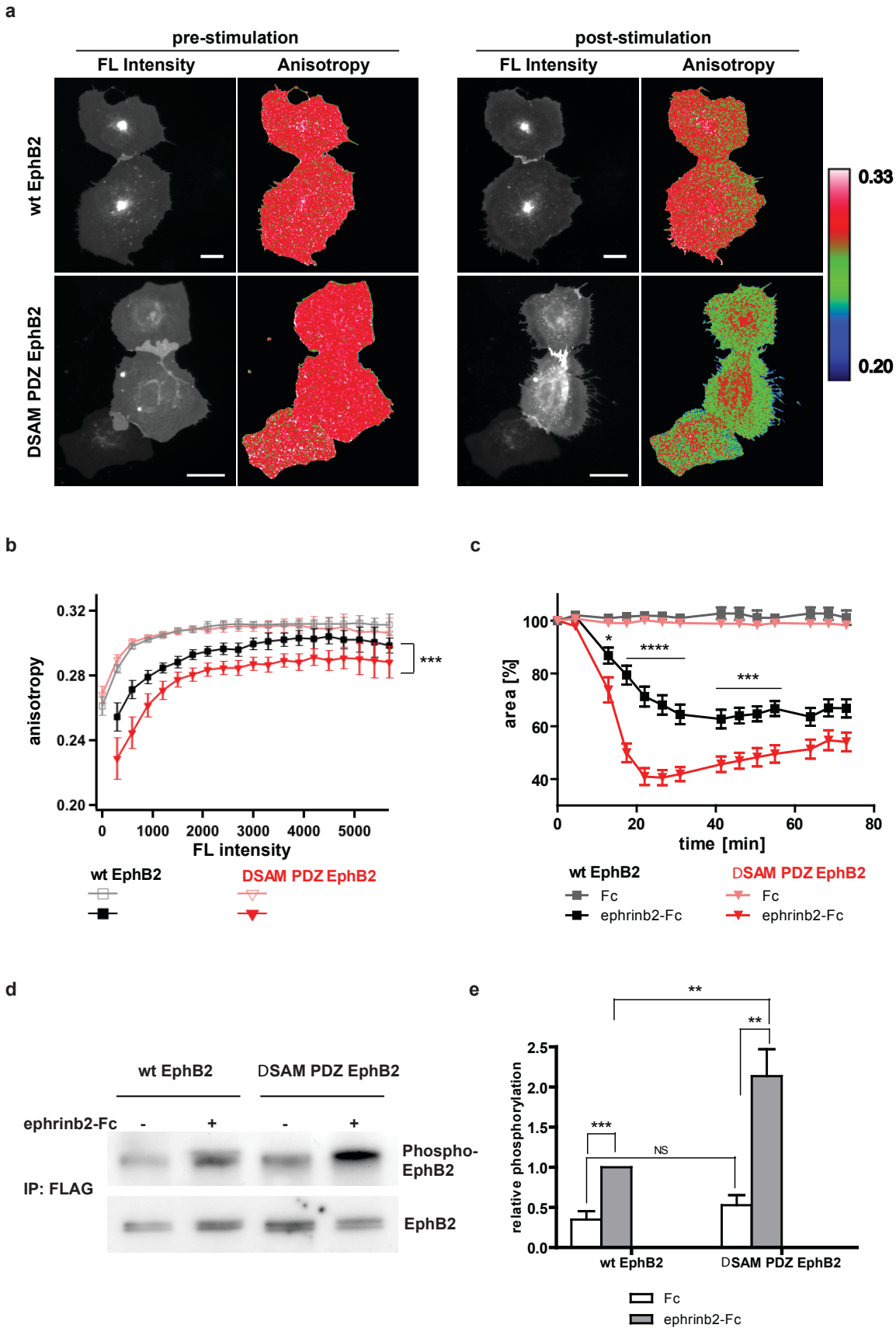
a
pre-stimulation
post-stimulation
FL Intensity
Anisotropy
FL Intensity
Anisotropy
wt EphB2
DSAM PDZ EphB2
0.33
0.20
b
anisotropy
0.32
0.28
0.24
0.20
0
1000
2000
3000
4000
5000
FL intensity
***
wt EphB2
DSAM PDZ EphB2
c
area [%]
100
80
60
40
0
20
40
60
80
time [min]
*
****
***
wt EphB2
Fc
ephrinb2-Fc
DSAM PDZ EphB2
Fc
ephrinb2-Fc
d
wt EphB2
DSAM PDZ EphB2
ephrinb2-Fc
-
+
-
+
IP: FLAG
Phospho-EphB2
EphB2
e
relative phosphorylation
2.5
2.0
1.5
1.0
0.5
0.0
**
**
***
NS
wt EphB2
DSAM PDZ EphB2
Fc
ephrinb2-Fc

3.3 Spatial-temporal regulation of EphA2 activity

3.3.1 Generation of a linker-optimized FRET based activity sensor for EphA2

Activation of Ephs correlates with auto-phosphorylation of two conserved tyrosines (Tyr587 and Tyr593, for EphA2) embedded in a highly conserved ~10-amino acid motif within the JMS, in addition to phosphorylation of the conserved Tyr_{ACT} (Tyr771 in the case of EphA2)[79]. In the crystal structure of murine EphB2, the JMS in its non-phosphorylated form adopts an ordered α-helical conformation that hinders the kinase domain from adopting an ordered, active structure. As a whole, the *auto*inhibited EphB2 kinase domain adopts a closed conformation that superficially resembles an active state. Because activation of Ephs is coupled to conformational change that leads to release of JMS *auto*inhibition, we previously we developed a 2-component FRET based imaging approach that is sensitive to the distance between the EphA3-C terminus and the PM. The use of a membrane-targeted acceptor fluorophore (FP), tkRas-RFP allowed use to measure FRET with EphA3-GFP as a change in GFP (donor) fluorescence lifetime, measured by time correlated single photon counting (TCSPC)-FLIM. Using this system, we showed that activation of EphA3 moves the kinase domain away from the PM [145]. However, this approach was limited in space and time, considering the rapid endocytosis occurring upon stimulation, that moves the receptor away from the membrane-restricted acceptor FP. In addition, whether the observed *auto*inhibited structure would be oriented in a certain fashion with respect to the inner surface of the membrane is impossible to extrapolate considering the lengthy sequence between the PM and the start of strand Ex1 [83].

This work formed the basis for designing a genetically encoded EphA2 intramolecular biosensor to study the spatial regulation of the *auto*catalytic activation mechanism of Eph receptors in living cells. The EphA2 biosensor is designed to report on the conformational changes taking place upon full Eph activation by phosphorylation, as a change in distance and/or orientation of two FPs in frame with the receptor. Changes in FRET are then measured by TCSPC-FLIM as a change in donor fluorescence lifetime. A stretch of (10) amino acids below the TM domain and away from the JMS conserved motif were chosen to screen for viable insertion points of the donor FP (**Fig. 3.16 (A)**). Insertion of the donor FP was optimized by using different sets of linkers that range in flexibility from being completely unstructured (amino acid sequence: NLSSDSSNS) [208], Beta-

sheet forming linker (amino acid sequence: KLRTDIKVV, from accession no.: 1A26), coiled-coil linker (amino acid sequence: LAAAYSSILSS, from accession no.: 1FB1) or a coiled-coil linker combined with a short flexible linker (amino acid sequence: LAAAYSSILSSNLSSDS). Several types of FPs were also tested for JMS insertion including: monomeric citrine (mCit), monomeric teal FP (mTFP) and circularly permuted variants of GFP (cp51, cp157 or cp173) [209] . Chimeras that were mislocalized inside cells, showed diminished *auto*phorphorylation (**Fig. 3.16 (B)),** or showed a low dynamic range in FRET experiments were eliminated from further experiments. In all cases, the acceptor FP was appended in-frame to the EphA2 C-terminus. We tested two FRET pairs: mCitrine, as an acceptor for mTFP or mCherry, as an acceptor for mCtirine. TCSPC-FLIM was then used to identify a functional sensor construct with high dynamic range. From all the constructs that were tested, the coiled-coil + flexible linker (CCL) chimera exhibited an optimal localization, *auto*phosphorylation, expression level and dynamic range and was therefore chosen for further experiments in living cells (**Fig. 3.17 (A))**. Ectopic expression of either the EphA2ccl mCit/mCherry FRET pair (**Fig. 3.17 (A), upper panels)**, or mTFP/mCit FRET pair (**Fig. 3.17 (A), lower panels)** showed a basal FRET signal as compared to the respective donor-only samples (**Fig. 3.17 (A), right side)**. As compared to a uniform distribution of fluorescence (FL) lifetime values in donor only samples, EphA2ccl FL lifetime (τ) decreased at points of cell-cell contact (**Fig. 3.17 (A), white arrow**) and increased towards the interior of the cell. To confirm that the observed drop in FL lifetime was due to FRET, an acceptor photo-bleaching experiment was undertaken using the EphA2ccl mCit/mCherry FRET pair which from now onwards will be dubbed as the **L**inker-optimized **I**ntramolecular **F**RET based activity sensor for **E**ph**A2** (LIFEA2). Bleaching of mCherry in living cells increased mCitrine FL lifetime (*τ*) back to donor only values, thereby confirming that the drop in FL lifetime was due to FRET (**Fig. 3.17 (B)).**

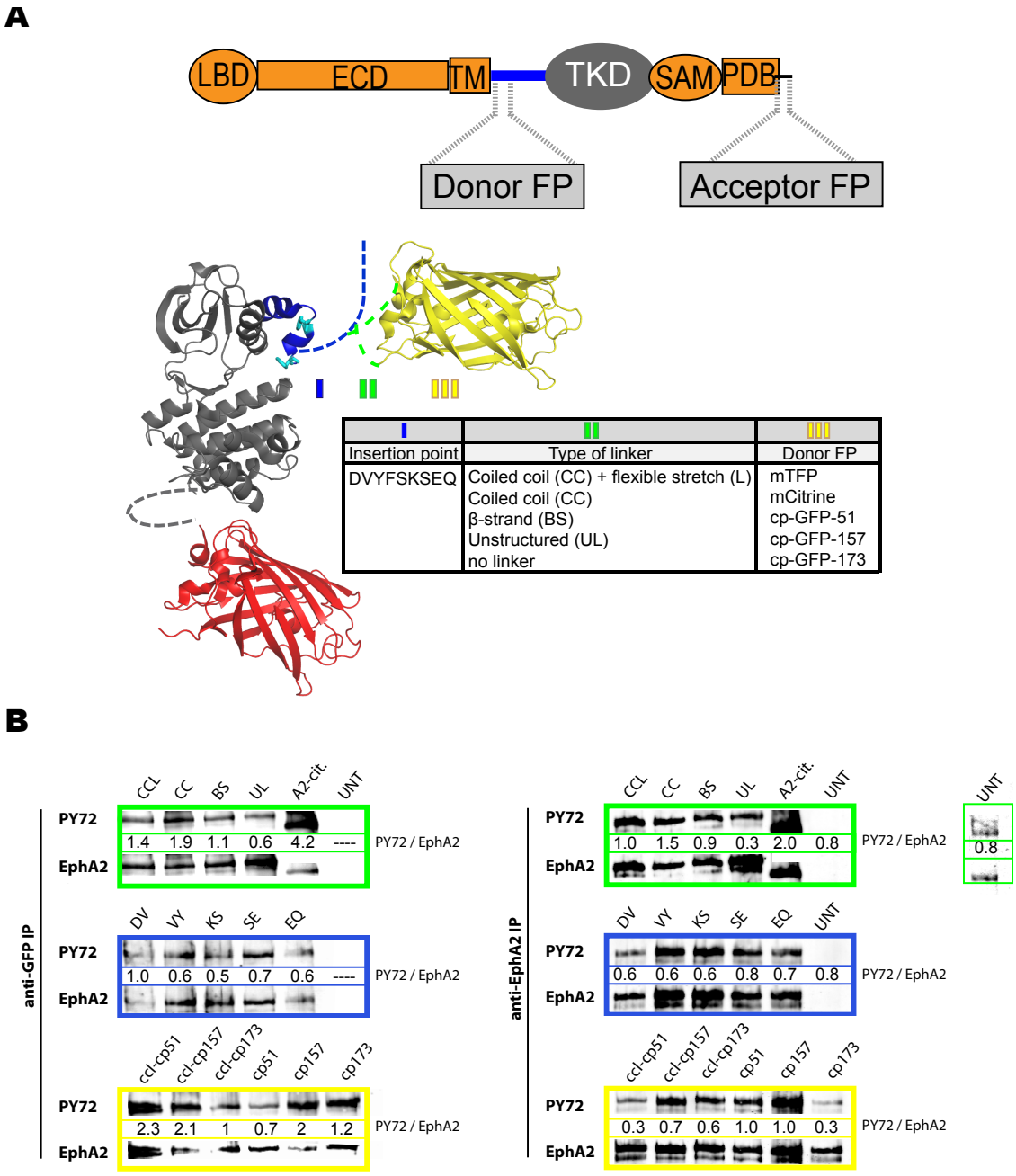

Fig 3.16 Design of a genetically encoded intramolecular FRET based EphA2 biosensor
(**A**) EphA2 biosensor domain structure with mCit/mCherry FRET pair. The biosensor was constructed by inserting the first fluorophore (FP) on a linker in the juxtamembrane segment (JMS, blue). This inserted FP is always the blue-shifted donor for any FRET-pair used. Several optimization parameters (I, II & III, see table) were used to enhance the biosensor FRET efficiency, its localization inside cells and its response to stimulation. A control biosensor was also generated, which contained only the JMS-inserted FP (Donor only LIFEA2). Abbreviations: LBD, ligand binding domain; ECD, extracellular domain; TM: transmembrane; TKD tyrosine kinase domain (grey); SAM: sterile-alpha motif; PDB: PDZ-binding motif. Structural model depicting murine 2YF mutant-EphB2 kinase domain (grey), JMS (blue) with conserved tyrosines (cyan) (modified from PDBs: 1JPA and 1EMA) [25]. (**B**) Representative *auto*phosphorylation blots of anti-GFP (left side), or anti-Eph (right side) immunoprecipitated EphA2-citrine, the different LIFEA2 chimeras or endogenous EphA2 in COS-7 cells. For blotting: mouse anti-phospho tyrosine (PY72); and goat anti-EphA2 were used. Ratio of phosphorylated to total Eph is depicted below each condition.

Abbreviations: green insets (CCL, coiled-coil + flexible linker; CC, coiled-coil only; BS, Beta-sheet linker; UL, unstructured flexible linker; UNT, untransfected), blue insets (refers to the donor FP insertion point in between the two given amino acids), yellow insets (cp, circularly permutated; number refers to the position of the new-termini within the GFP sequence). Note: the lane representing untransfected COS-7 cells was contrast-optimized separately to facilitate display.

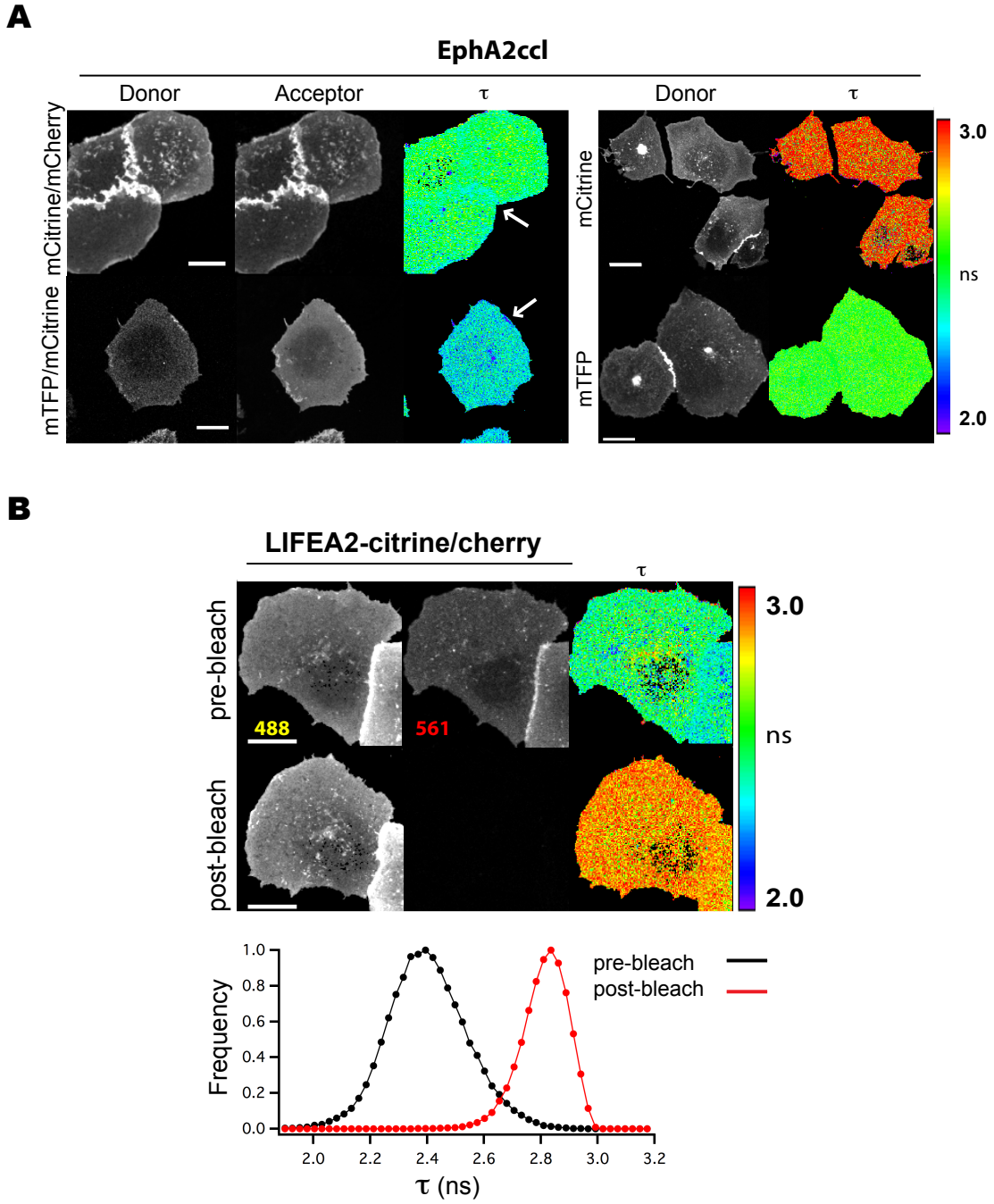

Fig 3.17 Characterization of LIFEA2 FRET signals inside living cells using FLIM
(**A**) Average fluorescence lifetime distribution of LIFEA2 in living cells measured by FLIM. Representative COS-7 cells transiently expressing EphA2ccl sensor (left panels) or donor only constructs (right panels). White arrows point to the lower FL lifetimes values detected at points of cell-cell contact and/or cell periphery. (**B**) Bleaching the acceptor returns the lifetimes of LIFEA2 to that of donor only values. Ectopic expression of LIFEA2 in COS7 cells before (upper row) or after mCherry photo bleaching (lower row). Scale bars: 10 μm. Lower panel shows average lifetime distribution before and after photo-bleaching.

3.3.2 Ligand-dependent activation of LIFEA2

FLIM was used to visualize EphA2 activation in single cells following ephrin stimulation. Ligand stimulation of donor-only LIFEA2 showed no change in FL lifetime (τ) over time (**Fig. 3.18**), thereby excluding the possibility of clustering dependent photo physical artifacts. Ligand stimulation (ephrinA1-Fc (2 μg/ml)) of ectopically expressed LIFEA2 caused a clear initial translocation of receptor to the PM, parallel to reduction of LIFEA2 FL lifetime (τ) (**Fig. 3.19 (A)**). The FL lifetime further decreased over time, reaching a maximum change at ~ 20 min. We observed an expression-level dependency of FL lifetime values upon transient expression of LIFEA2 (**Fig. 3.19, (A) compare cell 1 & 2**), which affected the relative change in FL lifetime (τ) in response to ligand (**Fig. 3.19, (B)**). The FL lifetime distributions over time for three independent experiments showed the same variance prior to ligand stimulation and a consistent trend upon stimulation (**Fig. 3.19, (C)**). By calibrating microscopy settings across the various experiments, we determined the conformational state of LIFEA2 (τ) as a function of its expression level (FL intensity) for many cells (n=60), before and after 20 min of stimulation (**Fig. 3.19, (D)**). Prior to ligand addition, the amount of active LIFEA2 conformation switched abruptly to lower values of LIFEA2 FL lifetime at intensity values of ~ 0.25 x10^6 (**Fig 3.19 (D) (dashed red line)**), suggesting the existence of an activation threshold in the system. At much higher intensity values, a slight gradual drop in LIFEA2 FL lifetime (τ) might be due to molecular crowding effects. The relative change in FL lifetime ($\Delta\tau$) of LIFEA2 per cell upon stimulation was larger in cells expressing low levels of the receptor (**Fig 3.19 (E)**).

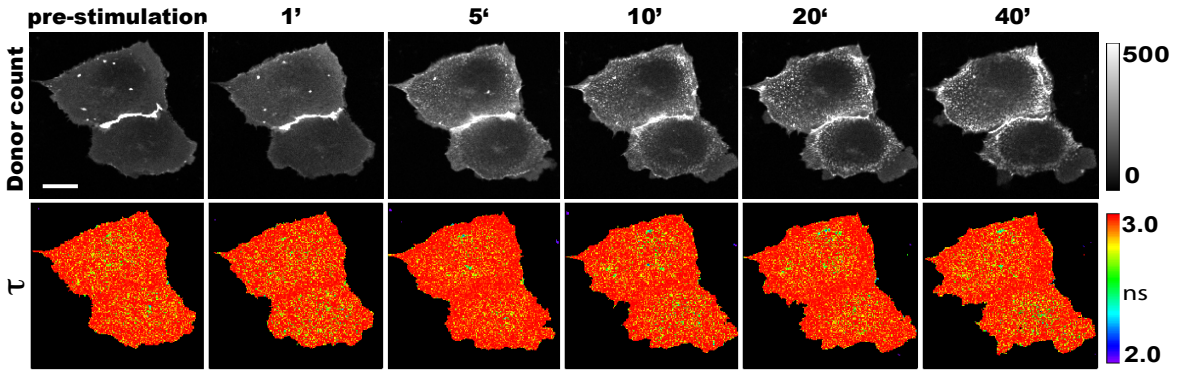

Fig 3.18 Ligand-induced stimulation of donor-only LIFEA2
Spatial-temporal profiling of donor-only LIFEA2 activation in living cells monitored by FRET-FLIM. (Upper row) show photon counts from the donor channel. (Lower row) show corresponding average FL lifetime (τ) maps in ns. Color-coding is shown on the right.

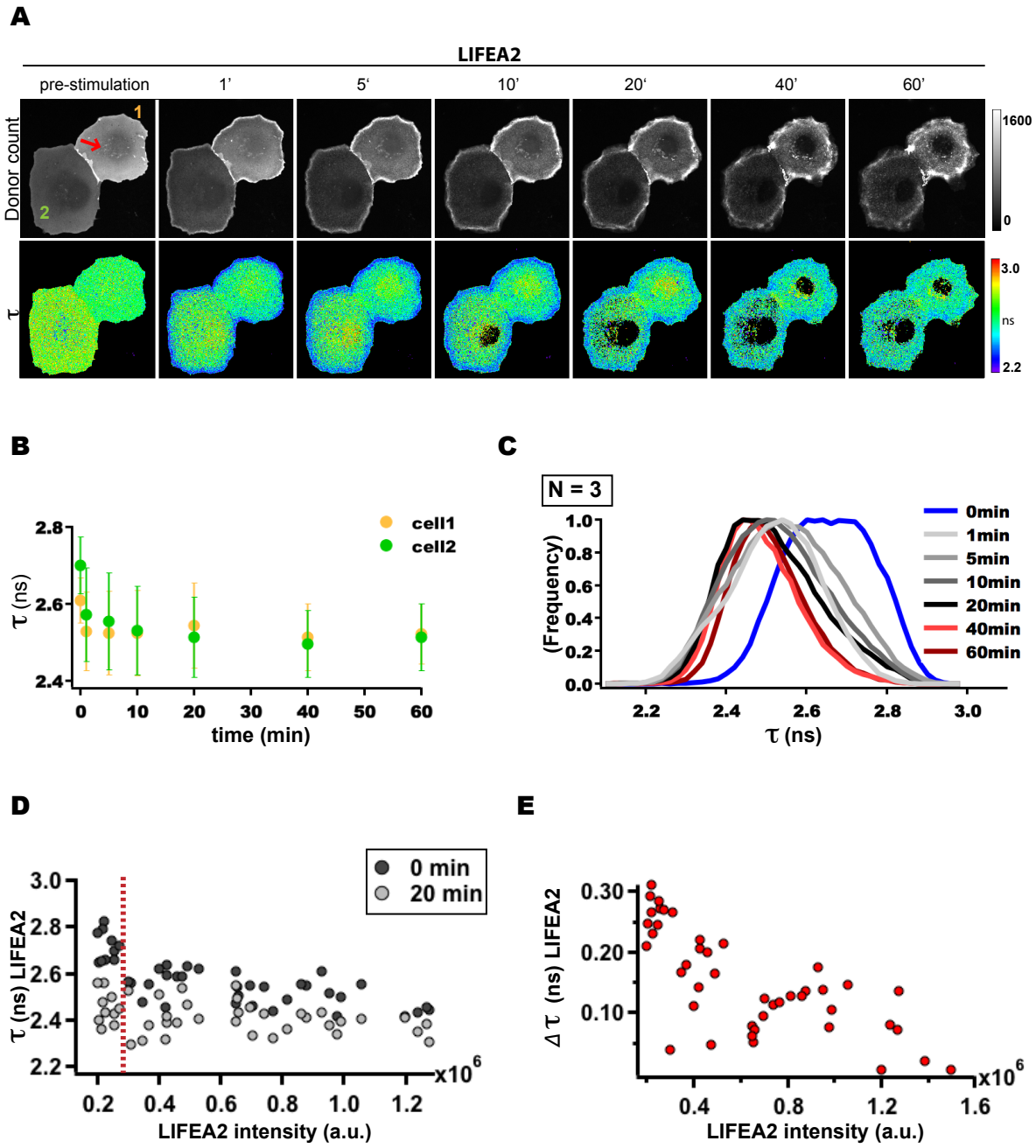

Fig 3.19 Spatial-temporal profiles of ligand-induced stimulation of LIFEA2
(**A**) LIFEA2 conformational dynamics in living cells monitored by FRET-FLIM. Upper row: show photon counts from the donor channel. Lower row: average FL lifetime (τ) maps, color-coding is shown on the right. An enhanced accumulation of LIFEA2 was observed on endomembranes before stimulation (red arrow). (**B**) Spatially averaged FL lifetime over the whole cell is plotted for the two cells over time (mean ± S.D). (**C**) Average FL lifetime distribution over time for three independent experiments shows that stimulation with ephrinA1 lowers LIFEA2 FL lifetime (τ) over time. (**D**) Expression level dependence of LIFEA2 conformational activation. Individual data points represent integrated intensity and the mean FL lifetime (τ) of LIFEA2 for selected cells 20 min with (grey) and without ligand (black). (**E**) Ligand stimulation of LIFEA2 induced a shift in the population of receptor with an active state. The relative change ($\Delta\tau$) of LIFEA2 FL lifetime was larger in cells expressing lower levels of the receptor.

3.3.3 LIFEA2 reports on conformational dynamics

To confirm that LIFEA2 reports changes in receptor conformational dynamics and not clustering, we resorted to fluorescence anisotropy. Unclustered ephrin-Fc can dimerize Ephs yet it does not allow for recpeptor activation, in fact it has been reported to act as an antagonist [46-49]. Ligand-induced Eph dimers can undergo Förster resonance energy transfer between identical FPs (homo-FRET), which results in a decrease of the steady state fluorescence anisotropy of the FP [193]. First, FLIM was used to visualize LIFEA2 active state in single cells following treatment with alexa647-labelled unclustered ephrinA5-Fc (500 ng/ml). (**Fig. 3.20 (A)**). Despite slow ligand binding kinetics, after 40-60 minutes of ephrinA5 addition, abundant Alexa647-ephrinA5 was bound to the cell surface with no apparent change in LIFEA2 average FL lifetime (τ). We also used ephrinA1-Fc (500 ng/ml), the high affinity ligand of EphA2 to exclude the possibility that ephrinA5 could not activate the receptor because of a reduced binding affinity and found no apparent change in average FL lifetime (τ) (**Fig. 3.20 (C)**). Second, using FL anisotropy imaging, we found that addition of unclustered ephrinA1-Fc (500 ng/ml) to the cells decreased anisotropy values, pointing at the occurrence of homo-FRET due to the formation of dimers (**Fig. 3.20 (B)**). These results show that clustering per se does not induce a change in the FL lifetime of LIFEA2 and thereby demonstrates that it reports on receptor conformation.

Fig 3.20 Ligand dimerization does not change LIFEA2 FL lifetime
(**A**) FL lifetime distribution of ephrinA5-induced clusters of LIFEA2 in living cells measured with FLIM. Upper row: photon counts from the donor channel. Middle row: average FL lifetime (τ) maps. Lower row: Alexa-647 conjugated ephrinA5-Fc, color coding is shown on the right of images. (**B**) Steady-state FL anisotropy of ephrinA1 induced clusters of LIFEA2 in living cells. Anisotropy values of representative cells pre- (upper row) and 20 min post-clustering (lower row) with ephrinA1-Fc are shown. The coding of anisotropy values is shown on the right. Graph shows quantification of steady-state FL anisotropy plots from pre- and post- treatment (20 min) with 500 ng/ml unclustered ephrinA1-Fc is shown. Data represent mean anisotropy ± SEM of n=10 cells. (**C**) FL lifetime (τ) distribution of ephrinA1 induced clusters of LIFEA2 in living cells measured by FLIM. Representative COS-7 cells ectopically expressing LIFEA2 pre- (upper row) and 20 min post-clustering (lower row) with ephrinA1-Fc are shown. Scale bars: 10 μm. The coding of (τ) values is shown on the right. Quantification of average FL lifetime from pre- and post- treatment (20 min) with 500 ng/ml unclustered ephrinA1-Fc is shown.

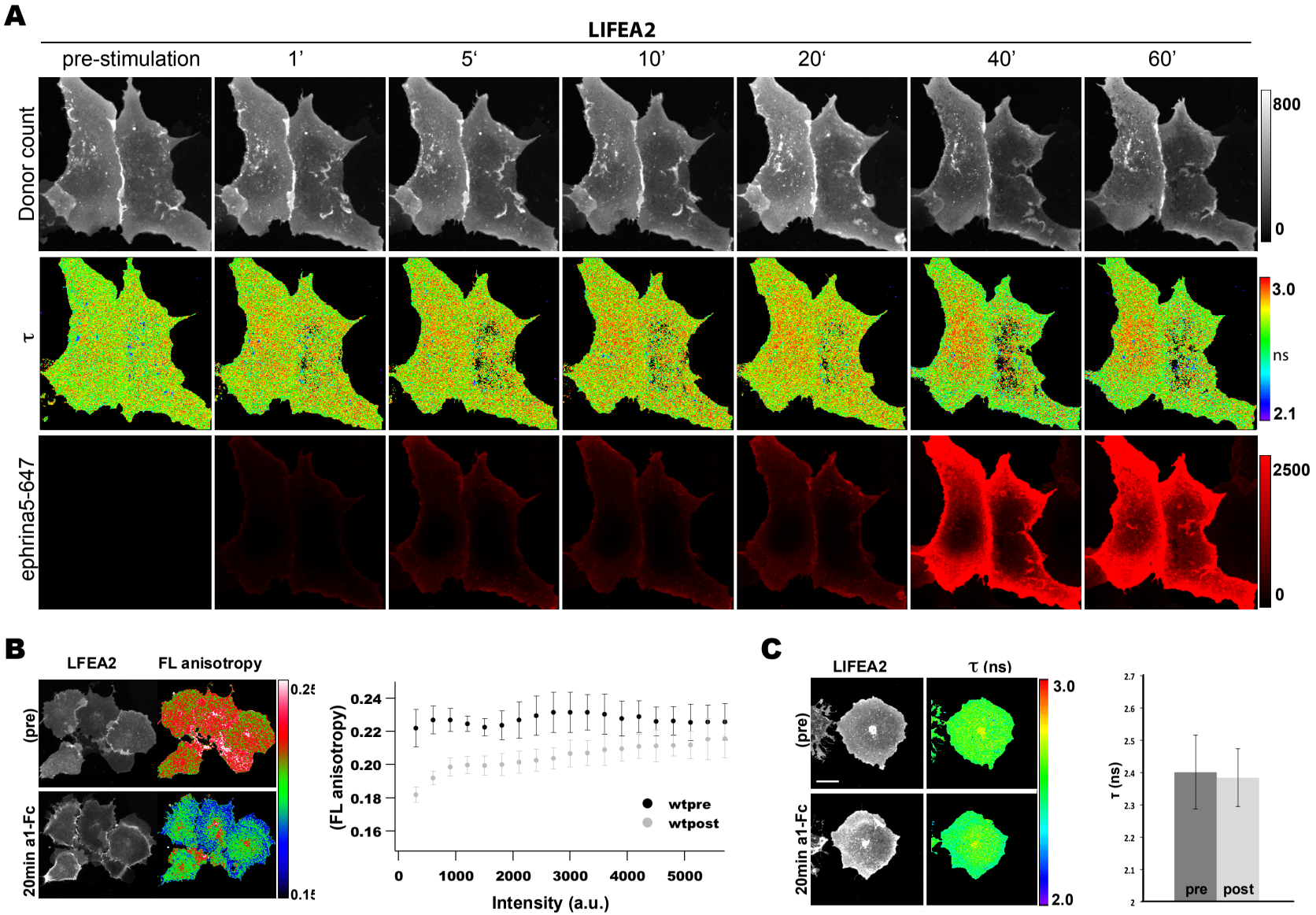
A
LIFEA2
pre-stimulation
1'
5'
10'
20'
40'
60'
Donor count
800
0
τ
3.0
ns
2.1
ephrina5-647
2500
0
B
LFEA2
FL anisotropy
(pre)
20min a1-Fc
0.25
0.15
(FL anisotropy)
0.24
0.22
0.20
0.18
0.16
0
1000
2000
3000
4000
5000
Intensity (a.u.)
wtpre
wtpost
C
LIFEA2
τ (ns)
(pre)
20min a1-Fc
3.0
2.0
τ (ns)
2.7
2.6
2.5
2.4
2.3
2.2
2.1
2
pre
post

3.3.4 Relating phosphorylation with conformational dynamics of LIFEA2

To assess whether average FL lifetime changes of LIFEA2 correlate to its phosphorylation, COS-7 cells expressing LIFEA2 were fixed and stained with a phospho-specific antibody (**Fig. 3.21 (A)**). Stimulation of LIFEA2 with pre-clustered ephrinA1-Fc shifted FL lifetime (τ) distribution to lower values in a time-dependent manner. COS-7 cells expressing LIFEA2 were then fixed, permeabilized and stained for phosphorylated JMS tyrosine residues (p-JM). The average FL lifetime of LIFEA2 (τ) was obtained in areas where we found p-JMS signal. From this it was apparent that the distribution of phosphorylated JMS coincided with areas inside cells where LIFEA2 FL lifetime was lower. In addition to immunofluorescence of single cells, LIFEA2 *auto*phosphorylation was tested by immunoblotting, which showed that LIFEA2 indeed exhibited increased *auto*phosphorylation after ephrinA1-Fc stimulation (**Fig. 3.21 (B)**). In the previous section a correlation between LIFEA2 expression level and its activity as a function average FL lifetime (τ) was described. To confirm that LIFEA2 reports on an active conformation, phosphorylation of JMS as a function of LIFEA2 FL lifetime (τ) was determined. LIFEA2 was transiently transfected in COS-7 cells and average FL lifetime (τ) was calculated for many cells (n=56). Cells were fixed and stained with p-JM and by calibrating microscopy settings across many experiments, we could correlate the intensity of p-JM across all data sets to obtain a cell-to-cell quantification of average FL lifetime (τ) as a function of p-JM staining (**Fig. 3.21 C (1)**) and of receptor expression as a function of p-JM staining (**Fig. 3.21 C (2)**).

Fig 3.21 Phosphorylation of LIFEA2
(**A**) Fraction of active LIFEA2 maps to phosphorylated JMS. COS-7 ectopically expressing LIFEA2 were fixed and stained with a phospho-specific antibody (p-JM) following an ephrinA1 stimulation time-series. FL Lifetime values (τ) of representative cells pre- (upper row), 15 min (middle row) and 60 min (lower row) post ephrinA1-Fc are shown. The drop in lifetime values post ephrinA1 treatment correlates with an increase in p-JM staining indicating that LIFEA2 maps phosphorylated, activated receptor. Scale bars, 10 μm. Right graph shows quantification of FL lifetime (τ) values with respect to masked p-JM channel for n= 6 cells. Data represent mean (τ) ± S.D. (**B**) Representative western blot of anti-GP immunoprecipitated LIFEA2, using p-JM and total-EphA2 antibodies. Blots show the time course of LIFE2 *auto*phosphorylation induced by preclustered ephrinA1-Fc. (**C**) Single cell analysis correlating JMS phosphorylation level to LIFEA2 FL lifetime (τ) (1) or LIFEA2 expression level (2). Individual data points represent integrated phospho-specific antibody intensity and the mean (τ) of LIFEA2 for selected cells. (2).

A

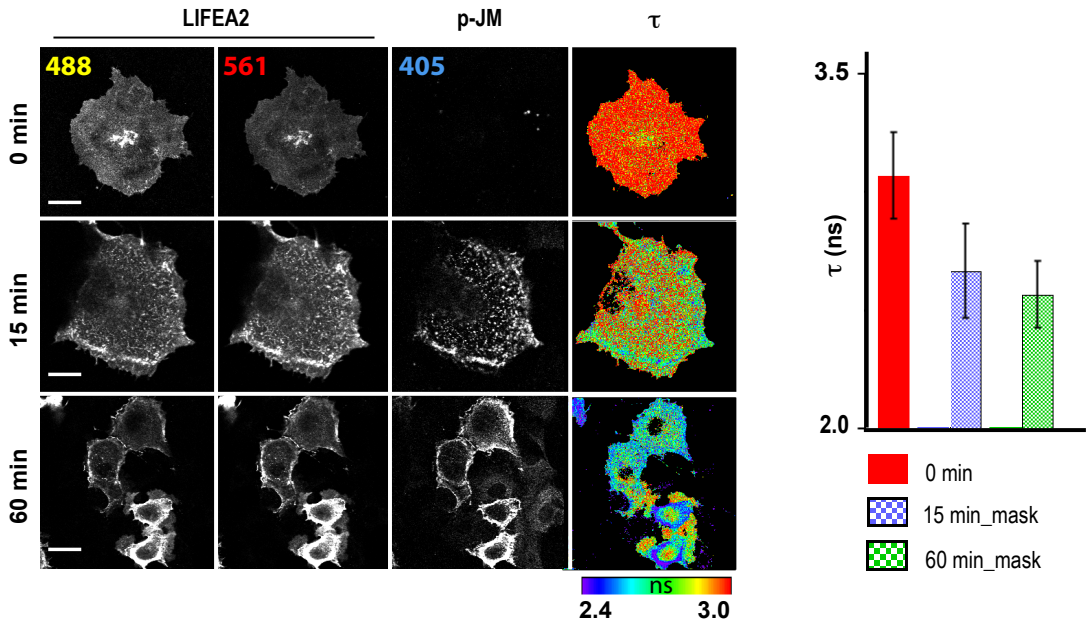

B

ephrina1-Fc	-	+	+	+	+	+
(min)	0'	5'	10'	15'	20'	40'
phospho JM						
Total LIFEA2						
Ratio	0.8	0.9	1.4	1.7	1.8	2.3

C

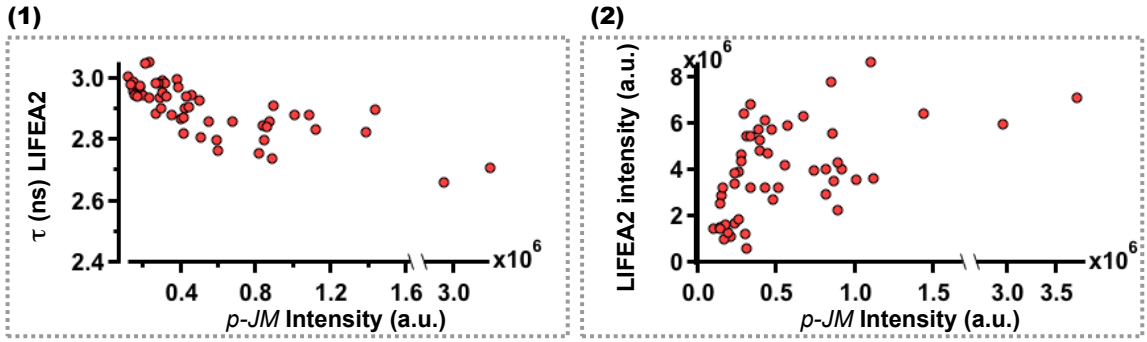

JMS phosphorylation of LIFEA2 could either be due to its intrinsic kinase activity or phosphorylation by other endogenous Eph receptors. To differentiate between these two possibilities, we assayed LIFEA2 kinase activity *in-vitro*. LIFEA2 *auto*catlytic activity measured as ratio of tyrosine *auto*phosphorylation to total receptor amount (**Fig. 3.22 (B)**) was measured in comparison to EphA2-citrine (**Fig. 3.22 (A)**) and endogenous EphA2 in MDA-468 cells (**Fig. 3.22 (C)**). In addition, we

measured the kinase activity of LIFEA2 using enolase as an external substrate for *trans*phosphorylation (**Fig. 3.22 (B)**) and compared our results to C-terminally tagged EphA2-citrine (**Fig. 3.22 (A)**). Our data indicate that the active conformation detected by the FL lifetime of LIFEA2 is an indicator of its intrinsic kinase activity that phosphorylates with comparable kinetics to endogenously expressed EphA2 in MDA-468 cells.

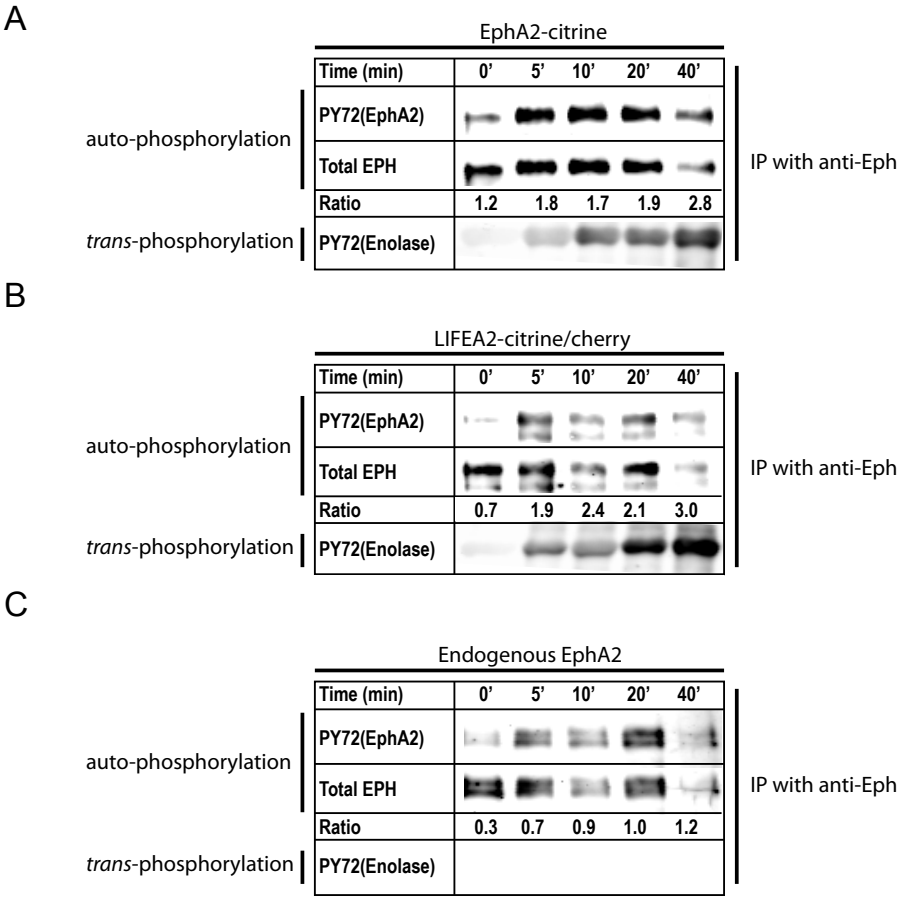

Fig 3.22 *In Vitro* kinase assays of LIFEA2, EphA2-Citrine and endogenous EphA2
Representative western blots of anti-Eph immunoprecipitated LIFEA2, EphA2citrine and endogenous EphA2 using anti-phospho-tyrosine (PY72) and anti-EphA2 protein levels (C-20). Blots show the time course of EphA2 (**A**), LIFEA2 (**B**) and Endogenous EphA2 (**C**), autophosphorylation as well as transhosphorylation of enolase as an external substrate.

To investigate how *auto*phosphorylation of EphA2 temporally correlates with its conformational dynamics, we monitored EphA2-citrine phosphorylation in live cells. We have previously shown that a fluorescent Src-homology 2 (SH2) domain can track Eph tyrosine phosphorylation[134]. Therefore, COS-7 cells ectopically expressing EphA2-citrine were co-transfected with a dimeric SH2 domain from $pp60^{src}$ labeled with mCherry (cherry-dSH2) and FLIM was used to visualize the degree of EphA2 phosphorylation in single cells. Ligand-induced stimulation of

EphA2 led to an initial translocation of receptor to the PM, in conjunction with localized reduction of EphA2-citrine FL lifetime (τ). The fraction of interacting EphA2-citrine and cherry-dSH2 (α) was calculated according to equation 12 and showed a linear increase in fraction of phosphorylated EphA2 for the duration of the experiment (60 min) (**Fig. 3.23**). Compared to EphA2 conformational dynamics reported by LIFEA2 (refer to **Fig. 3.19**), the kinetics of EphA2 phosphorylation are slower, pointing to a temporal precedence of attaining an active kinase conformation over *auto*phosphorylation. At later time points, there was still a large fraction of phosphorylated EphA2 on the PM, which could be due the to the high expression levels of dSH2 [185] that masks phosphorylation sites from phosphatases. Because many SH2-contatining proteins are coupled to Eph receptors through phosphorylated JMS tyrosine residues; thereby our data highlight a possible role for JMS-tyrosines in the regulation of EphA2 internalization and signal termination.

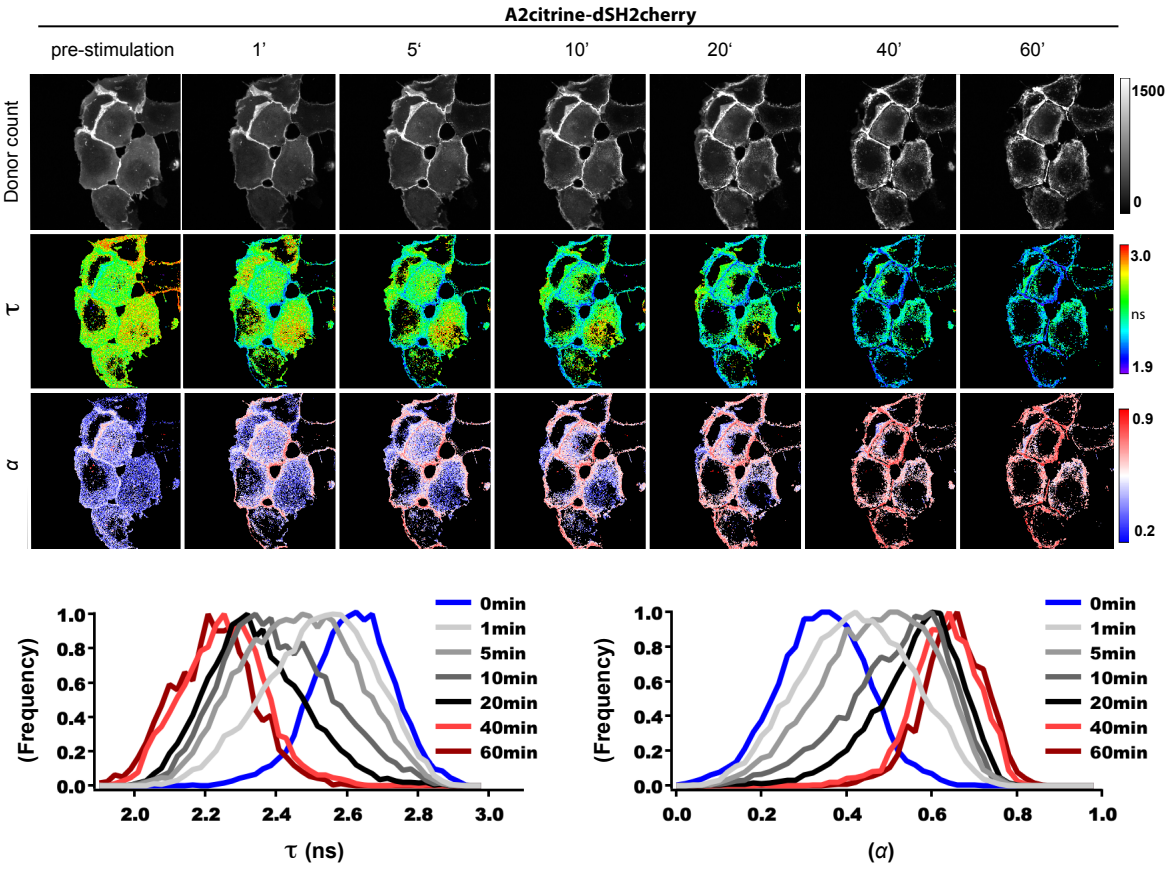

Fig 3.23 Spatial-temporal phosphorylation profiling of EphA2 measured by FLIM
Ephrin stimulation time series monitoring SH2-domain binding to phosphorylated EphA2. Upper row: photon counts from the donor channel. Middle row: average FL lifetime (τ) maps. Lower row: Fraction of phosphorylated EphA2 (α). Color-coding is shown on the right. Graphs represent average FL lifetime distribution over time (left) or fraction of phosphorylated EphA2 (α) over time (right).

3.3.5 JMS conformational dynamics in the *auto*regulation of EphA2 activity

Activation of Ephs correlates with *auto*phosphorylation of two conserved tyrosines (Tyr587 and Tyr593, for EphA2) embedded in a highly conserved ~10-amino acid motif within the JMS [79]. It has been shown that mutation of the conserved JMS tyrosines to phenylalanine (2YF) impairs kinase activity, while phospho-mimetic glutamic acid substitution (2YE) preserves kinase activity [80,81]. In the crystal structure of EphB2-KD, the JMS in its non-phosphorylatable form (2YF), adopts an ordered α-helical conformation that interacts with several elements in the KD, and prevents it from adopting an ordered, active structure [25]. Despite knowledge gained from structural studies on *auto*inhibited and active Eph KD, crystallographic snapshots do not explain how the *auto*catalytic activity of the kinase can be suppressed by the JMS in a dynamic way to allow for robust activation when ligand is added *in vivo*.

We therefore created 2YF- and 2YE- mutants of LIFEA2 and used FLIM to understand how the JMS can regulate the *auto*catalytic activity of EphA2. Ectopic expression of either 2YE-LIFEA2 or 2YF-LIFEA2 in COS-7 cells showed a distinct basal FRET signal for each mutant (**Fig. 3.24 (A)**), where the average FL lifetime (τ) of the 2YE mutant was higher than that of the 2YF mutant. The plots of FL lifetime (τ) values as a function of receptor FL intensity shows differences in the dependency of the FL lifetime values on the expression level between the two mutants (~ n= 23 cells for 2YE, n= 26 for 2YF and n= 30 for wild type) (**Fig. 3.24 (B)**). One can see that the average τ distribution of 2YE-LIFEA2 was shifted towards higher FL intensity values as compared to 2YF-LIFEA2. The distribution of LIFEA2 on the other hand, covered a broad FL lifetime (τ) range, indicating a mixed population of inhibited and open JMS at steady state. To confirm that the JMS mutants reports changes in receptor conformational dynamics and not clustering, we resorted to fluorescence anisotropy. Ectopically expressed 2YE-, 2YF- or wild type (wt) LIFEA2 all exhibited similar anisotropy values with no correlation between anisotropy and FL intensity (**Fig. 3.24 (C)**). This excludes differences in clustering as a cause for the difference in the observed FL lifetime (τ) of the LIFEA2 constructs.

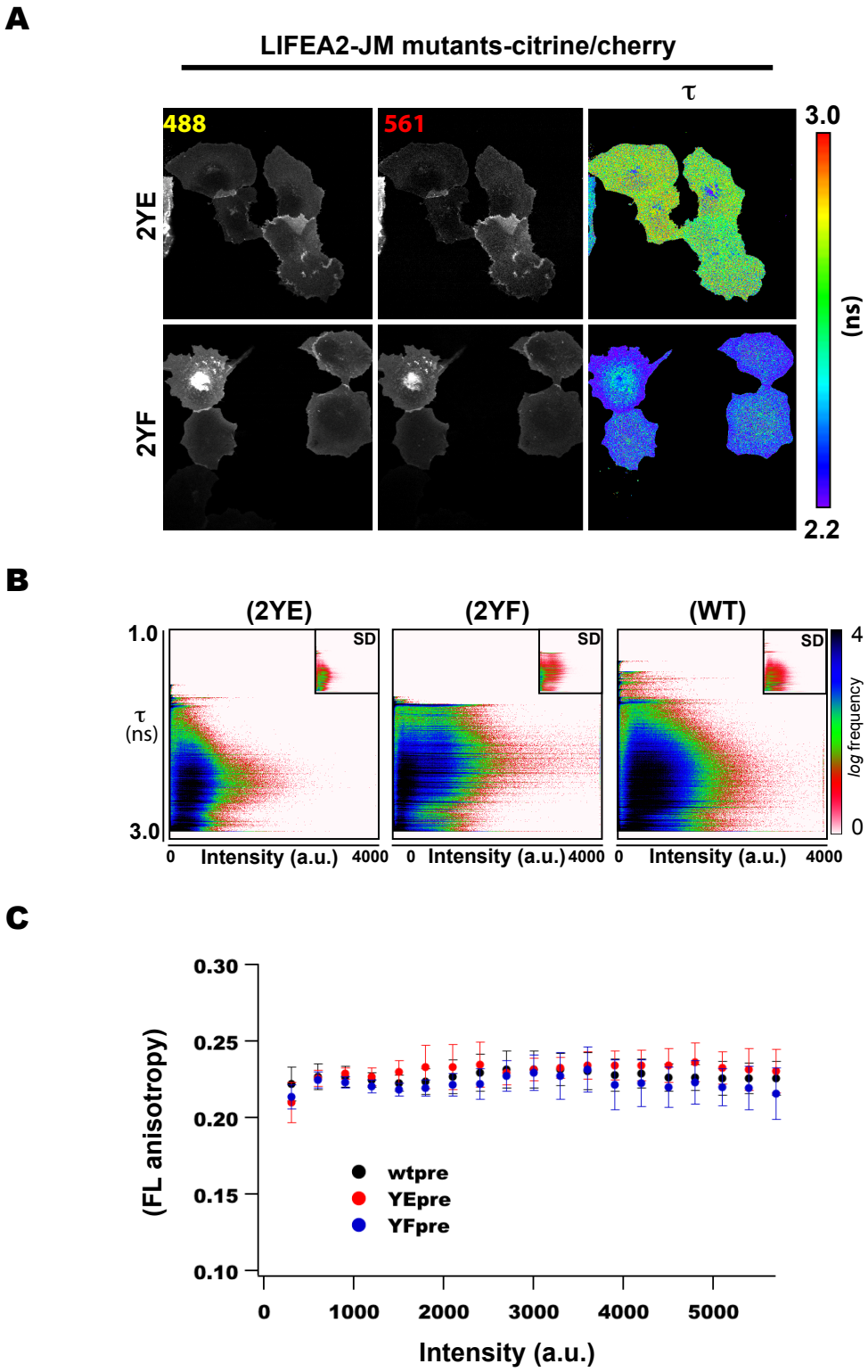

Fig 3.24 Characterization of LIFEA2 JMS mutants

Average FL lifetime (τ) distribution of LIFEA2-JMS mutants measured by FLIM. (**A**) Representative COS-7 cells ectopically expressing 2YE-LIFEA2 (upper row) or 2YF-LIFEA2 (lower row). Color-coding is shown on the right. (**B**) 2D-histograms of average FL lifetime (τ) distribution with respect to LIFEA2 intensity. Insets represent Standard Deviation. (**C**) Steady-state FL anisotropy of (wt, 2YE, 2YF) LIFEA2 in living cells show no difference in anisotropy values as a function of intensity indicating the absence of clustering-dependent propensities. Data represent mean anisotropy ± SEM (n=8 experiments).

FLIM was then used to follow ephrin-induced conformational dynamics of ectopically expressed LIFEA2 in comparison to the 2YE- and 2YF-LIFEA2 mutants. Similar to LIFEA2 (**Fig. 3.25 (A)**), stimulation with clustered ephrinA1-Fc (2 μg/ml) caused an initial net translocation of the phosphomimetic 2YE-LIFEA2 construct towards the PM, that was paralleled by a reduction of its average FL lifetime (τ) (**Fig. 3.25 (B)**). However, the relative drop in τ was larger as compared to LIFEA2. On the other hand, the non-phosphorylatable 2YF-LIFEA2 construct showed slower and minimal changes in average τ (**Fig. 3.25 (C)**). The average FL lifetime of wild type and 2YE-LIFEA2 approached the same value after long-time ephrin stimulation, whereas 2YF-LIFEA2 gradually shifted to even lower FL lifetime values (**Fig. 3.25 (D)**). We thereby find that the phospho-mimetic mutant of LIFEA2 (2YE) retained the ability to change conformation upon ligand-induced stimulation, in contrast to the non-phosphorylatable 2YF mutant. Prior to simulation, LIFEA2 depicted a mixed population of "activatable" and "tight" JMS-KD interactions as revealed from the FL lifetime distribution that was in between that of the 2YE- and 2YF-LIFEA2 mutants. These experiments show that the FL lifetime of the auto-inhibitied 2YF-LIFEA2 mutant and that of the ligand activated LIFEA2 have approximately the same value, causing a degeneracy in the FLIM-FRET based conformation detection system. However, because LIFEA2 fluctuates between an open and closed conformation in the absence of stimulation, this system allows the detection of the transition to the catalytically active conformation (**refer to Discussion**). Therefore, LIFEA2 is a proper conformational activity sensor.

Fig 3.25 Conformational breathing of Eph JM determines its activation barrier
COS-7 cells ectopically expressing wild type LIFEA2 (Upper panels), 2YE mutant (middle panels), or 2YF mutant (lower panels) are depicted. At steady state, FL lifetime (τ) maps of wild type (**A**), 2YE (**B**) and 2YF-LIFEA2 (**C**) show that wild type LIFEA2 represents a mixed population of "tight" and "activatable" JMS. Average lifetime distribution over time shows that the drop in lifetime values post ephrinA1 treatment correlates with Eph activation, with the active 2YE mutant showing the biggest relative change. (**D**) Average FL lifetime (τ) distributions of the three represented time-series over time shows that the 2YE mutant

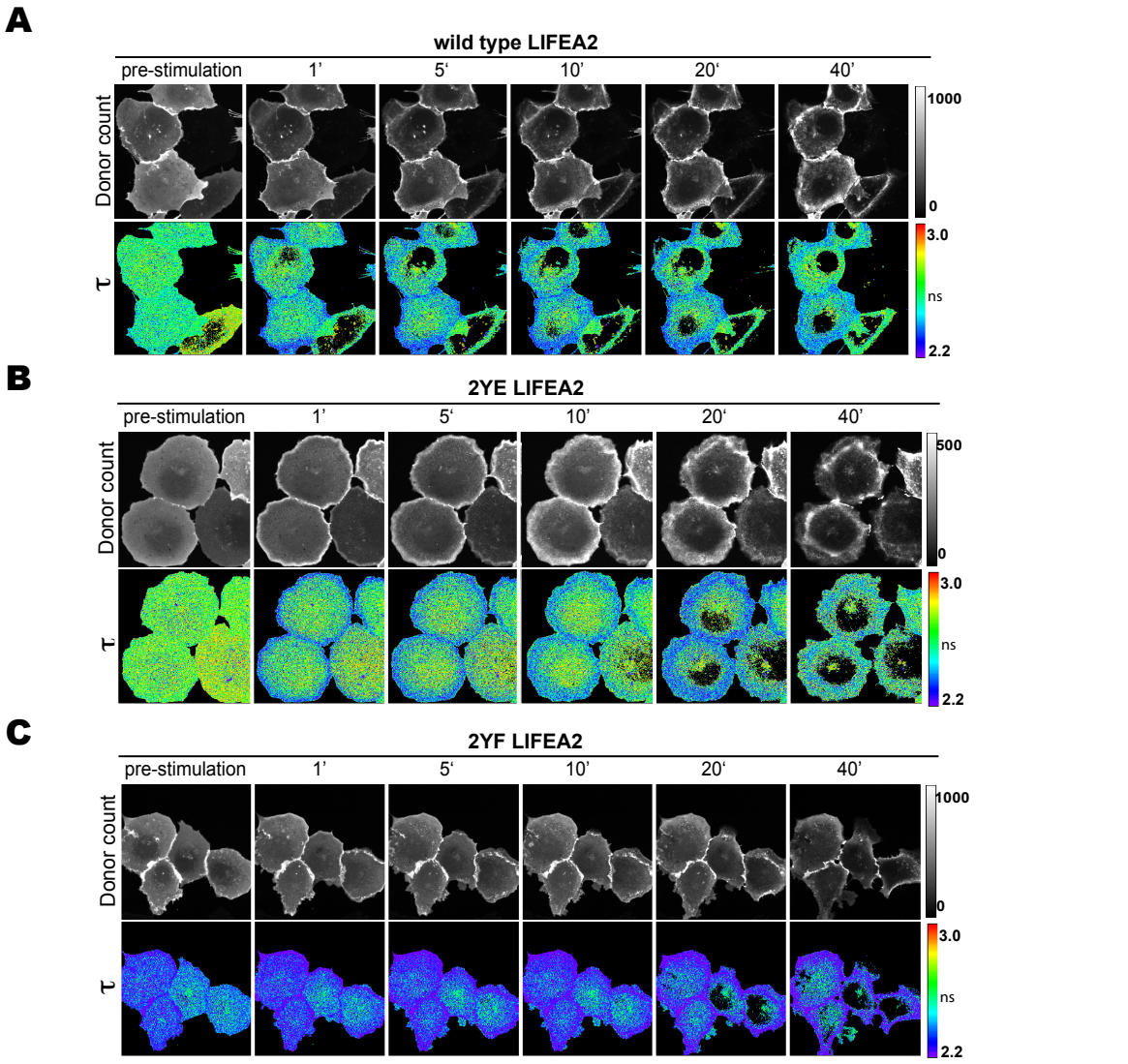
A
wild type LIFEA2
pre-stimulation
1'
5'
10'
20'
40'
Donor count
τ
1000
0
3.0
ns
2.2
B
2YE LIFEA2
500
C
2YF LIFEA2
D
wild type LIFEA2
2YE LIFEA2
2YF LIFEA2
(Frequency)
τ (ns)
Key:
0min
1min
5min
10min
20min
40min
60min

The slight change in 2YF-LIFEA2 FL lifetime possibly shows that a small fraction of receptors transited into an active conformation upon ligand stimulation. We therefore tested if the 2YF mutant exhibited any residual catalytic activity in comparison to wild type- and 2YE-LIFEA2 in an *in-vitro* kinase activity assay (**Fig. 3.26 (A)**). LIFEA2 *auto*catalytic activity was measured as a ratio of tyrosine *auto*phosphorylation to total receptor, as well as by the *trans*phoshorylation of an external substrate (enolase). As compared to wild type, the 2YE mutant retained full catalytic activity, while the 2YF-JMS mutant's activity was clearly impaired, but not completely inhibited. In a separate experiment the activity of the JMS mutants was compared to a kinase dead EphA2 mutant (K645R) (**Fig. 3.26 (B)**), which demonstrated that 2YF-LIFEA2 indeed retains residual activity.

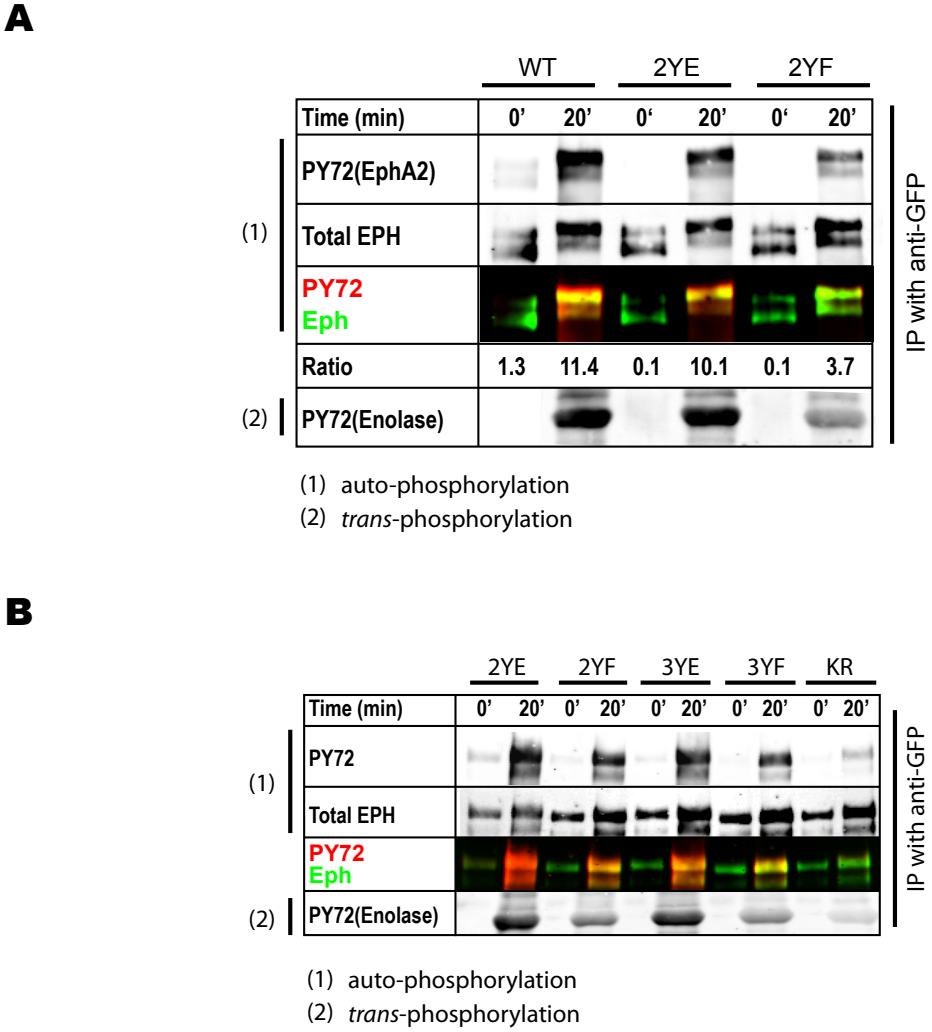

Fig 3.26 *In Vitro* kinase assays of the different LIFEA2 mutants
Representative western blots of anti-GFP immunoprecipitated wild type and mutant LIFEA2 using anti-phospho-tyrosine (PY72) and total EphA2 protein levels. (**A**) Blots show the *auto*- and *trans*- kinase activity of wild type LIFEA2 as compared to 2YF and 2YE JMS mutants (fixed time point, 20 min). (**B**) Kinase activity of JMS-mutants compared to kinase dead LIFEA2 (K654R). All assays were done at a fixed time point (20 min) for comparison.

3.3.6 Locking LIFEA2 in a specific conformation by dasatinib

A kinase inhibitor that locks EphA2-KD into a specific conformation was used to confirm that LIFEA2 indeed reports on EphA2 conformational dynamics. Dasatinib is a small-molecular kinase inhibitor that is currently being used in cases of chronic myeloid leukemia (CML) that develop resistance to imatinib [210]. Initially used as a selective inhibitor of BCR-Abl and Src kinaes [211], dasatinib's spectrum of inhibition later expanded to include members of the Eph family [212,213]. Dasatinib competes with ATP in a reversible manner and has been crystalized with many kinase domains in an active conformation.

Dasatinib inhibition of LIFEA2 reduced basal and ligand-induced phosphorylation inside cells as compared to the DMSO control (**Fig. 3.27 (A), right panel**). FLIM was used to visualize LIFEA2 conformation in single cells before and after dasatinib inhibition. COS-7 cells ectopically expressing LIFEA2 & treated with 200 nM dasatinib for 2 hrs exhibited reduced FL lifetimes (τ) (**Fig. 3.27 (A), left panel**). Cells that exhibit differential conformational states of LIFEA2 (due to differences in receptor expression level; **Fig. 3.27 (B)**) converge to a similar FL lifetime upon drug addition, indicating that dasatinib locks LIFEA2 into a unique conformational state. Importantly, ligand-addition after dasatinib inhibition did not further change the FL lifetime distribution of LIFEA2, thereby establishing that the sensor reports on conformational dynamics and not clustering.

In an attempt to identify which conformation dasatinib locks EphA2 into, we ectopically expressed 2YF-, 2YE- and wild type-LIFEA2 and then used dasatinib for inhibition (**Fig. 3.28 (A)**). Compared to LIFEA2, the 2YE mutant showed a reduced relative change in average FL lifetime (τ) while the FL lifetime values of the 2YF mutant remained the same. These experiments suggest that dasatinib: (1) cannot bind the non-phosphorylatatble 2YF mutant; (2) shifts the equilibrium of the phospho-mimetic 2YE mutant to an active KD conformation; (3) inhibits EphA2 by locking the KD in an active conformation. To rule out the contribution of clustering to the observed differences in average FL lifetime (τ) before and after dasatinib inhibition, we resorted again to fluorescence anisotropy. Ectopic expression of 2YE-, 2YF- or wild type-LIFEA2 in COS-7 followed by dasatinib inhibition (200 nM) showed no differences in anisotropy values over the range of recorded intensity values (**Fig. 3.28 (B)**), confirming that clustering does not contribute to the observed differences in FL lifetime.

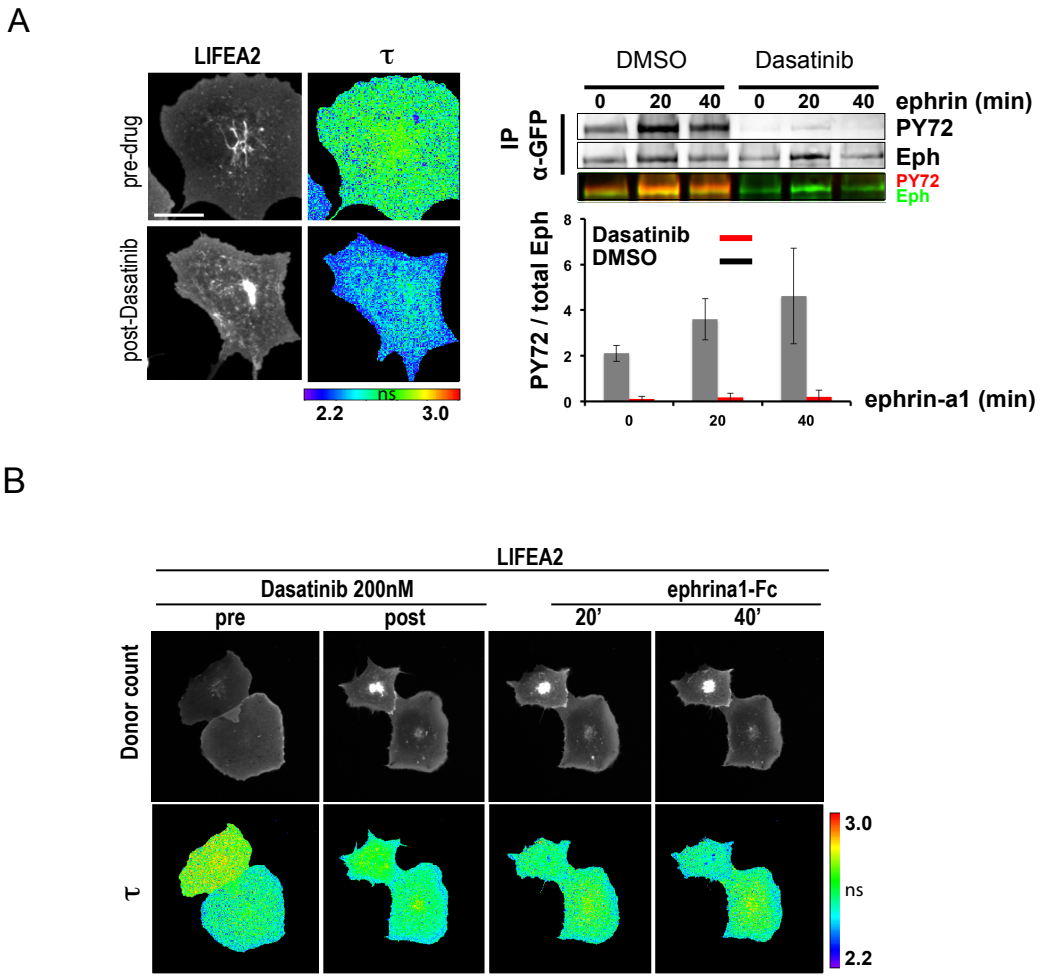

Fig 3.27 Dasatinib locks the kinase domain of LIFEA2 in a specific conformation
(**A**) Inhibition of EphA2 kinase activity with dasatinib locks LIFEA2 into an active state. Left: average FL lifetime (τ) distribution of representative COS-7 cells ectopically expressing LIFEA2, pre- (upper row) and 2 hr post-inhibition (lower row) with dasatinib (200 nM). Color-coding of FL lifetime (τ) values is shown below images. Scale bar: 10 μm. Right: Representative Western blots of anti-GFP immunoprecipitated LIFEA2 after inhibition with dasatinib (200nM) and stimulation with clustered ephrinA1-Fc (2 μg/ml), for the indicated time points. Blots were incubated with mouse anti-phospho tyrosine antibody (PY72) and goat anti-EphA2 for total Eph protein levels. Bottom: Quantitative analysis of receptor phosphorylation (**B**) Inhibition of EphA2 kinase activity with dasatinib hinders ligand-induced translocation and clustering. Average FL lifetime (τ) distribution of dasatinib-treated LIFEA2 shows that inhibition of kinase activity lowers biosensor FL lifetime (τ), in an activity-dependent manner. Stimulation with clustered ephrinA1-Fc (2 μg/ml) did not affect the average FL lifetime distribution. Color-coding of FL lifetime (τ) values is shown on the right.

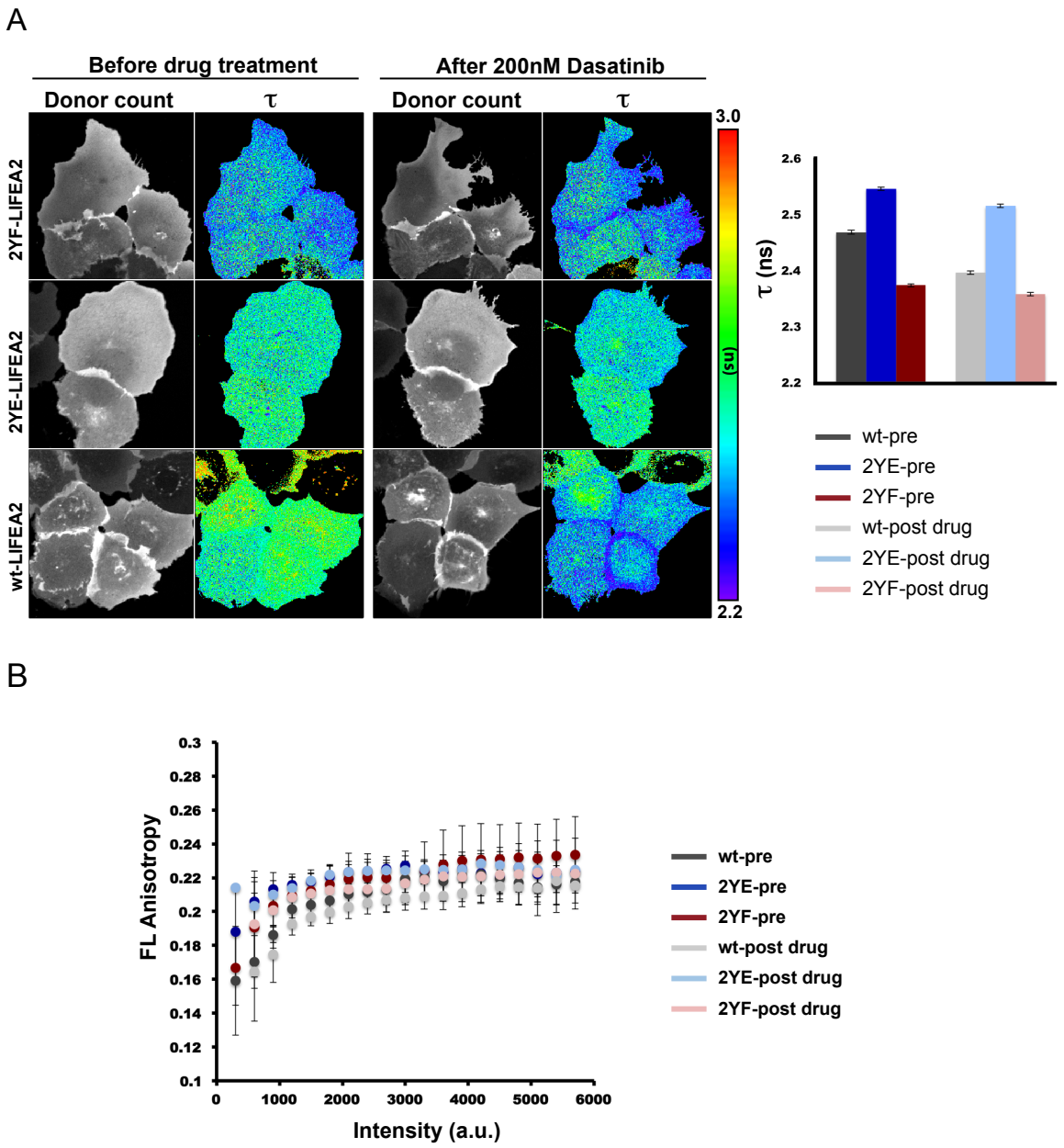

Fig 3.28 Dasatinib inhibition of the different LIFEA2 JMS mutants
(**A**) Left: Average FL lifetime distribution of representative COS-7 cells ectopically expressing 2YF-LIFEA2 (upper row), 2YE-LIFEA2 (middle row) or wild type LIFEA2 (lower row), before (left) and 2 hours post-dasatinib inhibition (right). Right: Representative Quantitative analysis of receptor FL lifetime (τ) distribution pre- and post-dasatinib inhibition. Data represent mean ± SEM (**B**) Steady-state fluorescence (FL) anisotropy of (wild type, 2YE, 2YF) LIFEA2 before and after dasatinib inhibition show no difference in anisotropy values over a range of intensity values indicating the absence of clustering-dependent change. Data represent mean anisotropy ± SEM of n=8 experiments.

3.3.7 Spatial regulation of EphA2 conformational dynamics by PTP1B

The phosphorylation level of a given RTK at a specific place in the cell is given by the balance between its intrinsic kinase activity and the local protein tyrosine phosphatase (PTP) activity. Therefore, one cannot account for the signaling capacity of a given Eph receptor system inside the cell without taking into consideration the opposing activities of PTPs. Consistent with this idea, elevated PTP activity in EphA3-positivie leukaemia cells provokes adhesion to an ephrin-A5 surface, while PTP inhibition reverses the adhesive response to a repulsive one [124]. Furthermore, changing the expression of PTP1B can modulate the duration and amplitude of EphA3 phosphorylation in response to ligand stimulation [127]. As previously indicated in **section 3.1**, we found that inhibition of PTP1B causes increased tyrosine phosphorylation of EphA2 at points of cell-cell contact. In the absence of stimulus, allosteric inhibition of PTP1B (Calbiochem #539741) reduces the average FL lifetime (τ) of LIFEA2 specifically at sites of cell-cell contact, indicating an *auto*phosphorylation-stabilized active conformation (**Fig. 3.29 (D & E)**). On the other hand, COS-7 cells ectopically expressing PTP1B and LIFEA2 showed a shift in LIFEA2 FL lifetime (τ) distribution towards higher values indicating reduced catalytically active states of the receptor (**Fig. 3.29 (A)**). This was corroborated by the reduced *auto*phosphorylation level of LIFEA2 in the presence of PTP1B as measured by immunobloting (**Fig. 3.29 (C)**)). 2D histograms of LIFEA2 FL lifetime (τ) as a function of PTP1B FL intensity showed an increase in LIFEA2 FL lifetime (τ) in intracellular regions with high PTP1B expression, i.e. peri-nuclear endomembranes (n= 3) (**Fig. 3.29 (B)**).

Fig 3.29 Regulation of LIFEA2 activity by PTP1B
(**A**) PTP1B negatively regulates activity of LIFEA2. Left: COS-7 ectopically expressing LIFEA2 and PTP1B show a uniform average FL lifetime map and no apparent colocalization between EphA2 and PTP1. Color-coding of FL lifetime is on the right. Right: Quantitative analysis of LIFEA2 FL lifetime (τ) distribution in the absence (black trace) and presence of PTP1B ectopic expression (red trace), n=3 experiments. (**B**) 2D-histograms of FL lifetime (τ) distribution with respect to PTP1B intensity, n=3 separate experiments. (**C**) Representative Western blot of LIFEA2 or LIFEA2 + PTP1B after stimulation with equal concentration of ephrinA1-Fc (2 μg/ml) using anti-phospho JMS antibody for phosphorylation, anti-GFP for total LIFEA2 and anti-PTP1B for endogenous and ectopic PTP1B. (**D**) COS-7 cells transiently expressing LIFEA2, pre (upper row) or after allosteric inhibition of PTP1B (lower row). Color-coding of FL lifetime is on the right. (**E**) COS-7 cells ectopically expressing LIFEA2, pre (upper row) or after inhibition of PTP1B (lower row). Cells were fixed and stained for tyrosine phosphorylation using PY72 antibody followed by Alexa647-labeled secondary antibody. Color-coding of FL lifetime is on the right.

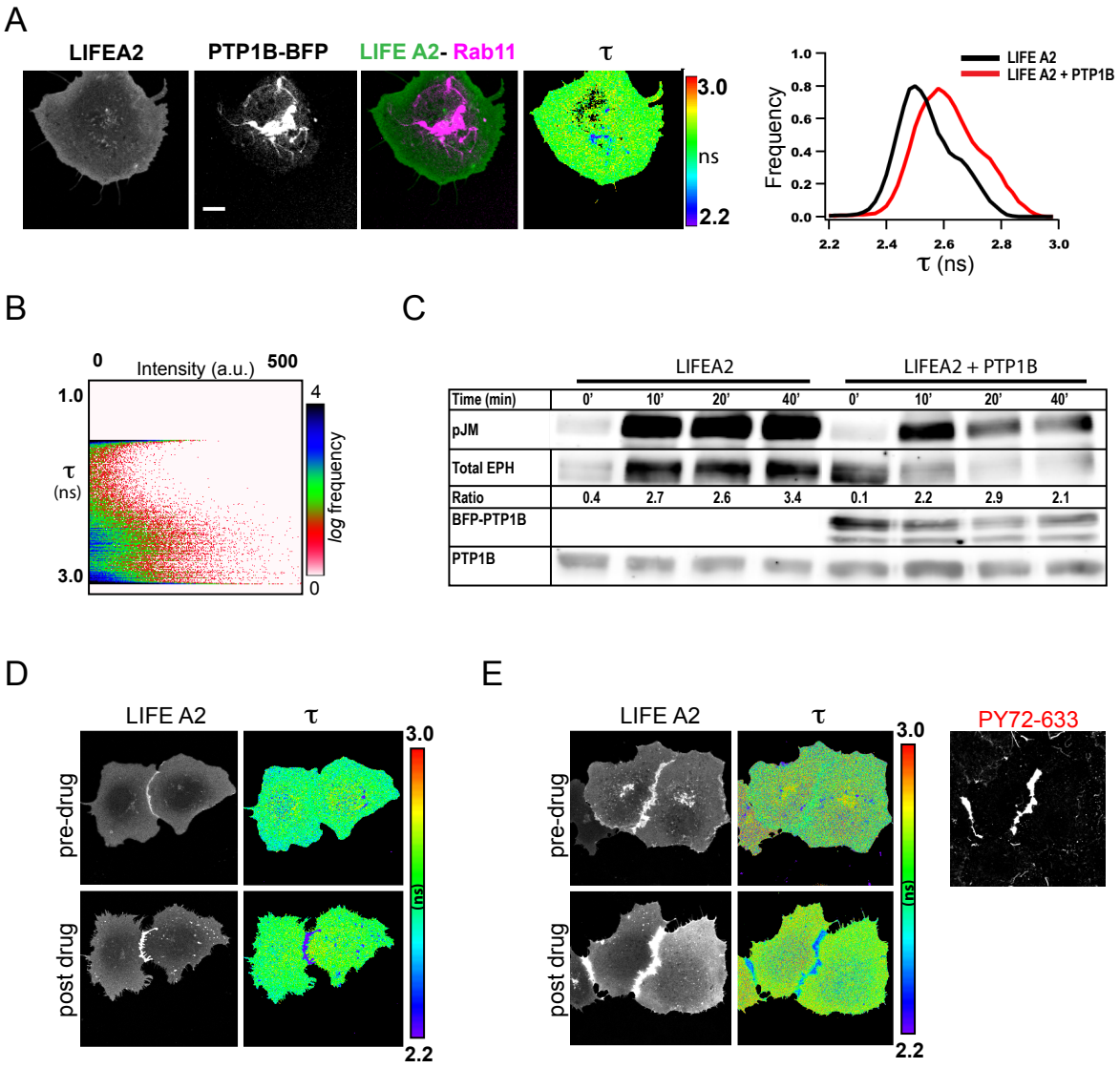

Ligand-dependent activation of RTKs may be coupled to transient PTP inactivation in order to enhance signal efficiency. This can happen through increased production of H_2O_2 upon activation of the NADPH oxidase complex and the subsequent inactivation of PTPs by oxidation of the catalytic cysteine [137-141]. To monitor the production of H_2O_2 in the vicinity of Eph receptors, we created a chimera consisting of full-length EphA2, attached via a linker to the H_2O_2–biosensor Hyper. Hyper consists of a circularly permuted YFP (cpYFP) inserted into the regulatory domain of the H_2O_2–sensing protein, OxyR. Exposure of OxyR to H_2O_2 results in a dramatic conformational change of the protein translated into an in crease in Hyper fluorescence [214] (**Fig. 3.30 (A)**). Ectopic expression of EphA2-Hyper in COS-7 cells showed enhanced EphA2-Hyper FL at point of cell-cell contact, on internalized vesicular structures and around the cell periphery. Stimulation with pre-clustered ephrinA1-Fc caused an initial increase in EphA2-

Hyper FL, indicative of increased H_2O_2 production, followed by a reduction in its intensity (**Fig. 3.30 (B)**). To account for changes in the local concentration of EphA2-Hyper after stimulation, EphA2-mCherry was ectopically co-expressed with EphA2-Hyper as a normalizing factor. Intensity curves in both channels were measured, and the ratiometric signal showed that the initial burst of H_2O_2 was sustained for longer duration of time (**Fig. 3.30 (C)**).

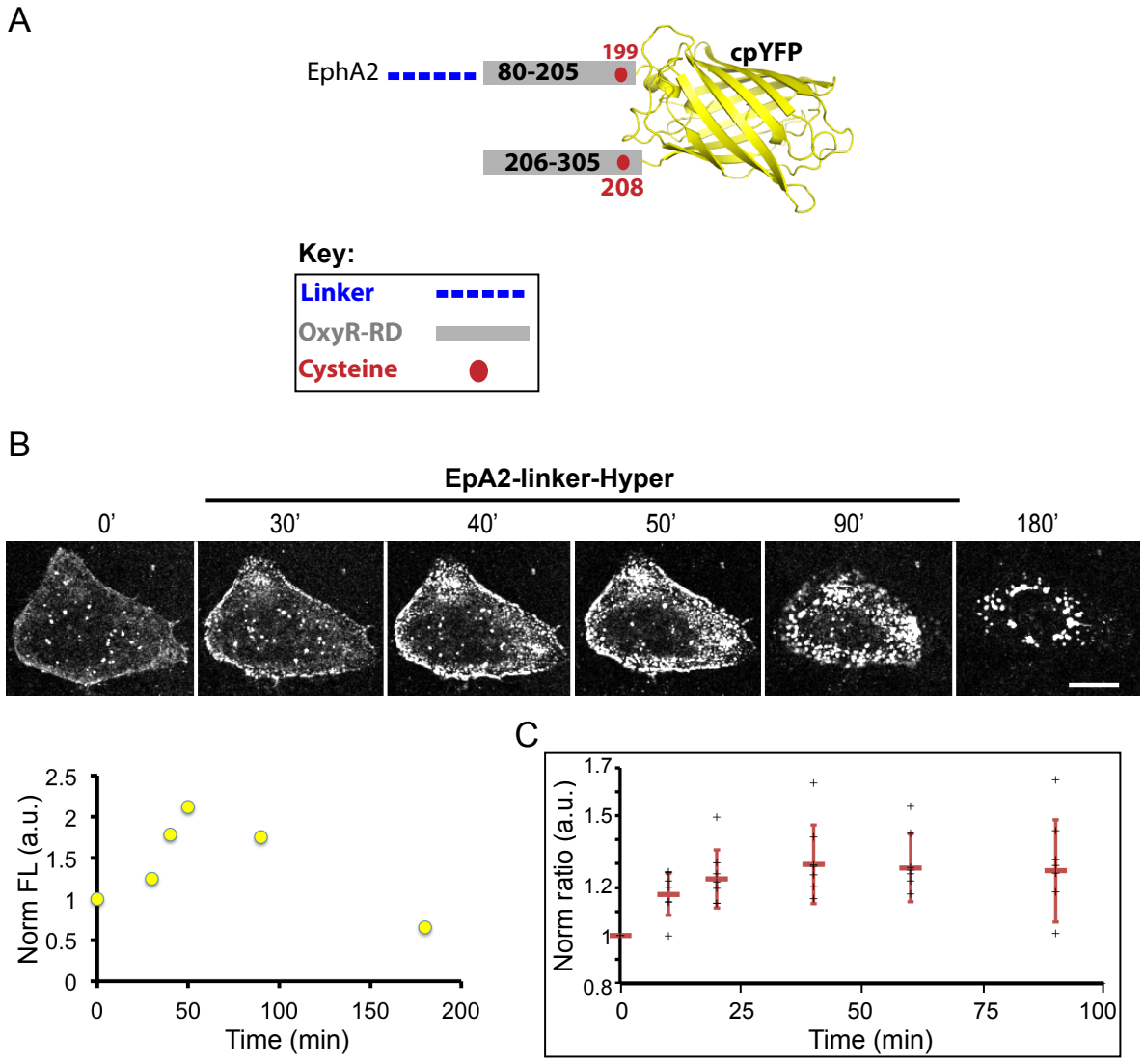

Fig 3.30 Mapping H_2O_2 production by EphA2
(**A**) Scheme of EPHA2-linker-Hyper chimera; circularly permuted YFP (cpYFP) is inserted within the H_2O_2 sensitive, regulatory domain of E.coli OxyR (grey). The two redox-sensitive conserved cysteines (red) are depicted with their respective number in the amino acid sequence. (**B**) Dynamics of H_2O_2 production in living cells before and after stimulation of EphA2 with ephrinA1-Fc. Representative COS-7 cells expressing EphA2-Hyper were stimulated with (2 μg/ml) preclustered ephrinA1-Fc and Hyper intensity fluctuations was monitored over time. Plot represents normalized intensity changes of EphA2-Hyper over time. Scale bar 10 μm.(**C**) EphA2cherry was used as a normalizing factor for intensity changes of EphA2-Hyper. Plot represents data from n=8 experiments. Error bar = Std.

3.3.8 PM-recycling as a safeguard mechanism against spurious EphA2 activation

Since the localization and activity of PTP1B is mostly perinuclear as shown in **Fig 3.29 (A),** we reasoned that at steady state, Ephs need to be transported to those areas for effective regulation by dephosphorylation. Indeed, we found EphA2 and/or LIFEA2 in the perinuclear area, but the strong PM-enrichment of the receptor impeded its clear detection on endomembranes. In the early endocytic pathway, Rab11 marks the recycling endosome (RE) [154] and is involved in recycling of cargo between the PM and the centrally localized RE. Ectopic expression of BFP/cherry-Rab11 enriched EphA2 in the perinuclear region and we observed substantial overlap between the spatial distribution of LIFEA2 and/or EphA2-citrine with Rab11 (**Fig. 3.31 (A) & 3.32 (A)**). In the presence of BFP-Rab11, LIFEA2 average FL lifetime (τ) distribution shifted towards higher values indicating a reduced catalytically active conformation (**Fig. 3.31 (A)**). In addition, single cell analysis of LIFEA2 conformational state as function of its expression level showed a shift in the response properties of the system in the presence of ectopically expressed BFP-Rab11. The ligand-independent switch-like response behavior of LIFEA2, as indicated in the FL lifetime versus FL intensity histograms, now occurred at higher receptor expression levels, indicating a higher activation threshold in the system as compared to LIFEA2 alone (**Fig. 3.31 (B & C)**). FLIM was also used to visualize the degree of EphA2 activation in single cells co-expressing LIFEA2 and BFP-Rab11 following addition of ephrin. Ligand-induced stimulation led to an initial translocation of LIFEA2 to the PM that was paralleled by a reduction of its average FL lifetime (τ). This was followed by internalization of receptors and increase in average FL (τ) (**Fig. 3.31 (D)**).

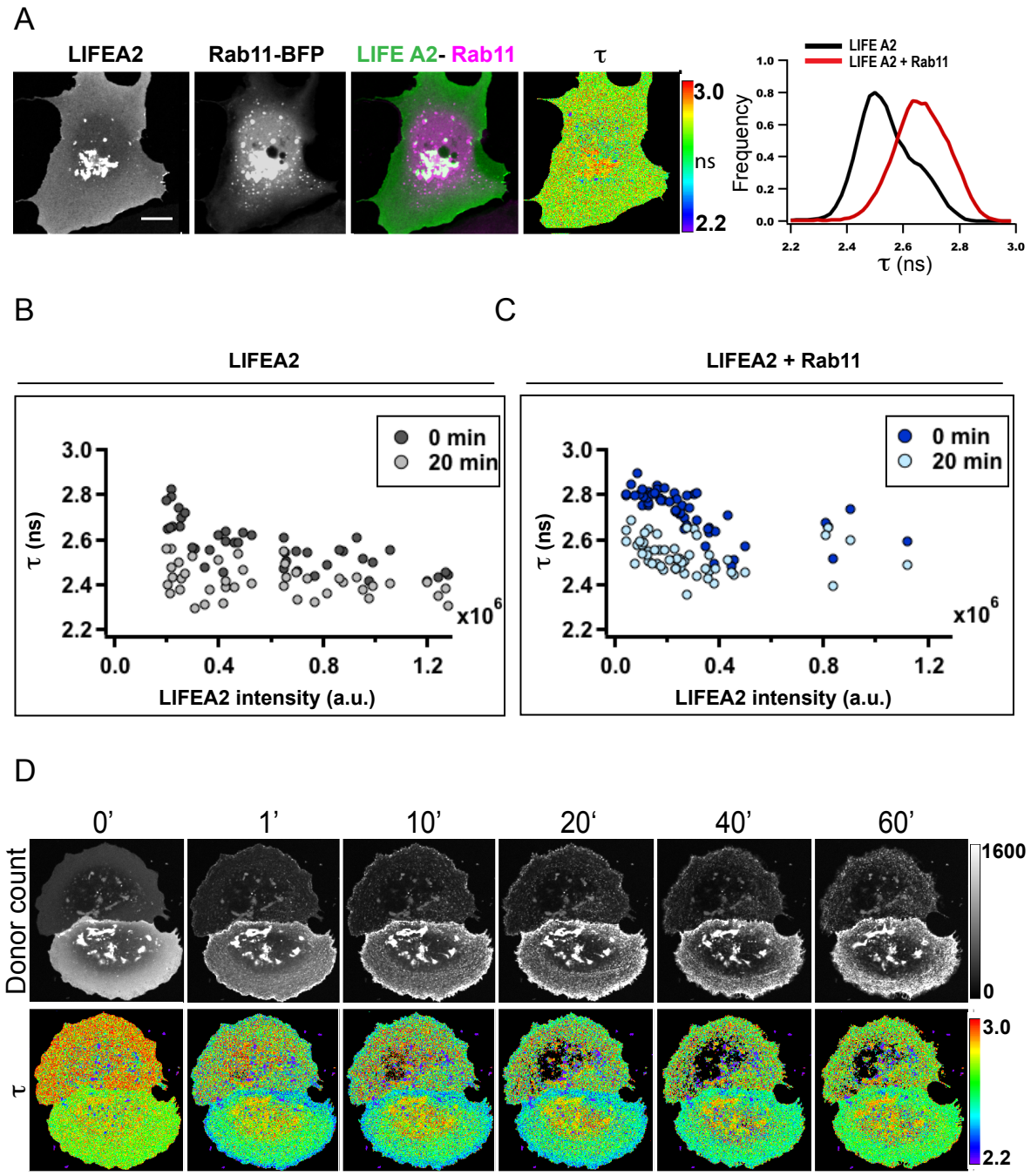

Fig 3.31 Recycling as a protective mechanism against spurious LIFEA2 activation
(**A**) Recycling of EphA2 protects against spurious phosphorylation and activation. Left: average FL lifetime maps of representative COS-7 cells transiently co-expressing LIFEA2 and Rab11. Scale bar: 10 μm. Right: Quantitative analysis of LIFEA2 FL lifetime (τ) distribution in the absence (black trace) and presence of Rab11 ectopic expression (red trace), n=3 experiments. (**B**) Individual data points represent integrated intensity and the mean FL lifetime (τ) of LIFEA2 for selected cells 20 min with (grey) and without ligand (black). (**C**) Individual data points represent integrated intensity and the mean FL lifetime (**τ**) of LIFEA2 for selected cells 20 min with (cyan) and without ligand (blue). (**D**) Spatial temporal organization of LIFEA2 active state in living cells monitored by FLIM. Upper row: photon counts from the donor channel. Lower row: average FL lifetime (**τ**) maps, color-coding is shown on the right.

To confirm that this recycling mechanism indeed protects against spuriously phosphorylated receptors, EphA2 *auto*phosphorylation when Rab11 is ectopically expressed was investigated. COS-7 cells ectopically expressing EphA2-citrine or EphA2-citrine and BFP-Rab11 were fixed, permeabilized and stained with a phospho-tyrosine specific antibody (PY72) labeled with Cy3.5 (**Fig. 3.32 (A)**). Phosphorylation of EphA2 leads to PY72 binding and FRET between citrine-tagged EphA2 and Cy3.5 PY72 can be detected by the reduction in citrine FL lifetime as monitored by FLIM. The Rab11 marked RE that showed substantial colocalization with EphA2-citrine did not show significant tyrosine phosphorylation (**Fig. 3.32 (A)**). Quantification of EphA2-citrine average FL lifetime (τ) in relation to EphA2-citrine intensity, showed a lower FL lifetime (τ) at higher receptor expression levels indicative of its *auto*catalytic activation. In the presence of Rab11, a shift to higher average FL lifetime (τ) could be observed, indicating a lower tendency for self-activation as compared to EphA2 alone (**Fig. 3.32 (B)**). The ligand-independent response behavior of EphA2 in the presence of an enlarged RE further strengthen the notion that constant receptor recycling to the PM acts as a safeguard mechanism against spurious receptor phosphorylation.

We next wanted to investigate the changes in EphA2 population residing on the RE after ligand-induced stimulation. If EphA2 is constantly being trafficked between the PM and the RE to safeguard against receptor self-activation, then how can the ligand disrupt such an equilibrium to ensure robust activation and subsequent termination of signaling. To investigate this, COS-7 cells ectopically expressing EphA2-citrine, BFP-Rab11 and cherry-Rab7 as a marker for the late endosomal (LE) compartment, were imaged with confocal microscopy. Prior to ephrin stimulation, EphA2 colocalized with Rab11 on the RE, with no apparent colocalization with Rab7 (**Fig. 3.32 (C)**). Ligand-induced activation initially caused a net translocation of EphA2 towards the cell-periphery with a reduction in amount of colocalization between EphA2 and Rab11. This was followed by massive internalization of the receptor with a delayed slight enrichment of EphA2 on the RE and more enrichment on the LE.

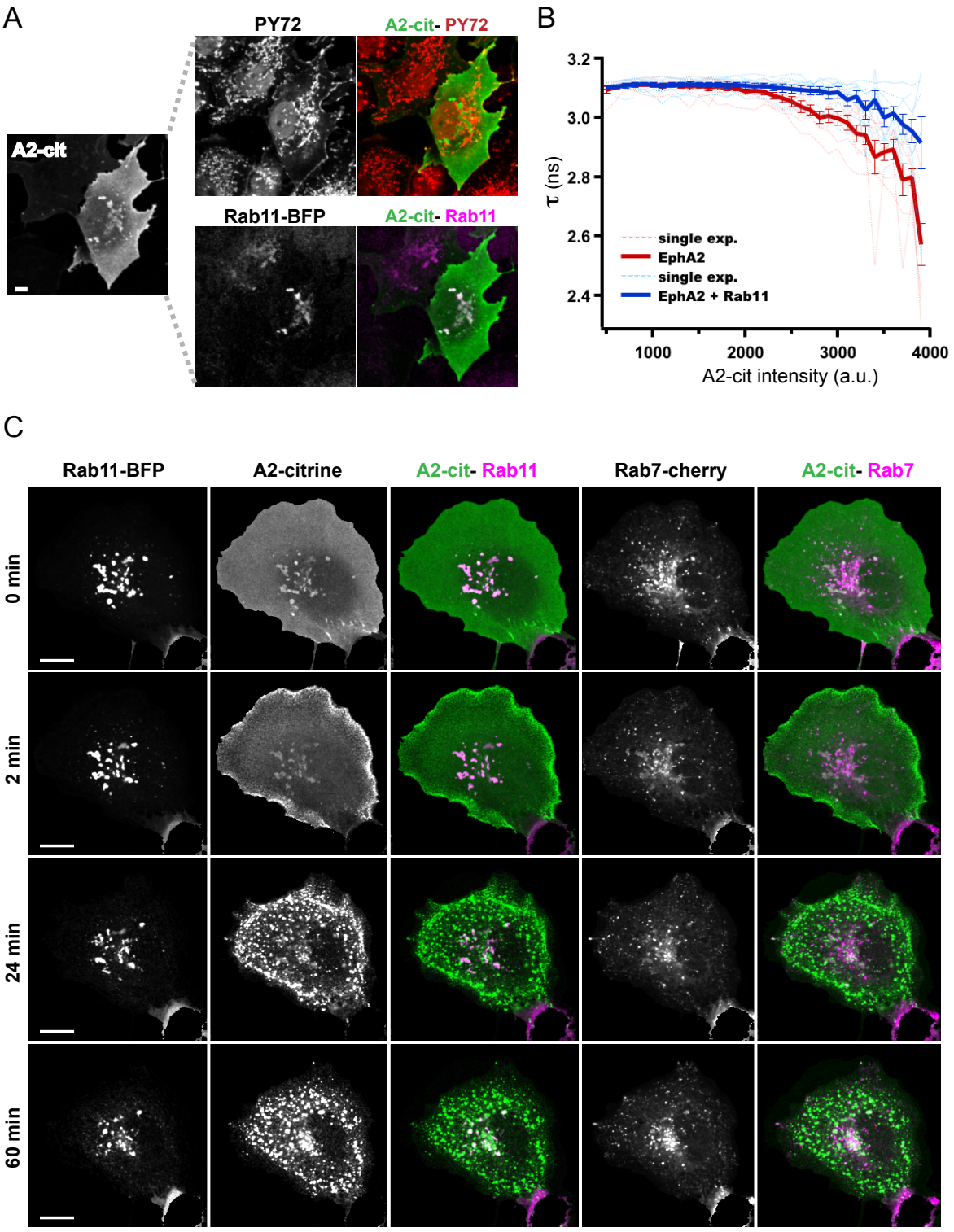

Fig 3.32 Constant recycling protects against spurious EphA2 phosphorylation.
(**A**) Representative COS-7 cells expressing EphA2-citrine and Rab11-BFP were fixed and stained with an anti-phospho tyrosine antibody (PY72). Scale bar: 10 μM (**B**) Quantification of intermolecular FRET between EphA2 citrine and Cy3.5 labeled PY72 in absence (red trace) or presence (blue trace) of Rab11. Histograms are a plot of EphA2-citrine average FL lifetime (τ) in correlation to EphA2-ctrine intensity (pixel by pixel) from n=40 cells. Data represent mean ± SEM. (**C**) The recycling endosome as a source for ligand-induced Eph translocation to PM. Spatial-temporal profile of EphA2-citrine activation in living cells coexpressing BFP-Rab11 and cherry-Rab7. Scale bars: 10 μm.

Quantification of EphA2/Rab11 colocalization prior to and after ephrin-induced stimulation showed an initial loss of EphA2 from the RE, suggesting the trafficking of receptors towards the PM (**Fig. 3.33**). Ligand-induced translocation of Ephs towards the PM enhances its activation and initiates a massive burst of signaling-mediated receptor internalization into the endocytic pathway.

Fig 3.33 Dynamic interactions between Rab11 and EphA2
(**A**) Representative COS-7 cells expressing EphA2-citrine and cherry-Rab11 were stimulated with preclustered ephrinA1-Fc. Scale bar: 10 μm (**B**) A mask of the RE was used to quantify changes in EphA2 citrine FL intensity in two ROIs and show an initial loss of EphA2 from Rab11 +ve endosomes followed by slight reentry.

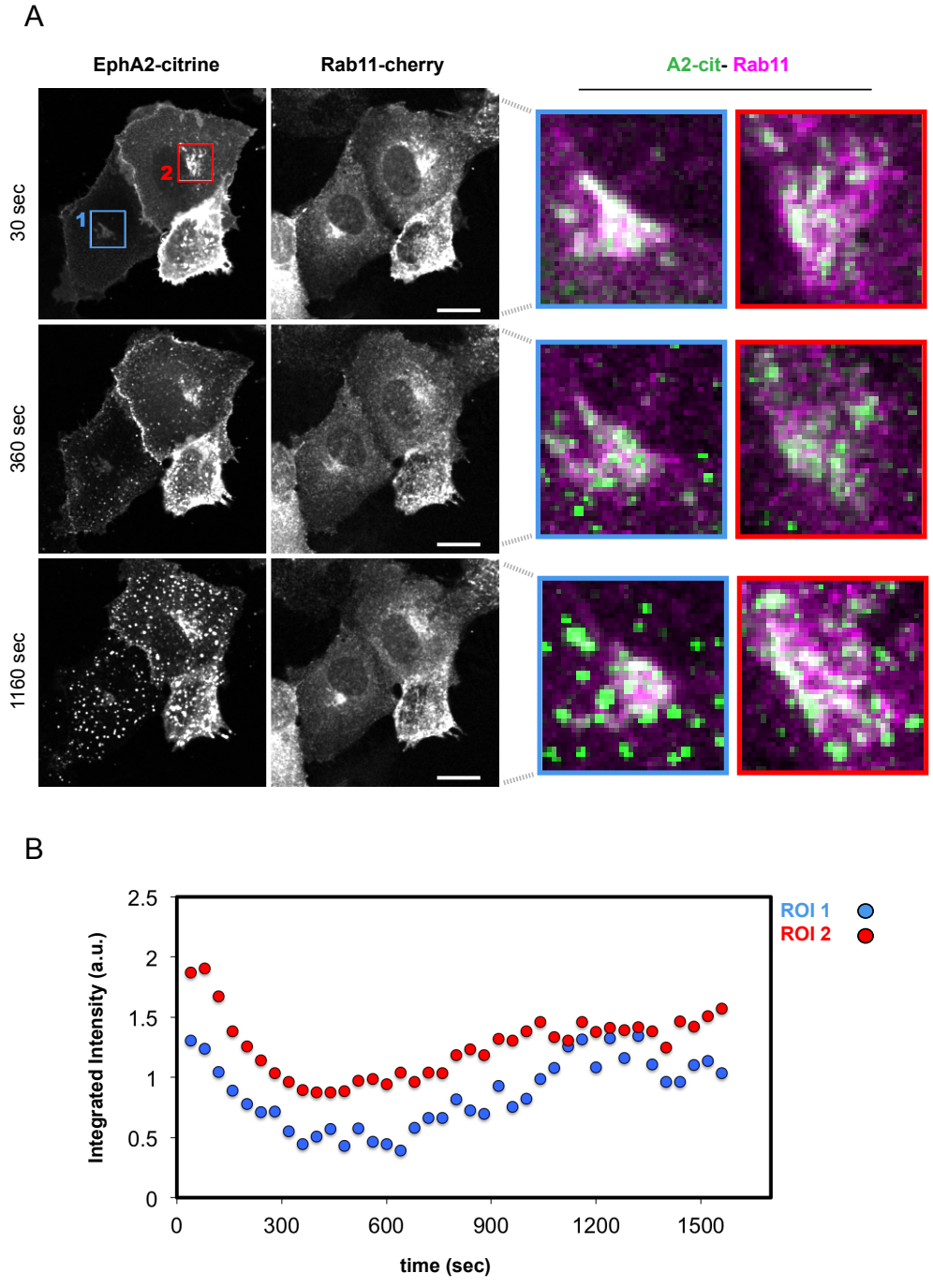

Quantification of EphA2/Rab7 colocalization showed a continuous and slow enrichment of EphA2 onto Rab7^{+ve} late endosomal (LE) compartments after ligand stimulation (**Fig. 3.34**). This indicates that ligand-induced signaling-mediated receptor internalization slowly targets Ephs to the degradative pathway.

Fig 3.34 Dynamic interactions between Rab7 and EphA2
(**A**) Representative COS-7 cells expressing EphA2-citrine and cherry-Rab7 were stimulated with preclustered ephrinA1-Fc. Scale bar: 10 μm (**B**) Quantification of EphA2-citrine FL mapping to Rab7 FL on the late endosomal compartment shows continuous slow entry of EphA2 into Rab7 +ve endosomes.

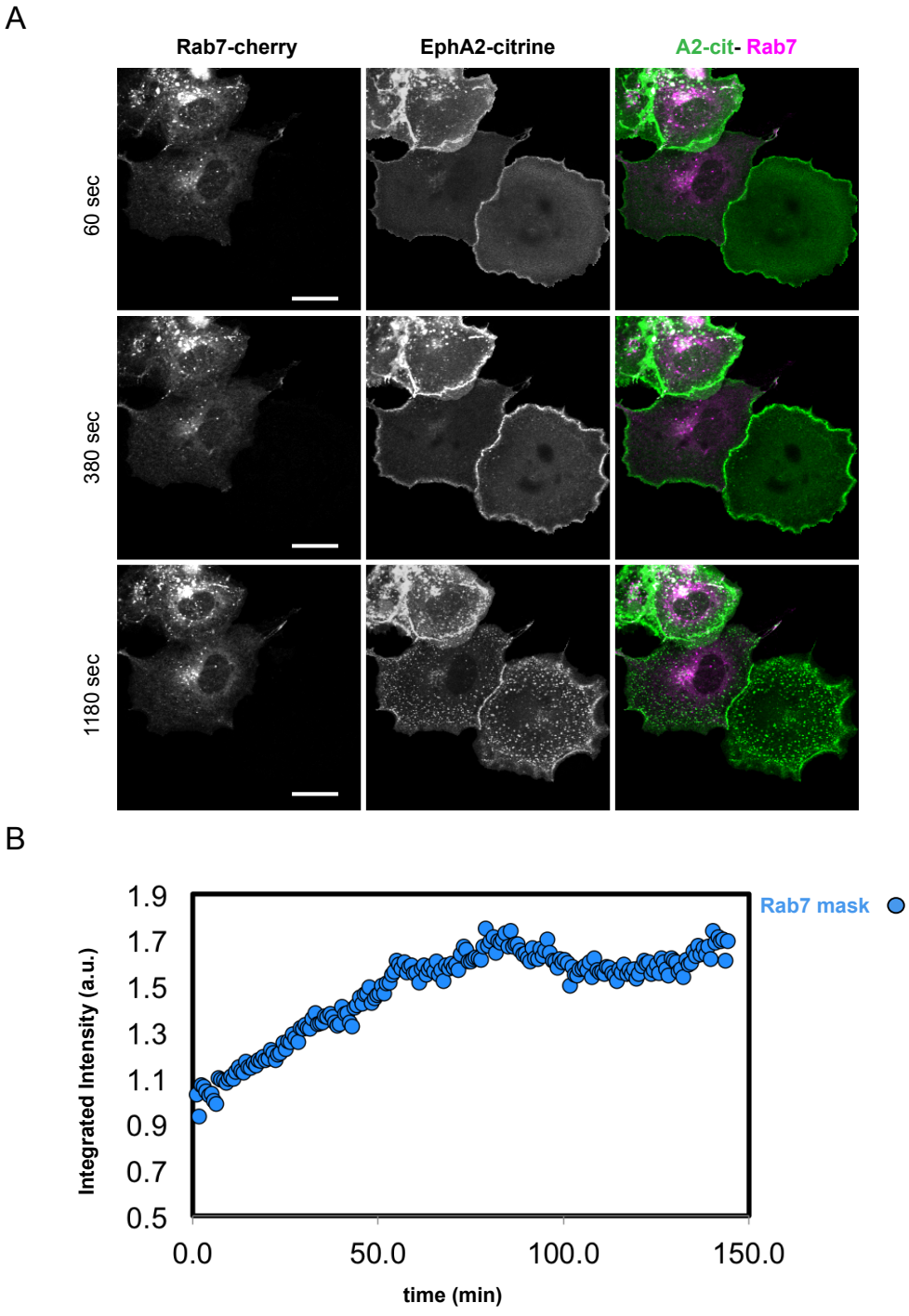

To demonstrate that EphA2 residing on the RE was continuously recycling to the PM, we tracked the mobility of EphA2 fused to photoactivatable GFP (EphA2-paGPF) in live cells [215]. EphA2-paGFP, EphA2-cherry and Rab11-BFP were ectopically expressed in COS-7 cells. EphA2-cherry served as a marker for RE population of EphA2 (**Fig. 3.35 (A)**). Photoactivation of EphA2-paGFP (405 nm) specifically at the RE resulted in increased fluorescence. Continuous imaging of photoactivated EphA2-paGFP as compared to EphA2-mcherry, revealed an increase of fluorescence intensity at the PM. Using EphA2-cherry as a normalizing factor for changes in the photoactivated EphA2-paGFP fluorescence, we quantified the time constants for fluorescence loss after photoactivation at the RE and the complementary fluorescence gain at the PM (**Fig. 3.35 (B) & (C)**).

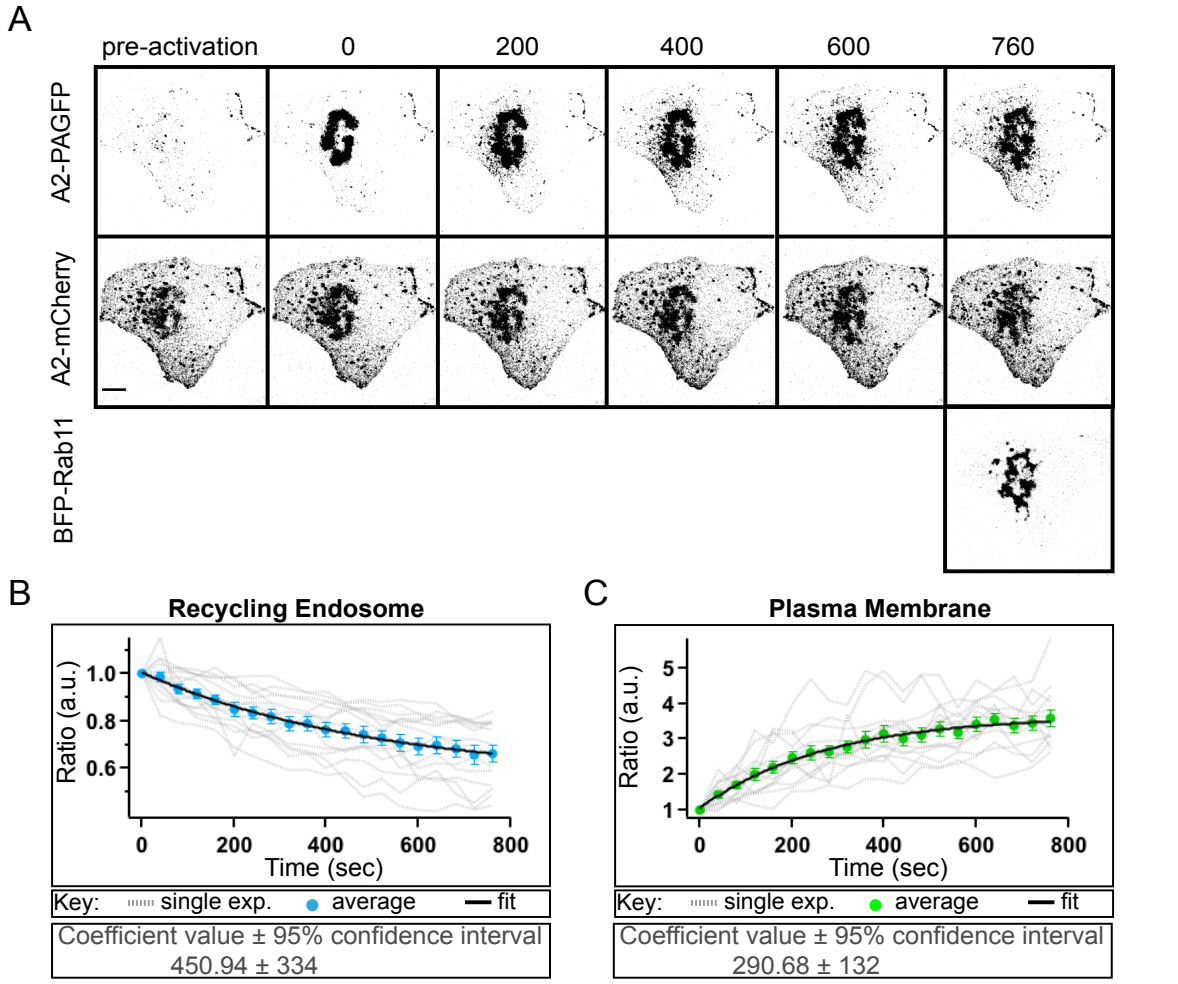

Fig 3.35 Vesicular transport of Eph from the RE to the PM
(**A**) COS-7 cells expressing EphA2-paGFP (upper row), EphA2-cherry (middle row) and Rab11-BFP (lower row) were photoactivated specifically at the RE, and the fluorescence intensity of EphA2-paGFP at the RE and at the PM was resolved. Scale bar: 5 μM. Quantification of the change in fluorescence ratio (EphA2-paGFP/EphA2-cherry) at the RE (**B**) and PM (**C**) was done and an average of FL decay curves was fitted with a single exponential equation to retrieve time constants, (n=14 independent experiments).

4. DISCUSSION

Eph RTKs and their membrane-bound ephrin ligands are involved in controlling cell positioning during development and disease. Eph/ephrin interactions can decide the fate of cell-contact points by promoting either cell-cell adhesion or repulsion. It is currently not clear how the same Eph/ephrin interaction can have opposing tendencies, and this will likely depend on several factors, including the degree of Eph and ephrin clustering, the activity of cellular phosphatases and the spatial organization of Eph activity [56,124,133,144,216]. In this thesis, the main aim was to understand how the activity of Eph RTKs, with inherent *auto*catalytic properties and intrinsic structural features that promote dimerization and clustering, is spatially-temporally regulated.

The formation of higher-order clusters is a unique feature of Eph/ephrin family among other RTKs [12]. Using an FKBP-based dimerizing system, we find that the relative abundance of oligomers over dimers within a cluster population determines the strength of EphB2 response. Furthermore, a negative regulatory effect on ephrin-induced clustering by C-terminal domains of EphB2 and a positive effect on receptor clustering by GRIP1 protein was identified. These results suggest that a given Eph-ephrin interaction can either cause cell-cell repulsion or adhesion depending on the context of the interacting cells.

In addition to Ephs structural features that allow for receptor clustering and activation, its phosphorylation-dephosphorylation cycle is partitioned spatially and temporally inside the cell owing to interactions with protein tyrosine phosphatases (PTPs). Recent work identified EphA3 as a substrate for the ER-anchored PTP1B [133]. We report EphA2 as an additional substrate for PTP1B at points of cell-cell contact. Non-competitive allosteric inhibition of PTP1B creates EphA2 phosphorylation hot spots at points of cell-cell contact, thereby highlighting ER-PM interactions as an emerging new paradigm in cellular signaling. On the other hand, ligand-induced activation of EphA2 locally increases cellular H_2O_2 levels raising the possibility of a double negative feedback-loop whereby EphA2 negatively regulates its own inhibitory PTP in order to spread the activation signal.

Using a genetically encoded biosensor that monitors EphA2 conformational dynamics (LIFEA2), we describe the dynamics of Eph activation with precise spatial & temporal resolution. Like other RTKs, Eph activity is regulated by reversible *auto*-phosphorylation of key tyrosine residues in its intracellular domain.

Self-amplifying systems as such have the propensity to self-activate even in the absence of stimulus, necessitating the need for suppressive mechanisms that yet allow for robust activation when needed. Suppressive mechanisms can be intrinsic structural features as with *auto*regulation of Eph kinase domain (KD) through intramolecular inhibitory interactions by the juxtamembrane segment (JMS), or cell-imposed regulatory machineries. We find that interactions between EphA2 JMS and KD are not ON-OFF as previously suggested, but a dynamic process where the JMS is continuously moving between an ordered state that inhibits the KD and a disordered state that allows for KD activation. This dynamic process allows the KD to continuously sample different conformations one of which is stabilized by ligand-induced phosphorylation and defines the catalytically competent state.

Finally, we identify continuous receptor recycling through Rab11-positive endosomes as a novel cell-intrinsic safeguard mechanism against concentration dependent EphA2 self-activation. The recycling endosome modulates the amount of Eph available for activation on the plasma membrane at steady state and traffics the receptor through the peri-nuclear region rich in active PTP1B for efficient dephosphorylation.

4.1 Functional significance of clustering for Eph signaling

The clustering propensity of Eph subfamily of RTKs raises questions about its role in signal transduction. It has been argued that receptor clustering confers a wide range of advantages including, tunable sensitivity to extracellular ligand [217,218], enhanced specificity [219] and segregation as a means of limiting cross-talk between signaling systems [220,221] . How clustering translates into molecular features defining Eph-ephrin response is still poorly understood. We used chemical dimerizers to generate defined oligomeric states of EphB2 receptors in living cells and analyzed their biochemical and physiological properties. Four important observations could be conferred: **(1)** Small-sized EphB2 clusters produce functional cell responses, an unexpected finding in light of the finding that EphA2 tends to form large signaling arrays [42]; **(2)** The relative abundance of active multimers (trimers, tetramers and oligomers) over inactive dimers determines the strength of EphB2 signaling, suggesting an ON-OFF activation mechanism; **(3)** Overexpression of the intracellular scaffolding protein GRIP1 can enhance ephrin-induced EphB2 clustering, indicating that intracellular clustering can provide a means to alter the cell's sensitivity towards extracellular stimuli **(4)** the C-terminal SAM domain and PDZ binding motif in the intracellular domain of EphB2 reduce EphB2 clustering in the presence of extracellular ephrins, an unexpected result in light of the inclination of SAM domains to oligomerize.

Small sized EphB2 clusters are fully activated

Crystal structures of whole EphA2 ectodomains bound to ephrinAs [42,43] suggested that Eph/ephrin clusters form large two-dimensional signaling arrays. However, it has so far been difficult to functionally assess the different oligomeric states of Ephs formed in living cells, in part because of the dynamic nature of the process [56,144]. Using different FKBP isoforms of EphB2, we generated and characterized defined clusters: dimers (1FKBP), mostly small-sized clusters (2FKBP) or larger clusters (3FKBP) (**Fig 3.10 & 3.11**). Fluorescence anisotropy imaging of physiological ephrinB/EphB interactions at cell contact sites, was then undertaken to determine the abundance of monomers, dimers and multimers in ephrin/Eph clusters (**Fig 3.12**). We find that ligand-free Eph receptors are monomeric and that clusters are heterogeneous consisting of dimers and multimers. Comparison of the relative phosphorylation of larger oligomers (trimers up to hexamers) in the two cluster populations (2FKBP and 3FKBP) did

not reveal significant differences (**Fig. 3.13 (B)**), suggesting that small-sized clusters (trimers/tetramers) are already fully activated and that the presence of larger clusters (pentamers, hexamers, etc.) serves a different purpose than enhancing phosphorylation of the system.

EphB2 follows an ON-OFF mechanism

While growth factor activation of RTKs generally occurs during transition from monomers to dimers [7], our data shows that the activation switch of EphB2 (and EphA4) receptors occurs during the transition from dimers to trimers/tetramers. The clearest difference between the two EphB2-FKBP cluster populations was the relative ratio of inactive states (monomers/dimers) to active states (≥trimers). The ratio of inactive to active states was 1:3 in cells expressing the 2FKBP isoform, but it became 1:10 in cells expressing the 3FKBP isoform (data not shown). This points to the fact that the strength of the cellular response is determined by the relative abundance of higher-order oligomers versus monomers/dimers within EphB2 clusters. This can explain how a possible ON-OFF mechanism can account for the documented Eph graded responses necessary for topographic mapping. Oligomerization might be important for Eph signaling to: **(1)** Relieve *auto*inhibition imposed on the receptor, since in bigger or more stable clusters the Eph intracellular domain may spend more time in the active conformation and produce stronger signaling output. **(2)** Produce a molecular crowding effect that limits the spatial freedom of each receptor molecule leading to a shift in the conformational steady state equilibrium as described by others [222,223]. **(3)** Protect phosphorylated residues of receptors in the center of the cluster from tyrosine phosphatases and thereby produce an overall stronger activity.

Adaptor proteins can precondition Eph response to extracellular ephrin

We provided direct evidence that cells may use intracellular Eph adaptors such as GRIP1 to precondition themselves towards extracellular ephrin (**Fig 3.14**). Because Eph/ephrin signaling is bi-directional, this raises the additional possibility that adaptor-induced clustering influences ephrinB reverse signaling. It has been shown that interaction of EphB2 with GRIP1 can regulate reverse signaling of ephrinB3 at specific hippocampal synapses [224]. It is possible to conceive that endogenous GRIP enhanced EphB2 clustering in these neurons, thereby providing stronger *trans* interactions with ephrinB3 that led to stronger reverse signaling.

SAM/PDB domains as steric spacers counteracting ephrin-induced EphB2 clustering

Finally we report that deletion of SAM domain and PDZ binding motif (PDB) from EphB2 augmented EphB2 clustering and signaling. This is contrary to expectations considering previous work identifying the positive effect isolated SAM domains have on clustering and the positive effect PDZ domain interactions have on Eph/ephrin signaling [225,226]. SAM/PDB deletion mutant showed a difference response to wtEphB2 only upon ephrin stimulation suggesting the following model: ephrinBs binding initiates EphB2 clustering and recruitment of cytoplasmic proteins via SAM and PDZ domain associations and that these interactions limit EphB2 clustering (for example: by protein modifications or steric hindrance). Freeing EphB2 from these interactions, as with the EphB2ΔSAM/PBM mutant will therefore increase receptor clustering and signaling. In line with this finding, a similar deletion mutant of EphA4 retained full activity in a Xenopus morphogenesis assay, and a conserved tyrosine residue in the SAM domain was proposed as a protein-protein interaction site for a negative regulator [56,227]. If indeed SAM/PDB domain acts as a steric spacer for Ephs *in vivo*, then this offers a mechanistic explanation for a switch from repulsive to adhesive cellular responses as seen in cells co-expressing truncated EphA7 splice forms or ephrins [228,229].

4.2 Spatial organization of the phosphorylation-dephosphorylation cycle

Classically, RTK-mediated signal transduction implied ligand binding for receptor dimerization and activation via *trans*-phosphorylation [230]. Such a view however, does not take into account the conformational dynamics and flexibility of a kinase domain, ligand gradients and random receptor collisions on membranes, all of which can lead to high basal receptor activity and spurious phosphorylation. Cell-imposed regulatory mechanisms that act as a safeguard mechanism against high RTK activity are therefore essential to understand and manipulate as a possible method for controlling aberrant RTK activity coupled to tumorigenesis. A receptor-extrinsic regulatory mechanism for tyrosine phosphorylation and an active partner in phosphotyrosine-based signaling is the process of dephosphorylation undertaken by protein tyrosine phosphatases (PTPs) [3,4,231]. Sufficient data suggests, that functions of these PTPs are controlled by changing their subcellular localization within the cell and/or through covalent modifications of their cysteine-dependent catalytic site [230,231]. The invariant Cys residue found in the PTP superfamily signature motif [I/V]HCXXGXXR[S/T] displays an unusually low pKa, which increase its susceptibility to oxidation [232]. Of particular interest in this study is PTP1B, which contains 35 predominantly hydrophobic residues at its C-terminus that target the enzyme to the endoplasmic reticulum (ER) membrane [199]. How the ER-anchored PTP1B can interact with and affect a PM receptor in a spatial-temporal manner is a conceptual dilemma that has been extensively investigated. We used quantitative cellular imaging techniques and mathematical modeling of protein mobility to explore how PTP1B can reach and interact with cell-cell contact bound substrates. The following observations could be conferred: **(1)** The ER network is in close proximity to the PM at regions of cell-cell contact, thereby allowing the ER-anchored PTP1B to interact with substrates at those sites; **(2)** The PTP1B ER-anchor plays a pivotal role in restricting its interactions with cell-cell contact bound substrates; **(3)** Selective inhibition of PTP1B leads to increased tyrosine phosphorylation and activation of EphA2, more so at regions of cell-cell contact, thereby identifying those sites as important target regions for regulation by PTP1B [134]; **(4)** Ligand induced activation of a H_2O_2 sensitive EphA2 chimera led to increased production of ROS, suggesting an underlying bistable reaction network as a possible mechanism for spreading Eph activation signal.

The ER extends to regions proximal to PM at cell-cell contacts

The contribution of the ER-anchored PTP1B to the regulation of phosphorylation of several RTKs was initially surprising considering their spatial segregation inside the cell. Where some studies showed that dephosphorylation by PTP1B takes place when endocytosed RTK transit past the ER [128,129], others suggested a direct contact between PTP1B and its PM and/or adhesion sites localized substrates [130,131], or a possible recruitment of PTP1B to the cell surface upon Eph-ephrin cell-cell contact [133]. We show that the accumulation of the substrate-trapping mutant of PTP1B (D181A) [233] at points of cell-cell contact can be abolished by thiol-reactive compounds like pervanadate [234]. Inactivation of PTP1B D/A by pervanadate occurred without altering its ER localization or that of the wild type PTP1B [134], indicating a substrate-mediated enrichment of PTP1B at points of cell-cell contact. However, nocodazole-based disruption of microtubules and hence destabilization of the ER-network [201,202], highlighted the ER's intrinsic polarity and stability at points of cell-cell contact. These findings indicate that PTP1B-substrate interactions at points of cell-cell contact do not solely account for the polarity of ER towards those specialized regions. Rather, the presence of an intrinsic polarity of the ER towards cell contact points, directs PTP1B to those regions. Varying rates of endocytosis at cell-cell contact regions as compared to the rest of the PM is a factor that we didn't investigate and might account for the differential ability of PTP1B to access cell-contact bound substrates. Varying amounts and types of substrates at point of cell-cell contact might also account for PTP1B recruitment to regions of cell-cell contact. However, uniform EGFR expression on the PM, still showed enhanced PTP1B (D/A)-EGFR interactions at regions of cell-cell contact [134]. One can of course still argue, that unequal density of other RTKs or tight junction specific proteins such as p120 catenin at points of cell-cell contact can dictate where PTP1B interacts with substrates.

Regulation of Eph signaling by PTP1B

Why then is the ER-anchored PTP1B oriented towards regions of cell-cell contact? Allosteric inhibition of PTP1B led to increased tyrosine phosphorylation of EphA2, seen as increased co-localization with SH2 domain of $pp60^{Src}$ (**Fig 3.7**). These findings identify cell contact points as important target regions for regulation by PTP1B and highlight a role for PTP1B in maintaining a dephosphorylated EphA2 receptor prior to stimulation. Indeed overexpression of

PTP1B reduced basal EphA2 phosphorylation and activation indicative of negative regulation (**Fig 3.29**). Ligand-independent EphA2 phosphorylation upon allosteric inhibition of PTP1B may still result from the action of a heterologous kinase. This argument can only be disproven if inhibition of PTP1B was coupled to a kinase inhibitor of EphA2 or if a kinase dead variant of EphA2 (K645R) was used. Pending these experiments, one can argue that PTP1B inhibition modulates endocytosis and recycling of EphA2 from and to points of cell-cell contact. Changes in receptor PM residence time, can increase the chances of receptor *auto*-activation at points of cell-cell contact. However, this argument would require a polarity of the endocytic/recycling machinery towards regions of cell-cell contact, a hypothesis that remains to be tested.

Regulation of PTP signaling by Eph-induced ROS production

If cell-contact points are rich in PTP1B activity, how can Eph signaling actively contribute to decision making at those sites? Ligand-dependent activation of RTKs may be coupled to transient PTP inactivation through increased production of H_2O_2 [137-141]. To detect H_2O_2, we created a chimera consisting of full-length EphA2, attached via a linker to the H_2O_2–sensitive Hyper[214]. Ectopic expression of EphA2-Hyper showed enhanced H_2O_2 production at cell contact points that could be further increased upon ligand stimulation. Opposing gradients of Eph and PTP activities might therefore comprise a reaction cycle required for the establishment of a signaling threshold close to the PM & points of cell-cell contact. Previous work defining the coupling between EGFR activity and protein tyrosine phosphatases has shown that the reaction network is characterized by bistable response properties, which explains how high levels of phosphorylated EGFR can be maintained on the PM prior to ligand exposure [235]. Production of H_2O_2 by EphA2 (**Fig 3.30**) or EphB2 (data not shown) indirectly points to such coupling with PTP1B. Further experiments are needed to verify the role of H_2O_2 in Eph system response. Reducing the amount of produced ROS with enzymatic-hydrogen-peroxide-scavenging systems such as catalase and/or with the NADPH oxidase inhibitor diphenyleneiodonium (DPI) [213]would change the response of the reaction network if indeed EphA2 and PTP1B activities were tightly coupled.

4.3 Spatial organization of EphA2 activity

Similar to other RTKs, activation of Ephs follows a general framework beginning with, ligand binding, receptor oligomerization at the PM, activation of the intrinsic KD activity and consequently *trans*-phosphorylation of key tyrosine residues on the intracellular domain. Tyrosine phosphorylation affects the signaling properties of Ephs in at least two ways. First, phosphorylation of two tyrosine residues in the conserved JMS relieves JMS-mediated *auto*inhibition of the KD and creates docking sites for downstream effectors [74-77]. Second, *auto*phosphorylation of a key tyrosine residue within the kinase activation loop (AL), known as Tyr_{ACT} changes the structure of the receptor and stabilizes the active conformation of the kinase domain. Despite knowledge gained from structural studies, how Eph receptor activates in living cells is still incompletely understood. In particular, how liganded receptor constitutes a different signaling entity when compared to overexpressed self-activated receptors that manage to evade *cis*-inhibiton by the JMS. To study the spatial regulation of the *auto*catalytic activation mechanism of Eph receptors, we generated a genetically encoded FRET-based activity sensor for EphA2.

Based on the conformational change that takes place upon full activation of Ephs by phosphorylation, we could confer the following observations: **(1)** Interactions between the JMS and the KD of Eph are not ON-OFF as previously suggested [25], but a dynamic process where the JMS is continuously switching between a tight (inactive KD) and a relaxed (activatable KD) conformation in the absence of ligand. This intra-domain "breathing" allows for *auto*catalytic activation when the local concentration of receptor is raised by ligand-induced crosslinking. **(2)** Ligand-induced clustering and activation of Ephs occurs through step-wise conformational transitions that involves both the JMS and AL and as such identify the JMS as an intrinsic safeguard mechanism against spurious receptor activity. **(3)** The ATP competitive inhibitor dasatinib, inhibits EphA2 activity by locking the KD in an active conformation and thereby uncouples conformational flexibility from ligand-induced receptor crosslinking. **(4)** Ligand-independent activation of EphA2 on the PM can occur at high receptor expression levels, necessitating the need for a cell-intrinsic control mechanism that maintains low levels of Ephs on the PM. **(5)** Ectopic expression of the ER-anchored PTP1B or enhancement of the slow recycling compartment through ectopic expression of Rab11 demonstrates such a cell-intrinsic regulatory mechanism. Constant recycling of EphA2 through Rab11-

positive endosomes controls its steady-state level at the PM, and traffics it through the peri-nuclear region rich in active PTP1B, thereby safeguarding against spurious receptor *auto*activation.

Design of an EphA2 sensor for mapping receptor activation in space and time

Our current understanding of KD regulation is mostly inferred from biochemical experiments done on large populations of cells and/or structural studies. So in a way it is either information gathered from an "averaged cell", with biological-relevant variance lying beyond the limits of detection [236], or information gathered from crystallographic snap shots that represent the most crystal favored conformation rather than the multiple states a full-length protein can adopt in living cells. Good spatial resolution of protein organization can be acquired through immunofluorescence experiments, but it offers poor temporal resolution considering that it requires fixation of cells, a strenuous process that changes the architecture of the cells and arrests dynamic processes. Precise spatial and temporal information of intracellular reaction dynamics can be attained with the help of functional fluorescence microscopy that exploits the photophysical properties of genetically encoded green-fluorescent proteins (GFPs). One of the photophysical phenomena regularly used in live-cell functional imaging is Förster Resonance Energy Transfer (FRET). FRET has proven to be an invaluable tool in measuring protein dynamics, as the efficiency at which Förster –type energy transfer occurs is steeply dependent on the distance (**Equation 4**) between two FPs (donor and acceptor) and the relative orientation of their transition dipoles (**Equation 5**) [177,179,237,238]. To design a sensor that reports on the conformational dynamics of EphA2 in living cells, we placed the donor FP before the regulatory JMS and acceptor FP at the C-terminus of EphA2. Conformational changes coupled to EphA2 activation translated into a change in the relative distance and/or angle of the two FPs, which results in a change in FRET measured by FLIM as a change in donor fluorescence lifetime (τ). To allow for inserted FP folding (average distance between N and C- terminus of GFP is ~20 Å) and at the same time reduce the extent of disruption to EphA2 secondary structure (average distance between adjacent amino acids ~3.5 Å), various linkers were tested for in-frame FP insertion. The idea was to use linkers with different secondary structures rather than varying their length, ranging from a strict coiled-coil to an unstructured linker or a combination of both. After screening, the combination of coiled-coil (next to

EphA2) and flexible linker (next to the JMS-inserted FP) (**Fig 4.1**) was picked as the **L**inker-optimized, **I**ntramolecular **F**RET-based activity sensor for **E**ph**A2** (LIFEA2).

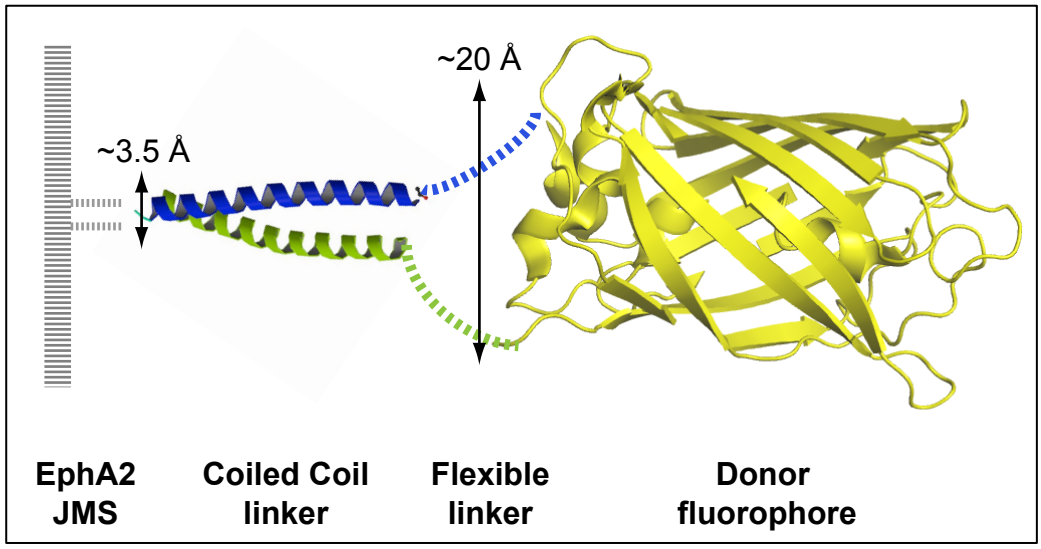

Fig 4.1 Model of donor FP insertion into EphA2 JMS via an optimized linker

Expression of LIFEA2 did not cause any protein mislocalization, cytotoxicity or changes in cell morphology (tested in COS-7, MDCK, MCF7 and HEK293 cells). In addition, stimulation of LIFEA2 with pre-clustered purified ephrinA1-Fc showed similar phosphorylation profiles to C-terminally tagged EphA2 or endogenously overexpressed EphA2 in MDA-468 cells, and induced cell shrinkage in cultured cells. In total, LIFEA2 as a genetically encoded single-chain biosensor allowed us the following possibilities: **(1)** the choice of detecting FRET with either intensity-based approaches, or FLIM. The latter is advantageous since fluorescence lifetime is an intrinsic property of the FP that is insensitive to variations in instrumental setting or probe emission intensity and concentration [172]. More importantly, FLIM measurements are robust across separate experiments and therefore allow for direct comparisons. **2)** Visualization of steady state JMS-KD conformational dynamics in living cells with high spatial and temporal resolution. **(3)** Correlation of receptor expression level to its active state in the same cells before and after ligand stimulation. Thereby overcoming the introduction of errors arising from averaging different populations of cells. **(4)** Monitoring the effect of the spatially organized phosphorylation-dephosphorylation cycle on Eph activity and conformational dynamics. **(5)** The chance of increasing the complexity of cell-culture systems to 3D vasculogenic models that can be imaged with single plane illumination microscopy (SPIM)-FLIM.

Autonomous activation of EphA2

Like other RTKs, EphA2 activity is regulated by reversible *auto*-phosphorylation of key tyrosine residues in its intracellular domain. Self-amplifying systems as such have the propensity to activate even in the absence of stimulus, necessitating the cell to evolve suppressive mechanisms that yet allow for robust activation when needed. To investigate the self-activating capacity of EphA2, we determined the ligand-independent activity of EphA2 as a function of its expression level. By calibrating our microscopy settings across all experiments, we obtained cell-to-cell variance in LIFEA2 expression relative to its activity state (**Fig 3.19**) and JMS phosphorylation (**Fig 3.21**). Steady-state conformational dynamics of LIFEA2 that report on the receptor's active state, exhibited a bimodal distribution of activated and nonactivated receptors with a switch-like response behavior that is sensitive to the expression levels of the receptor (**Fig 3.19**). Ultrasensitivity has been described before by Goldbeter-Koshland as an inherent property of reversible covalent modification schemes such as phosphorylation/ dephosphorylation cycles when both converting enzymes work under Michaelis-Menten saturable kinetics with respect to the protein substrate [239]. In this thesis we found that Eph activation generates H_2O_2 suggesting a reactive oxygen species (ROS)-mediated coupling between Ephs and phosphatases as described earlier for EGFR. ROS-mediated coupling between EGFR and PTPs create a bistable reaction network with switch-like rather than graded response properties and explain how high amounts of phosphorylated receptors reside on the PM prior to ligand stimulation [235]. The ability of Ephs to abruptly switch steady state conditions points to the *auto*catalytic nature of EphA2 activation and suggest ROS as the underlying mechanism allowing an increase in receptor expression to shift the system from the "stable" to the "bistable" or even the "constitutively active" state [235,240] (**Fig 4.2**).

Fig 4.2 Eph and PTP reaction network
(**A**) Reaction network scheme showing the possible coupling of PTP inhibition through H_2O_2 (dashed line) and Eph activation. Black arrows represent a change of protein state grey arrows indicate catalysis. (**B**) Calculated fraction of phosphorylated RTK (RTKp) at steady states as a function of the relative maximal PTP to RTK activity (PTP/RTK). Green and red lines are stable steady states (resting and activated, respectively). Where the red and green lines coincide (blue line), the system is bistable. Depending on the parameters, the system can operate in one of three possible conditions: (1) a single, stable steady state at low receptor phosphorylation; (2) a single, stable steady state at high receptor phosphorylation; (3) a bistable state wherein receptor phosphorylation can either be high "activated" or low "resting" depending on the conditions [235].

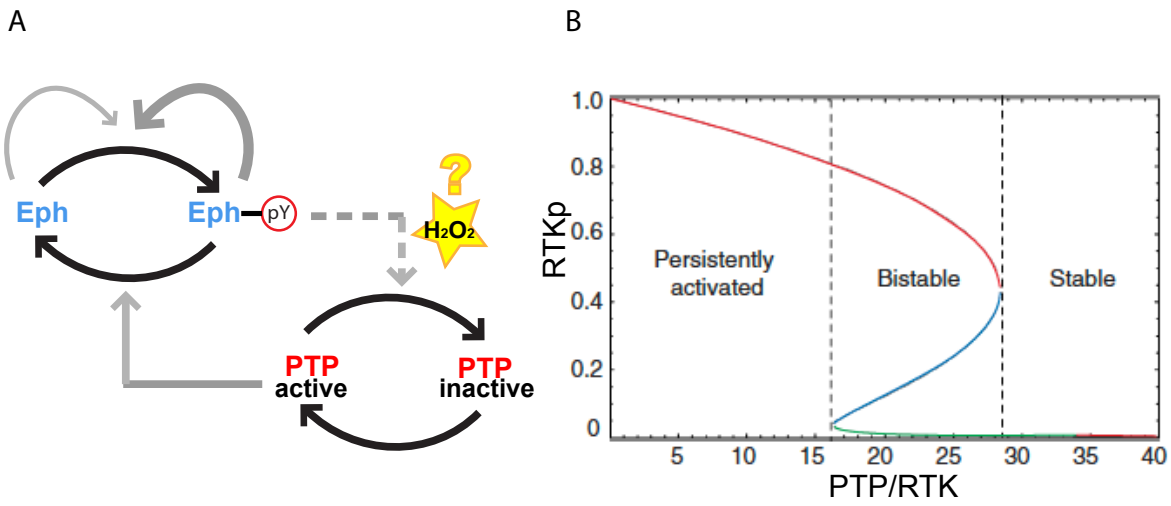

Ligand-independent activation of EGFR is already acquired during its maturation on the ER and Golgi apparatus [241]. Opposing gradients of centrally active pools of PTP1B would offer the negative regulation needed to counterbalance this endomembrane-based RTK activity [205]. However, one cannot entirely generalize the mechanism of ligand-independent activation between the different RTKs. EGFR's basal activity for example is likely attributed to a unique conformation its activation loop (AL) can adopt, which mimics the phosphorylated-active AL of other RTKs without the need for phosphorylation [242]. Despite an "active-like conformation" adopted by its AL, EGFR activity is sensitive to its surface density inside cells. Studies have shown that its autonomous signaling can be enhanced by phosphorylation of Tyr845 in the AL, a transition required for stabilizing the active conformation of the KD N-lobe [243].

Unlike our results with EphA2, ligand-dependent phosphorylation of EGFR was independent of the receptor surface density [28]. This discrepancy could be attributed to the nature of the read-out used to define an 'active" receptor, where EGFR surface-density studies were done with a phospho-specific antibody, our sensor in live-cells reports an "active conformation". In addition, rather than average studies of different cells prior to or after ligand-induced stimulation, we could track the relative change in activation for individual cells. Finally, ligand-induced clustering of EGFR and Eph is quite distinct and can be responsible for the difference in response properties of the system. What ligand clustering actually does to enhance Eph *auto*phosphorylation is discussed with more details earlier in this thesis (**section 4.1**). As for EGFR, it has been shown that the principal function of ligand is to change the conformation of the extracellular domain (ECD) in a way that does not hinder the intrinsic ability of the JMS to activate the KD [28,244].

Inhibition of EphA2 activation with the ATP competitive inhibitor dasatinib

To confirm that IFEA2 indeed reports conformational dynamics, we decided to use a kinase inhibitor that locks the KD into a specific conformation. Small-molecule inhibition of aberrant RTK activity usually traps the KD in a specific conformation, be it the active conformation (e.g. dasatinib) [245], or an inactive one (e.g. imatinib) [24,246,247]. Originally developed as a dual-specificity BCR-ABL & SRC-family kinase inhibitor [211], the ATP competitive inhibitor dasatinib proved to be a much more promiscuous inhibitor *in vitro* [248] & *in vivo* [249] & EphA2 was later established as a direct target of dasatinib (IC_{50} = 17 nMol) [250,251].

By correlating LIFEA2's *auto*phosphorylation capacity, conformational dynamics and clustering propensity upon dasatinib inhibition, we could show that dasatinib inhibits EphA2 by locking it in an active conformation without inducing clustering. Ligand-induced clustering of inhibited LIFEA2 can no longer change the conformation of the KD due to loss of its phosphorylating activity, thereby confirming that our sensor detects a conformation specific signal and not clustering. Although we still have no direct structural proof that dasatinib locks the KD of LIFEA2 specifically in its active conformation, we can draw parallels from dasatinib inhibition of other KDs, specifically EphA4. In the crystal structure of EphA4-KD in complex with dasatinib, the αC-helix was in the ATP proximal position forming the conserved ($Lys6^{53}$-Glu^{670}) salt bridge [18] and the AL in the "DFG-in" conformation [252], both are signatures for an active KD [78].

The JMS acts as an intrinsic safeguard mechanism against spurious receptor activation

Tolstoy had nothing to do with the world of kinases when he wrote Anna Karenina, but his opening lines of the novel "paraphrased" do not fail to sum up our current state of knowledge about KD activation "*All active kinases are alike but an inactive kinase is inactive after its own fashion*"[253]. If dasatinib locks EphA2 in the generic active conformation, which factors contribute to the formation of the inactive structure and the eventual switch-like release of inhibition? Activation of Ephs correlates with *auto*phosphorylation of two conserved tyrosines (Tyr587 and Tyr593, for EphA2) embedded in a highly conserved ~10 amino acid motif within the JMS and a key tyrosine residue (Tyr_{ACT}) within the kinase AL [79]. It has been shown that mutation of the conserved JM tyrosines to phenylalanine (2YF) impairs kinase activity, while glutamic acid substitution (2YE) preserves kinase activity [80,81].

In-vitro kinase assay performed on wild type (WT), 2YE and 2YF mutants of LIFEA2, indeed pointed to an impaired yet not completely inactive 2YF-LIFEA2. The presence of residual activity can be understood if one appreciates the dynamic character of JMS inhibition.

By comparing the response properties of the JMS phosphomimetic mutant (2YE-LIFEA2), and the non-phosphorylatable mutant, (2YF-LIFEA2) to WT LIFEA2, we could show that interactions between JMS and KD are not ON-OFF as previously suggested, but a dynamic process where the KD is continuously switching between a tight (inactive) and relaxed (activatable) conformation in the absence of ligand. This points to conformational flexibility, a property of kinase domains that would allow it to sample for the catalytically competent conformation in space and time. Reducing this "breathing" tendency by for example the YF mutation that forces an ordered closed JMS (**Fig 4.3** "**O**/**D**"), would prevent these activating transitions of the JMS (**Fig 4.3** "**D**/**D**") and prevent the KD from sampling of an active state (**Fig 4.3** "**D**/**O**").

Fig 4.3 Conformational fluctuation model for EphA2 activation

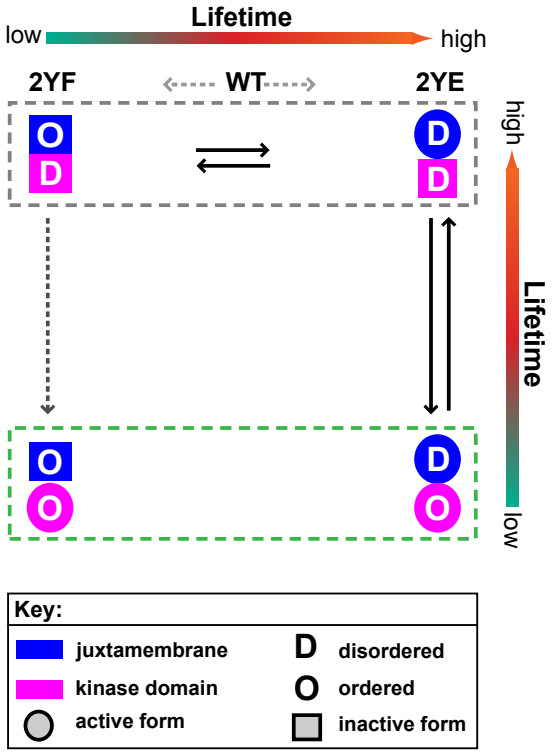

EphA2 activating transitions therefore represent a 3-state model for the conformational fluctuations that occur in its intracellular domain (**Fig 4.3**). The accessibility of the active site and thereby catalysis is regulated by the conformation of the JMS (blue) and the activation loop in the kinase domain (pink). The JMS- fluctuates between an "ordered" state that tightly interacts with and inhibits the KD by disordering the AL (**Fig 4.3** "**O**/**D**"), and a "disordered" state that allows for conformational breathing of the KD and AL (**Fig 4.3** "**D**/**D**"). *Auto*phosphorylation of the JMS tyrosines stabilizes this open JMS-kinase domain conformation allowing a dynamic KD and AL to sample many conformations compatible with catalysis. The catalytically competent KD is in turn stabilized by *auto*phosphorylation of the Tyr_{ACT}, a phosphorylation event that leads to ordering of the AL (**Fig 4.3** "**D**/**O**").

Fluctuations of catalytic domains are affected by phosphatases that counterbalance the action of "active conformation"-stabilizing phosphorylation events [254]. At steady state, phosphatases would be actively participating in the regulation of EphA2, by switching the JMS to an unphosphorylated ordered form that intrinsically inhibits EphA2 activity. EphA2-driven phosphorylation events would on the other hand stabilize the active conformation of JMS and AL. Beyond certain expression levels of EphA2, this autocatalytic system switches the population to an active state which is then stabilized by phosphorylation of the catalytic domains. Ligand-induced activation of EphA2 also makes use of this "breathing" of catalytic domains, as localized concentration of kinase activity allows for an *auto*catalytic initiation event that can propagate laterally[42,56].

An ordered unphosphorylated JMS can inhibit the KD, by preventing the AL from attaining a conformation that is compatible with catalysis. The extent to which the AL is ordered is commonly correlated with the phosphorylation state of the protein and the disordering of the JMS [25,85]. In the inactive state, Tyr_{ACT} blocks ATP binding by protruding into the active site. *Auto*-phosphorylation of Tyr_{ACT} repositions the AL and adjacent residues into a catalytically competent conformation (ordered), thereby freeing the active site to interact with substrates [72,73]. An ordered JMS can also inhibit Eph activity by restricting the flexibility of the N-terminal relative to the C-terminal kinase lobe, an inherent interlobe flexibility that allows the KD to adopt a range of conformations, among which lies the catalytically competent one [84].

A fourth highly unlikely conformational transition to an ordered AL despite of an ordered JMS can happen (**Fig 4.3** "**O**/**O**"), which might explain the residual activity we detect in our *in vitro* kinase assays for the 2YF mutant. Whether WT Eph-KD can overcome intrinsic inhibition by a closed, ordered JMS is speculative. However, a symmetric transition into an active state regardless of JMS structural inhibition would create no protective effect against Eph receptor *auto*activation and cannot explain the switch-like response properties of the system. Both the active state (**Fig 4.3** "**D**/**O**") & JMS-inhibited state (2YF) (**Fig 4.3** "**O**/**D**") exhibited a low fluorescence lifetime (τ), i.e. we observe degeneracy in our FRET-based system (**Fig 4.3, dashed green box**). One way of explaining this, is by appreciating the fact that in all RTKs, the catalytically competent conformation is the one in which the two kinase lobes clamp together to form an interfacial nucleotide binding site and catalytic cleft, i.e. it is superficially a closed structure [25]. In the crystal structure of 2YF-EphB2, the *auto*inhibited KD adopted a closed conformation that superficially resembled an active state [25]. In addition, the 2YF mutant used here as the "inactive" kinase mimic might represent a stabilization of a certain intermediate conformation that lacks certain aspects of catalysis such as nucleotide release and as such fail to faithfully translate into a conformational state that the WT is adopting [254].

As for the response properties of the phosphomimetic mutant (2YE), which points to a ligand-activatable transition state of EphA2, we detect enhanced catalytic activity in our *in-vitro* kinase assays. This goes in accordance with previous studies with 2YE-EphA4, which remained sensitive to ligand-induced receptor activation *in vivo* [255]. It has been suggested that JMS phosphorylation acts like a threshold that must be exceeded for proper receptor activation [256,257]. Loosing this intrinsic safeguard mechanism, as in the case of the 2YE mutant, will therefore not mean that the receptor is already in an active state. Indeed, structural and mutational studies have proposed that rather than fixing the AL or other elements of the KD into a catalytically competent conformation, dissociation of the JMS from the KD allows for more dynamic sampling of such a conformation [84]. This notion that the intrinsic plasticity of a protein is a key feature of catalysis is consistent with theoretical models and experimental observations [258].

The process of recycling acts as a safeguard mechanism against Eph *auto*activation

As gathered from our expression level versus activity state correlation, EphA2 as an RTK with intrinsic structural features that regulate its own activity can still bypass the JMS *cis*-inhibitory mechanism through its conformational flexibility. The cell must therefore impose another regulatory mechanism that maintains a low level of active Ephs at the PM. We find that ectopic expression of PTP1B (**Fig. 3.29**) as well as enhancement of the slow endosomal recycling compartment by ectopic expression of Rab11 (**Fig. 3.31**) represents a safeguard mechanism against ligand independent *auto*catalytic activation of EphA2. To investigate the protective effect imposed by vesicular recycling to the PM, we overexpressed Rab11 and determined the ligand-independent activity of LIFEA2 as a function of its expression level. By comparing FL intensity across all experiments, we obtained cell-to-cell variance in EphA2 expression level relative to its activity state (**Fig 3.31**) and phosphorylation (**Fig 3.32**). The switch-like activation described earlier for the receptor in the absence of Rab11 occurred at higher receptor expression levels when Rab11 was ectopically expressed, indicating a recycling-mediated safeguard mechanism.

The dependency of RTK self-activation on surface density has recently been detailed for EGFR [28]. Prior to ligand activation, EGFR on the PM is under dynamic flow, where it is continuously internalized at a comparable rate to basal membrane recycling (rate constant ~ 0.02-0.05 min^{-1}) [259]. Most of internalized EGFR is recycled back to the PM with a constitutive recycling rate of ($\geq$0.2 min^{-1}), which displays biphasic kinetics with a fast component ($t_{1/2}$ ~ 5 min) and a more prolonged one at ~ 20 min [260]. The higher recycling rate dictates a predominant steady-state PM localization of EGFR and a smaller endosomal pool. It is likely that EphA2 will follow the same steady state conditions. A higher density of RTKs on the PM would increase the chances of random-collisions, increasing the chances of ligand-independent activation. Eph recycling would therefore act as another level of protection against high basal KD activity. This is why we turned to Rab proteins, which play a pivotal role in relaying receptor signaling to the endosomal trafficking machinery & vice versa [157].

Rab11 has been shown to associate with the peri-centriolar recycling endosome (RE) and to regulate the "slow recycling component" of transferrin receptor [261]. Prior to ligand binding and in accordance with previous studies done on transferrin [261], we see less Eph on the PM and a more on the RE. By

photoactivating EphA2-paGFP specifically on the RE and following fluorescence loss from the RE and appearance on the PM over time, we could show that the population of EphA2 enriched on the RE is dynamic and contributes to the steady-state localization of receptor on the PM. The fluorescence intensity (FL) decay curves after photoactivation point to a slow vesicular transport from the RE ($t_{1/2}$ 7.5 ± 5.5 min) and simultaneous slow appearance of fluorescence on the PM ($t_{1/2}$ 4.8 ± 2.2 min). The specific rates of EphA2 recycling are within the range of rates measured for other receptors ($t_{1/2}$ of 12 min for EGFR) [259]. However, ligand induced activation of EphA2 induces a fast translocation of receptor towards the PM (~1 min). If the slow vesicular transport contributes to this initial increase in PM-population of receptor, it would mean the dynamics of RE-PM transport have to change upon addition of ligand. We plan to repeat our confocal FLAP experiments in the presence of ligand, to investigate whether the slow RE changes EphA2 PM-transport kinetics upon ligand-induced activation.

What then does trafficking through the slow RE do to Eph receptors? Ectopic expression of Rab11 can push more of the constitutively internalized Eph through the slow RE path, thereby depriving the receptor from a possible fast cycle back to the cell surface through Rab4-positive endosomes. In addition, considering the fast ligand-induced translocation of receptor towards the PM, the contribution of the fast RE to PM-RTK enrichment is more likely. To explore this hypothesis, we are investigating the role of Rab4 in the regulation of steady state and ligand-induced EphA2 recycling. Rab11 can also regulate incoming traffic to the RE, by enhancing movement of internalized cargo from the sorting endosome to the RE [261]. To address if Rab11 enhances internalization of Ephs from the PM towards the RE, we plan to photoactivate EphA2 (EphA2-paGFP) using total internal reflection fluorescence (TIRF) microscopy. TIRF restricts the excitation of EphA2-paGFP to the basal PM and its residence time can be derived from the loss fluorescence over time following photoactivation.

Following ligand-induced translocation and enrichment of EphA2 activity on the PM, we observed a delayed burst of receptor-signaling-mediated endocytosis that depletes the activated receptors from the PM. This pool of ligand-activated EphA2 slowly enriches on the late endosomal/lysosomal compartment. One of the principal determinants of ligand-induced receptor crosslinking is to create large clusters that are central for Eph signaling (refer to **section 4.1).** We therefore reason that this signaling-mediated switch between an active monomer

and oligomerized active receptor opens up a new route for internalized receptors (late endosome), to allow for termination of signaling. To test this hypothesis, we are investigating the ubiquitin-mediated molecular mechanism that regulates this differential endosomal sorting of ligand-activated clustered receptor versus monomeric active ones. It has already been shown that ligand binding causes EphA2 to be internalized and degraded by promoting its interaction with the ubiquitin ligase c-Cbl [262], an interaction that can be inhibited by dasatinib suggesting a dependency on kinase activity [251]. Receptor signaling-mediated switch in endosomal trafficking could arise from tyrosine phosphorylation of a consensus Cbl-docking sequence (Tyrosine-XXX-Proline) and hence sort more receptor for degradation. Mutation of the respective tyrosine (1045) to phenylalanine in EGFR inhibited receptor ubiquitination and degradation [263]. The corresponding residue on EphA2 (Tyrosine 813) is not an identified *in vivo auto*phosphorylation site, but ligand induced PM-enrichment might bring EphA2 in close proximity to other tyrosine kinases [264-266] that bring about its phosphorylation. It is therefore interesting to create the Y813F EphA2 mutant and investigate its effect on PM recycling and/or receptor degradation.

How then is Eph intrinsic *auto*catalytic activity dynamically controlled to prevent self-activation yet allow for robust ligand-induced activation (**Fig 4.4**):

(A) Steady state level of EphA2 on the PM is maintained by constant trafficking and represents a sum of slow internalization and faster recycling. PM-enriched EphA2 has a higher chance of random collision and spurious activation owing to its *auto*catalytic activity. Intrinsic structural elements of inhibition (for Eph, JMS) represent an initial threshold that can be surpassed. The cell must therefore impose additional control mechanisms that maintain low levels of active Eph on the PM. One of our main findings is that continuous slow recycling of EphA2 to the PM represents a cell intrinsic safeguard mechanism against *auto*activated receptors by: (1) maintaining a relatively low steady-state level of receptor at the PM and (2) transporting the receptor past areas rich in PTP1B activity [205], thereby dephosphorylating spuriously activated receptors. The contribution of the Rab4-positive fast recycling endosome to Eph kinetics remains to be tested (red arrow).

(B) Ligand induced clustering of Ephs causes a net translocation of receptors to the PM, ensuring robust *trans*phosphorylation and activation. This is followed by a delayed burst of signaling-mediated endocytosis. Most of internalized

receptors end up in the late endosomal compartment for degradation (blue arrow). Whether ligand-activated EphA2 is at all recycled back to and enriched on the PM is still under investigation, but is highly unlikely. We therefore conclude that ligand clustering rather than the receptor's intrinsic *auto*catalytic activity is what initiates Eph vesicular trafficking into the degradative pathway for efficient termination of signaling.

Fig 4.4 Model depicting factors affecting the activation of EphA2

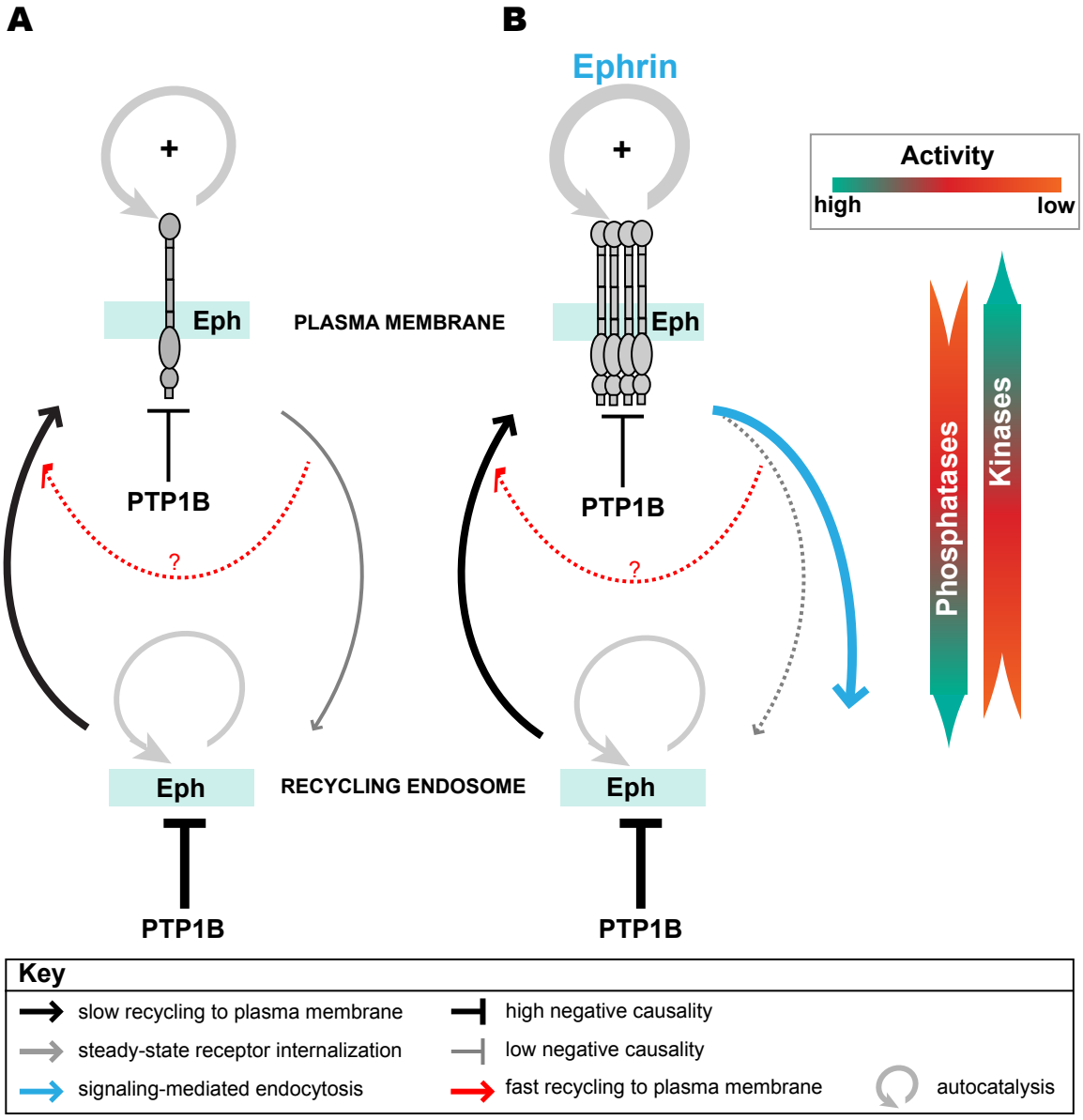

5. BIBLIOGRAPHY

1 Zamir, E. & Bastiaens, P. I. H. Reverse engineering intracellular biochemical networks. *Nat Chem Biol* **4**, 643-647, doi:Doi 10.1038/Nchembio1108-643 (2008).

2 Grecco, H. n. E., Schmick, M. & Bastiaens, P. I. H. Signaling from the Living Plasma Membrane. *Cell* **144**.

3 Hunter, T. Tyrosine phosphorylation: thirty years and counting. *Current opinion in cell biology* **21**, 140-146, doi:10.1016/j.ceb.2009.01.028 (2009).

4 Lim, W. A. & Pawson, T. Phosphotyrosine signaling: evolving a new cellular communication system. *Cell* **142**, 661-667, doi:10.1016/j.cell.2010.08.023 (2010).

5 Ullrich, A. & Schlessinger, J. Signal transduction by receptors with tyrosine kinase activity. *Cell* **61**, 203-212 (1990).

6 Blume-Jensen, P. & Hunter, T. Oncogenic kinase signalling. *Nature* **411**, 355-365, doi:10.1038/35077225 (2001).

7 Lemmon, M. A. & Schlessinger, J. Cell signaling by receptor-tyrosine kinases. *Cell* **141**, 1117-1134 (2010).

8 Wiesmann, C. *et al.* Crystal structure at 1.7 A resolution of VEGF in complex with domain 2 of the Flt-1 receptor. *Cell* **91**, 695-704 (1997).

9 Leppanen, V. M. *et al.* Structural determinants of growth factor binding and specificity by VEGF receptor 2. *Proceedings of the National Academy of Sciences of the United States of America* **107**, 2425-2430, doi:10.1073/pnas.0914318107 (2010).

10 Wiesmann, C., Ultsch, M. H., Bass, S. H. & de Vos, A. M. Crystal structure of nerve growth factor in complex with the ligand-binding domain of the TrkA receptor. *Nature* **401**, 184-188, doi:10.1038/43705 (1999).

11 Liu, H., Chen, X., Focia, P. J. & He, X. Structural basis for stem cell factor-KIT signaling and activation of class III receptor tyrosine kinases. *The EMBO journal* **26**, 891-901, doi:10.1038/sj.emboj.7601545 (2007).

12 Himanen, J.-P. & Nikolov, D. B. Eph signaling: a structural view. *Trends in Neurosciences* **26** (2003).

13 Wehrman, T. *et al.* Structural and mechanistic insights into nerve growth factor interactions with the TrkA and p75 receptors. *Neuron* **53**, 25-38, doi:10.1016/j.neuron.2006.09.034 (2007).

14 Garrett, T. P. *et al.* Crystal structure of a truncated epidermal growth factor receptor extracellular domain bound to transforming growth factor alpha. *Cell* **110**, 763-773 (2002).

15 Ogiso, H. *et al.* Crystal structure of the complex of human epidermal growth factor and receptor extracellular domains. *Cell* **110**, 775-787 (2002).

16 Yuzawa, S. *et al.* Structural basis for activation of the receptor tyrosine kinase KIT by stem cell factor. *Cell* **130**, 323-334, doi:10.1016/j.cell.2007.05.055 (2007).

17 Schlessinger, J. *et al.* Crystal structure of a ternary FGF-FGFR-heparin complex reveals a dual role for heparin in FGFR binding and dimerization. *Molecular cell* **6**, 743-750 (2000).

18 Huse, M. & Kuriyan, J. The conformational plasticity of protein kinases. *Cell* **109**, 275-282 (2002).

19 Nolen, B., Taylor, S. & Ghosh, G. Regulation of protein kinases; controlling activity through activation segment conformation. *Molecular cell* **15**, 661-675, doi:10.1016/j.molcel.2004.08.024 (2004).
20 Shewchuk, L. M. *et al.* Structure of the Tie2 RTK domain: self-inhibition by the nucleotide binding loop, activation loop, and C-terminal tail. *Structure* **8**, 1105-1113 (2000).
21 Zhang, X., Gureasko, J., Shen, K., Cole, P. A. & Kuriyan, J. An allosteric mechanism for activation of the kinase domain of epidermal growth factor receptor. *Cell* **125**, 1137-1149, doi:10.1016/j.cell.2006.05.013 (2006).
22 Hubbard, S. R. Juxtamembrane autoinhibition in receptor tyrosine kinases. *Nature reviews. Molecular cell biology* **5**, 464-471, doi:10.1038/nrm1399 (2004).
23 Mohammadi, M., Schlessinger, J. & Hubbard, S. R. Structure of the FGF receptor tyrosine kinase domain reveals a novel autoinhibitory mechanism. *Cell* **86**, 577-587 (1996).
24 Mol, C. D. *et al.* Structural basis for the autoinhibition and STI-571 inhibition of c-Kit tyrosine kinase. *The Journal of biological chemistry* **279**, 31655-31663, doi:10.1074/jbc.M403319200 (2004).
25 Wybenga-Groot, L. E. *et al.* Structural basis for autoinhibition of the Ephb2 receptor tyrosine kinase by the unphosphorylated juxtamembrane region. *Cell* **106**, 745-757 (2001).
26 Niu, X. L., Peters, K. G. & Kontos, C. D. Deletion of the carboxyl terminus of Tie2 enhances kinase activity, signaling, and function. Evidence for an autoinhibitory mechanism. *The Journal of biological chemistry* **277**, 31768-31773, doi:10.1074/jbc.M203995200 (2002).
27 Knowles, P. P. *et al.* Structure and chemical inhibition of the RET tyrosine kinase domain. *The Journal of biological chemistry* **281**, 33577-33587, doi:10.1074/jbc.M605604200 (2006).
28 Endres, N. F. *et al.* Conformational coupling across the plasma membrane in activation of the EGF receptor. *Cell* **152**, 543-556, doi:10.1016/j.cell.2012.12.032 (2013).
29 Arkhipov, A. *et al.* Architecture and membrane interactions of the EGF receptor. *Cell* **152**, 557-569, doi:10.1016/j.cell.2012.12.030 (2013).
30 Himanen, J.-P., Saha, N. & Nikolov, D. B. Cell-cell signaling via Eph receptors and ephrins. *Current Opinion in Cell Biology* **19**, 534-542 (2007).
31 Pasquale, E. B. Eph-ephrin bidirectional signaling in physiology and disease. *Cell* **133** (2008).
32 Nievergall, E., Lackmann, M. & Janes, P. W. Eph-dependent cell-cell adhesion and segregation in development and cancer. *Cell Mol Life Sci* **69**, 1813-1842, doi:10.1007/s00018-011-0900-6 (2012).
33 Davis, S. *et al.* Ligands for EPH-related receptor tyrosine kinases that require membrane attachment or clustering for activity. *Science* **266**, 816-819 (1994).
34 Stein, E. *et al.* Eph receptors discriminate specific ligand oligomers to determine alternative signaling complexes, attachment, and assembly responses. *Genes & Development* **12**, 667-678 (1998).
35 Hirai, H., Maru, Y., Hagiwara, K., Nishida, J. & Takaku, F. A novel putative tyrosine kinase receptor encoded by the eph gene. *Science* **238**, 1717-1720 (1987).

36 Eph Nomenclature, C. Unified Nomenclature for Eph Family Receptors and Their Ligands, the Ephrins. *Cell* **90**, 403-404 (1997).
37 Qin, H. *et al.* Structural Characterization of the EphA4-Ephrin-B2 Complex Reveals New Features Enabling Eph-Ephrin Binding Promiscuity. *Journal of Biological Chemistry* **285**, 644-654 (2010).
38 Takemoto, M. *et al.* Ephrin-B3,ÄìEphA4 interactions regulate the growth of specific thalamocortical axon populations in vitro. *European Journal of Neuroscience* **16**, 1168,Äì1172 (2002).
39 Himanen, J.-P. *et al.* Repelling class discrimination: ephrin-A5 binds to and activates EphB2 receptor signaling. *Nature Neuroscience* **7**, 501-509 (2004).
40 Drescher, U. Eph family functions from an evolutionary perspective. *Current opinion in genetics & development* **12**, 397-402 (2002).
41 Himanen, J. P. *et al.* Crystal structure of an Eph receptor-ephrin complex. *Nature* **414**, 933-938, doi:10.1038/414933a (2001).
42 Seiradake, E., Harlos, K., Sutton, G., Aricescu, A. R. & Jones, E. Y. An extracellular steric seeding mechanism for Eph-ephrin signaling platform assembly. *Nature structural & molecular biology* **17**, 398-402, doi:10.1038/nsmb.1782 (2010).
43 Himanen, J. P. *et al.* Architecture of Eph receptor clusters. *Proceedings of the National Academy of Sciences of the United States of America* **107**, 10860-10865, doi:10.1073/pnas.1004148107 (2010).
44 Leone, M., Cellitti, J. & Pellecchia, M. NMR studies of a heterotypic Sam-Sam domain association: the interaction between the lipid phosphatase Ship2 and the EphA2 receptor. *Biochemistry* **47**, 12721-12728, doi:10.1021/bi801713f (2008).
45 Gale, N. W. *et al.* Eph receptors and ligands comprise two major specificity subclasses and are reciprocally compartmentalized during embryogenesis. *Neuron* **17**, 9-19 (1996).
46 Carter, N., Nakamoto, T., Hirai, H. & Hunter, T. EphrinA1-induced cytoskeletal re-organization requires FAK and p130(cas). *Nature cell biology* **4**, 565-573, doi:10.1038/ncb823 (2002).
47 Dobrzanski, P. *et al.* Antiangiogenic and Antitumor Efficacy of EphA2 Receptor Antagonist. *Cancer Research* **64** (2004).
48 Lawrenson, I. D. *et al.* Ephrin-A5 induces rounding, blebbing and de-adhesion of EphA3-expressing 293T and melanoma cells by CrkII and Rho-mediated signalling. *Journal of Cell Science* **115** (2002).
49 Vearing, C. J. & Lackmann, M. "Eph receptor signalling; dimerisation just isn't enough". *Growth Factors* **23**, 67-76, doi:10.1080/08977190500055869 (2005).
50 Noren, N. K., Yang, N. Y., Silldorff, M., Mutyala, R. & Pasquale, E. B. Ephrin-independent regulation of cell substrate adhesion by the EphB4 receptor. *Biochem J* **422**, 433-442, doi:10.1042/BJ20090014 (2009).
51 Janes, P. W., Nievergall, E. & Lackmann, M. Concepts and consequences of Eph receptor clustering. *Seminars in cell & developmental biology* **23**, 43-50, doi:10.1016/j.semcdb.2012.01.001 (2012).
52 Lackmann, M. *et al.* Ligand for EPH-related kinase (LERK) 7 is the preferred high affinity ligand for the HEK receptor. *The Journal of biological chemistry* **272**, 16521-16530 (1997).
53 Smith, F. M. *et al.* Dissecting the EphA3/Ephrin-A5 interactions using a novel functional mutagenesis screen. *The Journal of Biological Chemistry* **279** (2004).

54 Day, B. *et al.* Three distinct molecular surfaces in ephrin-A5 are essential for a functional interaction with EphA3. *The Journal of biological chemistry* **280**, 26526-26532, doi:10.1074/jbc.M504972200 (2005).
55 Lackmann, M. *et al.* Distinct subdomains of the EphA3 receptor mediate ligand binding and receptor dimerization. *The Journal of biological chemistry* **273**, 20228-20237 (1998).
56 Wimmer-Kleikamp, S. H., Janes, P. W., Squire, A., Bastiaens, P. I. H. & Lackmann, M. Recruitment of Eph receptors into signaling clusters does not require ephrin contact. *J Cell Biol* **164**, 661-666, doi:Doi 10.1083/Jcb.200312001 (2004).
57 Himanen, J. P. *et al.* Ligand recognition by A-class Eph receptors: crystal structures of the EphA2 ligand-binding domain and the EphA2/ephrin-A1 complex. *EMBO Reports* **10** (2009).
58 Chrencik, J. E. *et al.* Structural and biophysical characterization of the EphB4*ephrinB2 protein-protein interaction and receptor specificity. *The Journal of Biological Chemistry* **281** (2006).
59 Bocharov, E. V. *et al.* Spatial structure and pH-dependent conformational diversity of dimeric transmembrane domain of the receptor tyrosine kinase EphA1. *The Journal of biological chemistry* **283**, 29385-29395, doi:10.1074/jbc.M803089200 (2008).
60 Stapleton, D., Balan, I., Pawson, T. & Sicheri, F. The crystal structure of an Eph receptor SAM domain reveals a mechanism for modular dimerization. *Nat Struct Biol* **6**, 44-49, doi:10.1038/4917 (1999).
61 Thanos, C. D., Goodwill, K. E. & Bowie, J. U. Oligomeric structure of the human EphB2 receptor SAM domain. *Science* **283**, 833-836 (1999).
62 Behlke, J., Labudde, D. & Ristau, O. Self-association studies on the EphB2 receptor SAM domain using analytical ultracentrifugation. *Eur Biophys J* **30**, 411-415 (2001).
63 Smalla, M. *et al.* Solution structure of the receptor tyrosine kinase EphB2 SAM domain and identification of two distinct homotypic interaction sites. *Protein Sci* **8**, 1954-1961, doi:10.1110/ps.8.10.1954 (1999).
64 Citri, A. & Yarden, Y. EGF-ERBB signalling: towards the systems level. *Nature reviews. Molecular cell biology* **7**, 505-516, doi:10.1038/nrm1962 (2006).
65 Freywald, A., Sharfe, N. & Roifman, C. M. The kinase-null EphB6 receptor undergoes transphosphorylation in a complex with EphB1. *The Journal of biological chemistry* **277**, 3823-3828, doi:10.1074/jbc.M108011200 (2002).
66 Truitt, L., Freywald, T., DeCoteau, J., Sharfe, N. & Freywald, A. The EphB6 receptor cooperates with c-Cbl to regulate the behavior of breast cancer cells. *Cancer research* **70**, 1141-1153, doi:10.1158/0008-5472.CAN-09-1710 (2010).
67 Warner, N., Wybenga-Groot, L. E. & Pawson, T. Analysis of EphA4 receptor tyrosine kinase substrate specificity using peptide-based arrays. *Febs J* **275**, 2561-2573, doi:10.1111/j.1742-4658.2008.06405.x (2008).
68 Bush, J. O. & Soriano, P. Ephrin-B1 forward signaling regulates craniofacial morphogenesis by controlling cell proliferation across Eph-ephrin boundaries. *Genes & development* **24**, 2068-2080, doi:10.1101/gad.1963210 (2010).
69 Jorgensen, C. *et al.* Cell-Specific Information Processing in Segregating Populations of Eph Receptor Ephrin-Expressing Cells. *Science* **326** (2009).
70 Vearing, C. *et al.* Concurrent binding of anti-EphA3 antibody and ephrin-A5 amplifies EphA3 signaling and downstream responses: potential as EphA3-

specific tumor-targeting reagents. *Cancer research* **65**, 6745-6754, doi:10.1158/0008-5472.CAN-05-0758 (2005).
71 Janes, P. W. *et al.* Eph receptor function is modulated by heterooligomerization of A and B type Eph receptors. *The Journal of cell biology* **195**, 1033-1045, doi:10.1083/jcb.201104037 (2011).
72 Johnson, L. N., Noble, M. E. & Owen, D. J. Active and inactive protein kinases: structural basis for regulation. *Cell* **85**, 149-158 (1996).
73 Hubbard, S. R. Crystal structure of the activated insulin receptor tyrosine kinase in complex with peptide substrate and ATP analog. *The EMBO journal* **16**, 5572-5581, doi:10.1093/emboj/16.18.5572 (1997).
74 Hubbard, S. R., Mohammadi, M. & Schlessinger, J. Autoregulatory mechanisms in protein-tyrosine kinases. *The Journal of biological chemistry* **273**, 11987-11990 (1998).
75 Hubbard, S. R. Structural analysis of receptor tyrosine kinases. *Prog Biophys Mol Biol* **71**, 343-358 (1999).
76 Pawson, T. Protein modules and signalling networks. *Nature* **373**, 573-580, doi:10.1038/373573a0 (1995).
77 Yamaguchi, H. & Hendrickson, W. A. Structural basis for activation of human lymphocyte kinase Lck upon tyrosine phosphorylation. *Nature* **384**, 484-489, doi:10.1038/384484a0 (1996).
78 Farenc, C., Celie, P. H. N., Tensen, C. P., de Esch, I. J. P. & Siegal, G. Crystal structure of the EphA4 protein tyrosine kinase domain in the apo- and dasatinib-bound state. *FEBS Letters* **585**.
79 Binns, K. L., Taylor, P. P., Sicheri, F., Pawson, T. & Holland, S. J. Phosphorylation of tyrosine residues in the kinase domain and juxtamembrane region regulates the biological and catalytic activities of Eph receptors. *Molecular and Cellular Biology* **20**, 4791-4805 (2000).
80 Zisch, A. H., Kalo, M. S., Chong, L. D. & Pasquale, E. B. Complex formation between EphB2 and Src requires phosphorylation of tyrosine 611 in the EphB2 juxtamembrane region. *Oncogene* **16**, 2657-2670, doi:10.1038/sj.onc.1201823 (1998).
81 Zisch, A. H. *et al.* Replacing two conserved tyrosines of the EphB2 receptor with glutamic acid prevents binding of SH2 domains without abrogating kinase activity and biological responses. *Oncogene* **19** (2000).
82 Nowakowski, J. *et al.* Structures of the cancer-related Aurora-A, FAK, and EphA2 protein kinases from nanovolume crystallography. *Structure* **10**, 1659-1667 (2002).
83 Connor, R. J. & Pasquale, E. B. Genomic organization and alternatively processed forms of Cek5, a receptor protein-tyrosine kinase of the Eph subfamily. *Oncogene* **11**, 2429-2438 (1995).
84 Wiesner, S. *et al.* A change in conformational dynamics underlies the activation of Eph receptor tyrosine kinases. *The EMBO Journal* **25**, 4686-4696 (2006).
85 Davis, T. L. *et al.* Autoregulation by the juxtamembrane region of the human ephrin receptor tyrosine kinase A3 (EphA3). *Structure (London, England: 1993)* **16** (2008).
86 Kalo, M. S. & Pasquale, E. B. Multiple in vivo tyrosine phosphorylation sites in EphB receptors. *Biochemistry* **38**, 14396-14408 (1999).

87 Kalo, M. S., Yu, H. H. & Pasquale, E. B. In vivo tyrosine phosphorylation sites of activated ephrin-B1 and ephB2 from neural tissue. *The Journal of Biological Chemistry* **276** (2001).
88 Singla, N., Erdjument-Bromage, H., Himanen, J. P., Muir, T. W. & Nikolov, D. B. A semisynthetic Eph receptor tyrosine kinase provides insight into ligand-induced kinase activation. *Chem Biol* **18**, 361-371, doi:10.1016/j.chembiol.2011.01.011 (2011).
89 Pasquale, E. B. Eph receptor signalling casts a wide net on cell behaviour. *Nature reviews. Molecular cell biology* **6**, 462-475, doi:10.1038/nrm1662 (2005).
90 Flanagan, J. G. Neural map specification by gradients. *Curr Opin Neurobiol* **16**, 59-66, doi:10.1016/j.conb.2006.01.010 (2006).
91 McLaughlin, T. & O'Leary, D. D. Molecular gradients and development of retinotopic maps. *Annu Rev Neurosci* **28**, 327-355, doi:10.1146/annurev.neuro.28.061604.135714 (2005).
92 Mellitzer, G., Xu, Q. & Wilkinson, D. G. Eph receptors and ephrins restrict cell intermingling and communication. *Nature* **400**, 77-81, doi:10.1038/21907 (1999).
93 Xu, Q., Mellitzer, G. & Wilkinson, D. G. Roles of Eph Receptors and Ephrins in Segmental Patterning. *Philosophical Transactions: Biological Sciences* **355** (2000).
94 Poliakov, A., Cotrina, M. L., Pasini, A. & Wilkinson, D. G. Regulation of EphB2 activation and cell repulsion by feedback control of the MAPK pathway. *The Journal of Cell Biology* **183** (2008).
95 Davy, A., Bush, J. O. & Soriano, P. Inhibition of gap junction communication at ectopic Eph/ephrin boundaries underlies craniofrontonasal syndrome. *PLoS Biol* **4**, e315, doi:10.1371/journal.pbio.0040315 (2006).
96 Tanaka, M., Kamo, T., Ota, S. & Sugimura, H. Association of Dishevelled with Eph tyrosine kinase receptor and ephrin mediates cell repulsion. *The EMBO journal* **22**, 847-858, doi:10.1093/emboj/cdg088 (2003).
97 Adams, R. H. *et al.* Roles of ephrinB ligands and EphB receptors in cardiovascular development: demarcation of arterial/venous domains, vascular morphogenesis, and sprouting angiogenesis. *Genes & development* **13**, 295-306 (1999).
98 Gerety, S. S. & Anderson, D. J. Cardiovascular ephrinB2 function is essential for embryonic angiogenesis. *Development* **129**, 1397-1410 (2002).
99 Adams, R. H. & Eichmann, A. Axon guidance molecules in vascular patterning. *Cold Spring Harb Perspect Biol* **2**, a001875, doi:10.1101/cshperspect.a001875 (2010).
100 Stephen, L. J., Fawkes, A. L., Verhoeve, A., Lemke, G. & Brown, A. A critical role for the EphA3 receptor tyrosine kinase in heart development. *Dev Biol* **302**, 66-79, doi:10.1016/j.ydbio.2006.08.058 (2007).
101 Frieden, L. A. *et al.* Regulation of heart valve morphogenesis by Eph receptor ligand, ephrin-A1. *Dev Dyn* **239**, 3226-3234, doi:10.1002/dvdy.22458 (2010).
102 Ogawa, K. *et al.* The ephrin-A1 ligand and its receptor, EphA2, are expressed during tumor neovascularization. *Oncogene* **19** (2000).
103 Brantley-Sieders, D. M. *et al.* EphA2 receptor tyrosine kinase regulates endothelial cell migration and vascular assembly through phosphoinositide 3-

kinase-mediated Rac1 GTPase activation. *Journal of cell science* **117**, 2037-2049, doi:10.1242/jcs.01061 (2004).
104 Sawamiphak, S. *et al.* Ephrin-B2 regulates VEGFR2 function in developmental and tumour angiogenesis. *Nature* **465**, 487-491, doi:10.1038/nature08995 (2010).
105 Wang, Y. *et al.* Ephrin-B2 controls VEGF-induced angiogenesis and lymphangiogenesis. *Nature* **465**, 483-486, doi:10.1038/nature09002 (2010).
106 Janes, P. W., Adikari, S. & Lackmann, M. Eph/ephrin signalling and function in oncogenesis: lessons from embryonic development. *Current cancer drug targets* **8**, 473-479 (2008).
107 Pasquale, E. B. Eph receptors and ephrins in cancer: bidirectional signalling and beyond. *Nat Rev Cancer* **10**, 165-180, doi:10.1038/nrc2806 (2010).
108 Campbell, T. N. & Robbins, S. M. The Eph receptor/ephrin system: an emerging player in the invasion game. *Curr Issues Mol Biol* **10**, 61-66 (2008).
109 Fournier, M. V. *et al.* Gene expression signature in organized and growth-arrested mammary acini predicts good outcome in breast cancer. *Cancer research* **66**, 7095-7102, doi:10.1158/0008-5472.CAN-06-0515 (2006).
110 Easty, D. J., Herlyn, M. & Bennett, D. C. Abnormal protein tyrosine kinase gene expression during melanoma progression and metastasis. *International journal of cancer. Journal international du cancer* **60**, 129-136 (1995).
111 Zelinski, D. P., Zantek, N. D., Stewart, J. C., Irizarry, A. R. & Kinch, M. S. EphA2 overexpression causes tumorigenesis of mammary epithelial cells. *Cancer Research* **61** (2001).
112 Gale, N. W. *et al.* Ephrin-B2 selectively marks arterial vessels and neovascularization sites in the adult, with expression in both endothelial and smooth-muscle cells. *Dev Biol* **230**, 151-160, doi:10.1006/dbio.2000.0112 (2001).
113 Guo, H. *et al.* Disruption of EphA2 Receptor Tyrosine Kinase Leads to Increased Susceptibility to Carcinogenesis in Mouse Skin. *Cancer Research* **66** (2006).
114 Kumar, S. R. *et al.* Receptor tyrosine kinase EphB4 is a survival factor in breast cancer. *The American journal of pathology* **169**, 279-293, doi:10.2353/ajpath.2006.050889 (2006).
115 Noren, N. K., Foos, G., Hauser, C. A. & Pasquale, E. B. The EphB4 receptor suppresses breast cancer cell tumorigenicity through an Abl-Crk pathway. *Nature cell biology* **8**, 815-825, doi:10.1038/ncb1438 (2006).
116 Noren, N. K., Lu, M., Freeman, A. L., Koolpe, M. & Pasquale, E. B. Interplay between EphB4 on tumor cells and vascular ephrin-B2 regulates tumor growth. *Proceedings of the National Academy of Sciences of the United States of America* **101**, 5583-5588, doi:10.1073/pnas.0401381101 (2004).
117 Wimmer-Kleikamp, S. H. & Lackmann, M. Eph-modulated Cell Morphology, Adhesion and Motility in Carcinogenesis. *IUBMB Life* **57** (2005).
118 Holmberg, J., Clarke, D. L. & Frisen, J. Regulation of repulsion versus adhesion by different splice forms of an Eph receptor. *Nature* **408** (2000).
119 Dravis, C. *et al.* Bidirectional signaling mediated by ephrin-B2 and EphB2 controls urorectal development. *Dev Biol* **271**, 272-290, doi:10.1016/j.ydbio.2004.03.027 (2004).
120 Huynh-Do, U. *et al.* Surface densities of ephrin-B1 determine EphB1-coupled activation of cell attachment through alphavbeta3 and alpha5beta1 integrins. *The EMBO journal* **18**, 2165-2173, doi:10.1093/emboj/18.8.2165 (1999).

121 Hansen, M. J., Dallal, G. E. & Flanagan, J. G. Retinal axon response to ephrin-as shows a graded, concentration-dependent transition from growth promotion to inhibition. *Neuron* **42**, 717-730, doi:10.1016/j.neuron.2004.05.009 (2004).
122 Matsuoka, H., Obama, H., Kelly, M. L., Matsui, T. & Nakamoto, M. Biphasic functions of the kinase-defective Ephb6 receptor in cell adhesion and migration. *The Journal of biological chemistry* **280**, 29355-29363, doi:10.1074/jbc.M500010200 (2005).
123 Holmberg, J. & Frisen, J. Ephrins are not only unattractive. *Trends in neurosciences* **25**, 239-243 (2002).
124 Wimmer-Kleikamp, S. H. *et al.* Elevated protein tyrosine phosphatase activity provokes Eph/ephrin-facilitated adhesion of pre-B leukemia cells. *Blood* **112** (2008).
125 Shintani, T. *et al.* Eph receptors are negatively controlled by protein tyrosine phosphatase receptor type O. *Nature neuroscience* **9**, 761-769, doi:10.1038/nn1697 (2006).
126 Konstantinova, I. *et al.* EphA-Ephrin-A-mediated beta cell communication regulates insulin secretion from pancreatic islets. *Cell* **129**, 359-370, doi:10.1016/j.cell.2007.02.044 (2007).
127 Nievergall, E. *et al.* PTP1B regulates Eph receptor function and trafficking. *The Journal of Cell Biology* **191**.
128 Boute, N., Boubekeur, S., Lacasa, D. l. & Issad, T. Dynamics of the interaction between the insulin receptor and protein tyrosine-phosphatase 1B in living cells. *EMBO Reports* **4** (2003).
129 Haj, F. G., Markova, B., Klaman, L. D., Bohmer, F. D. & Neel, B. G. Regulation of receptor tyrosine kinase signaling by protein tyrosine phosphatase-1B. *The Journal of biological chemistry* **278**, 739-744, doi:10.1074/jbc.M210194200 (2003).
130 Hernandez, M. V., Sala, M. G., Balsamo, J., Lilien, J. & Arregui, C. O. ER-bound PTP1B is targeted to newly forming cell-matrix adhesions. *Journal of cell science* **119**, 1233-1243, doi:10.1242/jcs.02846 (2006).
131 Anderie, I., Schulz, I. & Schmid, A. Direct interaction between ER membrane-bound PTP1B and its plasma membrane-anchored targets. *Cell Signal* **19**, 582-592, doi:10.1016/j.cellsig.2006.08.007 (2007).
132 Fuentes, F. & Arregui, C. O. Microtubule and cell contact dependency of ER-bound PTP1B localization in growth cones. *Molecular biology of the cell* **20**, 1878-1889, doi:10.1091/mbc.E08-07-0675 (2009).
133 Nievergall, E. *et al.* PTP1B regulates Eph receptor function and trafficking. **191**, 1189-1203.
134 Haj, F. G. *et al.* Regulation of signaling at regions of cell-cell contact by endoplasmic reticulum-bound protein-tyrosine phosphatase 1B. *PloS one* **7**, e36633, doi:10.1371/journal.pone.0036633 (2012).
135 Chiarugi, P. & Cirri, P. Redox regulation of protein tyrosine phosphatases during receptor tyrosine kinase signal transduction. *Trends Biochem Sci* **28**, 509-514, doi:10.1016/S0968-0004(03)00174-9 (2003).
136 den Hertog, J., Groen, A. & van der Wijk, T. Redox regulation of protein-tyrosine phosphatases. *Arch Biochem Biophys* **434**, 11-15, doi:10.1016/j.abb.2004.05.024 (2005).
137 Kwon, J. *et al.* Reversible oxidation and inactivation of the tumor suppressor PTEN in cells stimulated with peptide growth factors. *Proceedings of the*

National Academy of Sciences of the United States of America **101**, 16419-16424, doi:10.1073/pnas.0407396101 (2004).
138 Lee, S. R., Kwon, K. S., Kim, S. R. & Rhee, S. G. Reversible inactivation of protein-tyrosine phosphatase 1B in A431 cells stimulated with epidermal growth factor. *The Journal of biological chemistry* **273**, 15366-15372 (1998).
139 Lee, S. R. *et al.* Reversible inactivation of the tumor suppressor PTEN by H2O2. *The Journal of biological chemistry* **277**, 20336-20342, doi:10.1074/jbc.M111899200 (2002).
140 Meng, T. C., Fukada, T. & Tonks, N. K. Reversible oxidation and inactivation of protein tyrosine phosphatases in vivo. *Molecular cell* **9**, 387-399 (2002).
141 Mahadev, K., Zilbering, A., Zhu, L. & Goldstein, B. J. Insulin-stimulated hydrogen peroxide reversibly inhibits protein-tyrosine phosphatase 1b in vivo and enhances the early insulin action cascade. *The Journal of biological chemistry* **276**, 21938-21942, doi:10.1074/jbc.C100109200 (2001).
142 Hattori, M., Osterfield, M. & Flanagan, J. G. Regulated cleavage of a contact-mediated axon repellent. *Science (New York, N.Y.)* **289** (2000).
143 Janes, P. W. *et al.* Adam meets Eph: an ADAM substrate recognition module acts as a molecular switch for ephrin cleavage in trans. *Cell* **123**, 291-304, doi:10.1016/j.cell.2005.08.014 (2005).
144 Salaita, K. *et al.* Restriction of Receptor Movement Alters Cellular Response: Physical Force Sensing by EphA2. *Science* **327**, 1380-1385, doi:Doi 10.1126/Science.1181729 (2010).
145 Janes, P. W. *et al.* Cytoplasmic relaxation of active Eph controls ephrin shedding by ADAM10. *PLoS Biol* **7**, e1000215, doi:10.1371/journal.pbio.1000215 (2009).
146 Litterst, C. *et al.* Ligand binding and calcium influx induce distinct ectodomain/gamma-secretase-processing pathways of EphB2 receptor. *The Journal of Biological Chemistry* **282** (2007).
147 Wei, S. *et al.* ADAM13 induces cranial neural crest by cleaving class B Ephrins and regulating Wnt signaling. *Developmental cell* **19**, 345-352, doi:10.1016/j.devcel.2010.07.012 (2010).
148 Georgakopoulos, A. *et al.* Metalloproteinase/Presenilin1 processing of ephrinB regulates EphB-induced Src phosphorylation and signaling. *The EMBO Journal* **25** (2006).
149 Lin, K.-T., Sloniowski, S., Ethell, D. W. & Ethell, I. M. Ephrin-B2-induced cleavage of EphB2 receptor is mediated by matrix metalloproteinases to trigger cell repulsion. *The Journal of Biological Chemistry* **283** (2008).
150 Pascall, J. C. & Brown, K. D. Intramembrane cleavage of ephrinB3 by the human rhomboid family protease, RHBDL2. *Biochemical and biophysical research communications* **317**, 244-252, doi:10.1016/j.bbrc.2004.03.039 (2004).
151 Marston, D. J., Dickinson, S. & Nobes, C. D. Rac-dependent trans-endocytosis of ephrinBs regulates Eph-ephrin contact repulsion. *Nature Cell Biology* **5** (2003).
152 Zimmer, M., Palmer, A., K√ ∂ hler, J. & Klein, R. d. EphB-ephrinB bi-directional endocytosis terminates adhesion allowing contact mediated repulsion. *Nature Cell Biology* **5** (2003).
153 Schlessinger, J. Cell signaling by receptor tyrosine kinases. *Cell* **103**, 211-225, doi:Doi 10.1016/S0092-8674(00)00114-8 (2000).
154 Mizuno-Yamasaki, E., Rivera-Molina, F. & Novick, P. GTPase networks in membrane traffic. *Annu Rev Biochem* **81**, 637-659, doi:10.1146/annurev-biochem-052810-093700 (2012).

155 Zerial, M. & McBride, H. Rab proteins as membrane organizers (vol 2, pg 107, 2001). *Nat Rev Mol Cell Bio* **2**, 216-216 (2001).
156 von Zastrow, M. & Sorkin, A. Signaling on the endocytic pathway. *Current opinion in cell biology* **19**, 436-445, doi:10.1016/j.ceb.2007.04.021 (2007).
157 Stenmark, H. Rab GTPases as coordinators of vesicle traffic. *Nature reviews. Molecular cell biology* **10**, 513-525, doi:10.1038/nrm2728 (2009).
158 Eathiraj, S., Pan, X., Ritacco, C. & Lambright, D. G. Structural basis of family-wide Rab GTPase recognition by rabenosyn-5. *Nature* **436**, 415-419, doi:10.1038/nature03798 (2005).
159 Blumer, J., Wu, Y. W., Goody, R. S. & Itzen, A. Specific localization of Rabs at intracellular membranes. *Biochemical Society Transactions* **40**, 1421-1425, doi:Doi 10.1042/Bst20120225 (2012).
160 Sonnichsen, B., De Renzis, S., Nielsen, E., Rietdorf, J. & Zerial, M. Distinct membrane domains on endosomes in the recycling pathway visualized by multicolor imaging of Rab4, Rab5, and Rab11. *The Journal of cell biology* **149**, 901-914 (2000).
161 Barbero, P., Bittova, L. & Pfeffer, S. R. Visualization of Rab9-mediated vesicle transport from endosomes to the trans-Golgi in living cells. *The Journal of cell biology* **156**, 511-518, doi:10.1083/jcb.200109030 (2002).
162 Andersson, E. R. The role of endocytosis in activating and regulating signal transduction. *Cellular and Molecular Life Sciences* **69**, 1755-1771, doi:Doi 10.1007/S00018-011-0877-1 (2012).
163 Yoo, S., Shin, J. & Park, S. EphA8-ephrinA5 Signaling and Clathrin-Mediated Endocytosis Is Regulated by Tiam-1, a Rac-Specific Guanine Nucleotide Exchange Factor. *Mol Cells* **29**, 603-609, doi:Doi 10.1007/S10059-010-0075-2 (2010).
164 Bouvier, D. *et al.* EphA4 is localized in clathrin-coated and synaptic vesicles in adult mouse brain. *J Neurochem* **113**, 153-165, doi:Doi 10.1111/J.1471-4159.2010.06582.X (2010).
165 Vihanto, M. M., Vindis, C., Djonov, V., Cerretti, D. P. & Huynh-Do, U. Caveolin-1 is required for signaling and membrane targeting of EphB1 receptor tyrosine kinase. *Journal of Cell Science* **119**, 2299-2309, doi:Doi 10.1242/Jcs.02946 (2006).
166 Pitulescu, M. E. & Adams, R. H. Eph/ephrin molecules,Äîa hub for signaling and endocytosis. *Genes & Development* **24**.
167 Deininger, K. *et al.* The Rab5 guanylate exchange factor Rin1 regulates endocytosis of the EphA4 receptor in mature excitatory neurons. *Proceedings of the National Academy of Sciences of the United States of America* **105**, 12539-12544, doi:Doi 10.1073/Pnas.0801174105 (2008).
168 Sharfe, N., Freywald, A., Toro, A. & Roifman, C. M. Ephrin-a1 induces, c-Cbl phosphorylation and EphA receptor down-regulation in T cells. *J Immunol* **170**, 6024-6032 (2003).
169 Fasen, K., Cerretti, D. P. & Huynh-Do, U. Ligand binding induces Cbl-dependent EphB1 receptor degradation through the lysosomal pathway. *Traffic* **9**, 251-266, doi:Doi 10.1111/J.1600-0854.2007.00679.X (2008).
170 Zhang, G. A., Spellman, D. S., Skolnik, E. Y. & Neubert, T. A. Quantitative phosphotyrosine proteomics of EphB2 signaling by stable isotope labeling with amino acids in cell culture (SILAC). *J Proteome Res* **5**, 581-588, doi:Doi 10.1021/Pr050362b (2006).

171 Verveer, P. J. & Bastiaens, P. I. H. Quantitative microscopy and systems biology: seeing the whole picture. *Histochem Cell Biol* **130**, 833-843, doi:Doi 10.1007/S00418-008-0517-5 (2008).
172 Lakowicz, J. R. *Principles of fluorescence spectroscopy*. 3rd edn, (Springer, 2006).
173 Bader, A. N., Hofman, E. G., Voortman, J., en Henegouwen, P. M. & Gerritsen, H. C. Homo-FRET imaging enables quantification of protein cluster sizes with subcellular resolution. *Biophysical journal* **97**, 2613-2622, doi:10.1016/j.bpj.2009.07.059 (2009).
174 Yeow, E. K. & Clayton, A. H. Enumeration of oligomerization states of membrane proteins in living cells by homo-FRET spectroscopy and microscopy: theory and application. *Biophysical journal* **92**, 3098-3104, doi:10.1529/biophysj.106.099424 (2007).
175 Forster, T. *Zwischenmolekulare Energiewanderung Und Fluoreszenz. *Ann Phys-Berlin* **2**, 55-75 (1948).
176 Clegg, R. M. Fluorescence resonance energy transfer. *Current opinion in biotechnology* **6**, 103-110 (1995).
177 Bastiaens, P. I. & Pepperkok, R. Observing proteins in their natural habitat: the living cell. *Trends Biochem Sci* **25**, 631-637 (2000).
178 Patterson, G. H., Piston, D. W. & Barisas, B. G. Forster distances between green fluorescent protein pairs. *Anal Biochem* **284**, 438-440, doi:Doi 10.1006/Abio.2000.4708 (2000).
179 Yasuda, R. Imaging spatiotemporal dynamics of neuronal signaling using fluorescence resonance energy transfer and fluorescence lifetime imaging microscopy. *Curr Opin Neurobiol* **16**, 551-561, doi:10.1016/j.conb.2006.08.012 (2006).
180 Bastiaens, P. I. & Squire, A. Fluorescence lifetime imaging microscopy: spatial resolution of biochemical processes in the cell. *Trends Cell Biol* **9**, 48-52 (1999).
181 van Munster, E. B. & Gadella, T. W. Fluorescence lifetime imaging microscopy (FLIM). *Adv Biochem Eng Biotechnol* **95**, 143-175 (2005).
182 *Live Cell Imaging: A Laboratory Manual*. Second Edition edn, (Cold Spring Harbor Laboratory Press, 2010).
183 Walther, K. A., Papke, B., Sinn, M. B., Michel, K. & Kinkhabwala, A. Precise measurement of protein interacting fractions with fluorescence lifetime imaging microscopy. *Molecular bioSystems* **7**, 322-336, doi:10.1039/c0mb00132e (2011).
184 Grecco, H. E., Roda-Navarro, P. & Verveer, P. J. Global analysis of time correlated single photon counting FRET-FLIM data. *Optics express* **17**, 6493-6508 (2009).
185 Kirchner, J., Kam, Z., Tzur, G., Bershadsky, A. D. & Geiger, B. Live-cell monitoring of tyrosine phosphorylation in focal adhesions following microtubule disruption. *Journal of cell science* **116**, 975-986 (2003).
186 Gluzman, Y. SV40-transformed simian cells support the replication of early SV40 mutants. *Cell* **23**, 175-182 (1981).
187 Rumsby, G. An introduction to PCR techniques. *Methods Mol Biol* **324**, 75-89, doi:10.1385/1-59259-986-9:75 (2006).
188 Sanger, F., Nicklen, S. & Coulson, A. R. DNA sequencing with chain-terminating inhibitors. 1977. *Biotechnology* **24**, 104-108 (1992).

189 Holland, S. J. *et al.* Juxtamembrane tyrosine residues couple the Eph family receptor EphB2/Nuk to specific SH2 domain proteins in neuronal cells. *The EMBO Journal* **16** (1997).
190 Rocks, O. *et al.* The palmitoylation machinery is a spatially organizing system for peripheral membrane proteins. *Cell* **141**, 458-471, doi:10.1016/j.cell.2010.04.007 (2010).
191 Weber, G. Dependence of the Polarization of the Fluorescence on the Concentration. *T Faraday Soc* **50**, 552-560, doi:Doi 10.1039/Tf9545000552 (1954).
192 Bastiaens, P. I. H., Vanhoek, A., Benen, J. A. E., Brochon, J. C. & Visser, A. J. W. G. Conformational Dynamics and Intersubunit Energy-Transfer in Wild-Type and Mutant Lipoamide Dehydrogenase from Azotobacter-Vinelandii - a Multidimensional Time-Resolved Polarized Fluorescence Study. *Biophysical journal* **63**, 839-853 (1992).
193 Runnels, L. W. & Scarlata, S. F. Theory and application of fluorescence homotransfer to melittin oligomerization. *Biophysical Journal* **69**, 1569-1583 (1995).
194 Blackman, S. M., Piston, D. W. & Beth, A. H. Oligomeric state of human erythrocyte band 3 measured by fluorescence resonance energy homotransfer. *Biophysical journal* **75**, 1117-1130 (1998).
195 Varma, R. & Mayor, S. GPI-anchored proteins are organized in submicron domains at the cell surface. *Nature* **394** (1998).
196 Gautier, I. *et al.* Homo-FRET microscopy in living cells to measure monomer-dimer transition of GFP-tagged proteins. *Biophysical journal* **80**, 3000-3008, doi:10.1016/S0006-3495(01)76265-0 (2001).
197 Squire, A., Verveer, P. J., Rocks, O. & Bastiaens, P. I. Red-edge anisotropy microscopy enables dynamic imaging of homo-FRET between green fluorescent proteins in cells. *J Struct Biol* **147**, 62-69, doi:10.1016/j.jsb.2003.10.013 (2004).
198 Fish, K. N. Total internal reflection fluorescence (TIRF) microscopy. *Curr Protoc Cytom* **Chapter 12**, Unit12 18, doi:10.1002/0471142956.cy1218s50 (2009).
199 Frangioni, J. V., Beahm, P. H., Shifrin, V., Jost, C. A. & Neel, B. G. The nontransmembrane tyrosine phosphatase PTP-1B localizes to the endoplasmic reticulum via its 35 amino acid C-terminal sequence. *Cell* **68** (1992).
200 Woodford-Thomas, T. A., Rhodes, J. D. & Dixon, J. E. Expression of a protein tyrosine phosphatase in normal and v-src-transformed mouse 3T3 fibroblasts. *The Journal of cell biology* **117**, 401-414 (1992).
201 Terasaki, M., Chen, L. B. & Fujiwara, K. Microtubules and the endoplasmic reticulum are highly interdependent structures. *The Journal of cell biology* **103**, 1557-1568 (1986).
202 Terasaki, M. & Reese, T. S. Interactions among endoplasmic reticulum, microtubules, and retrograde movements of the cell surface. *Cell Motil Cytoskeleton* **29**, 291-300, doi:10.1002/cm.970290402 (1994).
203 Lu, L., Ladinsky, M. S. & Kirchhausen, T. Cisternal organization of the endoplasmic reticulum during mitosis. *Molecular biology of the cell* **20**, 3471-3480, doi:10.1091/mbc.E09-04-0327 (2009).
204 Maeder, C. I. *et al.* Spatial regulation of Fus3 MAP kinase activity through a reaction-diffusion mechanism in yeast pheromone signalling. *Nature cell biology* **9**, 1319-1326, doi:10.1038/ncb1652 (2007).

205 Yudushkin, I. A. *et al.* Live-cell imaging of enzyme-substrate interaction reveals spatial regulation of PTP1B. *Science* **315**, 115-119, doi:10.1126/science.1134966 (2007).
206 Wiesmann, C. *et al. Nat Struct Mol Biol* **11** (2004).
207 Torres, R. *et al.* PDZ proteins bind, cluster, and synaptically colocalize with Eph receptors and their ephrin ligands. *Neuron* **21**, 1453-1463 (1998).
208 van Leeuwen, H. C., Strating, M. J., Rensen, M., de Laat, W. & van der Vliet, P. C. Linker length and composition influence the flexibility of Oct-1 DNA binding. *The EMBO journal* **16**, 2043-2053, doi:10.1093/emboj/16.8.2043 (1997).
209 Topell, S., Hennecke, J. & Glockshuber, R. Circularly permuted variants of the green fluorescent protein. *FEBS letters* **457**, 283-289 (1999).
210 Shah, N. P. *et al.* Overriding imatinib resistance with a novel ABL kinase inhibitor. *Science* **305**, 399-401, doi:10.1126/science.1099480 (2004).
211 Lombardo, L. J. *et al.* Discovery of N-(2-chloro-6-methyl- phenyl)-2-(6-(4-(2-hydroxyethyl)- piperazin-1-yl)-2-methylpyrimidin-4- ylamino)thiazole-5-carboxamide (BMS-354825), a dual Src/Abl kinase inhibitor with potent antitumor activity in preclinical assays. *J Med Chem* **47**, 6658-6661, doi:10.1021/jm049486a (2004).
212 Karaman, M. W. *et al.* A quantitative analysis of kinase inhibitor selectivity. *Nature biotechnology* **26**, 127-132, doi:10.1038/nbt1358 (2008).
213 Li, J. *et al.* A chemical and phosphoproteomic characterization of dasatinib action in lung cancer. *Nat Chem Biol* **6**, 291-299, doi:10.1038/nchembio.332 (2010).
214 Belousov, V. V. *et al.* Genetically encoded fluorescent indicator for intracellular hydrogen peroxide. *Nat Meth* **3** (2006).
215 Patterson, G. H. & Lippincott-Schwartz, J. A photoactivatable GFP for selective photolabeling of proteins and cells. *Science* **297**, 1873-1877, doi:10.1126/science.1074952 (2002).
216 Janes, P. W., Nievergall, E. & Lackmann, M. Concepts and consequences of Eph receptor clustering. *Seminars in cell & developmental biology* **23**, 43-50 (2012).
217 Bray, D., Levin, M. D. & Morton-Firth, C. J. Receptor clustering as a cellular mechanism to control sensitivity. *Nature* **393**, 85-88, doi:10.1038/30018 (1998).
218 Care, B. R. & Soula, H. A. Impact of receptor clustering on ligand binding. *BMC Syst Biol* **5**, 48, doi:10.1186/1752-0509-5-48 (2011).
219 Chan, C., George, A. J. & Stark, J. Cooperative enhancement of specificity in a lattice of T cell receptors. *Proceedings of the National Academy of Sciences of the United States of America* **98**, 5758-5763, doi:10.1073/pnas.101113698 (2001).
220 Wadhams, G. H., Martin, A. C., Warren, A. V. & Armitage, J. P. Requirements for chemotaxis protein localization in Rhodobacter sphaeroides. *Mol Microbiol* **58**, 895-902, doi:10.1111/j.1365-2958.2005.04880.x (2005).
221 Duke, T. & Graham, I. Equilibrium mechanisms of receptor clustering. *Prog Biophys Mol Biol* **100**, 18-24, doi:10.1016/j.pbiomolbio.2009.08.003 (2009).
222 Feng, Y.-X. *et al.* Liver cancer: EphrinA2 promotes tumorigenicity through Rac1/Ak/NF-kB signaling pathway *Hepatology (Baltimore, Md.)* (2009).
223 Dong, H., Qin, S. & Zhou, H. X. Effects of macromolecular crowding on protein conformational changes. *PLoS Comput Biol* **6**, e1000833, doi:10.1371/journal.pcbi.1000833 (2010).

224 Contractor, A. *et al.* Trans-synaptic Eph receptor-ephrin signaling in hippocampal mossy fiber LTP. *Science* **296**, 1864-1869 (2002).
225 Kayser, M. S., McClelland, A. C., Hughes, E. G. & Dalva, M. B. Intracellular and trans-synaptic regulation of glutamatergic synaptogenesis by EphB receptors. *J Neurosci* **26**, 12152-12164, doi:10.1523/JNEUROSCI.3072-06.2006 (2006).
226 Qiao, F. & Bowie, J. U. The many faces of SAM. *Sci STKE* **2005**, re7, doi:10.1126/stke.2862005re7 (2005).
227 Parker, M. *et al.* Reverse endocytosis of transmembrane ephrin-B ligands via a clathrin-mediated pathway. *Biochemical and Biophysical Research Communications* **323** (2004).
228 Holmberg, J., Clarke, D. L. & Frisén, J. Regulation of repulsion versus adhesion by different splice forms of an Eph receptor. *Nature* **408**, 203-206 (2000).
229 Carvalho, R. F. *et al.* Silencing of EphA3 through a cis interaction with ephrinA5. *Nat Neurosci* **9**, 322-330 (2006).
230 Weiss, A. & Schlessinger, J. Switching signals on or off by receptor dimerization. *Cell* **94**, 277-280 (1998).
231 Tonks, N. K. Protein tyrosine phosphatases--from housekeeping enzymes to master regulators of signal transduction. *Febs J* **280**, 346-378, doi:10.1111/febs.12077 (2013).
232 Tonks, N. K. Redox redux: revisiting PTPs and the control of cell signaling. *Cell* **121**, 667-670, doi:10.1016/j.cell.2005.05.016 (2005).
233 Flint, A. J., Tiganis, T., Barford, D. & Tonks, N. K. Development of "substrate-trapping" mutants to identify physiological substrates of protein tyrosine phosphatases. *Proceedings of the National Academy of Sciences of the United States of America* **94**, 1680-1685 (1997).
234 Huyer, G. *et al.* Mechanism of inhibition of protein-tyrosine phosphatases by vanadate and pervanadate. *The Journal of biological chemistry* **272**, 843-851 (1997).
235 Reynolds, A. R., Tischer, C., Verveer, P. J., Rocks, O. & Bastiaens, P. I. EGFR activation coupled to inhibition of tyrosine phosphatases causes lateral signal propagation. *Nature cell biology* **5**, 447-453, doi:10.1038/ncb981 (2003).
236 Levsky, J. M. & Singer, R. H. Gene expression and the myth of the average cell. *Trends Cell Biol* **13**, 4-6 (2003).
237 Miyawaki, A. & Tsien, R. Y. Monitoring protein conformations and interactions by fluorescence resonance energy transfer between mutants of green fluorescent protein. *Methods in Enzymology* **327** (2000).
238 Heyduk, T. Measuring protein conformational changes by FRET/LRET. *Current Opinion in Biotechnology* **13** (2002).
239 Goldbeter, A. & Koshland, D. E., Jr. An amplified sensitivity arising from covalent modification in biological systems. *Proceedings of the National Academy of Sciences of the United States of America* **78**, 6840-6844 (1981).
240 Tyson, J. J., Chen, K. C. & Novak, B. Sniffers, buzzers, toggles and blinkers: dynamics of regulatory and signaling pathways in the cell. *Current opinion in cell biology* **15**, 221-231 (2003).
241 Slieker, L. J., Martensen, T. M. & Lane, M. D. Synthesis of epidermal growth factor receptor in human A431 cells. Glycosylation-dependent acquisition of ligand binding activity occurs post-translationally in the endoplasmic reticulum. *The Journal of biological chemistry* **261**, 15233-15241 (1986).

242 Stamos, J., Sliwkowski, M. X. & Eigenbrot, C. Structure of the epidermal growth factor receptor kinase domain alone and in complex with a 4-anilinoquinazoline inhibitor. *The Journal of biological chemistry* **277**, 46265-46272, doi:10.1074/jbc.M207135200 (2002).
243 Shan, Y. *et al.* Oncogenic mutations counteract intrinsic disorder in the EGFR kinase and promote receptor dimerization. *Cell* **149**, 860-870, doi:10.1016/j.cell.2012.02.063 (2012).
244 Jura, N. *et al.* Mechanism for activation of the EGF receptor catalytic domain by the juxtamembrane segment. *Cell* **137**, 1293-1307, doi:10.1016/j.cell.2009.04.025 (2009).
245 Tokarski, J. S. *et al.* The structure of Dasatinib (BMS-354825) bound to activated ABL kinase domain elucidates its inhibitory activity against imatinib-resistant ABL mutants. *Cancer research* **66**, 5790-5797, doi:10.1158/0008-5472.CAN-05-4187 (2006).
246 Schindler, T. *et al.* Structural mechanism for STI-571 inhibition of abelson tyrosine kinase. *Science* **289**, 1938-1942 (2000).
247 Nagar, B. *et al.* Crystal structures of the kinase domain of c-Abl in complex with the small molecule inhibitors PD173955 and imatinib (STI-571). *Cancer research* **62**, 4236-4243 (2002).
248 Fabian, M. A. *et al.* A small molecule-kinase interaction map for clinical kinase inhibitors. *Nature biotechnology* **23**, 329-336, doi:10.1038/nbt1068 (2005).
249 Rix, U. *et al.* Chemical proteomic profiles of the BCR-ABL inhibitors imatinib, nilotinib, and dasatinib reveal novel kinase and nonkinase targets. *Blood* **110** (2007).
250 Huang, F. *et al.* Identification of candidate molecular markers predicting sensitivity in solid tumors to dasatinib: rationale for patient selection. *Cancer research* **67**, 2226-2238, doi:10.1158/0008-5472.CAN-06-3633 (2007).
251 Chang, Q., Jorgensen, C., Pawson, T. & Hedley, D. W. Effects of dasatinib on EphA2 receptor tyrosine kinase activity and downstream signalling in pancreatic cancer. *Br J Cancer* **99** (2008).
252 Cowan-Jacob, S. W., Mobitz, H. & Fabbro, D. Structural biology contributions to tyrosine kinase drug discovery. *Current opinion in cell biology* **21**, 280-287, doi:10.1016/j.ceb.2009.01.012 (2009).
253 Noble, M. E., Endicott, J. A. & Johnson, L. N. Protein kinase inhibitors: insights into drug design from structure. *Science* **303**, 1800-1805, doi:10.1126/science.1095920 (2004).
254 Jura, N. *et al.* Catalytic control in the EGF receptor and its connection to general kinase regulatory mechanisms. *Molecular cell* **42**, 9-22, doi:10.1016/j.molcel.2011.03.004 (2011).
255 Egea, J. *et al.* Regulation of EphA 4 kinase activity is required for a subset of axon guidance decisions suggesting a key role for receptor clustering in Eph function. *Neuron* **47**, 515-528, doi:10.1016/j.neuron.2005.06.029 (2005).
256 Davis, T. L. *et al.* Autoregulation by the Juxtamembrane Region of the Human Ephrin Receptor Tyrosine Kinase A3 (EphA3). *Structure* **16**, 873-884 (2008).
257 Binns, K. L., Taylor, P. P., Sicheri, F., Pawson, T. & Holland, S. J. Phosphorylation of Tyrosine Residues in the Kinase Domain and Juxtamembrane Region Regulates the Biological and Catalytic Activities of Eph Receptors. *Mol. Cell. Biol.* **20**, 4791-4805, doi:10.1128/mcb.20.13.4791-4805.2000 (2000).

258 Eisenmesser, E. Z. *et al.* Intrinsic dynamics of an enzyme underlies catalysis. *Nature* **438**, 117-121, doi:10.1038/nature04105 (2005).
259 Wiley, H. S. *et al.* The role of tyrosine kinase activity in endocytosis, compartmentation, and down-regulation of the epidermal growth factor receptor. *The Journal of biological chemistry* **266**, 11083-11094 (1991).
260 Wiley, H. S. Trafficking of the ErbB receptors and its influence on signaling. *Exp Cell Res* **284**, 78-88 (2003).
261 Ullrich, O., Reinsch, S., Urbe, S., Zerial, M. & Parton, R. G. Rab11 regulates recycling through the pericentriolar recycling endosome. *The Journal of cell biology* **135**, 913-924 (1996).
262 Walker-Daniels, J., Riese, D. J. & Kinch, M. S. c-Cbl-Dependent EphA2 Protein Degradation Is Induced by Ligand Binding11 American Cancer Society (CSM) Grant RPG-97-105-01 and the NIH Grant CA91318-01. *Molecular Cancer Research* **1** (2002).
263 Levkowitz, G. *et al.* Ubiquitin ligase activity and tyrosine phosphorylation underlie suppression of growth factor signaling by c-Cbl/Sli-1. *Molecular cell* **4**, 1029-1040 (1999).
264 Zantek, N. D. *et al.* E-Cadherin Regulates the Function of the EphA2 Receptor Tyrosine Kinase. *Cell Growth Differ* **10** (1999).
265 Miao, H., Burnett, E., Kinch, M., Simon, E. & Wang, B. Activation of EphA2 kinase suppresses integrin function and causes focal-adhesion-kinase dephosphorylation. *Nature cell biology* **2**, 62-69, doi:10.1038/35000008 (2000).
266 Pandey, A., Lazar, D. F., Saltiel, A. R. & Dixit, V. M. Activation of the Eck receptor protein tyrosine kinase stimulates phosphatidylinositol 3-kinase activity. *The Journal of biological chemistry* **269**, 30154-30157 (1994).

ACKNOWLEDGEMENTS

"It was the best of times, it was the worst of times, it was the age of wisdom, it was the age of foolishness, it was the epoch of belief, it was the epoch of incredulity, it was the season of Light, it was the season of Darkness, it was the spring of hope, it was the winter of despair, we had everything before us, we had nothing before us, we were all going direct to heaven, we were all going direct the other way -"…… Charles Dickens "A Tale of Two Cities"

For all the people and events that go down in my book-of-memories as the "best of times" I will be eternally grateful. Philippe, a year ago I was caught off balance and the only thing that made sense at that point was to runaway, so I thank you for being a temporary "backbone" at work and for giving me the necessary space and time to recover. If there were anything I would love to forever retain from my PhD- thesis time, it would be the precious people I got to know. I would like to thank all the residents of room C2.24 (past and present ones) for the fun time we had and a special dedication to the present members Katrin, Janah, Rabea and Martin, for bearing my snappy pre-submission period. Jian, Christina, Rabea, Hernan, Thies, Sfengler, ChenChen, Johann and many more thank you for teaching me that friendship has no nationality and cannot be bound to any label. Sorry but did I say Jiannnnn?

Zeta-Zeta-Zeta, because family is a decision, I thank you for including me in yours and being part of mine, "είσαι η μία". Hendrike, Jutta, Anetta and LisaWeta, I cannot group you into "our lab mothers" anymore because of LisaWeta, yet I thank you all for your unconditional help and support. Astrid, Matle, Christa, Pedro, Tanja, Kirstin, Hernan, Ali, Sven Muller, Anastasia, Andy and Waltraud thanks for the help and advise I got from you through the years, I started off as a "mathematically-deficient biologist" and I end up being "mathematically-deficient" only, hurray!

For some reason and despite of any failures and misgivings, there are those people out there who always had faith in me. My Alia & Hend, you define Khalil Gibran's saying "*your friend is your needs answered, for you come to him with your hunger, and you seek him for peace*". My rock-Mai, Caroline, Helmy, Amira, Walid and many more back home, you guys constitute my never-ending supply of positive energy.

It is unfair to acknowledge the role my family played in a couple of sentences, but I will give it a shot. My family pillars, Abo-Samra and Mimi, thanks for your continuous faith in me and your unconditional love and support. The happiest moment in my life must have been when you decided to get married. Kiwi, Nany, Dist, Habeeba, Nada, Marc, Rasha, Youssef, Khaled, Yousra, Menna, Ismail and Adam, you are my biggest and most beautiful support network. Last but not least, the luckiest person in this life is he whose "unchosen" family member becomes a chosen best friend for life, Nahla you make me the luckiest girl, I love you.

CURRICULUM VITAE

Permanent address: 5 Amin Anis St., 4th Zone, Cairo, Egypt, 11341 •Mobile: (+490175) 1565543 •
olasabet@hotmail.com

Education:

2008-2013 (Nov-July)	Graduate Student, Max Planck Institute for Molecular Physiology, Dortmund, Germany Department of Systems Cell Biology (Prof. Dr. Philippe Bastiaens)
2006-2007 (Oct-Oct)	Maters of Research, Department of Biology and Biochemistry Bath University, Bath, UK Research Experience: Thesis 1 title: The role of Angiogenin-Amyotrophic Lateral Sclerosis variants in neuronal pathfinding and their subcellular localization (supervised by Dr. Vasanta Subramanian). Thesis 2 title: The contribution of Microtubules o the polarity and the migratory machineries of *Drosophila* hemocytes (supervised by Dr. Will Wood). Degree Awarded: Dec 2007, MRes in Biosciences with distinction (top of class).
1998-2003 (Sep-July)	Bachelor of Pharmaceutical Sciences, Cairo University, Cairo, Egypt Pharmacy College Degree Awarded: Aug 2003, B.S. very good with honors.

Work Experience:

2004-2006 (Aug-Sep)	Research/Teaching Assistant, German University in Cairo, Cairo, Egypt Department of Organic and Biochemistry
2004-2004 (Jan-June)	Research/Teaching Assistant, American University in Cairo, Cairo, Egypt Department of Chemistry
2003-2004 (Aug-Jan)	Community Pharmacist, Abdel Maksoud Pharmacy, Cairo, Egypt

Publications and Manuscripts in preparation:

Stramer, B., Moreira, S., Millard, T., Evans, I., Huang, C. Y., **Sabet, O**., Milner, M., Dunn, G., Martin, P. and Wood, W., " Clasp-mediated microtubule bundling regulates persistent motility and contact repulsion in Drosophila macrophages *in vivo*." *J Cell Biol. 2010 May* 189 (4), pp. 681-689.

Janes, PW., Winner-Kleikamp, SH., Frangakis, AS., Treble, K., Griesshaber, B., **Sabet, O**., Grabenbauer, M., Ting, AY., Saftig, P., Bastiaens, PI., Lackmann, M.," Cytoplasmic relaxation of active Eph controls ephrin shedding by ADAM10". PLoS Biol., 2009 Oct 7(10).

Haj, FG., **Sabet, O**., Kinkhabwala, A., Wimmer-Kelikamp, S., Roukos, V., Han, HM., Grabenbauer, M., Bierbaum, M., Anthony, C., Neel, BG., Bastiaens, P.," Regulation of signaling at regions of cell-cell contact by endoplasmic reticulum-bound protein tyrosine phosphatase 1B" PLoS ONE.

Schaupp, A., **Sabet, O**., Dudanova, I., Ponsere M., Bastiaens, PI., Klein, R.," Composition of EphB2 clusters determines strength of cellular response" (Submitted).

Sabet O, Stockert R, Schmick M, Bastiaens PIH (2013) "The Spatial Organizaiton of Eph Receptor Signaling" (In preparation).

Hou J* & **Sabet O***, Grecco H, Bastiaens P (2013) "Enzyme Substrate Imaging of Eph Receptors" (In preparation).

APPENDIX I

Key: F: forward primer R: reverse primer

Oligo Name	Sequence	Tm total (°C)	Use
EphA2-KpnI-F	CAG GGT ACC ATG GAG CTC CAG GCA GCC C	69.1	C-terminal FP introduction
EphA2-AgeI-R	CAT AC CGG TGA GAT GGG GAT CCC CAC AGT G	66.0	‘’
EphA2-XmaI-F	TTT CCC GGG AAG TCA GAA CAA CTG AAG CCC	66.6	Restriction site introduction
EphA2-SpeI-R	GGA CTA GTG GAG AAG TAA ACG TCC TCC G	61.2	‘’
EphB2-SpeI-pt-F	CGG ACA AGC TGC AAC ACT ACA CTA GTG GCC ACA TGA CCC C	70.0	‘’
EphB2-SpeI-pt-R	G GGG TCA TGT GGC CAC TAG TGT AGT GTT GCA GCT TGT CCG	70.0	‘’
Spe-CC1-L-PvuI-TFP-F & used for Citrine	GGACTAGTctggcggcggcgtatagcagcattctg agcagcaacctgagcagcgatagcCGATCG ATGGTGAGCAAGGGCGAGGAG	74.3	Donor amplification + linker insertion
Xma-CC1-L-PvuI-Cit-R	TCCC CCC GGG GCT GCT CAG AAT GCT GCT ATA CGC CGC CGC CAG GCT ATC GCT GCT CAG GTTC GAT CGCTT GTA CAG CTC GTC CAT GCC	75.8	‘’
Spe-CC1-PvuI-TFP-F & used for Citrine	GGACTAGTctggcggcggcgtatagcagcattctg agcagcCGATCG ATGGTGAGCAAGGGCGAGGAG	74.4	“
Xma-CC1-Pvu1-Cit-R	TCCC CCC GGG GCT GCT CAG AAT GCT GCT ATA CGC CGC CGC CAG C GAT CGCTTGTACAGCTCGTCCATGCC	76.8	‘’
BamH-CC1-PvuI-Cit-R	TTCG GGATCC GCT GCT CAG AAT GCT GCT ATA CGC CGC CGC CAG C GAT CGCTTGTACAGCTCGTCCATGCC	75.2	‘’
Spe-BS1-Pvu1-TFP-F	GGA CTA GT A AAC TGC GCA CCG ATA TTA AAG TGG TG C GAT CGA TGG TGA GCA AGG GCG AGG AG	71.2	“
Xma-BS1-PvuI-Cit-R	TCCC CCC GGG CAC CAC TTT AAT ATC GGT GCG CAG TTT C GAT CG CTTGTACAGCTCGTCCATGCC	74	‘’
BamH-BS1-Pvu1-Cit-R	TTCG GGATCC CAC CAC TTT AAT ATC GGT GCG CAG TTT C GAT CG CTTGTACAGCTCGTCCATGCC	72.2	‘’
Spe-UL1-PuvI-TFP-F	GGACTAGT AAC CTG AGC AGC GAT AGC AGC AAC AGC CGATCGA TGG TGA GCA AGG GCG AGG AG	72.8	“
Xma-UL1-PvuI-Cit-R	TCCC CCC GGG GCT GTT GCT GCT ATC GCT GCT CAG GTT C GAT CG CTTGTACAGCTCGTCCATGCC	75.5	‘’
BamH-UL1-PvuI-Cit-R	TTCG GGATCC GCT GTT GCT GCT ATC GCT GCT CAG GTT C GAT CG CTTGTACAGCTCGTCCATGCC	73.7	“
EphA2-2YE-F	GACAGAGGTGGACCCCCACACAGAG GAGGACCCCAACCAGGCTGTGTTG	73.7	A2-2YE-Mutagenesis
EphA2-2YE-R	GGGTCCTCCTCTGTGTGGGGGTCCAC CTCTGTCTTCAGGGGCTTCAGTTG	73.1	A2-2YE-Mutagenesis
EphA2-2YF-F	GAAGACATTCGTGGACCCCCACACA TTTGAGGACCCCAACCAGGCTGTG	71.9	A2-2YF-mutagenesis
EphA2-2YF-R	GGTCCTCAAATGTGTGGGGGTCCACG AATGTCTTCAGGGGCTTCAGTTG	71.4	A2-2YF-mutagenesis

BamHI-calretic-BFP-F	TTGGGATCCATGCTGCTATCCGTGCC GTTGCTGCTCGGCCTCCTCGGCCTGG CCGTCGCCGACCGGTCGatgagcgagctga ttaagg	76	ER-BFP
BFP-XbaI-R	CCGGGCCTAGTCTAGATTACAGCTCG TCCTTATTAAGCTTGTGCC CCA GTT TGC TAG GGAGGTCGCAGTATCTGGCCACTG CCA CC	73	ER-BFP
hephrinA1-BglII-F	ACGCGTCGACTCACGGGGTTTGCAGC AGCAGAAGTGG	72	PCR amplify
hephrinA1-SalI-R	ACGCGTCGACCGGGGTTTGCAGCAG CAGAAG	71	PCR amplify
hephrinA1-SalI-F	ACGCGTCGACATGGAGTTCCTCTGGG CCCCTCTCTTGGG SalI	72.6	PCR amplify
h-ephrinA1-Not1-R-stop codon	ATAAGAATGCGGCCGCTCACGGGGT TTGCAGCAGCAGAAG Not1	71.3	PCR amplify
acceptor_AgeI_F	cgcaccccgctgaacACCGGTatggtgagcaaggg cgaggagg (AgeI)	75	PCR amplify
acceptor_linker_R_1st	CAGGCTGCCGCTGCCGCCGCTGCTctt gtacagctcgtccatgcc	76	
8L_B2(PBD)_Not1_R_2nd	ATAGTTTAgcggccgcTCAAACCTCCAC AGACTGAATCTGGTTCATCTGGGCCA GGCTGCCGCTGCCG (Not1)	75	
A2_Cit_ccl_DONOR_fix_F	CGTTTACTTCTCCACTAGTctggccgccgcc tatagcagcattctgagc (SpeI)	72	
A2_Cit_ccl_DONOR_fix_R	caattgACCGGTGATCAGATGGGGATCC CCACAGTGTTCACCTGGTCC	71	
ephrinB1_BglII_F	GGAAGATCT ATGGCTCGGCCTGGGCAGC	67.5	Ephrin cloning
ephrinB1_SalI_R	ACGCGTCGACTCAGACCTTGTAGTAG ATGTTCGC	66	"
hephrinB2_BglII_F	GGAAGATCT ATGGCTGTGAGAAGGGACTCC		"
hephrinB2_SalI_R	ACGCGTCGACTCAGACCTTGTAGTAA ATGTTCG		"
mTFP_AgeI_F_pDisplay	ctgaacACCGGTGTGAGCAAGGGCGAG GAGAC	69	"
mTFP_BsrG1_R_pDisplay	attcagTGTACAGCTCGTCCATGCCGTC GGTGG	68	
A2-D738N-F	GAACTATGTGCACCGTAACCTGGCTG CCCGCAAC	69	Mutagenesis
A2-D738N-R	GTTGCGGGCAGCCAGGTTACGGTGC ACATAGTTC	69	"
Cp_51_A2_F	GGACGTTTACTTCTCCtccgccggcAAAT TACCTGTTCCTTGGCCAAC	70	Circularly permuted GFPs
Cp_51_A2_R	CTTCAGTTGTTCTGACTTggaggcgccAC CCGTAGTGCATATAAACTTCAG	68.5	"
Cp_145_A2_F	GGACGTTTACTTCTCCtccgccggcAACT CGCATAATGTGTACATTACAG	68.5	"
Cp_145_A2_R	CTTCAGTTGTTCTGACTTggaggcgccGA AATTATACTCAAGTTTATGGC	67	"
Cp_157_A2_F	GGACGTTTACTTCTCCtccgccggcAAGA ACGGAATTAAAGCG	69	"
Cp_157_A2_R	CTTCAGTTGTTCTGACTTggaggcgccTT GTTTGTCAGCTGTAATG	67.5	"
Cp_173_A2_F	GGACGTTTACTTCTCCtccgccggcGGGT CTGTTCAACTTGC	71	"
Cp_173_A2_R	CTTCAGTTGTTCTGACTTggaggcgccAT	70	'

	CTTCGACGTTGTGCC		
Cp_51_SpeI/ccl_F	ggACTAGTctggccgccgcctatagcagcatcctga gcagcaacctgagcagcgatagc **AAATTACCTGTTCCTTGGC**	73	To overcome using PvuI only and introduce the cpGFPs while retaining the linkers in different backgrounds
Cp_51_XmaI/ccl_R	tcccCCCGGGgctgctcaggatgctgctataggcggc ggccaggctatcgctgctcaggtt **ACCCGTAGTGCATATAAAC**	75	
Cp_157_SpeI/ccl_F	ggACTAGTctggccgccgcctatagcagcatcctga gcagcaacctgagcagcgatagc **AAGAACGGAATTAAAGCG**	73	
Cp_157_XmaI/ccl_R	tcccCCCGGGgctgctcaggatgctgctataggcggc ggccaggctatcgctgctcaggtt **TTGTTTGTCAGCTGTAATG**	75	
Cp_173_SpeI/ccl_F	ggACTAGTctggccgccgcctatagcagcatcctga gcagcaacctgagcagcgatagc **GGGTCTGTTCAACTTGC**	74	
Cp_173_XmaI/ccl_R	tcccCCCGGGgctgctcaggatgctgctataggcggc ggccaggctatcgctgctcaggtt **ATCTTCGACGTTGTGC**	76	
Cp_51_SpeI/cc_F	ggACTAGTctggccgccgcctatagcagcatcctga gcagc**AAATTACCTGTTCCTTGGC**	73	
Cp_51_XmaI/cc_R	tcccCCCGGGgctgctcaggatgctgctataggcggc ggccag**ACCCGTAGTGCATATAAAC**	75	
Cp_157_SpeI/cc_F	ggACTAGTctggccgccgcctatagcagcatcctga gcagc**AAGAACGGAATTAAAGCG**	72	
Cp_157_XmaI/cc_R	tcccCCCGGGgctgctcaggatgctgctataggcggc ggccag**TTGTTTGTCAGCTGTAATG**	75	
Cp_173_SpeI/cc_F	ggACTAGTctggccgccgcctatagcagcatcctga gcagc**GGGTCTGTTCAACTTGC**	74	
Cp_173_XmaI/cc_R	tcccCCCGGGgctgctcaggatgctgctataggcggc ggccag**ATCTTCGACGTTGTGC**	77	
(ED)A2-XmaI-F	tttcc CCC GGG gacgtttacttctccaagtcag	66	
(ED)A2-SpeI-R	GGA CTA GTctccggggactggcgggcac	70	Restriction site introduction at different points using homologous recombination
(DV)A2-XmaI-F	tttcc CCC GGG gtttacttctccaagtcagaac	65	
(DV)A2-SpeI-R	GGA CTA GTgtcctccggggactggcggg	70	
(VY)A2-XmaI-F	tttcc CCC GGG tacttctccaagtcagaac	64	
(VY)A2-SpeI-R	GGA CTA GTaacgtcctccggggactggc	66	
(YF)A2-XmaI-F	tttcc CCC GGG ttctccaagtcagaacaac	65	
(YF)A2-SpeI-R	GGA CTA GTgtaaacgtcctccggggac	63	
(FS)A2-XmaI-F	tttcc CCC GGGtccaagtcagaacaactgaag	66	
(FS)A2-SpeI-R	GGA CTA GTgaagtaaacgtcctccgggg	63	
(KS)A2-XmaI-F	tttcc CCC GGGtcagaacaactgaagcccc	67	
(KS)A2-SpeI-R	GGA CTA GT cttggagaagtaaacgtcctccg	62	
(SE)A2-XmaI-F	tttcc CCC GGG gaacaactgaagcccctgaag	69	
(SE)A2-SpeI-R	GGA CTA GTtgacttggagaagtaaacgtcctccgg	64	
(EQ)A2-XmaI-F	tttcc CCC GGGcaactgaagcccctgaagac	69	
(EQ)A2-SpeI-R	GGA CTA GT ttctgacttggagaagtaaacgtcctccggg	66	
(QL)A2-XmaI-F	tttcc CCC GGG ctgaagcccctgaagacatac	68	
(QL)A2-SpeI-R	GGA CTA GT ttgttctgacttggagaagtaaacgtcctccg	65	
ccl/cc-A2(SK)-Spe-out-F	GGAGGACGTTTACTTCTCCACCAGCct ggccgccgcctatagcag	72	
ccl/cc-A2(SK)-Spe-out-R	GGCTTCAGTTGTTCTGACTTCCCGGGg ctgctcaggatgctgctatag	71	
A2-cterm-HyPer-R	ccttccgcatctagattaaaccgcctgttttaaaactttatcg aaatg	71	
A2-intern-HyPer-F	ttggACTAGTtccgccggcatggagatggcaagcca gcag	77	

A2-intern-HyPer-R	attaccCCCGGGgaggcgccaaccgcctgttttaaaactttatcgaaatg	77	
C-term Hyper-F	GCCGGCatggagatggcaagccagcag	79.8	Mutagenesis
C-term Hyper-R	ctgctggcttgccatctccatGCCGGC	79.8	Quick change
Ptp1Bwt-BspE1-F	aatttctccggaggtggaggtggaggcatggag	73	Ligation/cloning
Prp1Bwt-SalI-R	taaacgcGTCGACctatgtgttgctgttgaacagg	71	"
A2-actYE-F	ccccgaggccaccGAGaccaccagtggcgg	84	Quick Change
A2-actYE-R	ccgccactggtggtCTCggtggcctcgggg	84	Quick Change
A2-actYF-F	ccccgaggccaccTTTaccaccagtggcgg	81	Quick Change
A2-actYF-R	ccgccactggtggtAAAggtggcctcgggg	81	Quick Change
GRIP_N_F	TATATAGTCGACGCCACCATGATAGCTGTCTCTTTTAAATGCC	71	Ligation/cloning
GRIP_N_R	TAGTAGcccgggcATGGTGATGGTGATGATGACC	73	Ligation/cloning
GRIP_C_F	TATATAGTCGACATGATAGCTGTCTCTTTTAAATGC	65	Ligation/cloning
GRIP_C_R	TAATAAcccgggTTAATGGTGATGGTGATGATGAC	69	Ligation/cloning
mChXmaI_F	TATATAcccggggcatggtgagcaagggcgagg	75	
mChNotI_R	TATATAgcggccgcCTActtgtacagctcgtcc	72	
BFP_AgeI_F	CCCCCC ACCGGT ATGAGCGAGCTGATTAAGG AgeI	67	Cloning
BFP_linker_BglII_R	TAATTTAGATCT CAGGCTGCCGCTTCCGCCGCTGCTAT TAAGCTTGTGCCCC	71	"
EBFP-AgeI-F	tttaatACCGGTatggtgagcaagggcgagg	70	
EBFP-BsrG1-R	tttaccttgtacagctcgtccatgccgagag	70	
EBFP-BglII-F	ttttccagatctatggtgagcaagggcgagg	70	